Doctoral theses at NTNU, 2022:257

Aleksandar Janković

Experimental methods and analysis for the thermal and fluid dynamics behavior of double skin facades

Doctoral thesis

NTNU
Norwegian University of Science and Technology
Thesis for the Degree of
Philosophiae Doctor
Faculty of Architecture and Design
Department of Architecture and Technology

NTNU
Norwegian University of
Science and Technology

Aleksandar Janković

Experimental methods and analysis for the thermal and fluid dynamics behavior of double skin facades

Thesis for the Degree of Philosophiae Doctor

Trondheim, September 2022

Norwegian University of Science and Technology
Faculty of Architecture and Design
Department of Architecture and Technology

NTNU

Norwegian University of
Science and Technology

NTNU
Norwegian University of Science and Technology

Thesis for the Degree of Philosophiae Doctor

Faculty of Architecture and Design
Department of Architecture and Technology

ISBN 978-82-326-5207-5 (printed ver.)
ISBN 978-82-326-6752-9 (electronic ver.)
ISSN 1503-8181 (printed ver.)
ISSN 2703-8084 (online ver.)

Doctoral theses at NTNU, 2022:257

Printed by NTNU Grafisk senter

Summary

The concept of a modern double-skin façade (DSF) as we know it today has been around for more than 100 years since the idea of Le Corbusier's active glass wall, although the origins of this design can be recognized far earlier in vernacular architecture. However, it is only in the last 30 years that the application of DSFs in buildings has become more common, indicating the lack of established building practice, best reflected in the frequent occurrence of the dual nature (behavior) of the DSF in practice. On one side, flexible control of mass and energy fluxes between indoor and outdoor environments offered by DSFs enables far better performance than static single-skin envelopes in terms of energy demand and thermal, visual, and even acoustic comfort. The other side of the coin is reflected through a necessity for proper design and constant administration, which, if not done correctly, can lead to a drastic underperform, even compared to conventional envelopes. Transport of mass, momentum, and energy (heat and light) highly interact with each other. In addition, they are non-linear in DSF systems due to their constant interaction with the varying boundary conditions and construction features. Therefore, it is not straightforward to link and quantify the influence of construction features, operational modes, and environmental conditions on the thermophysical behavior of DSFs. Systematic investigations allow comprehensive and reliable insights into such cause-and-effect relationships, but there are insufficient examples, which is the main reason why these links are not fully understood.

This doctoral research aims to expand the knowledge on thermal and fluid dynamics behavior of DSFs and quantify how this behavior is influenced by the construction elements and boundary conditions. As the most fundamental and reliable way of obtaining new knowledge, an experimental approach has been chosen to accomplish this, which had to be systematic to ensure the comprehensiveness of the results. Through several experimental campaigns, both in the field and in a controlled environment, the performance of real-scale DSF mock-ups has been monitored. Given that DSFs do not have a long building tradition and, at the same time, exert complex behavior atypical for conventional envelopes, their performance assessment and measurement procedures are under-researched or non-standardized. Moreover, the standard metrics for traditional envelopes are not suitable to describe the dynamic behavior of DSFs, so distinctive performance indicators were used to address these issues. Therefore, this doctoral research additionally seeks to improve the methodological approach to conducting experiments to enable a more comprehensive and reliable characterization of DSF behavior. The findings from this aspect of the research are equally important

since without proper experimental design, setup, and execution, valid conclusions about thermal and fluid-dynamics behavior cannot be drawn.

The state-of-the-art review in Chapter 2 frames the research by systematically depicitng current knowledge about the cause-and-effect relationships between construction features, boundary conditions, and thermophysical behavior of DSFs. In addition, an overview of both experimental and numerical methods appropriate for such investigation is provided. The outcomes of this activity inform the direction of the present research. More precisely, what aspects of the thermophysical behavior need to be studied and how this should be done. Accordingly, in the second stage of the research, an experimental testbed was developed to allow comprehensive and systematic testing of DSFs in a controlled environment. The assembled testbed was verified with experimental investigations of various levels of complexity suitable for different types of characterizations. It was concluded that for the developed flexible experimental testbed, the design of the experiment (DOE) method is most appropriate to systematically characterize the thermophysical behavior of a DSF. Therefore, in the following research activity, the focus was placed on optimizing the selected methodology to make the most of the experimental testbed. An extensive simulation study with nearly half a million simulations resulted in the recommended course of action for finding the optimal experimental design suitable to characterize the targeted complex behavior using resource-limited experiments.

The developed methodological approach using building performance tools and simulations was validated in the following research stage with the real 'physical' experiments in a climate simulator. An equally important result of this experimental campaign was the assessment of the impact of construction features and boundary conditions on the thermal and fluid-dynamics behavior of a single-story DSF naturally ventilated in a wide range of boundary conditions typical of summer. The analysis results indicated that the central regulators were environmental factors, while the influence of controllable features (venetian blinds and the opening size) was considerably limited. However, some aspects of behavior, such as net heat transfer and even the airflow rate, could be controlled by adjusting the angle of venetian blinds. Another experimental campaign in a climate simulator was conducted with the single-story DSF to examine the efficiency of mechanical ventilation and venetian blinds in controlling heat transfer. It was found that mechanical ventilation effectively relieved the thermally-overloaded DSF cavity but did not significantly reduce the net heat penetrating the indoor environment. Regarding air preheating, relatively low airflow rates were able to deliver enough fresh air and sufficiently preheated air, while any higher rates of supplied air significantly increased the energy required to keep the constant interior temperature. The way in which the research activities

are related to the research questions, publications, and the overall objective of the doctoral study is provided in the graphical abstract given below.

This thesis comprises several articles set as chapters, connected and arranged to coherently follow the course of the conducted research. The collection of articles is preceded by an introduction that discusses the theoretical background, defines the problem, and presents the overall goal, research questions, and the methodology of the study. The last chapter discusses the results of the study and provides answers to previously defined research questions, and also reflects on the limitations of the research. Finally, this doctoral thesis closes with conclusive remarks and presents possibilities for further research.

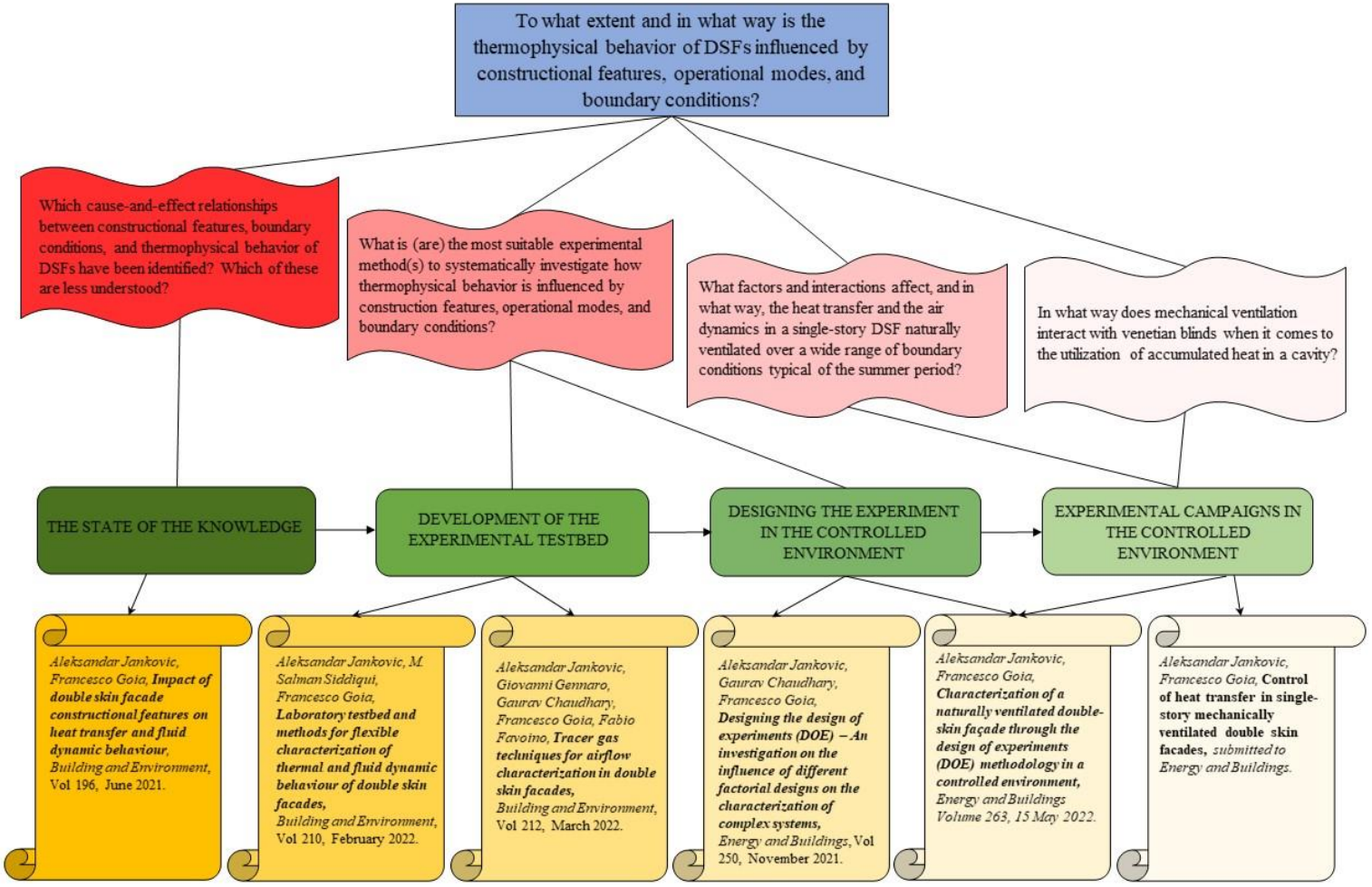

Graphical abstract - Relations of research questions, activities, and publications within doctoral research

Foreword

As has often befallen people in the Balkans, the time came for me to leave the homeland for the unknown to search for something better, somewhere where the past and present are less tumultuous, and the future is more certain. The choice, or perhaps more a set of circumstances, led me to Norway and Trondheim, the same city in which Miloš Crnjanski wrote in his travelogues almost 100 years ago that for every man there is one world unto himself and that all individuals together make one unusually pleasant society. However, deciding to leave your homeland in years when one should reap the fruits of their labor is not easy and carries many risks, especially when the haven is thousands of miles away, and where sky and air, culture, and ties within society are utterly different from those you're used to. Yet the desire for a life unencumbered by the past and all the bonds it carries was stronger than all the brakes created by the many differences. And here I am, with one stage in my life completed, almost four years after I arrived in Trondheim one rainy September morning with two suitcases. Throughout this time, it wasn't easy, but it was worth the effort. Everything from language learning, adaptation to climate and culture, meeting people from different backgrounds, fighting isolation, and having the opportunity to work with state-of-the-art technology and science has made me grow so much as a person, both professionally and personally. And perhaps this speaks best; if I could go back to summer 2018, I would do it all over again.

After almost four years of work, as the crown of my doctoral research, this thesis has seen the light of day, and therefore I would like to thank several people who contributed to the successful completion of this trip in various ways. First of all, I owe the greatest gratitude to my supervisor Francesco Goia, who made this experience much more accessible and enjoyable by having an excellent pedagogical approach and selflessly sharing his research experience and knowledge. Further, I would like to thank all those who helped carry out this study, either by collaborating on research or supporting me morally and affirmatively. Forgive me if I leave anyone out. A big credit should be given to Odne Oksavik, whom I want to thank for developing software to control and monitor the experiment and facilitating cooperation with SINTEF within the laboratory. My appreciation goes to Muhammad Salman Siddiqui and Gaurav Chaudhary for collaborating on several publications and assisting in the experimental setup. Thanks to Fabio Favoino and Giovanni Gennaro for cooperating in the experimental campaign at Politecnico di Torino and to Alesssandro Nocente, Egil Rognvik and Øystein Holmberget for support in the laboratory. I am thankful to Biljana Obradovic and other fellow doctoral students from the 4th and 8th floors for the many little things and

tips that helped me navigate this quest more easily. And of course, I thank the institution of NTNU itself, the REINVENT project, and the Research Council of Norway for funding this Ph.D. position.

Finally, I would like to thank my family, especially my wife Vanja, for accepting this journey into the unknown. She definitely carried the heaviest burden, especially during the long days when the whole world around us was shut down. Thanks to my mother for the selflessness she provided and my father for encouraging me to follow my dreams. He would surely be proud today. I dedicate this work to him.

Table of contents

List of figures

5. Designing the design of experiments (DOE) – An investigation on the influence of different factorial designs on the characterization of complex systems

6. Characterization of a naturally ventilated double-skin façade through the design of experiments (DOE) methodology in a controlled environment

List of tables

1. Introduction

1.1. Theoretical background

1.1.1. General considerations

The concentration of carbon dioxide in the atmosphere, most likely due to increased anthropogenic emission of greenhouse gasses, has increased at a record speed over the last 150 years to a level not seen for more than three million years (IPCC, 2014). Cities are the main drivers of the observed changes in climate since they are responsible for up to 70 % of global greenhouse gas emissions (UN-Habitat, 2011). Furthermore, the building sector represents a primary energy-consuming sector, accounting for more than a third of global energy consumption (Ahmad & Zhang, 2020)(Agency, 2013). Considering the statistics of the European Union, the energy consumption of the building sector amounts to about 40 % of final energy consumption, and residential buildings consume approximately two times more than commercial (Figure 1) (Belussi et al., 2019). Due to such a significant impact of the building sector on greenhouse gas emissions and energy consumption, increasingly stringent regulations aimed at reducing building energy demand have been present for some time, while new legislation encourages the construction of zero-energy buildings or buildings with zero net energy consumption (Marszal et al., 2011).

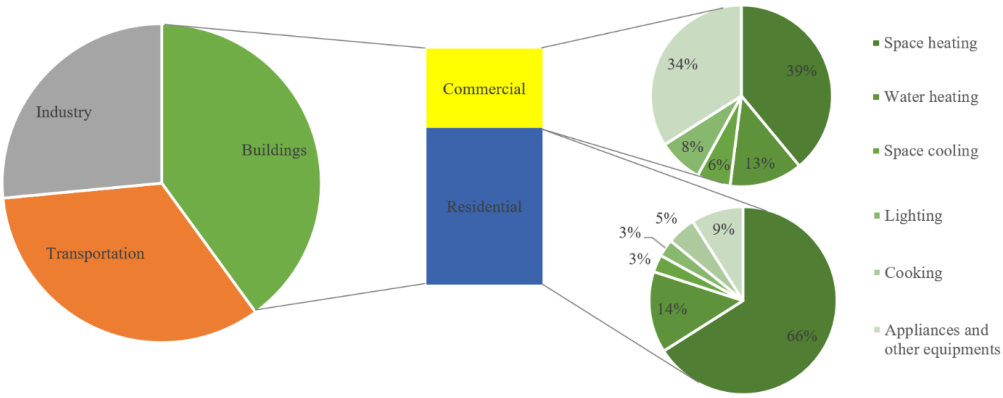

Fig. 1. – Final energy consumption by sector and end-use

With this approach, the built environment is expected to be nearly carbon-neutral in 2050, with greenhouse gas emissions 88-91 % lower than in 1990 (The European commision, 2011). In addition to reducing the emissions of greenhouse gases, this approach will also lead to economic benefits.

Concrete steps toward this goal are the Energy Efficiency Directive (The European Commision, 2012) and the European directive on the energy performance of buildings (EPBD) (The European Commision, 2010), as well as its updated and revised versions in 2016 (The European Commission, 2016) and 2018 (The European Commission, 2018). Directives suggest that all the European states should approve energy policies to promote the inclusion of very low and even close to zero energy buildings (De Gracia, Castell, Navarro, Oró, & Cabeza, 2013).

Final energy consumption in the building sector by end-use indicates that space heating occupies the largest share (Figure 1), while the energy demand for lighting and space cooling is also considerable. These types of energy consumption by end-use are directly dependent on the thermal insulation quality of the envelope and its ability to take advantage of the positive effects of the surrounding environment. Therefore, increased interest is evident in the search for building skin configurations that promise to minimize energy use for different purposes (heating, cooling, lighting, and ventilation) and maximize various aspects of user comfort (visual, thermal, and acoustic) (Cabeza et al., 2010). The most profitable strategy for achieving this is based on dynamic and responsive building envelope systems (Goia, 2013) capable of interacting with both indoor and outdoor environments and exploiting the effects of external stimuli instead of suppressing them (Taveres-Cachat, Grynning, Thomsen, & Selkowitz, 2019).

Recent qualitative research has identified four major families of dynamic (adaptive) facade technologies: dynamic shading, chromogenic, solar active, and active ventilated facades (Attia, Lioure, & Declaude, 2020). Although this study classifies double-skin façades (DSF) as solar-active facades, it must be emphasized that DSF systems can offer active ventilation and dynamic shading technology, depending on which design features are enabled. More precisely, a DSF is a multi-layered envelope element, most often highly transparent, with an external and internal skin separated by a ventilated space that can host a shading device for solar and visual control (Oesterle, Lieb, Lutz, & Heusler, 2001). Due to their visual attractiveness and flexibility in managing the interaction between indoor and outdoor environments, DSFs have become an interesting and important architectural and technological element in the last thirty years.

1.1.2. Double skin facades

The history of DSF architecture begins with the important invention of cast plate glassmaking in the middle of the 19th century, although the origins of this design date from a much earlier time when dwellings were built without professional guidance and with traditional materials and resources (Bonham, 2019a). Such examples are screened buffer zones (Jali screens or Mashrabiya from the

Middle East and India) or glazed buffer zones (traditional glass verandas in Balkan countries) (Lianos & Kostopoulos, 2006). The demand for better lighting, more than a need to exploit solar heat gains, brought the first glass curtain walls at the turn of the 20th century. However, the concept of active heating was first explored by Swiss-French architect Le Corbusier by inserting heating pipes between glass panes or between the glass pane and opaque wall construction (Bryan, 1991).

In addition to lighting and heating, through the second half of the 20th century, there were continuous attempts to employ DSF systems for better energy efficiency, thermal comfort, indoor air quality, and even better indoor acoustics. Empirical knowledge gained from these experimentations led to consolidating basic knowledge on the processes occurring in DSFs and increased confidence and interest in such technologies, resulting in the proliferation and increased application of DSFs since the early 1990s (Bonham, 2019a). Notable examples of buildings that incorporate DSF technology are 30 St Mary Axe (London), One Angel Square (Manchester), Manitoba Hydro Place (Winnipeg), and Pearl River Tower (Guangzhou). Some succesfull applications of DSF technology in Norwegian buildings are Sinsen Panorama, Hydro Vækerø and Helsfyr Atrium (Oslo), and Rådhus (Hamar). Although the application of DSFs is becoming increasingly popular globally, especially in regions with stricter energy efficiency regulations, significant knowledge gaps still exist regarding how the thermophysical behavior of DSFs is dictated by the boundary conditions, construction features, and operational strategies (Barbosa & Ip, 2014). Moreover, due to the lack of established building practices, there are no standardized procedures for designing and evaluating the performance of a DSF (Sinclair, Phillips, & Mezhibovski, 2009)(Choi, Joe, Kwak, & Huh, 2012).

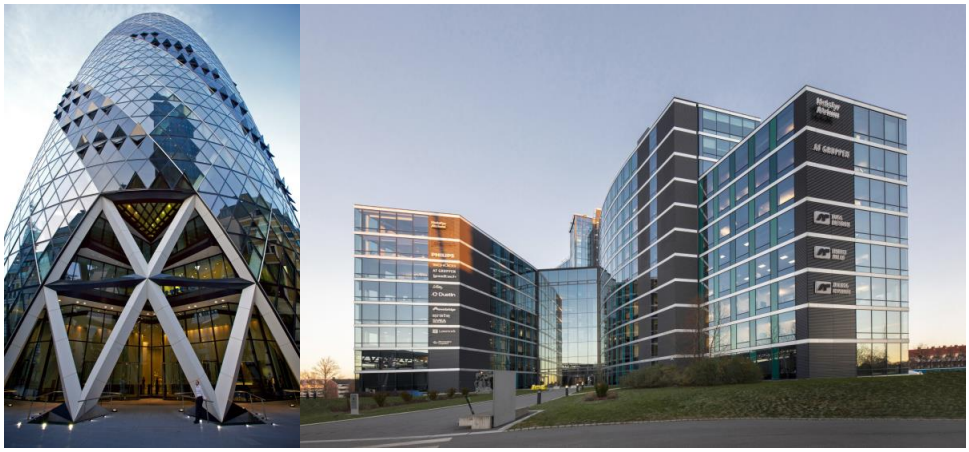

Fig. 2. – Examples of DSF building typology: a) 30 St Mary Axe (London) (Guichard, 2009) and b) Helsfyr Atrium (Oslo) (“Helsfyr Atrium building,” 2022)

DSFs can be classified according to three main criteria: ventilation type, cavity partitioning, and airflow path (or ventilation mode) (Loncour, Deneyer, Blasco, Flamant, & Wouters, 2005).

Ventilation of the cavity can rely on naturally induced airflow with wind action and thermal buoyancy as drivers. Both stimuli are often present, but an exact balance between them depends mainly on the climatic conditions and construction features of the DSF. The cavity of a DSF can be mechanically ventilated, most often utilizing powered fans. We can distinguish Box window, Shaft Box, Corridor, and Multi-Story configurations according to how the ventilation space is arranged, i.e., how the façade cavity is partitioned. In a box window configuration, the façade cavity is partitioned into smaller stand-alone units in which horizontal air movement is restricted between modules and, vertically, between floors. In a shaft-box configuration, the façade cavity is partitioned vertically, while in a corridor configuration, horizontally, most often by a story where the air moves laterally across façade elements. Vertical segmentation of the façade cavity is favorable for promoting the stack (chimney) effect, while horizontal is advantageous for fire safety and acoustic insulation (Poirazis, 2004). In the multi-story configuration, the façade cavity is not partitioned, and air can move freely through it (Hachem-Vermette, 2020).

Finally, the following ventilation (airflow) path arrangements exist: indoor air curtain, outdoor air curtain, exhaust, supply, and air buffer mode (Haase, Marques da Silva, & Amato, 2009). In the indoor air curtain and exhaust air ventilation modes, the air is drawn from the interior, whereby after passing through the cavity, it is returned to the interior in the former, while it is released to the outside in the latter mode. The flow is opposite in the outdoor air curtain and the supply air ventilation modes, with air drawing from the outdoor environment. The former ventilation mode releases the air back to the outside, while the latter, toward the interior. The DSF cavity is insulated from air exchange with the indoor and outdoor environment in the air buffer mode. Additionally, the air handling unit (AHU) can be connected to the DSF system to mechanically draw air from the cavity and release it to the interior space after the air treatment. This is the case with the climate façade where the air mechanically circulates in the indoor air curtain loop from the indoor space through the HVAC system and back into the interior (BBRI, 2002)(Serra, Zanghirella, & Perino, 2010).

DSFs have potential to be one of the best solutions for managing the interaction between the indoor and outdoor environment by providing minimum energy use and maximizing user comfort (Ahmed, Abel-Rahman, Ali, & Suzuki, 2015). For example, a fully glazed façade with integrated shading brings transparency without glare, which is often desired by architects when designing a residential or commercial building (Kuznik, Catalina, Gauzere, Woloszyn, & Roux, 2011). Besides visual comfort, DSFs bring appealing aesthetics and improve acoustic and thermal performance compared to single-skin glazed facades (Shameri, Alghoul, Sopian, Zain, & Elayeb, 2011). DSFs can provide air preheating in the façade cavity in the colder parts of the year through the greenhouse effect and solar heat gains (Carlos, Corvacho, Silva, & Castro-Gomes, 2011). Aside from air preheating, DSFs

offer the possibility of fresh air supply and heat recovery (Faggembauu, 2006). However, some disadvantages are known, such as overheating in the peak summer and insufficient air preheating in cold and overcast weather. Generally, dynamic envelope elements increase construction and maintenance costs compared to conventional envelopes. (Oesterle et al., 2001). Furthermore, DSFs must be well designed and managed since real-time optimization requires adjusting and fine-tuning the response of construction features to varying weather conditions. If this is not achieved, the desired optimization may turn into performance far below expectations due to the delicacy of interactions between controllable and uncontrollable factors.

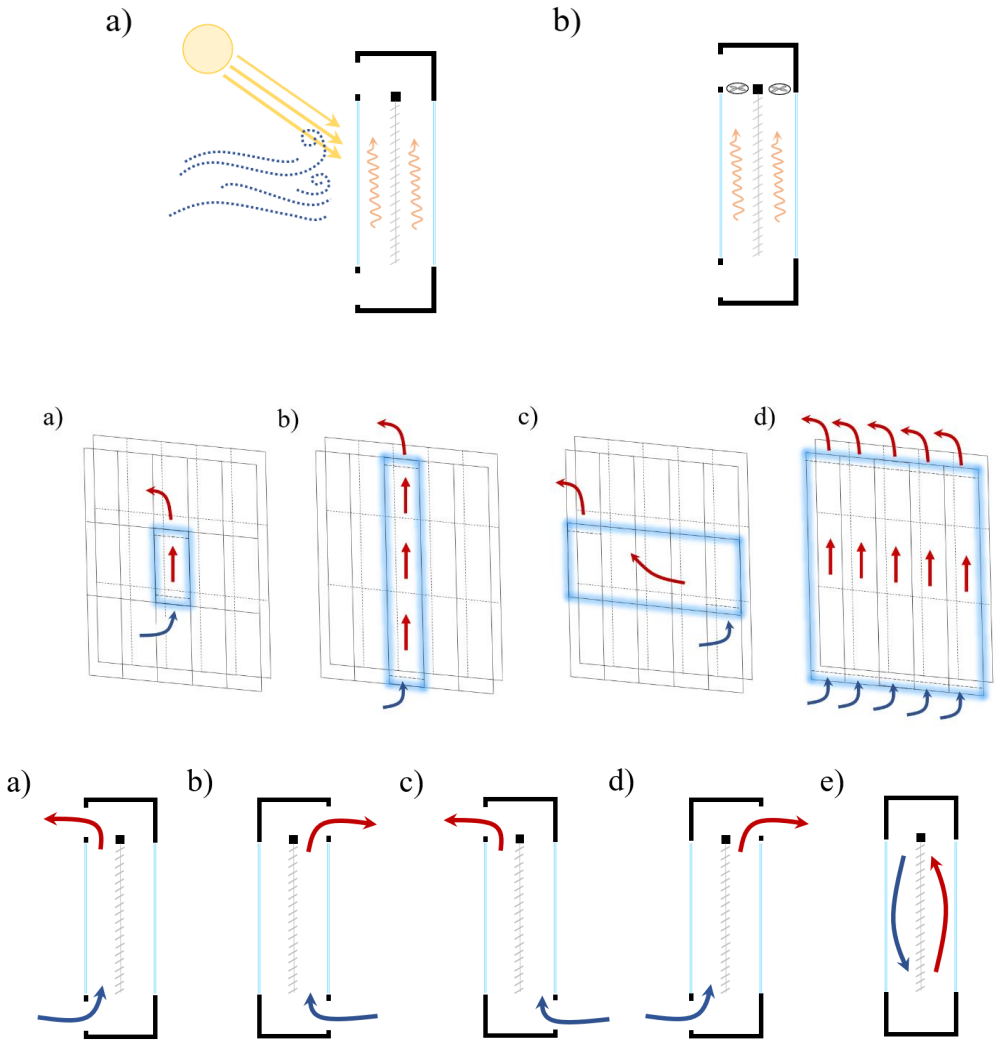

Fig. 3. – Classification of DSF according to
I) ventilation type: a) natural and b) mechanical
II) cavity partitioning: a) box window, b) shaft box, c) corridor, and d) multi-story configuration
III) ventilation mode: a) outdoor air curtain, b) indoor air curtain, c) exhaust, d) supply, and e) air buffer.

The concept of the DSF has been around for over 100 years, and it is constantly increasing in complexity through the addition of novel components such as photovoltaic (PV) elements (Preet, Sharma, Mathur, Chowdhury, & Mathur, 2020)(Luo et al., 2018), phase-change materials (PCM)(Li, Darkwa, & Kokogiannakis, 2017)(Elarga, Goia, Zarrella, Dal Monte, & Benini, 2016), plants (Yang, Yuan, Qian, Zhuang, & Yao, 2018), or thermochromic smart materials (Iken et al., 2019)(Liang et al., 2017). Predicting the thermal performance of DSFs, including conventional types, is far more complex than for other building envelope elements. Transports of heat, mass, and momentum in DSFs are highly dynamic and nonlinear, constantly driven by the varying boundary conditions and influenced by the construction features. Therefore, it is not a straightforward task to determine how the thermophysical behavior of DSFs is dictated by environmental, structural, and operational factors. Systematic research, both numerical and experimental, is the best way to translate the complexity of underlying processes in DSF systems into more accessible and pragmatic relations between the impacting factors and DSF behavior.

Nevertheless, these studies are very rare, which is one of the reasons why these links are generally not well understood and quantified. For that reason, decisions regarding the design and optimization of DSFs are not straightforward and may lead to performances far below expected, and even worse than those of conventional envelopes (Pasut & De Carli, 2012). Expertise in underlying physical processes and knowledge of prevailing on-site climatic conditions are required in the design phase to select suitable optical and geometric properties of glazing, shading device, cavity, and openings. Moreover, decisions regarding real-time optimization, including control of ventilation strategy and shading device, are even more complicated, and few researchers have addressed this. The flexibility offered by DSFs adds costs to architectural solutions, which may not always be a justified trade-off against high-performance single-skin facades (Bonham, 2019b). Nowadays, control strategies for ventilation and blinds in DSF systems are being developed (Gomes, Santos, & Rodrigues, 2014; Oh, Lee, & Yoon, 2012). However, their further development and success, to a large extent, depends on whether systematic investigations support them.

1.1.3 Experimental and numerical methods to investigate DSFs

Experiments and numerical modeling represent powerful tools for engineers and researchers to study DSF behavior and expand knowledge on heat transfer and fluid dynamics in such systems. According to Dopudi, numerical models can be grouped into three classes, depending on how detailed the cavity is modeled: simplified, zonal, and computational fluid dynamics (CFD) models (Dopudi, 2017). However, to address the full complexity of DSFs, modeling needs to be capable of representing heat, mass, and momentum transfer with a high degree of accuracy and detail (Gavan, Woloszyn, Kuznik,

& Roux, 2010). CFD modeling is the only type of numerical modeling capable of accurately capturing temperature and velocity fields (especially in the cavity), from which precise thermal and energy performance indicators can be derived. CFD modeling can be used for optimization purposes in the design phase, such as selecting the most favorable glazing or shading device type. It can also be used to extract simpler models that are easy to employ for real-time optimization, usually limited to a specific DSF type. The main advantage is higher flexibility than experiments when it comes to the comprehensive study of complex interactions between construction features and boundary conditions. However, at the same time, numerical simulations are highly dependent on experiments, as unvalidated results can give an erroneous picture of thermal and fluid-dynamic behavior. Due to the complex numerical set-up and detailed information they offer, CFD simulations require high computing and time costs. Furthermore, due its nature, only steady state or short-time transient states can be studied with CFD, which is why they are used mainly for research purposes far from everyday use.

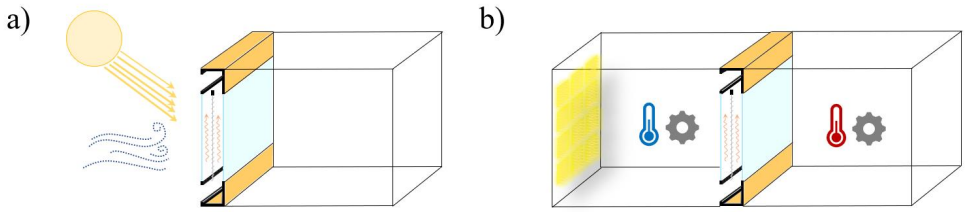

Fig. 4. – Sketch of a natural and controlled experiment

Experimental studies represent the principal and most reliable source of information for building knowledge on any phenomena, without which numerical models cannot be used properly. Generally, two types of experiments can be recognized: natural and controlled. In natural experiments, the test element is exposed to actual, outdoor, and transient conditions, while in controlled experiments, the surrounding environment is manipulated. In the latter experiment type, a mock-up is usually placed in a facility where the thermal or radiative environment can be controlled. For example, a climate simulator consists of two chambers intended to replicate the indoor and outdoor environment, with the mock-up placed in-between. Some facilities can simulate wind conditions, such as wind tunnels, but testing a real-scale DSF mock-up is challenging.

The first experiments that could be indirectly linked to the processes taking place in DSFs were realized in the second half of the twentieth century, where the heat and fluid flow were observed in the cavity between two vertical and opaque parallel plates (Batchelor, 1954)(Eckertf & Carlson, 1961)(King, 1989). At the beginning of this century, the first experiments with real DSFs as mock-

ups appeared, and all of them were natural (Zöllner, Winter, & Viskanta, 2002)(Manz, Schaelin, & Simmler, 2004)(Saelens, 2002). The scientific community had to wait until 2007 for the first experiment in a controlled environment, where the solar irradiance could be manipulated in addition to temperature (Mei et al., 2007). After the experiment at Loughborough University, only two laboratories provided testing of DSFs in both thermally and radiative controlled environments, the Center de Thermique de Lyon CETHIL (Gavan et al., 2010) and the Building Physics Laboratory at the İzmir Institute of Technology (Inan, Basaran, & Erek, 2017). No experiment has been performed to date in which thermal and radiative environments were controlled in addition to wind conditions.

No more than thirty experimental campaigns, where conventional DSFs (testbeds) were subjected to experimental investigations of varying complexity levels, have been performed under natural and controlled conditions. In most experiments, the temperature of various constructive elements was measured along with heat flux, incident, and transmitted solar radiation. The complexity of the experiments differed on the detailedness of the temperature field monitoring. For example, whether the temperature of the glazing surface was measured at only one point or multiple points were used. Also, how closely the physical quantities in the DSF cavity were monitored, whether temperature profiles could be extracted, and whether it was possible to obtain the airflow rate and velocity distribution in the cavity. The largest uncertainty in DSF thermal/energy performance assessment originates from the airflow measurements in the cavity since the instruments intended for measuring velocity and temperature represent perturbations in momentum fields. Generally, we can distinguish three categories of experimental airflow assessments: bulk airflow, direct velocimetry, and non-intrusive techniques. Each of these techniques differs in complexity and depth of insight they offer. Most experimental studies on DSF behavior use bulk airflow techniques, such as gas tracer techniques (Zeng, Li, Li, & Zhu, 2012)(Corgnati, Perino, & Serra, 2007)(Marques da Silva, Gomes, & Rodrigues, 2015), pressure difference methods (Manz et al., 2004)(Başaran & İnan, 2016), or one-point measurement of velocity to determine the bulk airflow (Zhang, Gang, Wang, Xu, & Du, 2019)(Curpek, Cekon, & Hraska, 2019). Very few experiments allowed the assessment of airflow patterns and velocity distribution in the cavity using multi-punctual direct velocity measurement, such as velocity profile method VPM (Zöllner et al., 2002)(Kalyanova & Heiselberg, 2008)(Mei et al., 2007)(Gavan et al., 2010)(Hassanli, Hu, Kwok, & Fletcher, 2017) or particle image velocimetry (PIV)(Safer, 2006)(Sánchez, Giancola, Blanco, Soutullo, & Suárez, 2019).

Unlike natural experiments, investigations in a controlled environment offer the possibility of focusing on certain phenomena by deliberately setting boundary conditions and even repeating or adjusting tests to make the effects of a specific phenomenon more detectable. In such investigations, parametric analyses are often performed based on a series of experiments in steady-state conditions.

The response of a particular performance indicator is examined through systematic alteration in controllable factors such as construction features or boundary conditions. In this way, controlled experiments offer a systematic and comprehensive approach to studying cause-and-effect relationships between variables in a system or process. The reason why there are more CFD studies than experimental studies lies in the high economic costs and the complex setup of experiments. The obtained results depend highly on the accuracy of instruments, reliability of measurement methods, and compliance with measuring procedures, which are most often non-standardized and insufficiently researched when it comes to DSF. Experiments in a controlled environment are even more sparse due to even higher expenses and specialized facilities not always being available for research.

1.2. Research objective and scope

1.2.1. Problem statement

This Ph.D. project is framed within the broader project: REsponsive, INtegrated, VENTilated - REINVENT – windows, financed by The Research Council of Norway, under the program FRINATEK – Young Research Talents. The project aims to introduce substantial innovation in how transparent facade elements are conceived and managed. On the one hand, the project aims to deepen understanding of the performance and the challenges of integrating dynamic components into building envelopes. On the other hand, it seeks to develop an advanced façade system for enhanced energy and environmental performance. The project involves designing, manufacturing, and testing a flexible and integrated façade system with incorporated sensing and control logic technology based on a double-skin façade architecture suitable for new and refurbished buildings. The research project is led by the Faculty of Architecture and Design (NTNU) with Hydro Extrusion AS as an industrial partner and SINTEF as a scientific partner. A collaboration with the Polytechnic University of Turin and Aalto University took place as well, and the results of this joint effort are also reflected in this doctoral thesis.

Double-skin facades are not a novel concept, but their more significant application only began in the 1990s. Due to their complex nature and to the absence of well-established building practice, a set of guidelines on designing DSFs to meet the building energy needs and users' requirements in terms of comfort do not exist. Unlike static envelope elements, transport processes in DSFs are highly coupled and dependent on interaction with construction features and external stimuli, meaning that the variability of exchanged energy and mass fluxes are also significantly greater. DSFs interact with the indoor and outdoor environment quite differently from traditional façade elements, such as opaque façades or windows, meaning that standard metrics (U- and g-value) are not good indicators of

thermal and energy performance of DSFs. Therefore, standardized procedures for assessing the performance of existing DSFs do not exist, meaning that the improvement and optimization of existing facades are more of a research process full of uncertainty than a well-established procedure. Although underlying physics and governing laws behind processes occurring in DSFs are more or less well understood, they are not translated into practical knowledge on DSF performance. For example, regarding the extent and how construction features, operational modes, and boundary conditions affect the thermophysical behavior of DSFs.

From the theoretical considerations in the previous section, it is clear that DSFs have been the subject of research, both experimental and numerical, for only twenty years. With such a short period of interest with a relatively small number of studies and insufficient experience from building practice, the scientific community has not been able to build a comprehensive knowledge base on thermal and fluid-dynamics behavior. This is best reflected through the typical problems DSFs encounter, such as overheating in a hot season or insufficient air preheating in cold periods. It is entirely wrong to say that these are common problems that are not solvable; rather, they are, in fact, examples of poorly designed DSFs or non-optimized functioning. The maximum potential of DSFs can be exploited once it is quantified and understood how different arrangements of construction features and operational modes in combination with boundary conditions influence the heat transfer and fluid dynamics in DSFs. In general, it can be said that the combined effects of environmental conditions, construction features and operational modes on the thermal and energy performance of DSFs are less known and studied, which represents an obstacle to optimal DSF design and operation.

Experiments in a controlled environment, especially when it comes to the simultaneous regulation of several flow drivers (such as solar irradiance, temperature difference, and wind conditions), represent valuable potential for examining these interactions and broadening the knowledge of cause-and-effect relationships in DSFs. Systematic investigations can translate these complex and (sometimes) nonlinear interrelations into accessible and practical relationships and provide answers to what extent and how various factors influence DSF performance. Moreover, the results of controlled experiments enable the validation of CFD models, which are another tool offering the opportunity to study DSFs more comprehensively. However, few experiments have been able to fully replicate and control the complexity of the external environment, which is one of the main reasons the knowledge base on DSF behavior is expanding slowly. To my best knowledge, only three laboratories (Gavan et al., 2010; Inan & Basaran, 2019; Mei et al., 2007) have run experimental campaigns in which real-scale DSFs were placed in facilities where the thermal and radiative environment was manipulated. Furthermore, no experiment has been performed where the surrounding temperature, incident solar radiation, and wind conditions were controlled simultaneously.

Generally, we can identify the following research gaps in the form of insufficient knowledge on:

- the overall impact of factors over a wide range of boundary conditions (comprehensive depictions of thermal and fluid behavior of DSF),
- the combined effect of several factors, i.e., interactions between construction features, on the thermophysical behavior.

Research gaps in the form of insufficient knowledge are caused by the lack of research on a given topic. In this case, how certain factors and their interactions influence the thermophysical behavior of DSF. Therefore, we can recognize a lack of systematic investigations in a controlled environment, especially those where two or more factors can be held constant, as a valuable resource for better understanding cause-and-effect relationships in DSF systems.

1.2.2. Research questions and objective

This doctoral study aims to fill these research gaps by expanding knowledge on DSF thermophysical behavior and quantifying how DSF performance is influenced by construction features, operational modes, and environmental conditions. Moreover, this research aims to demonstrate how experimental methods can be applied to successfully investigate thermophysical behavior of DSFs as atypical building envelope elements. A flexible experimental testbed was designed and developed, which, combined with optimized experimental procedures, offered the possibility to fill the existing knowledge gaps. Several experimental campaigns aimed at thoroughly examining the DSF performance were carried out.

Therefore, the main research question around which the doctoral research is centered is:

"To what extent and in what way is the thermophysical behavior of a DSF influenced by construction features, operational modes, and boundary conditions?"

The main research question can be divided into more specific sub-questions to facilitate decomposing a rather large problem into attainable elements to be systematically investigated.

- Which cause-and-effect relationships between construction features, boundary conditions, and thermophysical behavior of DSFs have been identified? Which of these are less understood?
- What is (are) the most suitable experimental method(s) to systematically investigate how the thermophysical behavior of DSFs is influenced by construction features, operational modes, and boundary conditions?

- What factors and interactions affect, and in what way, the heat transfer and the air dynamics in single-story DSF naturally ventilated over a wide range of boundary conditions typical of the summer period?
- In what way does mechanical ventilation interact with venetian blinds when it comes to the utilization of accumulated heat in a cavity?

The first research sub-question relates to the problem statement and identifying research gaps, while the second relates to developing a methodological approach for solving the previously recognized problem. The answers to the last two research sub questions represent the results and new knowledge about the thermophysical behavior of DSFs obtained by applying the previously developed methodological approach. These research questions are answered through published or recently submitted research and review articles in highly influential scientific journals. Four published conference papers are not presented in the thesis since they mainly provide the results of the initial research phase and do not bring any new findings compared to the articles.

Table 1. – Journal article contributions

	NAME	**AUTHORS**	**JOURNAL**
Journal article I (Aleksandar Jankovic & Goia, 2021)	**Impact of double skin facade constructional features on heat transfer and fluid dynamic behaviour**	Aleksandar Jankovic, Francesco Goia	*Building and Environment, Vol 196, June 2021, 107796*
Journal article II (Aleksandar Jankovic, Chaudhary, & Goia, 2021)	**Designing the design of experiments (DOE) – An investigation on the influence of different factorial designs on the characterization of complex systems**	Aleksandar Jankovic, Gaurav Chaudhary, Francesco Goia	*Energy and Buildings, Vol 250, November 2021, 111298*
Journal article III (Aleksandar Jankovic, Siddiqui, & Goia, 2022)	**Laboratory testbed and methods for flexible characterization of thermal and fluid dynamic behaviour of double skin facades**	Aleksandar Jankovic, M. Salman Siddiqui, Francesco Goia	*Building and Environment, Vol 210, February 2022, 108700*
Journal article IV (Aleksandar Jankovic, Gennaro, Chaudhary, Goia, & Favoino, 2022)	**Tracer gas techniques for airflow characterization in double skin facades**	Aleksandar Janković, Giovanni Gennaro, Gaurav Chaudhary, Francesco Goia, Fabio Favoino	*Building and Environment Volume 212, 15 March 2022, 108803*
Journal article V (Aleksandar	**Characterization of a naturally ventilated double-skin façade through the design of experiments (DOE)**	Aleksandar Jankovic, Francesco Goia	*Energy and Buildings*

Jankovic & Goia, 2022a)	**methodology in a controlled environment**		*Volume 263, 15 May 2022, 112024*
Journal article VI (Aleksandar Jankovic & Goia, 2022b)	**Control of heat transfer in single-story mechanically ventilated double skin facades**	Aleksandar Jankovic, Francesco Goia	Sent for review to Energy and Buildings in May 2022
Conference paper I (A Jankovic & Goia, 2019)	**A simulation study on the performance of double skin façade through experimental design methods and analysis of variance**	Aleksandar Jankovic, Francesco Goia	*IOP Conference Series: Materials Science and Engineering, Volume 609, 2019, 062003*
Conference paper II (A Jankovic, Goia, Eckert, & Müller, 2019)	**A test bed for thermal fluid dynamic analysis of double skin facade systems**	Aleksandar Jankovic, Francesco Goia	*IOP Conference Series: Materials Science and Engineering, Volume 609, 2019, 032006*
Conference paper III (Aleksandar Jankovic, Gennaro, Chaudhary, Goia, & Favoino, 2021)	**Gas traces techniques for airflow characterization in double skin facades**	Aleksandar Janković, Giovanni Gennaro, Gaurav Chaudhary, Francesco Goia, Fabio Favoino	*Proceedings of 15th RoomVent virtual conference: Energy Efficient Ventilation for Healthy Future Buildings, 2021, s. 226-229.*
Conference paper IV (Siddiqui, Jankovic, & Goia, 2021)	**Design and testing of a flexible test bed for thermal and fluid mechanic investigations of double skin facades**	Aleksandar Jankovic, M. Salman Siddiqui, Francesco Goia	*Proceedings of 15th RoomVent virtual conference: Energy Efficient Ventilation for Healthy Future Buildings, 2021, s. 558-561.*

1.2.3. Structure of the research

All research questions are related to specific activities within the doctoral project, which can be identified as:

1) The state of the knowledge;
2) Development of the experimental testbed;
3) Designing the experiment in a controlled environment;
4) Experimental campaigns in the controlled environment;

Figure 5 shows how this doctoral research is organized through activities and how these activities are related to the overall aim of the study, research questions, and contributions through publications.

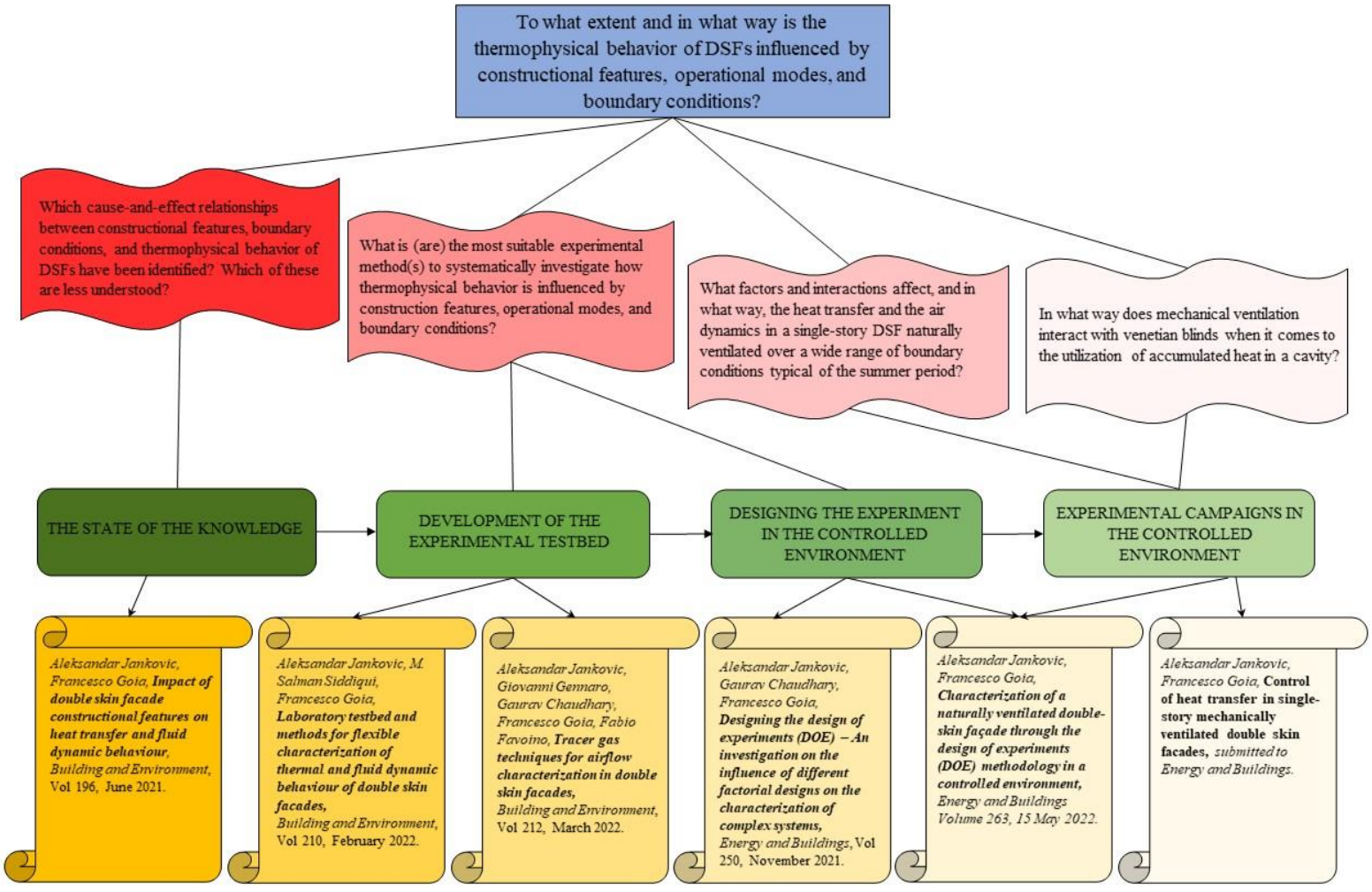

Fig. 5. - Relations of research questions, activities, and publications within doctoral research

1.3. Research methodology

The main activity around which the doctoral research revolved is the experimental testing of a full-scale DSF prototype in a climate simulator at the shared laboratories of NTNU and SINTEF. This involved equipping the test element with sensors, developing the onboard system for monitoring and control, calibrating set-up, designing and performing the experiments, and analyzing experimental data. Accordingly, a calibrated testbed for experimental analysis was developed, which was used (and is being used still) to assess the thermo-fluid behavior of DSF systematically. In planned experimental activities, numerous operational modes and configurations of the DSF were tested under different boundary conditions. Experimental analyses aimed to assess the energy performance and investigate the complex interrelation of thermophysical phenomena occurring in the systems, that is, the thermophysical behavior of the DSF in relation to cavity features, shadings, airflow rates, and more. The results of each of these research activities aimed to provide the answers to one or more of the research questions.

1.3.1. The state of the knowledge

This research activity aimed to systematically synthetize the current knowledge provided in the literature on the cause-and-effect relationships between construction features, operational modes, and boundary conditions and the resulting thermophysical behavior of DSFs. The body (of knowledge) was built and systematically organized by analyzing all previous relevant experimental and numerical research investigating topics of interest. The relevant publications for review were identified using the academic web search engines (Google Scholar, ScienceDirect, and Scopus) using specific keywords. The so-called snowball method (Wohlin, 2014) was then employed to expand the collection of publications (articles in journals and, to a lesser extent, doctoral dissertations and conference papers) as a source of information. Personal experience and general knowledge of heat transfer and fluid mechanics phenomena were used to complement and shape the information found in the literature. This was especially evident in systematizing the influence of structural elements and drawing conclusions and generalizations from the reviewed sources. In addition to shaping the current knowledge about thermophysical behavior, an overview of methods appropriate for such investigations (both experimental and numerical) was provided. Finally, knowledge gaps regarding methods for investigation and unexplored aspects of DSF behavior in the literature were pinpointed.

The literature review indicated a further course of research by recognizing problems not addressed in the current state of knowledge and determining the way in which they could be tackled. More precisely, what aspects of the thermophysical behavior of DSFs need to be studied and how that

should be done. Therefore, besides answering RQ1, this research activity aimed to answer the following sub question: “How can relationships in complex systems, such as DSFs, be studied?”. Besides formal review, activities in this phase of the research and associated publication (Aleksandar Jankovic & Goia, 2021) can be considered a state-of-the-art review since the publication history on experimental and numerical studies of DSFs only spans the last 20 years.

1.3.2. Development of the experimental testbed

In the framework of this activity, a flexible testbed was developed that, combined with optimized experimental procedures, would increase the possibilities for comprehensive and systematic investigation of DSF behavior and performance. The testbed was designed as an adaptable DSF mock-up equipped with a system for measurement and control of the experiment, placed into a cutting-edge climate simulator with an integrated artificial solar system. Features of this experimental testbed enabled relatively easy investigation of the response of thermophysical indicators to different configurations, operational modes, and boundary conditions replicated in the climate simulator. As such, it was possible to investigate how construction features, environmental conditions, and interactions among them influence the thermal and fluid dynamics behavior of a DSF. Activities at this stage of the research led to the publication of the article (Aleksandar Jankovic, Siddiqui, et al., 2022), where possible characterization methods suitable for addressing open questions about DSF thermophysical behavior were presented, including systematic investigations. This activity required the most time within the entire research, representing a central part of the doctoral study that paved the way for its overall success.

The methodological approach in this research activity can be divided into four steps:

I) Development of DSF mock-up;
II) Equipping the DSF mock-up with sensors and control features;
III) Airflow measurements by various techniques;
IV) Verification of the experimental set-up and preliminary measurements.

Development of DSF mock-up - The DSF mock-up was conceived as a flexible real-scale DSF prototype that can change its features. It was possible to manipulate the depth of the cavity, the slat angle of venetian blinds, size of the opening, fan speed, and airflow path by closing two of the four possible openings (Figure 6). The test element was planned to be subjected to a series of experimental investigations in the climate simulator located at the shared facilities of NTNU and SINTEF in Trondheim. The facility consists of two chambers for replicating indoor and outdoor conditions in

terms of air temperature and humidity conditions. The chamber replicating external conditions contains a solar simulator that can irradiate energy of maximum intensity of around 1000 Wm^{-2}.

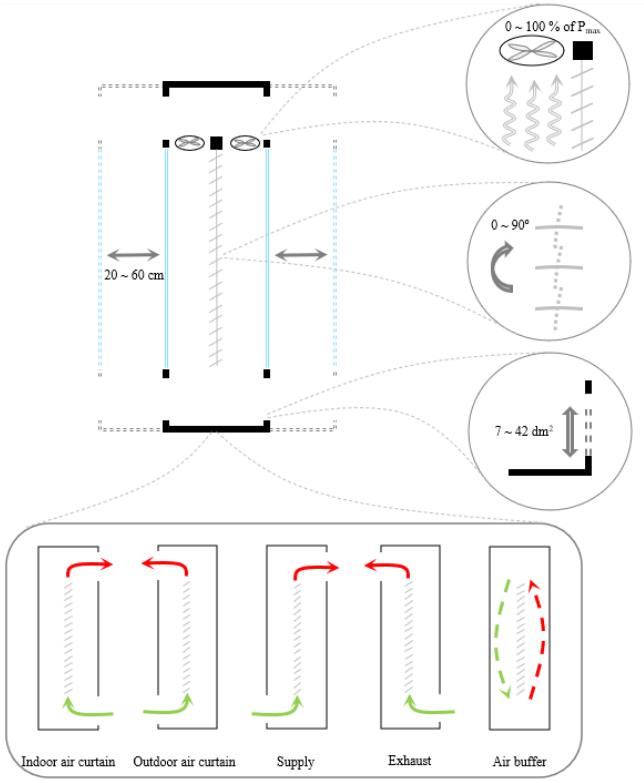

Fig. 6. - Alterable features of the DSF mock-up

Equipping the DSF mock-up with sensors and control features - Instrumentation of the DSF mock-up with sensors and control features required a long and thorough engagement. Over 70 sensors were installed for monitoring thermal and velocity fields in the cavity, temperature and irradiance distribution on the glazing and shading device, transmitted solar radiation, heat flux through glazing surfaces, and much more. Apart from standard metrics, such as U- or g-value, measurements of all other quantities in the DSF are not standardized. Therefore, selecting sensor type, positioning, and protection against adverse effects and providing physical support had to be guided by experience and best practices from literature. Recommended methods available in the literature were implemented to reduce the adverse impact of solar irradiance on temperature, heat flux, and airspeed measurements. For example, sensors were protected from additional heating from absorbed solar radiation by placing adhesive reflective aluminum tape in the suggested way.

Many sensors and control functions of the test element had to be connected into one system to monitor and control the experiment. The hardware of the communication system was made by wiring the sensors and control functions to devices that can communicate with and power them. The monitoring and control system software was developed in the LabVIEW environment. It was equipped with a graphic interface and built to control the measurements and main functions of the test element in real-time (cavity depth, fans rotation, shading proximity to glazing, and blind angle).

Airflow measurements by various techniques - The airflow rate measurements in the cavity represent the most delicate part of the experimental characterization of the thermal and fluid-dynamics behavior of the DSF. Techniques can be grouped into three main categories: bulk airflow, direct velocity, and non-intrusive velocity measurements; each of them has its advantages and disadvantages, differing in the complexity of the experimental set-up and the amount of information they can provide. In order to determine which method would best suit the planned tests, a separate experimental campaign was conducted to assess how reliably various techniques can characterize airflow. The campaign was conducted in outdoor conditions using a full-scale mock-up installed in the outdoor test facility at the Politecnico di Torino, where an effort was made to achieve the highest possible control over the experimental domain. In addition to determining airflow rate by direct velocity measurement, two other techniques were tested; the constant injection and the decay method. One of the aims was to expand the knowledge about tracer gas techniques that are rarely employed in DSFs and see what limitations may be encountered in characterizing airflow rate.

In order to achieve this, it was necessary to equip a full-scale mock-up of a DSF installed on an outdoor test facility with multiple sensors and run several experimental rounds. Different techniques for airflow rate measurement were employed over multiple airflow ranges generated by varying controllable features, i.e., the opening size and the fan speed. The measurement results obtained by the considered techniques were compared and supplemented by statistical analysis to obtain a more comprehensive picture of the relevance and the role of controllable and uncontrollable variables. Finally, based on experiences from the entire experimental campaign, a better insight was gained into the limitations linked to the instruments, requirements in terms of the experimental set-up, and applicability of each technique. The outcomes of this experimental campaign were published in the journal article (Aleksandar Jankovic, Gennaro, et al., 2022).

Verification of the experimental set-up and preliminary measurements - Although all deployed sensors were factory calibrated without further adjustment, periodic checks of their functionality were performed. For example, coherence tests between temperature sensors were performed approximately twice a year by comparing measurements of different sensors in thermal equilibrium. Similarly,

coherence tests between the same types of energy flux meters were performed by placing them close to each other, after which a stimulus of the same intensity was induced towards all. Sensors deviating from others by a larger quantity than the instrumental uncertainty were replaced or calibrated with respect to more accurate sensors. Finally, it was assessed how reliably the airflow rate could be determined in certain ranges by the chosen velocity profile method (VPM), as this method was selected to balance the accuracy and complexity of the experimental setup. The evaluation was done with respect to measurements obtained using an ultrasonic flowmeter, a technique that allows highly-accurate measurements using a special setup in laboratory conditions.

Prior to experimental campaigns aimed at thermophysical characterization of the DSF, the entire experimental testbed underwent preliminary testing, where four different types of experimental investigation with various levels of complexity were performed. From one side, this activity aimed to validate the experimental testbed by comparison with expected (theoretical) results. From the other side, the intention was to examine the possibilities offered by this flexible experimental testbed in terms of suitable characterization methods: measurement of standardized metrics, one-factor analysis, design of experiment, and dynamic profiles measurement.

1.3.3. Designing the experiment in the controlled environment

Previous research activity has indicated the possibilities for systematic characterization offered by the developed experimental testbed when paired with the various experimental methods. In this research activity, the focus was placed on optimizing the DOE methodology as the selected methodology to make the most of the experimental testbed. The DOE quantifies, in a systematic and efficient way, the relations between input variables (i.e., factors) and output variables (i.e., responses or performance indicators). In order to identify and link the influence of factors and interactions among them to the response quantities, a series of tests (experimental runs) needs to be devised systematically, where several factors are altered across each run. These series in which deliberate changes are made to the input variables are called experimental designs (or arrays). Their characteristics affect the outcome of the experiments, so the choice of representative runs that can sample the experimental domain effectively is crucial. After selecting the appropriate experimental design, a series of tests (experimental runs) are performed according to the pattern, after which statistical tools, such as ANOVA and regression analysis, are then employed to process the results. Finally, based on the statistical analysis results, it is determined to what extent and how the selected factors and interactions influence the indicators of the behavior of some process or system.

Since there are many experimental designs available for characterization, this research activity aimed to find an optimal array that would offer a comprehensive insight into the DSF behavior using as few resources as possible. That was not a straightforward task as, on the one hand, the thermophysical processes occurring in DSFs are very complex and nonlinear and, therefore, are not easy to describe. On the other hand, experiments in a controlled environment are rigid and highly demanding in terms of time and material resources. This research activity resulted in the journal article (Aleksandar Jankovic, Chaudhary, et al., 2021), which further clarified the answer to RQ2 by developing a set of guidelines for selecting optimal DOE. The following sub questions were answered to accomplish this: "What features should an experimental design have to adequately characterize the behavior of dynamic envelope elements, such as a DSF? What are the recommended steps to be followed to design experiments optimally?"

Finding optimal design was tackled through a case study, where the thermal and fluid-dynamic behavior of an advanced façade system was examined through building performance simulation tools and many different experimental designs. An effort was made to identify general guidelines that can facilitate finding optimal experimental designs for different types of investigations and processes, thus overcoming the specific case used in a case study. A wide range of experimental designs was compared and analyzed using numerical simulations to find one or more optimal designs that best and most efficiently describe the thermophysical behavior of the advanced façade system (mechanically ventilated DSF). Nearly half a million simulations were performed to evaluate the performance of more than 30 different DOEs by comparing their outputs with full factorial design (FFD) as the "ground truth." The assumption that the behavior of a system seen by the FFD is very similar to its actual behavior was not so far from the real truth since this design combines all the different levels and variables, allowing insight into the impact of every single permutation on the response variable.

1.3.4. Experimental campaigns in the controlled environment

The methodological approach, developed through building performance tools and simulation, needed to be validated with physical experiments with the DSF in a climate simulator and then employed to learn as much as possible about the thermophysical behavior of DSF. Therefore, two experimental campaigns, one with a naturally- and the other one with a mechanically-ventilated DSF, were performed in a controlled environment. In the first one, different configurations of a naturally-ventilated one-story DSF were exposed to a series of boundary conditions typical of the summer period replicated in the climate simulator. The developed experimental testbed was utilized through a systematically designed series of experiments to expand knowledge about the influence of

construction elements (venetian blinds and the opening size), boundary conditions, and their interactions on the thermophysical behavior of naturally-ventilated DSF. The results from this experimental campaign and the adopted methodology were presented in the journal article (Aleksandar Jankovic & Goia, 2022a).

In order to accomplish defined objectives, four applicable experimental designs were chosen according to the recommendations given in the previous research activity. Afterward, a series of experiments was performed using the climate simulator according to selected arrays. Data were collected and processed by ANOVA and associated statistical methods. Outputs from selected experimental designs were compared quantitively and qualitatively in order to identify common patterns in the behavioral depictions. Based on the resemblance between obtained characterizations, it could be assessed with a reasonable degree of accuracy which factors affected and in what way heat transfer and air dynamics in the DSF. The conclusions drawn here were intended to provide the answer to RQ3. Moreover, a comparison between designs led to synthesizing the main take-home lessons when it comes to using different experimental designs to characterize complex systems, such as DSFs. They were expected to be consistent with those derived in the simulation-supported study, which would validate the simulation-developed approach for finding the optimal design.

The effect of mechanically-induced airflow and venetian blinds in control of heat transfer in the one-story DSF was assessed in the second campaign. Unlike in the first experimental campaign, the impact of environmental factors (boundary conditions) was not examined here to gain a deeper insight into the extent of the influence of operable factors. Therefore, fixed boundary conditions were selected for two representative situations, according to which the appropriate ventilation modes were adapted. More precisely, supply-air ventilation mode for mid-season/winter conditions and outdoor air curtain for summer. A series of experiments were performed using a full-scale mock-up combined with a climate simulator, according to the full factorial design, where ventilation rate and venetian blind set-up were altered. After data collection, an analysis was performed to assess how effective chosen controllable elements were in preheating and delivering fresh air in supply-air mode and removing excess heat accumulated in the cavity in the outdoor air curtain mode. One journal article (Aleksandar Jankovic & Goia, 2022b) was developed and sent for review based on the results of this experimental campaign, and the conclusions drawn there were directed to answer RQ4.

1.4. References

Agency, I. E. (2013). *Transition to Sustainable Buildings*. https://doi.org/https://doi.org/10.1787/9789264202955-en

Ahmad, T., & Zhang, D. (2020). A critical review of comparative global historical energy consumption and

future demand: The story told so far. *Energy Reports*, *6*, 1973–1991. https://doi.org/10.1016/j.egyr.2020.07.020

Ahmed, M. M. S., Abel-Rahman, A. K., Ali, A. H. H., & Suzuki, M. (2015). Double Skin Façade: The State of Art on Building Energy Efficiency. *Journal of Clean Energy Technologies*, *4*(1), 84–89. https://doi.org/10.7763/jocet.2016.v4.258

Attia, S., Lioure, R., & Declaude, Q. (2020). Future trends and main concepts of adaptive facade systems. *Energy Science \& Engineering*, *8*, 3255–3272.

Barbosa, S., & Ip, K. (2014). Perspectives of double skin façades for naturally ventilated buildings: A review. *Renewable and Sustainable Energy Reviews*, *40*, 1019–1029. https://doi.org/10.1016/j.rser.2014.07.192

Başaran, T., & İnan, T. (2016). Experimental investigation of the pressure loss through a double skin facade by using perforated plates. *Energy and Buildings*, *133*, 628–639. https://doi.org/10.1016/j.enbuild.2016.10.020

Batchelor, G. K. (1954). Heat transfer by free convection across a closed cavity between vertical boundaries at different temperatures. *Quarterly of Applied Mathematics*, *12*(3), 209–233. https://doi.org/10.1090/qam/64563

BBRI, B. (2002). Source book for a better understanding of conceptual and operational aspects of active façades. *Department of Building Physics, Indoor Climate and Building Services, Belgian Building Research Institute*.

Belussi, L., Barozzi, B., Bellazzi, A., Danza, L., Devitofrancesco, A., Fanciulli, C., … Scrosati, C. (2019). A review of performance of zero energy buildings and energy efficiency solutions. *Journal of Building Engineering*, *25*, 100772. https://doi.org/10.1016/j.jobe.2019.100772

Bonham, M. Ben. (2019a). Double-Skin Façade History, Part I. In *Bioclimatic Double-Skin Façades* (1st ed., pp. 77–104). New York: Routledge. https://doi.org/10.4324/9781315661384

Bonham, M. Ben. (2019b). Double-Skin Façades: Motivations and Alternatives. In *Bioclimatic Double-Skin Façades* (1st ed., pp. 131–156). New York: Routledge. https://doi.org/10.4324/9781315661384

Bryan, H. (1991). Le Corbusier and the “Mur Neutralisant:” An Early Experiment in Double Envelope Construction. In S. Alvarez, J. L. Asiain, De, S. Yannas, & O. Fernandes (Eds.), *Architecture and Urban Space, Proceedings of the Ninth International PLEA Conference* (pp. 257–262). Seville, Spain: Springer Netherlands.

Cabeza, L. F., Castell, A., Medrano, M., Martorell, I., Pérez, G., & Fernández, I. (2010). Experimental study on the performance of insulation materials in Mediterranean construction. *Energy and Buildings*, *42*(5), 630–636. https://doi.org/10.1016/j.enbuild.2009.10.033

Carlos, J. S., Corvacho, H., Silva, P. D., & Castro-Gomes, J. P. (2011). Modelling and simulation of a ventilated double window. *Applied Thermal Engineering*, *31*(1), 93–102. https://doi.org/10.1016/j.applthermaleng.2010.08.021

Choi, W., Joe, J., Kwak, Y., & Huh, J.-H. (2012). Operation and control strategies for multi-storey double skin facades during the heating season. *Energy and Buildings*, *49*, 454–465. https://doi.org/10.1016/j.enbuild.2012.02.047

Corgnati, S. P., Perino, M., & Serra, V. (2007). Experimental assessment of the performance of an active transparent façade during actual operating conditions. *Solar Energy*, *81*(8), 993–1013. https://doi.org/10.1016/j.solener.2006.12.004

Curpek, J., Cekon, M., & Hraska, J. (2019). PCM Integrated in BiPV Ventilated Facąde Concepts: Experimental Test Cell Platform and Initial Full-Scale Measurements. *IOP Conference Series: Earth and Environmental Science*, *290*(1), 12072. https://doi.org/10.1088/1755-1315/290/1/012072

De Gracia, A., Castell, A., Navarro, L., Oró, E., & Cabeza, L. F. (2013). Numerical modelling of ventilated

facades: A review. *Renewable and Sustainable Energy Reviews*, *22*, 539–549. https://doi.org/10.1016/j.rser.2013.02.029

Dopudi, M. (2017). *Naturally ventilated double skin facade : CFD and simplified model for parametric energy simulation*. PhD Thesis, Politecnico Milano.

Eckertf, E. R. G., & Carlson, W. O. (1961). Natural convection in an air layer enclosed between two vertical plates with different temperatures. *International Journal of Heat and Mass Transfer*, *2*(1–2), 106–110. https://doi.org/10.1016/0017-9310(61)90019-9

Elarga, H., Goia, F., Zarrella, A., Dal Monte, A., & Benini, E. (2016). Thermal and electrical performance of an integrated PV-PCM system in double skin façades: A numerical study. *Solar Energy*, *136*, 112–124. https://doi.org/10.1016/j.solener.2016.06.074

Faggembauu, D. (2006). *Heat transfer and fluid-dynamics in double and single skin facades*. Universitat Politècnica de Catalunya.

Gavan, V., Woloszyn, M., Kuznik, F., & Roux, J.-J. (2010). Experimental study of a mechanically ventilated double-skin façade with venetian sun-shading device: A full-scale investigation in controlled environment. *Solar Energy*, *84*(2), 183–195. https://doi.org/10.1016/j.solener.2009.10.017

Goia, F. (2013). *Dynamic Building Envelope Components and nearly Zero Energy Buildings: Theoretical and experimental analysis of concepts, systems and technologies for an adaptive building skin*. PhD Thesis, Norges teknisk-naturvitenskapelige universitet, Fakultet for arkitektur og design.

Gomes, M. G., Santos, A. J., & Rodrigues, A. M. (2014). Solar and visible optical properties of glazing systems with venetian blinds: Numerical, experimental and blind control study. *Building and Environment*, *71*(Complete), 47–59. https://doi.org/10.1016/j.buildenv.2013.09.003

Guichard, A. (2009). 30 St Mary Axe. Retrieved April 25, 2022, from https://commons.wikimedia.org/wiki/File:30_St_Mary_Axe.jpg

Haase, M., Marques da Silva, F., & Amato, A. (2009). Simulation of ventilated facades in hot and humid climates. *Energy and Buildings*, *41*(4), 361–373. https://doi.org/10.1016/j.enbuild.2008.11.008

Hachem-Vermette, C. (2020). Selected High-Performance Building Envelopes BT - Solar Buildings and Neighborhoods: Design Considerations for High Energy Performance. In C. Hachem-Vermette (Ed.) (pp. 67–100). Cham: Springer International Publishing. https://doi.org/10.1007/978-3-030-47016-6_3

Hassanli, S., Hu, G., Kwok, K. C. S., & Fletcher, D. F. (2017). Utilizing cavity flow within double skin façade for wind energy harvesting in buildings. *Journal of Wind Engineering and Industrial Aerodynamics*, *167*, 114–127. https://doi.org/10.1016/j.jweia.2017.04.019

Helsfyr Atrium building. (2022). Retrieved April 25, 2022, from https://www.helsfyratrium.no/

Iken, O., Fertahi, S. ed-D., Dlimi, M., Agounoun, R., Kadiri, I., & Sbai, K. (2019). Thermal and energy performance investigation of a smart double skin facade integrating vanadium dioxide through CFD simulations. *Energy Conversion and Management*, *195*, 650–671. https://doi.org/10.1016/j.enconman.2019.04.070

Inan, T., & Basaran, T. (2019). Experimental and numerical investigation of forced convection in a double skin façade by using nodal network approach for Istanbul. *Solar Energy*, *183*, 441–452. https://doi.org/10.1016/j.solener.2019.03.030

Inan, T., Basaran, T., & Erek, A. (2017). Experimental and numerical investigation of forced convection in a double skin façade. *Energies*, *10*(9). https://doi.org/10.3390/en10091364

IPCC. (2014). *Climate Change 2014: Synthesis Report. Contribution of Working Groups I, II and III to the Fifth Assessment Report of the Intergovernmental Panel on Climate Change*. *IPCC*. Geneva, Switzerland.

Jankovic, A, & Goia, F. (2019). A simulation study on the performance of double skin façade through

experimental design methods and analysis of variance. *IOP Conference Series: Materials Science and Engineering*, *609*, 62003. https://doi.org/10.1088/1757-899x/609/6/062003

Jankovic, A, Goia, F., Eckert, D., & Müller, P. (2019). A test bed for thermal fluid dynamic analysis of double skin facade systems. *{IOP} Conference Series: Materials Science and Engineering*, *609*, 32006. https://doi.org/10.1088/1757-899x/609/3/032006

Jankovic, Aleksandar, Chaudhary, G., & Goia, F. (2021). Designing the design of experiments (DOE) – An investigation on the influence of different factorial designs on the characterization of complex systems. *Energy and Buildings*, *250*, 111298. https://doi.org/10.1016/j.enbuild.2021.111298

Jankovic, Aleksandar, Gennaro, G., Chaudhary, G., Goia, F., & Favoino, F. (2021). Gas traces techniques for airflow characterization in double skin facades. In *RoomVent 2020*. Torino.

Jankovic, Aleksandar, Gennaro, G., Chaudhary, G., Goia, F., & Favoino, F. (2022). Tracer gas techniques for airflow characterization in double skin facades. *Building and Environment*, *212*, 108803. https://doi.org/10.1016/j.buildenv.2022.108803

Jankovic, Aleksandar, & Goia, F. (2021). Impact of double skin facade constructional features on heat transfer and fluid dynamic behaviour. *Building and Environment*, *196*, 107796. https://doi.org/10.1016/j.buildenv.2021.107796

Jankovic, Aleksandar, & Goia, F. (2022a). Characterization of a naturally ventilated double-skin façade through the design of experiments (DOE) methodology in a controlled environment. *Energy and Buildings*, *263*, 112024. https://doi.org/10.1016/j.enbuild.2022.112024

Jankovic, Aleksandar, & Goia, F. (2022b). Control of heat transfer in single-story mechanically ventilated double skin facades. *Submitted to Energy and Buildings in May 2022*.

Jankovic, Aleksandar, Siddiqui, M. S., & Goia, F. (2022). Laboratory testbed and methods for flexible characterization of thermal and fluid dynamic behaviour of double skin facades. *Building and Environment*, *210*, 108700. https://doi.org/10.1016/j.buildenv.2021.108700

Kalyanova, O., & Heiselberg, P. (2008). *Experimental Set-up and Full-scale measurements in the 'Cube'*. DCE Technical reports No. 34, Department of Civil Engineering, Aalborg University.

King, K. J. (1989). *Turbulent Natural Convection in Rectangular Air Cavities*. PhD Thesis, Queen Mary University of London.

Kuznik, F., Catalina, T., Gauzere, L., Woloszyn, M., & Roux, J. J. (2011). Numerical modelling of combined heat transfers in a double skin facade - Full-scale laboratory experiment validation. *Applied Thermal Engineering*, *31*(14–15), 3043–3054. https://doi.org/10.1016/j.applthermaleng.2011.05.038

Li, Y., Darkwa, J., & Kokogiannakis, G. (2017). Heat transfer analysis of an integrated double skin façade and phase change material blind system. *Building and Environment*, *125*, 111–121. https://doi.org/10.1016/j.buildenv.2017.08.034

Liang, Z., Zhao, L., Meng, W., Zhong, C., Wei, S., Dong, B., … Wang, S. (2017). Tungsten-doped vanadium dioxide thin films as smart windows with self-cleaning and energy-saving functions. *Journal of Alloys and Compounds*, *694*, 124–131. https://doi.org/10.1016/j.jallcom.2016.09.315

Lianos, N., & Kostopoulos, K. (2006). Double-skin Façades and their Influence on the Form of Contemporary Buildings. Democritus University of Thrace. Retrieved from https://www.researchgate.net

Loncour, X., Deneyer, A., Blasco, M., Flamant, G., & Wouters, P. (2005). *Ventilated double facades. Classification & illustration of façade concepts*. *Belgian Building research institute* (Vol. 2).

Luo, Y., Zhang, L., Liu, Z., Xie, L., Wang, X., & Wu, J. (2018). Experimental study and performance evaluation of a PV-blind embedded double skin façade in winter season. *Energy*, *165*, 326–342. https://doi.org/10.1016/j.energy.2018.09.175

Manz, H., Schaelin, A., & Simmler, H. (2004). Airflow patterns and thermal behavior of mechanically ventilated glass double facades. *Building and Environment*, *39*(9), 1023–1033. https://doi.org/10.1016/j.buildenv.2004.01.003

Marques da Silva, F., Gomes, M. G., & Rodrigues, A. M. (2015). Measuring and estimating airflow in naturally ventilated double skin facades. *Building and Environment*, *87*, 292–301. https://doi.org/10.1016/j.buildenv.2015.02.005

Marszal, A. J., Heiselberg, P., Bourrelle, J. S., Musall, E., Voss, K., Sartori, I., & Napolitano, A. (2011). Zero Energy Building – A review of definitions and calculation methodologies. *Energy and Buildings*, *43*(4), 971–979. https://doi.org/10.1016/j.enbuild.2010.12.022

Mei, L., Loveday, D., Infield, D., Hanby, V., Cook, M., Ji, Y., … Bates, J. (2007). The influence of blinds on temperatures and air flows within ventilated double-skin facades. In O. S. Säteri & S. Jorma (Eds.), *Proceedings of Clima 2007 WellBeing Indoors* (p. 1606). Helsinki, Finland: REHVA World Congress. Retrieved from http://usir.salford.ac.uk/15870/1/Clima_2007_B02E1606.pdf

Oesterle, E., Lieb, R.-D., Lutz, M., & Heusler, W. (2001). *Double-skin facades : integrated planning*. München : Prestel. Retrieved from http://lib.ugent.be/catalog/rug01:000695707

Oh, M. H., Lee, K. H., & Yoon, J. H. (2012). Automated control strategies of inside slat-type blind considering visual comfort and building energy performance. *Energy and Buildings*, *55*, 728–737. https://doi.org/10.1016/J.ENBUILD.2012.09.019

Pasut, W., & De Carli, M. (2012). Evaluation of various CFD modelling strategies in predicting airflow and temperature in a naturally ventilated double skin faade. *Applied Thermal Engineering*, *37*, 267–274. https://doi.org/10.1016/j.applthermaleng.2011.11.028

Poirazis, H. (2004). *Double skin façades for office buildings*. Literature review, Lund University, Lund Institute of Technology.

Preet, S., Sharma, M. K., Mathur, J., Chowdhury, A., & Mathur, S. (2020). Performance evaluation of photovoltaic double-skin facade with forced ventilation in the composite climate. *Journal of Building Engineering*, *32*, 101733. https://doi.org/10.1016/j.jobe.2020.101733

Saelens, D. (2002). Energy performance assessment of single storey multiple-skin facades.

Safer, N. (2006). *Modélisation des façades de type double-peau équipées de protections solaires : Approches multi-échelles*. *PhD Thesis*. L'Institut National des Sciences Appliquées de Lyon.

Sánchez, M. N., Giancola, E., Blanco, E., Soutullo, S., & Suárez, M. J. (2019). Experimental Validation of a Numerical Model of a Ventilated Façade with Horizontal and Vertical Open Joints. *Energies*, *13*(1), 146. https://doi.org/10.3390/en13010146

Serra, V., Zanghirella, F., & Perino, M. (2010). Experimental evaluation of a climate façade: Energy efficiency and thermal comfort performance. *Energy and Buildings*, *42*(1), 50–62. https://doi.org/10.1016/j.enbuild.2009.07.010

Shameri, M. A., Alghoul, M. A., Sopian, K., Zain, M. F. M., & Elayeb, O. (2011). Perspectives of double skin façade systems in buildings and energy saving. *Renewable and Sustainable Energy Reviews*, *15*(3), 1468–1475. https://doi.org/10.1016/j.rser.2010.10.016

Siddiqui, M. S., Jankovic, A., & Goia, F. (2021). Design and testing of a flexible test bed for thermal and fluid mechanic investigations of double skin façades. In *Conference Proceedings of 15th RoomVent 2020 Conference*. Torino: Politecnico di Torino.

Sinclair, R., Phillips, D., & Mezhibovski, V. (2009). Ventilating façades. *Ashrae Journal*, *51*, 16–27.

Taveres-Cachat, E., Grynning, S., Thomsen, J., & Selkowitz, S. (2019). Responsive building envelope concepts in zero emission neighborhoods and smart cities - A roadmap to implementation. *Building and Environment*, *149*, 446–457. https://doi.org/10.1016/j.buildenv.2018.12.045

The European commision. (2011). *Communication from the Commission to the European Parliament, the Council, the European Economic and Social Committee and the Committee of the Regions - A Roadmap for moving to a competitive low carbon economy in 2050*. Brussels.

The European Commision. (2010). *Directive 2010/31/EU of the European Parliament and of the Council of 19 May 2010 on the energy performance of buildings*. Brussels.

The European Commision. (2012). *Directive 2012/27/EU of the European Parliament and of the Council of 25 October 2012 on energy efficiency, amending Directives 2009/125/EC and 2010/30/EU and repealing Directives 2004/8/EC and 2006/32/EC*. Brussels.

The European Commission. (2016). *Proposal for a Directive of the European Parliament and of the Council amending Directive 2010/31/EU on the energy performance of buildings 2016/0381 (COD)*. Brussels.

The European Commission. (2018). *Directive 2018/844/EU of the European Parliament and of the Council of 30 May 2018 amending Directive 2010/31/EU on the energy performance of buildings and Directive 2012/27/EU on energy efficiency PE/4/2018/REV/1 OJ L 156*. Brussels.

UN-Habitat. (2011). *Cities and Climate Change. Global Report on Human Settlements 2011*. *The Town Planning Review* (Vol. 83).

Wohlin, C. (2014). Guidelines for snowballing in systematic literature studies and a replication in software engineering. In *Proceedings of the 18th international conference on evaluation and assessment in software engineering* (pp. 1–10).

Yang, F., Yuan, F., Qian, F., Zhuang, Z., & Yao, J. (2018). Summertime thermal and energy performance of a double-skin green facade: A case study in Shanghai. *Sustainable Cities and Society*, *39*, 43–51. https://doi.org/10.1016/j.scs.2018.01.049

Zeng, Z., Li, X., Li, C., & Zhu, Y. (2012). Modeling ventilation in naturally ventilated double-skin façade with a venetian blind. *Building and Environment*, *57*, 1–6. https://doi.org/10.1016/j.buildenv.2012.04.007

Zhang, C., Gang, W., Wang, J., Xu, X., & Du, Q. (2019). Numerical and experimental study on the thermal performance improvement of a triple glazed window by utilizing low-grade exhaust air. *Energy*, *167*, 1132–1143. https://doi.org/10.1016/j.energy.2018.11.076

Zöllner, A., Winter, E. R. F., & Viskanta, R. (2002). Experimental studies of combined heat transfer in turbulent mixed convection fluid flows in double-skin-façades. *International Journal of Heat and Mass Transfer*, *45*(22), 4401–4408. https://doi.org/10.1016/S0017-9310(02)00160-6

2. Impact of double skin facade constructional features on heat transfer and fluid dynamic behavior

2.1. Abstract

Double skin facades (DSF) are an interesting and important architectural element in buildings as they are visually very attractive and can, at the same time, lead to better performance than single skin facades. DSFs need to be properly designed and operated, or their potential benefits might vanish. For this reason, the physical processes occurring in a DSF should be well understood and predicted. However, they are highly dynamic and in constant interaction with each other, and they depend on the geometric, thermo-physical, optical and aerodynamic characteristics of the different DSF elements. This literature review reports experimental and numerical studies of DSFs that investigate and assess the cause-effect link between constructional features and the thermophysical phenomena occurring in the systems. These studies are analyzed to better understand the current knowledge available to design both naturally and mechanically ventilated DSFs. The review shows that it is possible to understand simple links between families of constructional properties and performance, but only when one parameter at a time is analyzed. General trends can be defined, such as that the optical properties and especially shading (when present) properties are driving factors for both mechanically ventilated and naturally ventilated DSF, while other features seem to be less relevant (at least alone) to determine the behaviour of these systems. However, the complex interaction between more than one constructional feature is seldom investigated, if not completely explored, and this leaves a relatively large knowledge gap to support the optimal design and operation of DSF systems.

Graphical abstract

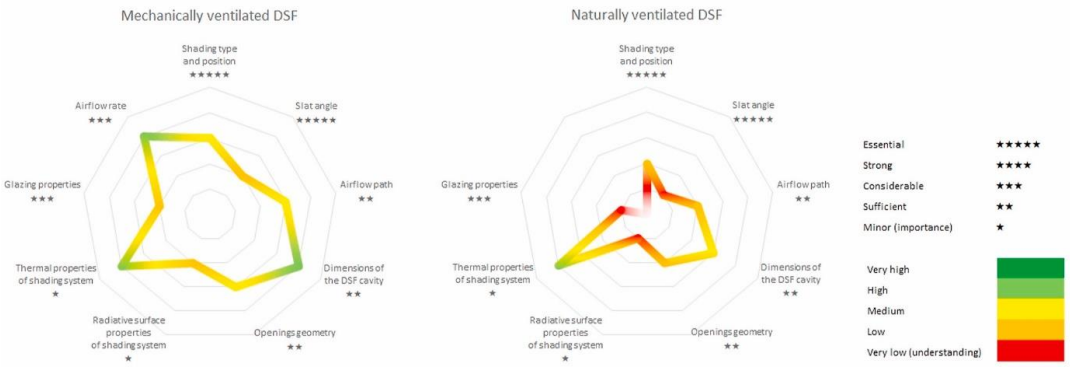

2.2. Introduction

A double skin façade (DSF) is composed of a multi layered structure, most often a highly transparent one, which has an external and internal layer, and a ventilated buffer space in between, sometimes hosting a device for solar and visual gain control [1]. DSFs can assume a different appearance and can be realized with different layouts, usually called Box Window, Shaft-Box, Corridor DSF, and Multi-Storey DSF (Fig. 1), relaying either on naturally induced or on mechanically induced airflow in the ventilated cavity, where by the last one is considered the flow driven by a powered fan.

A double skin façade is, in theory, an advanced system to manage the interaction between outdoors and the internal spaces due to its flexibility [3] thanks to the possibilities enabled by the different airflow paths that can be created in the DSF, ranging from outdoor air curtain to indoor air curtain, from supply air to exhaust air, and to the so-called climate façade configuration, with the possibilities to stop the ventilation flow and obtain a thermal buffer space (Fig. 2).

Besides better thermal performance and abundant daylight, a DSF brings visual attractiveness and provides an improvement in sound insulation, thermal comfort [5]. However, the large glazed surface can underperform conventional envelopes if they are not well designed and managed [6], for example through control of the ventilation flow and the activation of the shading devices in the DSF system [7,8].

The benefits that a DSF brings to the indoor environmental quality are of great interest to the professional and scientific community, while the interaction of DSFs with the outdoor urban environment is a less explored topic. The atypical radiative surface properties of DSF, where the outer skin is often almost fully glazed, may influence the overall energy balance in the urban environment, potentially leading to what is known as the urban heat island effect. However, some latest researches show that, contrary to the negative effect of large vertical glazed surfaces on the urban heat balance, DSF may actually contribute to dampening the urban heat island effect [9–11].

The DSF is widely explored as a technological solution, but it is not straightforward to link the constructional features of a DSF to its thermal and fluid mechanic behaviour. Transport of mass, momentum, and heat/ energy are highly dynamic and in constant interaction, and driven by the indoor and outdoor temperatures, the wind speed and direction, the intensity of incoming/outgoing radiation, and the pressure difference between the cavity and the two surrounding environments. Only once all the physical processes are understood, design actions (e.g. selecting and optimizing the constructional features of the DSF as. geometric, thermo-physical, optical and aerodynamic characteristics) [12] and the operational strategies can be consciously planned to achieve the desired performance goals.

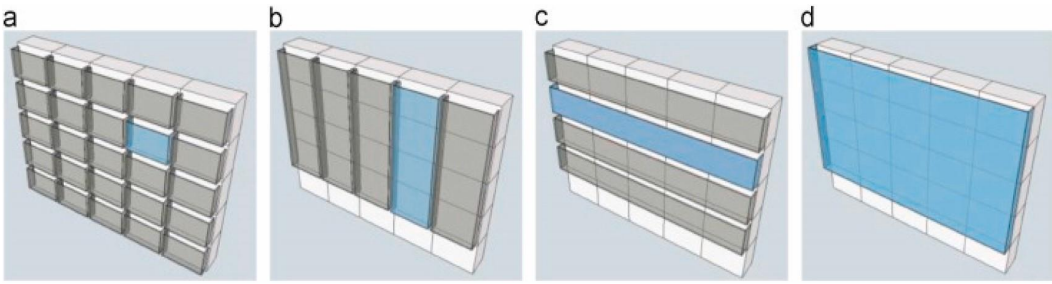

Fig. 1. DSF classification: (a) Box Window, (b) Shaft-Box, (c) Corridor and (d) Multi-Storey double skin façade. Original figure in [11].

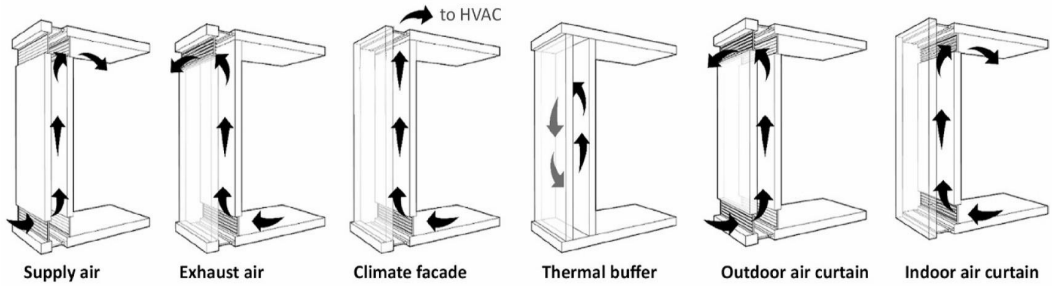

Fig. 2. DSF airflow path alternatives. Derived from illustration in [12].

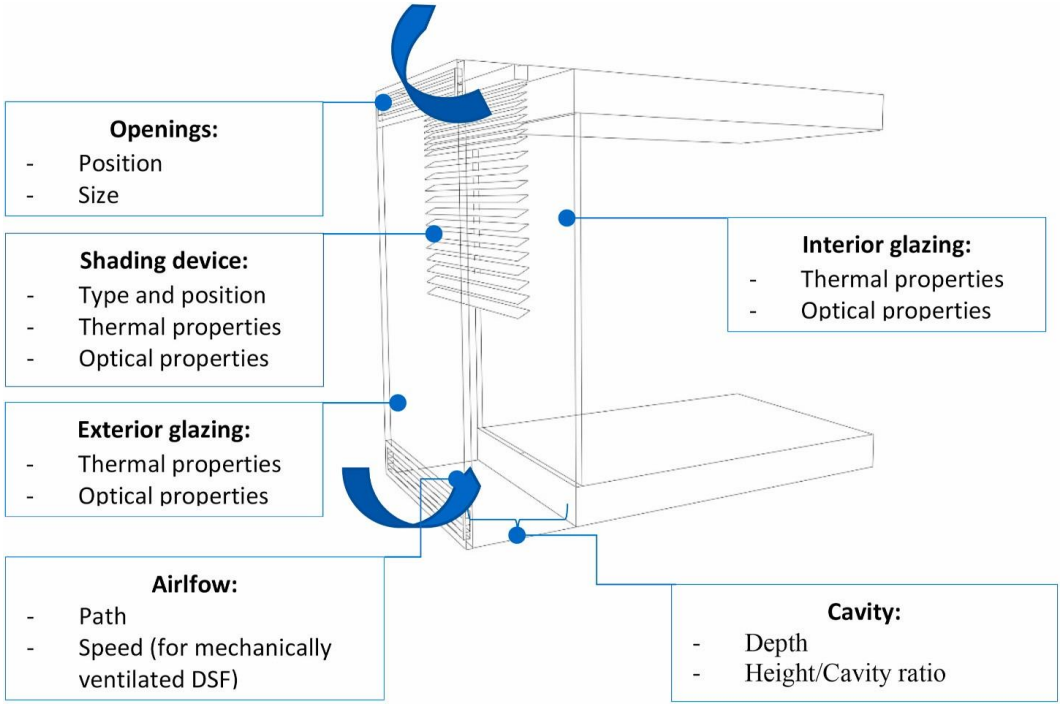

Fig. 3. Schematic representations of the constructional features investigated in this study (exemplified for the case of an outdoor air curtain DSF).

Although much knowledge about transport processes in DSFs is known, we experienced that the literature still lacks a systematic overview of how the constructional configurations of DSFs (e.g. cavity features, shadings, and airflows) affect the performance of a DSF. Through a comprehensive analysis of the established knowledge available in the scientific literature, we aim with this article to: i) explicitly examine the link between constructional features and heat transfer and fluid dynamic behavior in DSF systems; ii) to show how such relationships can be studied; and iii) to identify current knowledge gaps and unexplored relationships. The constructional features that we consider in this work, grouped in Fig. 3 for the different components of the DSF, are:

- geometric features:
    - dimensions of the cavity;
    - airflow path;
    - openings geometry;
    - shading position (and for venetian blinds, slat angle);
- material properties:
    - glazing properties;
    - radiative surface properties of the shading system;
    - thermal properties of the shading system;
- airflow rate (driven by the fan, only valid for mechanically ventilated DSF).

The main objectives of this article are therefore: to review research articles that clarify the influence how different structural parameters of DSF in conjunction with boundary conditions influence its performance and behavior; through such a review, to highlight what are the best, or at least most used techniques for numerical and experimental analysis of DSF behavior; and finally, to identify the current knowledge, as well as the knowledge gaps and unexplored relationships in the literature.

The identification of the relevant researches for review was done by using the freely accessible web search engines dedicated to scientific literature, using keywords to initiate the search of key documents, and then using a so-called snow-ball method to build up the corpus of manuscripts (articles in journals, and to a lesser extent doctoral dissertations and conference papers) used as a source of information. We also used our own experience and general knowledge of heat transfer and fluid mechanics phenomena to complement and assess the information we found in the literature.

The paper begins with Section 2, with a short part that recalls the theoretical background of heat transfer and focuses on its most complex components, especially for DSF systems, i.e. the convective heat transfer. A systemized overview of experimental and numerical methods to study DSFs is presented in Section 3. Because of the nature of the most complex phenomena occurring in the DSF,

after a brief general classification, when talking about numerical methods we place the focus on computational fluid dynamics (CFD) approaches, as they are the most advanced simulation technique to unveil the relationship between constructional features and fluid mechanic behaviour. In Section 4, based on the lessons learned from the literature, we summarize the explicit links between different families and sub-categories of constructional parameters and the fluid mechanics and thermal behavior of DSFs. The article is concluded with Section 5, where we give a comprehensive overview of the identified current know-how and knowledge gaps to be explored in the future to support a more grounded design of DSFs

2.3. Theoretical background

The prediction of the thermal performance of a DSF is sensibly more complex than for other building envelope systems. The temperature field in the solid/fluid layers of a DSF is determined by the heat transfer mechanisms occurring in the layer and in the surroundings, which can be a combination of conductive, radiative and convective components. The weight of conduction in the total heat transfer in a DSF is almost negligible, is well understood, and usually modeled within each glass layer or shading if it is present, while it is disregarded in the air channel. Heat transfer by radiation (also called thermal radiation) occurs between glass layers, between these and the shading, and between the interfaces of the DSF and the surrounding environments. Radiative heat exchange, as all the other mechanisms, is strongly influenced by solar radiation absorption and other optical phenomena [13] of the glass panes and the shading surface. The physical-mathematical background behind these two modes of heat transfer is well understood [14] and is not particularly complex in DSFs. Likewise, the numerical modeling of these two types of heat transfer does not pose real problems.

Conversely, the main uncertainty in the prediction of thermal performance of DSF originates from convective heat transfer and more complex knowledge on its physical and numerical background. The convective heat transfer is in its most general form described by the Newton law of cooling, where it is assumed that a rate of heat transfer by convection is proportional to the difference between surface and fluid temperature at an undisturbed location. In engineering practice, for internal flows such as double-skin facades, local temperature difference along cavity should be known, which is dependent on the distribution of both, temperature and velocity inside the cavity and on the surface of the glazing.

For conduits such as the ventilated gap in a DSF, there are several additional factors/influences that brings complexity and stochasticity in a calculation, e.g. asymmetrical boundary conditions and mutual impact of bordering surfaces which is why the entire temperature field across the cavity is affected simultaneously by more than one convective heat exchange. Drivers of the flow vary

inconsistently (solar radiation intensity and incident angle, outdoor temperature and especially wind speed and direction), which introduces unsteadiness and randomness in the flow. If geometrically complex elements such as venetian blinds are part of a conduit and if the dependence of thermophysical properties of air and solid parts on temperature is considered, then identification of the relevant quantities describing heat transfer by convection (heat transfer coefficient, Nusselt number etc.) is much more complicated than for more general cases. Before numerical methods became more widely adopted because of increased possibilities given by available computational power, empirical and dimensional analysis have been usually employed for a development of relationship for Nusselt number and evaluation of heat transfer by convection. Nowadays, computational fluid dynamics (CFD) methods are considered suitable tools to obtain a comprehensive solution to these problems [15].

2.4. Research methods to investigate the thermal and fluid mechanics phenomena in DSFs

This section gives a brief description of the different modelling approaches and the reason why CFD modelling is the best approach to offer a full insight into the cause-effect relationship between different variables in DSFs. Experimental studies represent the first and more reliable source of information, though they suffer from the lack of flexibility given by CFD studies. Furthermore, experiments are very important as they represent the only way of calibration and validation of numerical models.

2.4.1. Numerical analysis

A detailed numerical modelling of DSFs that wants to address the full complexity of these systems requires the combined representation of heat, mass, and momentum transfer [16]. Modeling and simulation of fluid dynamics in the DSF cavity requires a high degree of accuracy/detail to achieve a high degree of fidelity representation of the reality, and it is only possible to obtain with a specific type of numerical modelling (CFD or multi-zonal approach). However, different approaches to the modelling of phenomena in DSFs are seen with a different degree of accuracy, depending on the overall goal of the modelling activity. These approaches can be grouped in three categories, ranked in growing order of complexity of the model of the air cavity, according to the following list: 1) simplified models, 2) zonal models and 3) CFD models [17].

Simplified models are the broadest category of models that is the least detailed and accurate. Simplified models cover different subcategories, such as: analytical and lumped, airflow-network and control volume models and models derived from the non-dimensional analysis [18]. They are

able to predict the thermal performance of DSF by means of simulating heat and mass transfer through bulk airflow rates, but they cannot simulate fluid dynamics (momentum transfer). The most frequently used type of simplified model are lumped models, which are usually employed for parametric optimization analysis, representation of the overall thermal characteristics of the DSF systems, and prediction of the energy performance of DSF as a design assisting tool [19]. They usually are mono-dimensional and assume constant temperatures on the surfaces and cavity of the DSF [17], where heat transfer is represented by Newton law of cooling and occurs between more than two isothermal boundaries. The solution is obtained by the construction of a thermal network characterized by a fictitious thermal resistances and capacitances [20]. Furthermore, building energy simulation tools couple the airflow network with thermal network in order to account the influence of airflow and pressure fields on heat transfer [21]. However, these models are represented by approximate relations, which do not reflect the thermal phenomena in detail and are, because of their intrinsic limitation, not fully representative of the complex interacting phenomena.

In order to overcome these issues, an extension of the Newton formulation was proposed by Foroushani [22], where the convective heat transfer is represented by interaction between each pair of isothermal boundaries characterized by multiple functionality coefficients. The values of these multiple functionality coefficients can be calculated analytically or numerically by the so-called *dQdT technique*, which also can determine the limits of the applicability of the resistor-network model to the convection problem [23]. The extended Newton formulation and the *dQdT technique* were applied with a success to a wide variety of problems: natural [24,25] and forced convection [26,27], laminar [24,26] and turbulent flows [25,28], developed [26, 29] and hydrodynamically developing flows, constant- and variable-property flows [22]. This technique can be used for the improvement of accuracy of lumped models and calculation of more accurate convection coefficients (including heat transfer coefficient) for a wide range of DSF configurations, while still keeping the computational requirements for the simulation at a much lower level than for fully explicit models.

Zonal models are more advanced representations than lumped parameter models and other types of simplified models. They offer an intermediate approach with half-way accuracy and computational cost between CFD and control-volume models. Zonal models divide the DSF system into coarse cells (larger than cells in CFD models), where conservation laws are formulated for each cell, without momentum equations [19]. Yet, these models rely on a series of assumptions (e.g. constant temperature within the zone, require semi-analytical formulations based on the knowledge of the flow physics) which need to be considered when assessing the relevance of the predictions.

Computational fluid dynamics modelling divides a DSF system into a number of cells, where for each cell at least three conservation principles (mass, momentum and energy) must be satisfied [30].

Partial differential equations representing these conservation principles (Navier-Stokes equations) can be numerically represented and solved by using finite difference or finite volume method. The second method is the most common method for discretization, except very few researches such as Han's [31]. A certain number of researchers developed their own CFD code or software for thermal and air flow analysis of DSF [32,33], but most researchers in their studies use commercial or open-source CFD software packages such as OpenFOAM, Ansys FLUENT, Tas Engineering, COMSOL or Phoenics. In general terms, the numerical solution can be obtained using three CFD approaches: direct numerical simulation (DNS), large-eddy simulation (LES) and Reynolds-averaged Navier-Stokes (RANS) equations simulation with turbulence models [34].

While DNS has not been used for modelling flow inside the DSF cavity, LES [35,36] has been adopted by some researchers who obtained excellent fit with experimental data, but none of them included solar radiation models [37,38]. Numerical results provided excellent statistics about turbulence quantities, which has been used later as a validation tool by other models of lower accuracy.

The selection of a proper RANS turbulent model for the characteristic flow inside the cavity determines to the greatest extent the accuracy [39] of thermal and fluid dynamic simulation when this approach is chosen. Two-equation turbulent models are the most used category of models for building related researches, because they offer a good level of accuracy along with satisfactory computing time [39]. Among them renormalization group k-ε (RNG k-ε) is the most applied because it showed a very good performance in modelling naturally ventilated DSF [40]. In several studies, there was no need for the introduction of turbulence models, due to examination of laminar flow inside naturally ventilated cavities [41]. Besides turbulence models, other components in a CFD model that influence the level of confidence in the results and computation time are the pressure-velocity algorithm, the type of computational grid, the uncertainty in boundary conditions, and the radiation model.

The level of confidence in numerical simulations and in CFD models can be determined through an experimental validation procedure, but only a small number of CFD studies have validated both thermal and airflow (velocity) field, while most studies rely purely on the simulation or have validated only thermal part of the model.

The main strength of CFD analysis is its ability to accurately simulate velocity, temperature and pressure field from which detailed information about thermal and energy performance of DSF can be extracted, though this comes at the cost of high computational time and resources needed. CFD analysis is usually employed for the process of optimization or resolving design issues: finding optimal cavity depth, materialization of DSF elements, selection of shading system, glazing type,

airflow path and examination of flow around venetian blinds. Furthermore, CFD can assess specific parameters such as convective heat transfer coefficient between the DSF surfaces and ventilated cavity. The results from CFD simulations can be used for developing simple correlations for parameters that describe thermal and energy performance of DSF (e.g. correlation between Nusselt and Reynolds/Rayleigh number) [42–44].

2.4.2. Experimental analysis

The first experiments that can be linked to phenomena occurring in DSF systems were carried out in the middle of the XX century and were intended for a better understanding of buoyancy induced flow between vertical opaque parallel plates [45,46]. These experiments were performed in a laboratory where the temperature or heat flux of bordering surfaces was controlled, investigating the turbulent behavior of the flow and not the overall thermal and energy performance of the system. Because a large number of quantities were monitored with the high spatial and temporal resolution, the results from these studies were later used as validation tools for more recent CFD models of DSFs [37,42].
Experimental investigations can be divided into natural and controlled, depending on the possibility to control the surrounding environment. In natural experiments, the (full-scale) model of the DSF is exposed to a real outdoor (and indoor) transient environment, while in controlled experiments the outdoor conditions are replicated, where in the most cases only the thermal environment is controlled. Quite a few experiments were performed in both thermally and radiative controlled environments [16,43,47] and, to our best knowledge, no experiment was ever performed at controlled wind conditions. Usually, in these types of experiments, parametric analyses are done in steady state conditions and by deliberate variation of parameters such as physical properties of DSF (cavity depth or venetian blind angle) or boundary conditions (incident solar radiation or outdoor temperature).
The thermal environment in a DSF is usually monitored by measuring surface temperatures of glazing and shading devices, the temperature of the air in cavity, as well as the temperature of all the other surfaces and volumes that are part or have an influence on boundary conditions. The air cavity measurements require the greatest attention when it comes to the complexity of the measuring system due to non-isotropic features of the flow and the air temperature in the cavity, where several vertical and horizontal temperature profiles need to be monitored. In general, temperature sensors need to be shielded against direct radiation and in some situations ventilated to avoid that the radiative heat absorbed by the shield affects the measurements [48]. These protection measures may reduce experimental error, but at the same time they may represent obstruction to the air flow in the cavity, and more in general a perturbation of the thermal field around the measurement point.

The fluid dynamics behavior can be monitored by three main classes of techniques: bulk airflow methods; direct velocimetry; and non- intrusive velocimetry.

Bulk airflow methods determine bulk airflow rate inside ventilated cavities by measuring either the pressure loss across the cavity or by tracer gas technique. In the pressure difference method, airflow rate is estimated based on the pressure difference between the surface pressure at the opening and referent pressure inside of DSF, or across the cavity, where incense sticks can be used to judge the airflow direction [49]. This method is not suited for naturally ventilated cavities because the driving forces of the flow are usually weak. Such a method, moreover, requires that the pressure loss across the opening is previously calibrated against another measurement method of the airflow rate, or that the coefficient of discharge for the opening is simulated/measured experimentally. In the other class of methods, a tracer gas (usually carbon dioxide, CO_2 or sulfur hexafluoride, SF6) is monitored inside the cavity, where constant injection method (CIM), decay method (DM) and constant concentration method (CCM) could be used for evaluation of bulk airflow. CIM is probably the most used method by researchers, but generally all tracer gas methods are challenging for airflow measurements in naturally ventilated DSFs, due to the assumption of good mixing inside the cavity. In naturally ventilated DSFs, it is hard to achieve this because the flow is driven by weak forces and it is highly fluctuating. Large measurement error is expected there, when a significant amount of tracer gas is dispersed, and this can happen due thermal and velocity heterogeneities in the gap, insufficient mixing and variability of outdoor conditions [50].

The amount of information and its complexity that it is delivered through direct velocimetry vary from the most basic one, where only one bidirectional anemometer can be used for evaluation of bulk airflow, to the most advanced such as the velocity profile method. The velocity profile method ensures the airflow rate estimation, but also gives an indication of velocity distribution inside the cavity. Anemometers should be placed along several heights in the cavity in order to provide both horizontal and vertical velocity profiles. The accuracy of measurement needs to reach a tradeoff with the desired amount of information, because anemometers also represent an obstacle to the flow and a large number of these sensors in the cavity may significantly alter the flow. However, these methods are suitable for long term measurements and can therefore be very useful when infield investigations are carried out.

Non-intrusive velocimetry technique employs optical/acoustic methods for particle tracking upon which asses velocities, such as laser Doppler (LDV), particle image (PIV) or ultrasound velocimetry (USV) [51]. The first method allows the velocity to be measured only at one point, does not disrupt the flow and requires one initial fast calibration before measurement. Poor signal to noise ratio and consequent large measurement error that can be caused by attenuation and reflection of the signal

inside the cavity [52], together with the need for a relatively complex instrumentation that is hard to use outside a laboratory, limit the application of this technique. The PIV method obtains instantaneous velocity fields by recording images of particles at successive times though the "trace" left by the fine particle used as a marker when illuminated by a monochromatic light. This method allows one to analyze the flow in the plane, and recent attempts are trying to expand this technique to 3D measurements. One of the main advantages of this technique is that it can measure a wide range of velocities, while costs and complexity of the experimental set-up is the main drawback. Different parameters affect the accuracy and reliability of this method, such as the characteristics of the particles (larger particles affect the flow, while smaller scatter insufficient amount of light, so a compromise needs to be reached [53]), non-uniform dispersion near the inlet, sedimentation, and induration of seeding material on the blades and casing of the fan [54]. Ultrasound velocimetry is another non-intrusive technique that has been recently applied in HVAC system and it is based on the interaction of ultrasonic sound with moving fluid [51], and seems a promising possibility for long-term monitoring in DSFs too, though applications of this method for DSFs have not been reported in the literature.

The radiative environment, or at least the radiation linked to short- wave sources like the Sun, is usually replicated in laboratory studies through the use of a solar simulator, i.e. matrix of multiple lamps with spectral properties close to natural solar radiation. Solar simulators are placed close to DSF and emit continuous light [55]. The calibration and verification of the solar simulator are very important, because asymmetry in the irradiating surface may occur [56]. The measurement of the incoming and transmitted irradiance is mostly carried out with pyranometers [57], though other sensors based on other photoelectric phenomena are also used even if their accuracy is lower. Pyranometer placed in the interior space behind DSF system is used for the measurement of transmitted solar radiation and solar gains, as well as the calculation of efficiency parameters (e.g. the dynamic insulation efficiency) [58]. In the case of measurement points behind DSF or shading, data from pyranometers has to be adjusted to the view factors calculated for the complex geometry in the DSF [48]. The longwave radiation flux (far infrared) exchanged with surroundings surfaces can be assessed with pyrgeometers [59].

2.5. Constructional features and thermal and fluid dynamics behavior of double skin façade

2.5.1. Literature data on experimental and numerical (CFD) studies

The comprehensive review of the scientific literature of studies that investigated the impact of different constructional features on the DSF's performance is summarized in two tables which are reported in the Appendix for the sake of brevity of the manuscript. Table A.1 and Table A.2 are for experimental analysis and numerical (CFD) simulation, respectively.

We reviewed and organized nearly 70 studies in those tables according to the chronological order, we identified the main constructional feature(s) investigated and the type of ventilation mode (mechanical or natural ventilation) of the cavity, and we summarized for each study some important features. While for experimental studies we focused on the experimental instrumentation and the type of control over the boundary conditions (e.g. an experiment in fully controlled conditions or under uncontrolled conditions), for numerical studies, we also focused modelling setting such as simulation tool, dimensionality, discretization method, turbulence and radiation model, grid type, as well as the presence of a validation procedure. CFD models can be validated against results from own experiments or against open literature experimental databases or results, or finally as intersoftware comparison, i.e. against other more precise/detailed numerical models. In the analysis of the validation procedure, we differentiated how the fluid mechanics part of the model is validated. If it is validated against measured velocity at several positions and heights or with the PIV technique, then we defined it as a CFD model with detailed validation (fully validated). If it is validated against bulk airflow rate measurements by pressure difference, tracer gas or any other bulk airflow method, then we indicated it as partially validated (since the spatial structure of simulated flow is not verified).

The detailed analysis of the literature data led us to summarize the pieces of evidence and established knowledge on how different characteristics affect the performance of the DSF, which we summarized in the following two sections 4.2 and 4.3, for mechanically ventilated DSFs and naturally ventilated DSFs, respectively. For the sake of completeness, we need to mention that in the past two decades a wide variety of novel types of mechanically and naturally ventilated DSFs has been investigated. The list below is intented to be a non-exhaustive overview of a few of such investigations, together with the performance improvement that the new solutions are targeting.

- DSF with solar chimney [49] (enhancement of natural convection),
- opaque DSFs [60],
- DSF containing PV elements: DSF with PV modules encapsulated in glazing (semi-transparent PV elements) [31,61], DSF with integrated PV blinds (PVB-DSF) [62] PV vent window with PV

module installed on a louver that covers opening [63] (generation of electric power and reduction of transmitted solar radiation for DSF with semi-transparent PV elements),

- DSF with incorporated PCM materials: DSF with integrated PCM shading [64,65], ventilated windows with the PCM solar air heat exchanger [56], PCM layers in combination with PV integrated in DSFs [66,67] (absorption of excessive heat and reduction of the temperature in a cavity),
- a pipe-embedded double-skin façade (PDSF) with water as heat absorber [64] (absorption of excessive heat and reduction of the temperature in a cavity),
- Slim-Type Double Skin Window System [68] (easy to operate and reduction of SHGC in comparison to non-ventilated DSF and typical windows),
- triple glazed exhaust-air window (TGEW) [69] (removes excessive heat from the cavity)
- double-skin green façade (DSGF) [70] (reduction of the air cavity and surface glazing temperature),
- conditioned Trombe wall with installed venetian blinds [71] (enhancement of natural convection and reduction of the air cavity temperature).
- smart double skin facades that integrate Tungsten (W) doped Vanadium dioxide (VO_2) and a high absorbing aluminum nitride (AlN) coating. (SDSF) [72,73] (active control of the green-house effect in the cavity with the amplification in the winter and dampening in the summer period)

However, even if all or some of these developments might be interesting, and might add a large range of additional constructional features, we decided to keep the main focus of this analysis on conventional DSFs, as these systems still represent the largest type of DSF that are investigated and used.

2.5.2. Mechanically ventilated DSFs

In this paper, we classify under the category “mechanically ventilated DSF” all those configurations where the airflow is driven by one or more powered fans which transform the rotational kinetic energy of the blades into the translational kinetic energy of the flow. DSFs where the flow interacts (but is not induced) by the other powered elements such as operable vents, dampers, or louvers, and which are usually adopted to a module or control the airflow, are not considered as mechanically ventilated DSFs. Mechanically driven flow can significantly enhance some of the phenomena that affect the thermal behavior of such facades compared to a naturally driven flow, as well as lower the net heat transfer in comparison to conventional façade systems during the entire year, but especially in winter [74].

Geometric features

Dimension of the DSF cavity – Among all geometric properties of DSF, the influence of aspect ratio/cavity depth on fluid flow and heat transfer inside the cavity is the most investigated one. In the natural experiment where mechanically ventilated DSF with outdoor air curtain circulation was tested at high-noon summer conditions, it was concluded that mixed convection induced both by solar radiation and fan is strongly influenced by the aspect ratios (ratio between depth and height of cavity, D/H) [75]. Additionally, decreased aspect ratio leads to higher solar heat gains [68], both due to increased air temperature in the cavity and amplified multiple reflections.

Airflow path – We can distinguish five possible airflow paths in DSF: supply air (outdoor-indoor), exhaust air (indoor-outdoor), static air buffer (closed configuration), external air curtain (outdoor-outdoor) and indoor air curtain (indoor-indoor) airflow path [21]. For the indoor air curtain ventilation strategy, a further increase of the heat gain into a room can occur from the exhaust duct [76]. In the typical winter week and with the air supply ventilation strategy, preheating of delivered air can be significant during sunny days (15–25 ˚C) due to heat loss recovery and solar heat absorption. During periods without solar radiation temperature increase of supplied air is moderate (10 ˚C) [59]. Such air mass could be used for heating purposes in winter, thus leading to a reduction of the energy use for space heating or ventilation air heating [77].

Openings geometry - The size and shape of the inlet and outlet significantly affect the energy consumption of the fan. For example, when air circulates in outdoor air curtain mode, flow rises along with glazing opposite to the inlet, while lower velocities occur near the outer glazing. If the sharp edges and turns are present, a portion of the low- velocity zone near the inlet can be transformed into a recirculation zone, creating a pressure drop. Therefore, sharp edges should be avoided because they create a large pressure drop and behave like an obstacle to the airflow [38]. Attention should be paid to the inlet's width because it directly affects the average velocity within the channel [53], making it higher for narrower cavities. That is a consequence of the principle of mass conservation, based on which extracted airflow from the cavity does not change considerably either with dimensions of the air inlet or with the shading system's position.

Shading type and position – The heat transfer by radiation is dominant over convection and conduction for most environmental conditions and DSF configurations. It is found that the transmitted solar and exchanged long-wave radiation prevails over convective heat flux [58] and therefore the most important structural parameter in controlling thermal and fluid mechanics part of the double skin façade is, when installed in the cavity, the shading system. There are various types of shading systems installed in the DSF cavity, where the most common are vertical louvre, venetian

and roller blinds. The velocity fields are highly complicated [64] with an integrated shading system in the cavity, with sometimes accentuated three-dimensional patterns that cannot always be ignored by the assumption of two-dimensional flow [54]. However, due to the higher surface roughness and frictional drag, the velocity field is more complicated in cavities with installed louvre and venetian blinds than in roller (screen) blinds.

Most studies on mechanically ventilated DSF analyzed the influence of venetian blinds on thermal performance, while other types of shading systems are less explored. Venetian blinds allow a greater flexibility in the management of the cavity thermal gain, as a different, dynamic surface can be exposed to the solar radiation, hence it is a more interesting solution when it comes to modulate the thermophysical and fluid mechanical behavior of the system.
The shading position has a large influence on air velocity distribution in the cavity. In the case where both the channels created by shading have different widths, velocity will naturally be higher in narrower channels, unless very different glazing types are used on the indoor and outdoor skin. When the shading is closer to outer glazing, the solar heat gains will be lower, while for the opposite situation, the temperature of the inner glass surface will be highest, which is preferable when the outdoor temperature is significantly lower than indoor [78].

Slat angle – Different properties of the shading system such as thermal and optical properties, position, as well as slat angle influence the thermal behavior of DSF. However, if it is a shading system with built-in slats, the most significant parameter in the control of the heat transfer is slat angle. For example, when a DSF system is exposed to solar radiation, the slat surfaces have usually higher temperatures than glazing and the air inside the cavity. These temperatures and temperatures of other structural elements of DSF can be primarily controlled through the slat angle and secondarily through the airflow rate [79]. The tilt angle of slat influences to the largest extent radiative heat transfer, which is a very important fact during the high-irradiation periods [78].

For a typical summer situation, when the slat and the incidence angle of solar rays are lower than 60° and 45°, respectively, transmitted solar flux is higher than exchanged long-wave radiation. The dynamic insulation efficiency, which is a measure to quantify the ability of a DSF to reduce the thermal fluxes entering an indoor environment, is independent of the ventilation strategy when the slat angle is higher than 75° [58]. The average velocity of the air in the middle of the channels created by venetian blinds increases as slats are getting closed, and in the case of fully closed slats (0°), the outdoor air channel and slats itself will have higher temperatures than if it is opened (90°) [53].

Materials properties

Glazing properties – Regardless of DSF type, solar heat gain into a building can be reduced almost by the order of the magnitude by the appropriate combination of optical properties of the inner and outer glazing [77]. For unshaded mechanically ventilated DSF, solar heat gain in a typical summer day can be reduced to double if the internal glazing is replaced with low-e glass and up to 40% if the transmissivity of outer glazing is reduced by 55% [80]. Other dedicated analyses investigating combinations of different spectrally selected glazing solutions have not been found in the current literature.

Therefore, in warm climates, it is not recommended to have a low aspect ratio (<0.1). Firstly, due to the merging of thermal boundary layers in a long channel and increased air temperature and secondly, due to decreased optical losses and increased multiple reflections in the thin cavity. On the contrary, this may be the preferred configuration for cold climates since higher solar heat gains and air temperature in the cavity are desired.

Radiative surface properties of shading system – The heat transfer by radiation is the main driver of the thermal performance of DSF, and therefore the radiative properties of the shading system play an important role. However, only in the last few years several numerical studies have specifically investigated this aspect. Increased emissivity of the front surface of venetian blinds reduces transmitted heat flux into the interior environment [58], while the thermal performance of DSF can be further enhanced, considering the cavity as a device to capture solar energy, when the absorptivity of the back surface of venetian blinds is increased, which reduces double reflection towards indoor [12].

Thermal properties of the shading system – High thermal capacity materials incorporated in the shading devices, such as PCM materials or water [56,64,81,82], can play an important role in controlling heat processes in DSF. However, the application of this technology has been limited only to naturally ventilated DSF. It would be interesting to see how mechanical flow can promote the release of the stored heat during night-time when external conditions do not favor (low wind speeds) [65]. What is the coupled effect of PCM and mechanical flow on the thermal performance of DSF in ventilation modes other than outdoor air curtain?

Airflow rate

In summer, a solar energy absorbed by DSF elements can be reduced efficiently by mechanical ventilation. In particular, SHGC can be reduced by one-third along with the temperature of outer glazing and installed PV panels with the right combination of the forced airflow velocity and cavity

depth (e.g. 5 m/s and 200 mm [61]). However, one has to be careful, because the potential prevention of overheating can be overshadowed by operational costs [12]. Increasing the airflow rate, clearly, does not influence the transmitted solar radiation, but it reduces long-wave radiation exchange and increases dynamic insulation efficiency [58,83]. However, even the very high airflow rates may not be sufficient to reduce the overheating of the façade during the very warm weather in typical south-European climates. The only way to avoid this is to carefully plan the shading device, the glass type, and to adapt the airflow path [83]. From the point of the heat transfer, a key role is played by the fluid-dynamic characteristics of the flow, i.e. whether it is fully developed or is it still in the thermal and hydrodynamic developing phase. In a study where mechanically ventilated DSF with outdoor air curtain circulation was tested in a climate simulator without artificial sun [43], the flow was undeveloped in both senses for all environmental conditions (air temperature near inlet varied between 3 ˚C and 7 ˚C) and airflow rates (low, medium and high). Hence, heat transfer coefficients were found to be relatively higher, than it would be the case if the flow was developed. In typical summer conditions, circulatory motion with upward directed flow close to internal glazing and downward directed flow close to the opposite side has been observed [75], especially when the outer skin has low or little thermal resistance. These patterns create additional pressure drops and consequently increase the operational costs of DSF [80]. Therefore, in order to efficiently control the thermal performance of DSF, fan capacity needs to be designed based on pressure drops created by different structural elements of DSF [43].

2.5.3. Naturally ventilated DSFs

Because of the intricate nature of the flow and uncertain predictability of thermal, optical, and fluid mechanical behavior of naturally ventilated DSF, this type of DSF has been more studied than mechanically ventilated. However, some general conclusions can be drawn about performance, flow characteristics, and driving forces behind flow in naturally ventilated DSF. This type of DSF is a less recommendable choice for warm climates characterized by high irradiation levels, because structural elements of DSF can become hot (up to 70 ˚C) which can lead to overheating [84] and damage of delicate components like shading motors [85], while naturally induced airflow may be too modest to be used to remove the (solar) heat collected by the structures of the DSF. Therefore, the strengthening of naturally induced convective flow and heat transfer is desirable in periods with a high outdoor temperature and irradiation, with high Rayleigh number of the flow that ranges from 10^3 to 10^5 [31]. In several studies on the buoyancy-induced flow between two vertical parallel plates [6,41,86,87], circulation (bidirectional) flow with upward acceleration near the heated side has been observed along with downward deacceleration near the opposite side. This pattern is followed by the existence

of a vortex in the central portion of the cavity. The most intensive fluctuations of velocity and temperature correspond to this cavity region, producing lower wall temperatures in this area [37, 88]. For a similar configuration where the central part of one plate is heated with constant heat flow, a recirculation zone appears at the outlet near the colder surface with the property that its size increases with Rayleigh number [41]. More unsteady vortices in the corners of the channel have been observed, too [32]. If the channel is non-uniformly heated from both sides [38], two plumes driven by buoyancy appears. This is opposite to the case where the channel is heated from one side only and where only one plume appear. It can be concluded that a channel heated non-uniformly from both sides generates a larger mass flow rate and more vigorous mixing than in a channel heated from only one side.

A common assumption in naturally ventilated DSF is that flow inside the cavity is buoyancy-driven [89]. However, several recent studies show that wind dominates as the driver of the mass flow rate [33,90]. Through CFD investigations [91] it has been shown that free-stream wind can be amplified to 1.8 times in the corridors of story-high DSFs, which makes this system especially convenient for wind energy harvesting by incorporating wind turbines in corridors. Both the buoyancy and wind as driving forces are investigated in the validated CFD research [90], where DSF with outdoor air curtain ventilation mode is subjected to four typical conditions. The complicated and nearly isothermal flow pattern with several recirculation zones characterizes the situation where the wind (regardless of wind pressure orientation) is more dominant than buoyancy. On the contrary, when buoyancy is dominant over the wind, circulation is weak with a temperature gradient that can be amplified if the wind pressure is opposed to buoyancy.

However, in addition to the general characteristics that are recognizable, there are many more unknowns, which led us to appropriately design the ventilation strategies, geometrical configurations, materials, and layers in order to provide the best condition to remove excessive heat from the cavity when desired [68].

Geometrical features

Dimensions of the DSF cavity – The height of the DSF is a very important factor as it enhances the stack effect and accelerates airflow inside the cavity [92]. For that reason, multi-story and shaft-box facades are more suitable for natural ventilation and preferred over the box window and corridor type facades [2]. During the cold season for supply ventilation mode, air velocity in the cavity is approximately proportional to the height of the DSF and roughly inversely proportional to the depth of the cavity. The temperature of the supply air, i.e. the air that leaves the DSF's cavity, is inversely proportional to cavity depth as well [93]. Some studies support the claim that a narrower cavity accentuates the natural flow inside the cavity. Others [94] emphasize that cross-sections of DSF

should not be too shallow due to heat diffusion from hot surfaces and the consequent possibility of overheating. If DSF needs to deliver cold air, the channel width should not be larger than 0.6 m, while if it needs to provide warm air, then the width needs to be lower than 0.2 m [92]. With a reduction of aspect ratio, the transition from laminar to turbulent flow shifts higher and flow has a shorter entrance path. For turbulent flow, convective Nusselt number and local heat transfer coefficient increases when the aspect ratio increases, while for laminar flow, the opposite behavior is observed [86,87]. The length of the single recirculation zone that occurs at the outlet decreases with increasing aspect ratio [41].

Considering tilted (i.e. not perfectly vertical) DSFs, it can be said that the maximum heat and airflow rate occurs for the perfectly vertical channel. Tilting one side of the channel leads to a reduction of the Nusselt number and of the airflow rate [95]. In the same study, a recirculation zone near the outlet is observed, which increases in size with increasing positive tilt angle. Unconventional geometric configuration of DSF like this can reduce solar heat gains by self-shading and reduction of incoming solar radiation. However, according some researchers [94], if the adequate distribution of outlets is not provided, this configuration can lead to trapping of hot air in certain regions of the DSF.

Airflow path – Different airflow paths significantly influence the solar heat gain coefficient when the shading is not lowered [68]. In summer conditions, and with the absence of solar radiation, the closed configuration of the cavity is preferred because of low average temperature. In the presence of solar radiation in summer, outdoor air curtain ventilation type is a more efficient due to enhancement of stack effect and consequent lower transmitted heat gains and cooling load [96]. More advanced concepts have been proposed where a triple glazing divides the cavity in two separate elements. The shading device is placed in the outer zone through which air circulates in exhaust mode, while inner zone is closed. This configuration can effectively trap and remove the heat accumulated in the cavity during cooling periods with high outdoor temperature and irradiation and according experimental campaign it increases the temperature of the exhaust airflow [69]. A similar concept that uses inner closed zone and outer zone in the outdoor air curtain ventilation mode without installed shading device is proposed by Koo [97]. Experiments showed that natural ventilating of outer zone reduces SHGC and temperature of the cavity; however, at a significantly lower level than in the case of the previous configuration. In winter conditions, both with solar radiation and without, closed vents are recommended due to the higher average temperature of the cavity. Ventilation is not recommended as it lowers the air cavity temperature [84]. Otherwise, if it is necessary to provide fresh air during cloudy and cold weather, passive preheating of air in supply ventilation mode may not be enough [93].

Openings geometry - The size and arrangement of the openings and the cavity width significantly impact the overall performance of the DSF [98]. For typical summer conditions in very hot climates [99], the opening size has a more significant impact on the cavity's air temperature than cavity depth when the DSF is operated as an outdoor air curtain. An increase in the cavity depth leads to a rise in the cavity's temperature, while a larger opening size leads to the opposite situation. These two factors influence less the air velocity. For DSF consisting of both venetian blinds and high thermal-mass elements, larger openings area leads to stronger buoyancy flows [71]. The joint influence of cavity depth and opening size is very complicated and non-optimal dimensions can reduce to a great extent the naturally induced airflow in air supply ventilation mode in typical summer conditions [100]. Automatically controlled or manually controlled dampers and vents on the openings have been commonly used in naturally-ventilated DSFs to regulate and control the airflow to enhance the performance of the DSFs – i.e. reducing or suppressing the airflow when unwanted, while enabling it when required by the planned operational mode A comprehensive review on how dampers, vents, louvres, and any other controllable device impact on the airflow in terms of pressure drops for the naturally-induced flow would probably require a long list of individual cases, which is outside the scope of this paper. However, it is herewith important to point out that the use of such devices has been a practice in DSF design with several real-word implementations [101].

Velocities near openings are greatest because air is forced through the smaller area [44], and heat transfer to the inner side of DSF near the inlet is enhanced due to this amplified inflow of buoyant jet [102]. High intake speeds up to 1.6 m/s are possible on a typical summer day without wind [85], causing noise and the suction of dust. Through experimental analysis [86], the effect of entrance bell-mouth shape on buoyancy induced-flow is investigated for the case of vertical parallel plates set in outdoor air curtain ventilation mode. This type of inlet has found its application in practice due to round ends that can control the inlet disturbances more easily. Experiments showed that entrance bell-mouth shape leads to a delayed start and the end of the transition to turbulence and weaker disturbances, heat transfer, and velocity intensities, in the laminar and transition region. In a similar fashion, recessed regions at inlet and outlet along with rounded corners at walls increase mean velocity by one quarter at the middle of the passage of a corridor type DSF [103,104].

For naturally ventilated DSF, the position of the openings plays important role in the control of the heat transfer. Due to natural tendency of buoyant air to move vertically upwards, it is highly preferred to have openings located at the top and bottom of DSF, unlike for example lateral openings. If the wind is considered as a driving mechanism, central-placed (front) opening is preferred beside lateral openings, because this arrangement is less dependent on the wind direction. For normal winds, this configuration amplifies the airflow and makes a more uniform rate in the cavity, making that position

especially effective for enabling natural circulation [105,106]. DSF naturally ventilated reduces overheating and amplifies airflow rate when approaching wind direction is normal to the surface of the DSF [2]. Placing louvers on the openings can significantly assist naturally driven flow, where a small change in the shape, position and inclination of louvers can enhance natural ventilation considerably [107]. If the air velocity is not strong enough to reach deeper in the cavity, louvers should be placed at the top of inlets so that they can direct air movement [94]. Open horizontal and vertical joints in ventilated facades can be used as well to induce more effective airflow, reducing heat transfer in this way [108].

Shading type and position – In naturally ventilated DSF heat transfer by radiation is even more dominant over convective and conductive compared to mechanically ventilated DSF, and therefore the most important structural element in controlling heat transfer is the shading device, just like in the mechanically ventilated DSF. The shading device reduces solar radiation and heat gains in the interior by absorbing heat and increasing the air temperature and the stack effect inside the cavity [2,109]. It separates the cavity into two vertical channels, where the type of blinds has a major impact on temperature and velocity distribution in the cavity [110].

Roller blinds can be assumed airtight, so there is no exchange of mass between two cavities. Airflow is less effective in extracting heat from roller blinds than from louvered blinds due to higher roughness and more contact of the latter type of shading device. Louvered blinds reduce the airflow rate compared to a roller blinds, but the overall velocity profile stays the same [44]. Additionally, horizontal louvers enhance stronger buoyancy and higher airflow compared to vertical louvers [109]. The presence of venetian blinds has little effect on the convective heat transfer coefficient at glazing surfaces [111].

The shading position (distance from the inner or the outer glazing) leading to optimal energy behaviour can only be found considering the different external conditions and specific performance goals. In general it is possible to see that the best position is similar in both naturally and mechanically ventilated DSF, with a preference of placing the shading closer to outer glazing when the outdoor temperature is significantly lower than the indoor temperature, and next to inner glazing in the other case [2,98].

Slat angle – Natural convection is complex and sensitive to an incident angle of direct solar radiation on slat [33] and generally is enhanced by the increment of slat angles [71,112]. Slats placed in open positions (0°~30°) cause obstruction to the airflow in the cavity, while in a vertical position, drag in flow is reduced [2]. If slats are opened (0°), the two channels' temperatures approach each other, indicating higher interaction between them. For almost fully opened slats (15°), the temperature of

the inner channel will be higher. The opposite situation happens when slats are nearly or fully closed (60°~90°). In addition to this, heat fluxes to indoor can be reduced to 85% of incoming energy, and the blinds' temperature becomes higher [113]. The slat angle mainly influences the inner glass's surface temperature due to multiple reflections and absorption processes. However, this influence is additionally dependent on the shading position and aspect ratio of the cavity, as closing the blinds enhances heat transfer and absorption and reflection of sunlight [98].

Materials properties

Glazing properties – The effect of glazing radiation properties on thermal performance and fluid flow inside the cavity is even more accentuated for naturally than for mechanically ventilated DSF because these properties mainly determine glazing temperature, which represents a main driver of naturally induced fluid flow. For enhancement of the buoyancy induced flow, external glazing should be highly transparent, allowing high heat gain into the cavity [2]. However, suppose intensive heat transfer by radiation within the cavity is not preferred, like in hot summer conditions. In that case, it can be reduced by installing a low-emissivity glass [40] or other solutions with lower solar transmittance (e.g., PV glazing with low e-coating [31]), including smart, dynamic layers [73], where transmissivity of glazing decreases with increasing the ambient temperature [72]. PCM materials (mainly paraffin) can be applied on the inner façade to extend the ventilation period for several hours after sunset, making them potentially usable the DSF as a supply for fresh air not only in diurnal but in a nocturnal period as well [114]. For warm and dry subtropical climates, the two skins' thermal resistance is not crucial, and single-pane clear glass with a thickness of 6 mm is recommended for both sides with an optimum transmissivity of glass should lie between 0.7 and 0.9 [98].

Radiative surface properties of shading system – The size and the emissivity of the slats influence the naturally induced flow inside the cavity [98]. If the emissivity of the shading system (front surface) increases, the globally absorbed solar heat flux is reduced, and buoyant flow is enhanced inside the cavity. Consequently, the surplus heat is removed by the flow, and the cooling load is reduced [115]. However, the shading system's radiative properties do not influence only the thermal behavior of DSF; daylighting performance is highly determined by it as well, when the optical properties are analyzed in the visible spectrum. Therefore, one should be very careful in choosing the shading system's radiative properties, as improving thermal performance can lead to deterioration of daylighting performance and vice versa [98].

Thermal properties of the shading system – Adding heat capacity to the shading device (e.g. PCM integrated in blinds [64]) may reduce the outlet and air cavity temperature in summer conditions compared to conventional aluminum venetian blinds with no significant difference in comparison

with ambient temperature [65,116]. Under this case, excess heat in the cavity is absorbed by the PCM layer, making the convective heat transfer in the cavity reduced, the airflow more stable and the exchange of long-wave radiation from high-temperature surfaces lower. It was also shown that the air temperature in the cavity is highest when the blinds with PCM are close to the external glazing, while it is opposite when it is placed closed to the internal glazing [117]. DSF with venetian blinds that use water as a cooling medium in embedded pipes is able to significantly reduce the temperature in the cavity (around 29 °C) [118], accumulated heat and peak heat transfer during summer days with high radiation compared to the traditional ones. However, they are not effective when the DSF is exposed to low irradiation levels (e.g. toward the north on the northern hemisphere or at night [119]).

2.6 Conclusive remarks: current knowledge, knowledge gaps and possibilities for further research

The analyzed experimental and numerical studies provided a heterogeneous range of information and current knowledge on how the features of a DSF lead to different thermal and fluid mechanics behaviors. We tried to organize such current know-how to explicit the link between material properties and geometrical properties and DSF's performance.

The shading system represents the most influential structural element in controlling the thermal behavior of both naturally and mechanically ventilated DSF. Venetian blinds represent the most applied and investigated type of shading system, due to theirs flexibility in managing solar heat gains by changing several of its characteristics. Among the different properties of venetian blinds, the slat angle for both types of DSF plays a crucial role because it efficiently controls transmitted solar radiation. Glazing represents the second most influential structural element. However, this element's contribution is not in the same order of magnitude as the slat angle. In naturally ventilated DSFs, the influence of the glazing properties is generally more significant than in mechanically ventilated because glazing temperature drives buoyancy in the cavity.

For the same reason, the shading system's radiative surface properties may be significant in naturally ventilated DSF, though not with the same order of magnitude as the glazing optical (and to a lower extent, thermal) properties. In mechanically ventilated DSFs, the airflow rate is a parameter in the same range of relevance as the glazing properties. In the conventional shading system such as aluminum venetian blinds or roller blinds, the thermal properties are rather insignificant, but if more complex shading devices are installed (e.g. shading with phase change materials or high-capacity materials, or combined with systems that provides a heat sink effect in the shading device, the effect

of the thermal properties of the blinds in some situations can be in the same order of magnitude as the slat angle.

The airflow path, the dimensions of the cavity, and openings geometry represent factors closely related, and they need to be carefully coordinated to optimize the thermal performance of DSF. However, individual adjusting of these factors may not lead to significant performance improvements, though they can lead to severe performance deterioration if they are not adequately designed. Both wind (when present) and buoyancy play an important role in driving airflow inside the DSF cavity, yet the wind makes the flow pattern more complex. What drives the flow to a greater extent depends on climatic conditions (ambient temperatures, dominant wind intensity, and orientation) and the DSF configuration (opening size and position, cavity depth, glazing, and shading properties). However, if the conditions are so that both factors are present (e.g. for an outdoor air curtain façade), the wind will likely be a more dominant mechanism.

There are relevant unexplored or underexplored links regarding how different arrangements of structural parameters in conjunction with boundary conditions influence the thermophysical and fluid mechanics processes in DSF. These unknowns are accompanied by uncertainties and limitations regarding methods and techniques used for the investigation of these phenomena.

We can see that wind-induced flow is usually dominating over buoyancy-driven flows, however the exact balance of these two mechanisms, or the coexistence of buoyancy-driven flows and artificially (though fans) induced flows is mostly unexplored. There is a noticeable lack of numerical and experimental studies where the simulated flow is driven simultaneously by more than one mechanism. When it comes to wind-driven flows, the outside environment is usually not directly modeled, and therefore it is impossible to examine how different wind intensities and directions will influence the flow in conjunction with buoyancy.

We could summarize general cause-effect links between property families, property subcategories, and thermophysical and fluid mechanic behavior (Fig. 4). Usually, the influence of a single parameter at a time can be quite often explained and, to some extent, quantified, even if with different degrees of understanding. However, the combined and complex effects of more parameters together are almost never analyzed. For example, it is difficult to understand what is the effect resulting from two features that affect in an opposite way a certain performance, whether one or the other is dominant, and to what extent. Dedicated analyses investing the balance of effects between different driving forces and different constructional features would therefore give a more grounded understanding of these systems and thus support their optimization.

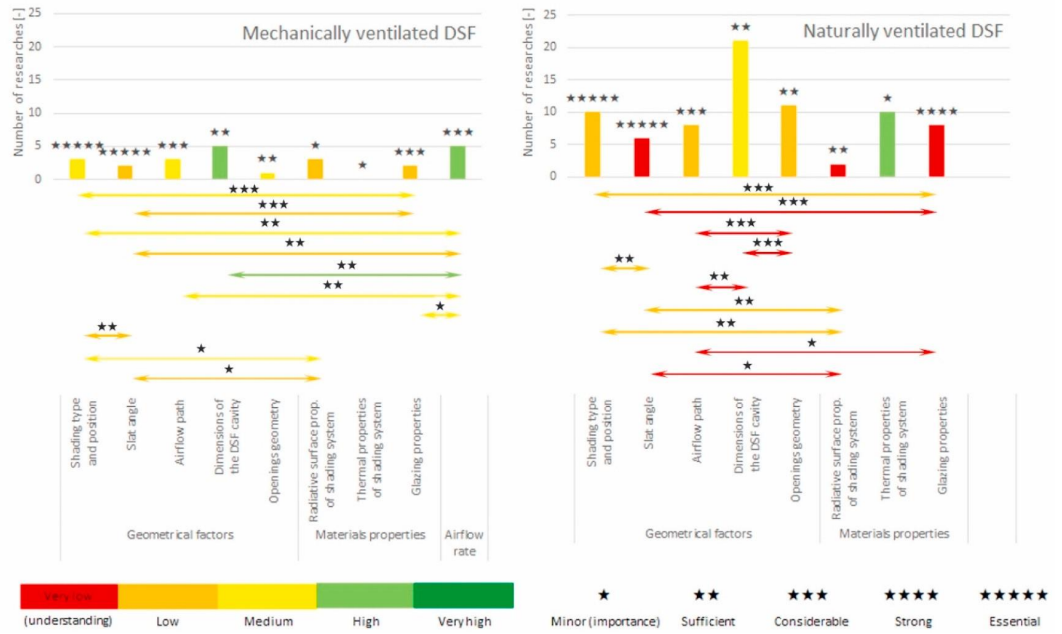

Fig. 4. A summary of the current understanding of the impact of structural elements and their interactions on the thermal and fluid dynamics behavior of DSFs

Studying experimentally the variation of two or more parameters at the same time require high control of the boundary conditions. Experiments with fully controlled thermal and radiative environments are however very rare as they require suitable indoor facilities. These analyses should be highly prioritized, and dedicated experimental methods developed, to provide evidence and quantifications of the effects of multiple features on the thermophysical and fluid mechanical behavior of DSFs. Experiments in controlled environments can also provide invaluable data for numerical models' validation, thus contributing to the possibility to study more comprehensively the complex interactions among different constructional features in a numerical way.

Best practices and recommendations for CFD models targeting typical situations and configurations of DSF are currently missing, and a comprehensive, systematic review of CFD modeling that gives recommended strategies (in terms of suggested turbulence and radiation model, solution algorithm, grid type, dimensionality, etc.) would be definitely beneficial to enhance the robustness of advanced numerical studies of DSF systems.

2.7. Appendix A

Table A.1. Experimental studies on thermal and fluid dynamics behavior of DSF

Appendix

Table A.1
Experimental studies on thermal and fluid dynamics behavior of DSF

Place	Year	Examined configuration	Examined constructional features/ quantities	The description	Type of experiment	Controlled environment	Thermal field	Velocity field	Other important variables
Queens Mary College, University of London, England and L'Ecole Nationale Superieure de Mecanique et d'Aerotechnique, Poitiers, France [52]; [42]	1989	Vertical parallel plates channel naturally ventilated (buoyancy only)	Two heights: 2.0 m and 2.5 m, Two widths: 0.5 m and 0.2 m, Three temperature differences: 32K, 46 K and 61 K.	The doctoral dissertation that investigates turbulent natural convection in rectangular air-cavities which can be suitable for DSF under certain conditions. Valuable information on correct experimental set-up and common issues. Final results from the study served as a validation tool for more recent CFD models.	Controlled	Radiative: no Thermal: yes Wind: no	Thermocouple (25 μm chromel-alumel) for measuring surface and air cavity temperatures	Laser Doppler anemometer	–
Yamaguchi University, Ube, Japan [86]; [37]	1991	Vertical parallel plates channel naturally ventilated (buoyancy only)	Three different channel spacing (500, 100 and 200 mm), with and without bell-mounted inlet and three different heat fluxes on the heated wall (50, 100 and 200 Wm^{-2}).	Experimentally study of a flow between vertical parallel plates with valuable information on various turbulent quantities. Used as validation source for later studies on similar topics. Results from research applicable to DSF under certain conditions.	Controlled	Radiative: no Thermal: yes Wind: no	Thermocouples for measuring surface (100 μm chromel-alumel) and air temperature in the channel (25 μm chromel-alumel).	Laser Doppler anemometer	–
Imperial College, London, England [88]	1996	Vertical parallel plates channel naturally ventilated (buoyancy only)	Fluid dynamics and thermal behavior of air cavity with an aspect ratio of 28.6 and with a Rayleigh number of 0.83×10^6.	Experimentally study of a flow between vertical parallel plates with valuable information on various turbulent quantities. Used as validation source for later studies on similar topics. Results from research applicable to DSF under certain conditions.	Controlled	Radiative: no Thermal: yes Wind: no	Thermocouples (75 μm chromel-alumel) for surface and air temperature in the channel.	Laser Doppler anemometer.	–
Technical university of München, Germany [75]; [110]	2002	Hybrid (buoyancy only)and mechanically ventilated DSF.	Three cavity depths: 0.3, 0.6 and 0.9 m. Different airflow rates: 0.06–0.6 kg/s. All experiments were performed at high noon for conditions with mixed convection.The height of the air inlet can be changed.	This experimental study provides the time and locally averaged heat transfer coefficients for mixed convection in DSF facades. Furthermore, it describes general features of the flow and its dependence on gap width and mechanical airflow rates.	Natural	–	Resistance thermometer for surface temperatures (PT100) and thermocouples (type K) for air cavity temperatures.	Impeller wheel (plate) thermal anemometers for measuring velocity of air in cavity.	Pressure difference method for measuring airflow rate. Venturi section for measuring airflow rate in ventilation duct. Pyranometer for measuring incident and transmitted solar radiation.
Catholic University of Leuven, Belgium [84]; [44]; [89]	2002	Mechanically and naturally ventilated DSF (both, buoyancy and wind) with	One-year measurement, where roller blind is activated when solar radiation	The doctoral dissertation of Saelens provides valuable information on thermophysical	Natural	–	Thermocouples (T-type) for measuring surface, air cavity and openings temperatures.	Not measured	Pressure difference and tracer gas method for measuring airflow rate.

(continued on next page)

Table A.1 (*continued*)

Place	Year	Examined configuration	Examined constructional features/ quantities	The description	Type of experiment	Controlled environment	Thermal field	Velocity field	Other important variables
		integrated roller blind.	exceeds 150 W/ m^2.	behavior of DSF from both numerical and experimental work, where both natural and field experiments were performed. Useful information about the correct experimental set-up that will minimize installation errors is provided along with a list of advantages and limitations of different methods for evaluation of the airflow (pressure difference, tracer gas and velocity profile method). Thermal behavior of DSF is described for two types of DSF, naturally and mechanically ventilated, for summer and winter period along with assumptions whether wind or buoyancy dominate naturally induced flow.					
Swiss Federal Laboratories for Materials Testing and Research EMPA, Duebendorf, Switzerland [12]; [33]; [76]; [120]	2004	Mechanically ventilated DSF with integrated metalized shading screen.	Mechanical airflow rate of 60 m^3/h. Several days measurement.	Mechanically ventilated DSF with integrated metalized shading screen were subjected to outdoor conditions and all-day measurements. Valuable findings on how to decrease solar heat gains are given.	Natural	–	Thermocouples for measuring surface, air cavity and openings temperatures.	Not measured.	Differential pressure airflow meter for measuring airflow rate in the cavity.
Waseda University, Tokyo, Japan [49]	2005	Naturally ventilated DSF (buoyancy only) with solar chimney	Different sizes of openings on top of the solar chimney with a different temperature rise of blinds.	Experimental study on natural ventilation behavior of reduced scale model (1/25) of the south-oriented facade with double-skin and a thermal storage space (solar chimney) above the DSF. Panel heaters used to simulate the temperature rise of DSF and its absorption. Results from experiments have been used for validation of CFD models.	Controlled	Radiative: no Thermal: yes Wind: no	Thermocouples for surface, air cavity, solar chimney and occupant space.	Not measured	Pressure difference distribution is measured at points in solar chimney relative to interior space.
Centre de Thermique de Lyon CETHIL, INSA Lyon, France. [53]; [58]	2006	Mechanically ventilated DSF with integrated venetian blinds.	Slat angles: 0, 15, 30, 45 and 60°. The shading system position: 5, 15 and 25 cm from the inner glazing.	In the doctoral dissertation of Safer, experimentally and numerically mechanical DSF is tested with external air curtain ventilation mode	Natural/ Controlled	Radiative: no Thermal: yes/no Wind: no	Not measured	Particle Image Velocimetry (PIV) technique for measuring velocity of air in cavity.	–

(*continued on next page*)

Table A.1 (*continued*)

Place	Year	Examined configuration	Examined constructional features/ quantities	The description	Type of experiment	Controlled environment	Thermal field	Velocity field	Other important variables
			The width of the inlet: 2 and 3 cm.	and integrated venetian blinds. The main influent structural parameters are recognized: slat angle, position of shading system, airflow rate, opening position, incident of the direct solar radiation and weather conditions. Valuable information and recommendations regarding the PIV technique are given. Characteristics of the flow in the cavity are given in response to slat angle, shading position, the width of the opening.					
Politecnico di Torino, Italy [83]; [78]	2007	Mechanically and naturally ventilated DSF (buoyancy only) with integrated venetian blinds.	Monitoring lasted for two years with different operating conditions: a) with and without venetian blinds; b) mechanical ventilation with the nominal air flow rate 50 m^3/h; c) mechanical ventilation with an increased air flow rate 75 m^3/h; d) natural ventilation with the filter on the supply opening of the air gap; e) natural ventilation without the filter.	An extensive measurement campaign is performed on the DSF connected with HVAC through exhaust ventilation mode during actual operating conditions in order to assess the energy and comfort performance.	Natural	–	Thermocouples for measuring surface, air cavity and openings temperatures.	Hot wire anemometer for air velocity in the cavity.	Tracer gas method for measuring airflow rate. Solarimeter for measuring incident and transmitted solar radiation. Heat flux meters for measuring heat flux through DSF element.
Loughborough University, England [47]; [6]; [113]; [115]; [109]; [99]; [112]; [111]; [98]	2007	Natural (buoyancy only) DSF with integrated venetian blinds.	Incident solar radiation: 187, 360, 540 and 715 W/m^2. Outside air temperature: 12, 20 and 30 °C. Slat angles: 0, 30, 45, 60 and 90°.	CFD model of natural DSF is developed based on the results from a controlled experiment in a climate chamber with a solar simulator. Interesting conclusions are found about the thermal and fluid dynamic behavior of DSF in response to the presence of shading element and tilt angle of its venetian blinds.	Controlled	Radiative: yes Thermal: yes Wind: no	Thermocouple (T-type) for measuring surface, air cavity and openings temperatures.	TSI air velocity transducers (omnidirectional) for measuring air velocity in cavity.	Pyranometer for measuring incident solar radiation.

(*continued on next page*)

Table A.1 (*continued*)

Place	Year	Examined configuration	Examined constructional features/ quantities	The description	Type of experiment	Controlled environment	Thermal field	Velocity field	Other important variables
Aalborg University, Denmark [48]; [102]; [90]	2008	Mechanically and naturally ventilated DSF (both, buoyancy and wind).	Three ventilation modes: 1 (outdoor air curtain), 2 (buffer zone) and 3 (air supply).The a irflow of 143 m^3/h was used as a supply in 3rd ventilation mode. Several days of monitoring.	Technical report as a part of the doctoral dissertation of Kalyanova provides information about thermophysical behavior of DSF with integrated both natural and mechanical ventilation mode based on several days of monitoring. Valuable information about the correct set-up for pressure difference, tracer gas and velocity profile methods are given. Conclusion on what drives more natural flow in the cavity is given.	Natural	–	Thermocouples (K-type), for measuring surface, air cavity and openings temperatures.	Hot sphere anemometers for measuring air velocity in cavity.	Pressure difference and tracer gas method for measuring airflow rate. Pyranometers for measuring incident and transmitted radiation. Ultrasonic anemometer for evaluation of wind velocity profile.
San Vendemiano, Treviso, Italy [121]	2010	Mechanically ventilated DSF with integrated venetian blinds	For different incident radiation and outdoor temperatures with an airflow rate of 40 m^3/h.	Paper presents validation of CFD model from experimental data obtained from a full-scale test room with DSF located in San Vendemiano (TV), Italy.	Natural	–	PT1000 temperature sensors for measuring air cavity temperatures. Resistance temperature detectors (RTD) for measuring surface temperatures of glazing and blinds.	Not measured	Pyranometer for measuring incident solar radiation. Automatic mini weather station.
Centre de Thermique de Lyon CETHIL, INSA Lyon, France [79]; [16]	2011	Mechanically ventilated DSF with integrated venetian blinds.	Airflow rates: 0, 200, 400 and 600 $m^3\ h^{-1}$. Slat angles: 0, 30, 45, 60 and 90°.	Full-scale experiment in climate chamber equipped with solar simulator provides information about the influence of airflow rate and slat angle of venetian blinds on the thermal behavior of mechanically ventilated DSF. Valuable information about correct experimental set-up in a controlled environment is given.	Controlled	Radiative: yes Thermal: yes Wind: no	Thermocouples type (T-type) for measuring surface, air cavity and openings temperatures.	TSI air velocity transducers (omnidirectional) for measuring air velocity in cavity.	Differential pressure airflow meter for measuring airflow rate in the cavity. Mobile pyranometer for measuring distribution of incident solar radiation.
Tsinghua University, Beijing, China [122]; [119]; [118]	2012	Natural (both, wind and buoyancy) DSF with integrated venetian blinds	Three different outdoor conditions: incident solar radiation, angle and outdoor temperature.	Paper presents the validation of CFD model based on field experiments on DSF model. It provides a database for validation of other more recent CFD models.	Natural	–	Thermocouple (T type) for measuring surface and air cavity temperature.	Not measured	Tracer gas method for measuring airflow rate.
University of Reims, France [41]; [95]	2012	Vertical parallel plates channel naturally ventilated	Different aspect ratios and modified Rayleigh numbers	Numerical results of the CFD model are compared with experiments carried out in the water.	Controlled	Radiative: no Thermal: yes Wind: no	Measured, but not analyzed, because water was used as working medium.	Particle Image Velocimetry (PIV) technique for deducing	Heat flux distribution was assessed based on temperature measurement

(*continued on next page*)

Table A.1 (*continued*)

Place	Year	Examined configuration	Examined constructional features/ quantities	The description	Type of experiment	Controlled environment	Thermal field	Velocity field	Other important variables
		(buoyancy only)	(between $2 \cdot 10^5$ and 4 and $2 \cdot 10^6$).	Simulation points to the patterns of the recirculation zone observed in the experiments.				streamline patterns.	along heating plate.
University of Technology Graz, Austria [123]	2014	Three types of naturally ventilated DSF (both, buoyancy and wind): naturally ventilated DSF with PV module and inner opaque facade, natural opaque DSF with solar collector and standard DSF design	Cross-comparison of thermal behavior via recorded surface temperatures of three different types of DSF for two summer days in Graz.	This study determines thermal behavior and airflow characteristics inside different types of natural DSF. Experimental campaign for one year was performed in order to validate the CFD model and to cross-compare the thermal behavior of these three types of DSF.	Natural	–	Pt 100 elements for measuring surface temperature of PV module and inner wall (DSF with PV module), surface temperature of thermal insulation and interior wall (opaque DSF) and surface temperature of interior glazing and interior wall (standard DSF).	Two hot wire anemometers for measuring velocity in the cavity of DSF with integrated PV modules	Automatic weather station.
University of Science and Technology of China, Hefei, China [71]; [124]	2015	Trombe wall naturally ventilated (only buoyancy) with integrated venetian blinds	Location of the venetian blinds (Z/m): 0.04, 0.05, 0.06, 0.07, 0.08, 0.09 and 0.10. Width of the air cavity (m): 0.18, 0.16, 0.14, 0.12, 0.10 and 0.08. Area of inlet/ outlet vent (m^2): 0.2 x 0.1, 0.3 x 0.1, 0.4 x 0.1, 0.5 x 0.1, 0.6 x 0.1 and 0.7 x 0.1.	The paper presents an experimental rig that was constructed and utilized to validate the CFD prediction.	Natural	–	Thermocouples for measuring surface and air openings temperature.	A kanomax A533-type anemometer for measuring velocity in the cavity.	Pyranometer.
Centre de Thermique de Lyon CETHIL, INSA Lyon, France [38]	2016	Vertical parallel plates channel naturally ventilated (buoyancy only)	Two examined configurations: 1) uniformly heated one side and 2) both sides heated with spatial periodicity 1/15 of the overall height with a heat input of 220 W/m^2	The experiment in the laboratory on the naturally induced flow between two vertical parallel plates provides recommendations on a preferred arrangement of PV panels that will reduce overheating of the cavity.	Controlled	Radiative: no Thermal: yes Wind: no	Thermocouples type (K-type) for measuring surface and air cavity temperatures.	Particle Image Velocimetry (PIV) technique for measuring velocity of air in cavity.	–
Building Physics Laboratory, İzmir Institute of Technology, Turkey [42]; [43]; [125]; [126]	2016	Naturally (buoyancy only) and mechanically ventilated DSF	7 experiments with naturally ventilated DSF with different Rayleigh numbers ranging from $8.59 \cdot 10^9$ to $1.41 \cdot 10^{10}$. [42] 18 experiments with mechanically ventilated DSF using perforated plates with two holes different in size: flow (low, medium and high) in combination with three incident solar	Several experiments on both naturally and mechanically ventilated DSF are performed in the laboratory in Izmir, based on which numerical models have been developed.	Controlled	Radiative: yes/no Thermal: yes Wind: no	Thermocouples (T-type) for measuring surface, air cavity and openings temperatures.	Not measured	Pressure difference method for measuring airflow rate. Pyranometer for measuring incident solar radiation.

(*continued on next page*)

Table A.1 (*continued*)

Place	Year	Examined configuration	Examined constructional features/ quantities	The description	Type of experiment	Controlled environment	Thermal field	Velocity field	Other important variables
			radiation. [125] 9 experiments with mechanically ventilated DSF: Three cavity depth (25, 32.5 and 40 cm) in combination with three airflow rates (low medium and high). [43] 12 experiments with mechanically ventilated DSF: two cavity depths (25 and 35 cm) in combination with three airflow rates (low, medium and high) and two radiation levels (around 185 and 350 Wm^{-2}). [126]						
The Hong Kong University of Science and Technology, China [106]; [105]; [104]	2017	Natural (wind only) DSF	Different incident wind angles.	A series of wind tunnel tests have been conducted to investigate the characteristics and related mechanisms of flow within the cavity of DSF integrated with a tall building model (1:150 scaled CAARC building model) at different incident wind angles.	Controlled	Radiative: no Thermal: no Wind: yes	No measured	60 Kanomax omni-directional anemometer probes for measuring velocities inside cavity.	–
Korea Institute of Civil Engineering and Building Technology, Goyang-si, Korea [97]	2017	Natural (buoyancy only) DSF in the laboratory. Both driving mechanism in outdoor tests.	Two different glazing configurations with and without ventilation (O–O mode) in the laboratory test. Thermal behavior of chosen configuration in outdoor conditions during several day measurements.	This paper proposes a configuration of the DSF that reduces SHGC without using a shading device, only by ventilating the outer zone of the cavity, while the inner zone is closed. Thermal performance is confirmed by the tests in the controlled environment and in the outdoor conditions.	Both, controlled and natural	Radiative: yes Thermal: yes Wind no.	Thermocouples for surface and air cavity temperatures	Not specified	Pyranometer. Indoor thermal comfort parameters (PMV and PPD).
The University of Nottingham Ningbo China. [64]; [116]; [65]; [117]	2017–2019	Natural (both, buoyancy and wind) DSF with integrated PCM blinds	Several days monitoring during hot summer days. Comparison with thermal behavior of standard aluminum DSF.	Experimental campaign during hot summer days in Ningbo where thermal behavior of small representative DSF element (1.05 × 0.95 m) has been analyzed. The influence of wind has not been analyzed. Data from	Natural	–	Thermocouples (K-type) for surface, and air cavity temperatures	Hot-wire anemometers for measuring velocity in the cavity	Meteo-station for monitoring outside conditions

(*continued on next page*)

Table A.1 (*continued*)

Place	Year	Examined configuration	Examined constructional features/ quantities	The description	Type of experiment	Controlled environment	Thermal field	Velocity field	Other important variables
				this campaign has been used for the validation of several CFD models.					
The Korean Institute of Construction Technology KICT, Ilsan, Korea [68]	2018	Natural (buoyancy only) DSF	Tree different configuration of slim-type DS window system has been subjected to the fixed incident solar radiation (around 500 Wm-2) and indoor (25 °C) and outdoor temperature (30 °C) in order to assess SHGC and temperature distribution in the cavity.	A novel type of DSF which reminds on the two double-glazed windows separated with the slim cavity was exposed to tests in the metering box and climate chamber with an installed solar simulator in order to assess SHGC and temperature distribution in the cavity. Results from experiments were used for validation of the CFD model.	Controlled	Radiative: yes Thermal: yes Wind: no	Thermocouples for the air cavity	Not measured	Measurement of SHGC according to KS L 9107 Test (Korean standard).
Universidade Federal de Ouro Preto, Brazil [60]	2018	Natural opaque (both, buoyancy and wind) DSF	Comparison of three days measurement between the wall with added external façade (opaque DSF) and standard wall without external layer.	The thermal performance of opaque DSF has been analyzed through a three-day measurement campaign and compared to the thermal performance of a one-skin wall. The influence of wind has not been analyzed. Results from the experiment served also for validation of the CFD model.	Natural	–	Thermocouples (K-type) for measuring surface temperatures	Hot wire anemometer for measuring air velocity in the cavity	–
Tongji University, Shanghai, China [70]	2018	Natural (both buoyancy and wind) DSF with green vertical greening system	Comparison of thermal behavior (air cavity, surface and indoor temperature) of DSF with vertical greening system and masonry wall.	Experimental summertime campaign on the thermal performance of DSGF of a 5-story administrative building in Shanghai.	Natural	–	Thermocouple (K-type) for surface temperature of outer vegetated skin, Temperature/RH smart sensor for air cavity temperature.	–	Automatic weather station. Equipment for indoor thermal quality assessment (globe temperature sensor and wind velocity sensor)
Hunan University, Changsha, China [62]	2018	Naturally ventilated DSF (both buoyancy and wind) with integrated PV blinds.	Comparison between ventilated and non-ventilated modes. Comparison of thermal performance between traditional opaque façade, and naturally ventilated DSF with integrated PV blinds.	This experimental research compares thermal behavior and electric performance of PVB-DSF with a traditional envelope element.	Natural	–	Thermocouples Pt100 for measuring glazing, PV cells surface temperatures and air duct temperature.	Hot wire anemometer for measuring velocity of air near inlet.	Pyranometers for direct and diffuse solar radiation. Output voltage of PV blinds.
La Rochelle University, France [59]	2019	Mechanically ventilated DSF	The volumetric flow rate across the airflow window has been gradually increased from 8 m^3h^{-1} to 48	The experimental campaign is performed in order to validate the numerical model and to investigate the thermal	Natural	–	Thermocouples (K-type) for measuring surface and air cavity temperatures.	The extracted airflow rate from test cell is assessed from air velocity measurements at the exhaust duct	Pyranometer and pyrgeometer measured total incident solar flux and exchanged

(*continued on next page*)

Table A.1 (*continued*)

Place	Year	Examined configuration	Examined constructional features/ quantities	The description	Type of experiment	Controlled environment	Thermal field	Velocity field	Other important variables
			m^3h^{-1} in order to investigate its effect on the thermal behavior of the window during a typical sunny and a quite warm winter week.	performances of a triple-glazed airflow window, by comparison to the convectional double-glazed window.				(hot wire anemometer).	longwave radiation flux. A cup anemometer and a weathervane measured the wind speed and its direction.
Huazhong University of Science and Technology, Wuhan, China [69]	2019	Naturally ventilated DSF with venetian blinds integrated into the switchable cavity.	Comparison of thermal behavior of triple glazed exhaust window and classic window along with validation of numerical study.	Experimental campaign on the novel DSF that is able to work in two modes (summer and winter) using switchable cavity were performed during two typical summer days in Wuhan in order to validate the numerical study.	Natural	–	Temperature sensors for measuring temperature of surface and air near openings.	–	Pyranometer for measuring incident radiation. Hot wire anemometer for measuring airflow delivered to the chamber (not installed in the cavity).
Brno University of Technology, Czech Republic [66]	2019	Naturally ventilated DSF with integrated PV cells and PCM material on the inner opaque side.	Two types of ventilated BiPV façade are tested: with and without PCM layer located behind the PV cells.	Experimental investigation of a novel combination of BiPV/PCM integrated in naturally ventilated DSF. The study does not contain specific information about used sensors.	Natural	–	Temperature sensors for surface and air in the cavity.	Sensor for velocity in the cavity.	Heat flux for measuring heat flow.
Yongin, Gyeonggi-do, Korea [40]	2019	Naturally ventilated DSF (slim type)	Cavity	This study analyzes the cooling energy performance of SDSW through field measurement.	Natural	–	Thermocouples for measuring surface and air cavity temperatures	–	Pyranometer for incident solar radiation. PMV meter for indoor space.
The University of Sydney, Australia [103]	2019	Naturally ventilated DSF (wind only)	Opening configuration (recessed regions, curved walls, converging and diverging passages)	Experimental research in a wind tunnel investigates mean flow characteristics inside the opening of a corridor-type DSF on a high building replica.	Controlled	Radiative: no Thermal: no Wind: Yes	–	Particle Image Velocimetry (PIV) technique for measuring velocity of air in the cavity.	Cobra multi-hole pressure probe for validating PIV technique.
Centre for Energy and Environment, Jaipur, India [61]	2020	Photovoltaic DSF naturally and mechanically ventilated	Cavity depth (50, 100, 150, 200 and 250 mm) and ventilation type (naturally and mechanically ventilated: 2, 2.75, 3.5, 4.25 and 5 m/s)	Comparison of experimental performance of naturally and mechanically ventilated photovoltaic DSF with outdoor air curtain ventilation mode during the typical cloudless day in a cooling period.	Natural	–	K-type thermocouples for inner surface of the PV panel and glass and the air cavity temperature	Hot wire anemometer for air velocity inside the cavity.	Pyrheliometer and two pyranometers for incident radiation and transmitted radiation. Automatic weather station. Conductive and radiative heat flux sensors.
Laboratoire de Genie Civil et geo-Environnement (LGCgE), Bethune, France [87]	2020	Vertical parallel plates channel naturally ventilated (buoyancy only)	Five different aspect ratios (5; 6.25; 8.34; 12.5 and 25) and four different temperatures (303 K, 313 K, 323 K and 342 K).	Experimental study of natural convection inside an asymmetrically heated open double vertical façade applicable to DSF under certain conditions. The intelligent way to make experiments with low investment.	Controlled	Radiative: no Thermal: yes Wind: no	Thermocouples for measuring surface and air temperature in the channel.	–	Heat flux sensors for measuring heat flow.

Table A.2. CFD studies on thermal and fluid dynamics behavior of DSF

Table A.2
CFD studies on thermal and fluid dynamics behavior of DSF

Name	Year	Examined configuration	Examined constructional features/ quantities	Used tool	Discretization method and dimensionality	Turbulence model	Grid type	Validation	Solution algorithm	Radiation model	The description
Airflow patterns and thermal behavior of mechanically ventilated glass double facades [76]	2004	Mechanically ventilated DSF with integrated shading screen	Cavity	Flovent	Finite volume (2D)	RNG k-ε model	Structured (rectangles)	By own experiment: thermal part: yes dynamical part: no	SIMPLE	Spectral optical model	A procedure for spectral optical and a CFD modelling is described and simulated results are compared with an experimental investigation built in an outdoor test facility
Influence of glass properties on the performance of double-glazed facades [77]	2005	Naturally and mechanically ventilated DSF	Ten different combination of glasses with different values of reflectance, transmittance and absorption coefficient.	Ansys Fluent (version not specified)	Finite volume (2D)	Standard k-ε model	Structured (rectangles)	Not validated	Not specified	Not specified	In this research the influence of the glass properties on the thermal performance of DSF has been studied through the unvalidated 2D model of both, naturally and mechanically ventilated DSF without venetian blinds.
Natural ventilation performance of a double-skin facade with a solar chimney [49]	2005	Naturally ventilated DSF with solar chimney	Different height of solar chimney and size of the openings	Not specified	Finite volume (3D)	Indoor zero-equation model (low turbulence)	Structured (rectangles)	By own experiment: thermal part: yes dynamical part: incomplete	Not specified	Not specified	CFD analysis is carried out in conjunction with a reduced scale model experiment in order to evaluate the natural ventilation performance of the prototype building.
CFD modelling of naturally ventilated double-skin facades with Venetian blinds [111]	2008	Naturally ventilated DSF with integrated venetian blinds	Different slat angles	Ansys CFX10	Finite volume (2D)	k-ω model	Hybrid mesh (rectangles + triangles)	By own experiment: thermal part: yes, dynamical part: incomplete.	Fully implicit	Multi-band Monte Carlo model	Numerical study on naturally ventilated DSF that inspects influence of venetian blinds on the flow and heat transfer in the cavity.
Nodal network and CFD simulation of airflow and heat transfer in double skin facades with blinds [112]	2008	Naturally ventilated DSF with integrated venetian blinds	Numerical approaches comparison.	Ansys CFX5.7.1	Finite volume (3D)	k-ω model	Not specified	By own experiment: thermal part: yes, dynamical part: incomplete.	Not specified	Multi-band Monte Carlo model	A simplified and CFD model was developed in order to compare their performance in the prediction of heat transfer and buoyancy-driven airflow. First developed three-dimensional CFD model of naturally ventilated DSF with integrated venetian blinds.
Numerical investigation on thermal	2008	Naturally ventilated DSF with	Different cavity depth, aspect ratio, height,	Phoenics 3.6	Finite volume (3D)	RNG k- ε model	Structured mesh (rectangles)	By open literature experimental	Not specified	Not specified	Based on the CFD simulation results,

(*continued on next page*)

Table A.2 (*continued*)

Name	Year	Examined configuration	Examined constructional features/ quantities	Used tool	Discretization method and dimensionality	Turbulence model	Grid type	Validation	Solution algorithm	Radiation model	The description
performance and correlations of double skin facade with buoyancy-driven airflow [44]		integrated roller blind	opening size, type of shading and environmental conditions					database [84]: thermal part: yes, dynamical part: incomplete			correlations for cavity airflow rate, air temperature stratification, and interior convection coefficient were provided.
Natural ventilation in the double skin facade with venetian blind [33]	2008	Naturally ventilated DSF with integrated venetian blinds	Shading position (fixed angle 45^0 and position: middle).	Not specified	Finite volume	Not specified	Not specified	By open literature experimental database [76]: thermal part: yes, dynamical part: no	Not specified	Separate model	In the paper, a detailed analysis of the thermal process in DSF with venetian blind was made. The governing equations were solved by incorporating CFD, optical and heat balance model. There is a lack of information on the CFD model.
Double skin façades for warm climate regions: Analysis of a solution with an integrated movable shading system [74]	2009	Naturally and mechanically ventilated DSF with integrated blinds.	Winter configuration: closed natural, O–O natural and forced O–I ventilation mode. Summer configuration with closed blinds.	Ansys Fluent 6.2	Finite volume (2D/3D)	RNG k-ε model	Unstructured mesh (triangles for 2D and tetrahedral for 3D)	By open literature experimental database [127]: thermal part: yes, dynamical part: incomplete.	Not specified	The solar ray tracing model	CFD model has been built and in order to compare the energy performance of one summer and three winter configurations with the energy performance of traditional enclosures.
A CFD approach to evaluate the influence of construction and operation parameters on the performance of active transparent facades in Mediterranean climates [80]	2009	Mechanically ventilated DSF	Different Reynolds number, length-to-depth ratio, glazing emissivity and transmittivity and inlet configuration.	Ansys Fluent 6.3	Finite volume (3D)	RNG k-ε model	Structured mesh (rectangular cuboids)	CFD model has been validated in previous works [120] by experimental database [76]. No further information.	PISO	P1 radiation model	This study assess, using CFD as a tool, the influence of optical properties of the materials, geometrical relations of the façade and flow stream conditions on energy savings, measured through reduction of the solar heat gain.
Numerical evaluation of the mixed convective heat transfer in a double-pane window integrated with see-through a-Si PV cells with low-e coatings [31]	2010	Naturally ventilated DSF	Different Rayleigh numbers and effects of low-e coatings applied on glazing.	Own numerical code (Fortran 90)	Finite difference (2D)	No turbulence model (laminar)	Not specified	Not validated	successive under-relaxation method (SUR)	Radiosity equation	2D numerical analysis of the control strategies on potential energy savings in double-pane window integrated with transparent a-S photovoltaic with low emittance (low-e) coatings.
CFD Analysis of Turbulent Natural Ventilation in Double-Skin	2010	Naturally ventilated DSF with integrated	Cross-comparison of different DSF types: no	Ansys Fluent 6.3	Finite volume (2D)	Standard k-ε model	Hybrid mesh (rectangles + triangles)	By open literature experimental database [75]:	Not specified	The discrete ordinates	This work summarizes the results of a computational

(*continued on next page*)

Table A.2 (*continued*)

Name	Year	Examined configuration	Examined constructional features/ quantities	Used tool	Discretization method and dimensionality	Turbulence model	Grid type	Validation	Solution algorithm	Radiation model	The description
Facade: Thermal Mass and Energy Efficiency [110]		venetian blinds	blinds, with aluminum blinds and with thermal mass concrete.					thermal part: no, dynamical part: incomplete.		(DO) model	fluid dynamic (CFD) analysis, which was carried out to investigate the effect of blind and thermal mass concrete on the thermal performance of a double-skin façade.
Natural Convection in PV-Integrated Double-Skin Façade using Large-Eddy simulation [37]	2011	Vertical parallel plates channel naturally ventilated	Cavity	Own numeric code	Finite volume (3D)	No. Large Eddy Simulation (Vreman subgrid-scale model)	Not specified	By open literature experimental database [86]: thermal part: yes, dynamical part: fully.	Two-stage predictor corrector method	Not included	First LES simulation on DSF. Useful observations on the advantages of LES over RANS in modeling naturally induced turbulent flow have been made.
Airflow and heat transfer in double skin facades [78]	2011	Mechanically ventilated DSF with integrated venetian blinds	Different slat angles and position of the blinds	Ansys Fluent 6.3	Finite volume (2D)	RNG k-ε model	Not specified	By own experiment: thermal part: yes, dynamical part: no	SIMPLE	The S2S (surface to surface) radiation model	CFD model has been developed for mechanically ventilated DSF with integrated venetian blinds in order to asses thermal and fluid dynamics behavior of DSF in response to position and angle of venetian blinds.
Numerical simulation of dynamical aspects of natural convection flow in a double-skin façade [41]	2012	Vertical parallel plates channel naturally ventilated (filled with water)	Different Rayleigh numbers and aspect ratios	Ansys Fluent (version not specified)	Finite volume (2D)	No turbulence model (laminar).	Structured mesh (rectangles)	By own experiment: thermal part: no dynamical part: incomplete	Not specified	Not included	A 2D numerical study of the laminar flow in an asymmetrically heated vertical plane channel with variable different Rayleigh numbers and aspect ratios. Water as a working medium.
Evaluation of various CFD modelling strategies in predicting airflow and temperature in a naturally ventilated double skin façade [6]	2012	Naturally ventilated DSF	Numerical approaches comparison	Ansys Fluent 6.3	Finite volume (2D/3D)	SST k-ω and RNG k-ε model.	Not specified	By open literature experimental database [47]: thermal part: yes, dynamical part: fully.	SIMPLE	Not included (measured values used)	A useful numerical study that highlights which segments of the CFD model are important in the simulation of thermo-physical behavior of naturally ventilated DSF. Dimensionality, turbulence models, modelization of external environment and fluid

(*continued on next page*)

Table A.2 (*continued*)

Name	Year	Examined configuration	Examined constructional features/ quantities	Used tool	Discretization method and dimensionality	Turbulence model	Grid type	Validation	Solution algorithm	Radiation model	The description
											properties are subjected to a sensitivity analysis, upon which a conclusion about the preferred CFD strategy has been drawn.
An experimentally validated mathematical and CFD model of a supply air window: Forced and natural flow [54]	2013	Naturally and mechanically ventilated DSF	Mechanically ventilated DSF with two different airflow rates and one naturally ventilated DSF.	Ansys Fluent 12.1	Finite volume (3D)	SST k–ω model	Structured mesh (rectangular cuboids)	By own experiment: thermal part: yes, dynamical part: incomplete	SIMPLE	The solar ray tracing model	CFD 3D model has been used for modelling airflow in DSF with supply ventilation mode for both types of DSF (naturally and mechanically ventilated) without venetian blinds.
Analysis of ventilation effects and the thermal behavior of multifunctional facade elements with 3D CFD models [123]	2014	Three different naturally ventilated DSFs: with integrated photovoltaic module (PV), a solar collector (ST) and a classic DSF design with two transparent glazing.	Cross comparison of three DSF types in typical summer conditions (25 °C, 500 Wm^{-2} and 60° incident angle)	Ansys Fluent 14.0	Finite volume (3D)	RNG k- ε model	Structured mesh (rectangular cuboids)	By own experiment: thermal part: yes, dynamical part: incomplete	SIMPLE	The discrete ordinates (DO) model	This study determines thermal behavior and airflow characteristics of three types of naturally ventilated DSFs using CFD simulations.
Double Skin Façade: Modelling Technique and Influence of Venetian Blinds on the Airflow and Heat Transfer [113]	2014	Naturally ventilated DSF with integrated venetian blinds	Different blind angles and position of the shading system.	Ansys Fluent 14.0	Finite volume (3D)	RNG k- ε model	Hybrid (tetrahedral and rectangular cuboids)	By open literature numerical database [47]: thermal part: yes, dynamical part: no.	SIMPLE	The solar ray tracing model/The discrete ordinates (DO) model	In this paper four modelling strategies and the influence of blind tilt angle and their proximity to the façade walls are investigated through 3D CFD simulations.
Thermal Performance of Ventilated Double Skin Façades with Venetian Blinds [12]	2015	Mechanically ventilated DSF with integrated venetian blinds	Different emissivity and absorptivity of blinds, shading position and airflow rate.	Ansys Fluent 15.0	Finite volume (3D)	RNG k-ε model	Structured mesh (rectangular cuboids)	By open literature experimental database [76]: thermal part: yes, dynamical part: fully.	PISO	P1 radiation model	The influence of several optical and geometrical properties of blinds and ventilation rate conditions of a DSF on the reduction of solar heat gains has been evaluated in this CFD study.
A numerical analysis of the air ventilation management and assessment of the behavior of double skin facades [58]	2015	Mechanical DSF with integrated venetian blinds	Different slat angles, incident angle of solar radiation, the slat emissivity and the airflow rate.	Ansys Fluent 6.3	Finite volume (2D)	Realizable k–ε model	Unstructured (triangles)	By open literature experimental database [53]: thermal part: no, dynamical part: fully.	SIMPLE	The discrete ordinates (DO) model	This research through developed CFD model examines the effect of solar radiation, incidence angle and slat angle on the thermal properties and the solar transmission

(*continued on next page*)

Table A.2 (*continued*)

Name	Year	Examined configuration	Examined constructional features/ quantities	Used tool	Discretization method and dimensionality	Turbulence model	Grid type	Validation	Solution algorithm	Radiation model	The description
											into the interior environment for a DSF equipped with a venetian blind.
Modelling natural ventilation in double skin façade [102]	2015	Naturally ventilated DSF	Numerical approaches comparison	OpenFOAM	Finite volume (2D)	The q-ζ model/RNG k-ε model	Structured (rectangles)	By open literature experimental database [48]: thermal part: yes, Dynamical part: incomplete.	SIMPLE	Not included (measured values used)	The CFD modelling activity presented in this work aims at investigating the reliability of the assumptions and hypotheses employed in the simplified model.
Solar heat gain reduction of double-glazing window with cooling pipes embedded in venetian blinds by utilizing natural cooling [118]	2016	Naturally ventilated DSF with integrated cooling pipes embedded in the venetian blinds	Cross-comparison of three types of DSF: no blinds, with blinds and with blinds accompanied with cooling pipes. Influence of glazing type.	Ansys Fluent 14.5	Finite volume (2D)	RNG k-ε model	Hybrid (rectangles and triangles)	By open literature experimental database [122]: thermal part: yes dynamical part: incomplete	SIMPLE	The Discrete Ordinate Method (DOM)	Cooling pipes embedded in the venetian blinds of a DSF are presented in this study along with a CFD model for the analysis of the effect of embedded pipes, different structures and glass assemblies on the thermal behavior of DSF.
Thermal performance of double skin façade with built-in pipes utilizing evaporative cooling water in cooling season [119]	2016	Naturally ventilated DSF with integrated cooling pipes embedded in the venetian blinds	Six different DSF configuration with open/ closed vents and Y/N built-in pipes. Different climate and orientation of DSF.	ANSYS Fluent 14.5	Finite volume (2D)	Standard k-ε model	Hybrid (rectangles and triangles)	By open literature experimental database [122]: thermal part: yes dynamical part: incomplete	SIMPLE	The Discrete Ordinate Method (DOM)	A comprehensive numerical model is presented to simulate the dynamic heat transfer during the cooling season where the performance of the pipe embedded DSF is investigated regarding different ventilation and operation strategies. The heat transfer process of the novel DSF is analyzed and compared with the traditional DSF. And influencing factors such as climate and orientation are evaluated.
Experimental and numerical investigation of natural convection in a double skin façade [42]	2016	Naturally ventilated DSF	Different Rayleigh numbers.	Ansys Fluent 14.5	Finite volume (3D)	Realizable k-ε model	Structured mesh (rectangular cuboids)	By own experiment: thermal part: yes. By open literature experimental database [52]: dynamical part: fully.	SIMPLE	Not included (measured values used)	Based upon the developed CFD model, the correlation for Nusselt number as a function of a Rayleigh number are given.

(*continued on next page*)

Table A.2 (*continued*)

Name	Year	Examined configuration	Examined constructional features/ quantities	Used tool	Discretization method and dimensionality	Turbulence model	Grid type	Validation	Solution algorithm	Radiation model	The description
Numerical and experimental investigation of unsteady natural convection in a non-uniformly heated vertical open-ended channel [38]	2016	Vertical parallel plates channel naturally ventilated	Uniformly and non-uniformly heated side of cavity.	Own numeric code	Finite volume (3D)	No. Large Eddy Simulation (Vreman subgrid-scale model)	Structured mesh (rectangular cuboids)	By own experiment: thermal part: yes, dynamical part: fully.	Two-step predictor corrector method	The radiosity model	LE simulation that includes the radiosity model describes characteristics of the flow behavior in and gives a preferred arrangement of PV panels in order to avoid overheating in the cavity.
Effect of Emissivity of Shading Device and Air Flow Inside Cavity of Double Skin Facade for Energy Saving and Thermal Comfort in Buildings: A CFD Modeling [115]	2016	Naturally ventilated DSF with integrated venetian blinds	Different airflow rate and emissivity of shading device.	Ansys Fluent 14.0	Finite volume (2D)	RNG k-ε model	Unstructured (triangles)	CFD model has been fully validated in previous works [113] by experimental measurements [47].	Not specified	The Discrete Ordinate Method (DOM)	The influence of different airflow rates and emissivity of the shading device is analyzed through the CFD model.
Influence of natural ventilation due to buoyancy and heat transfer in the energy efficiency of a double skin facade building [96]	2016	Naturally ventilated DSF	Different cavity widths in winter/ summer conditions with opened/closed vents and with/ without solar radiation.	Ansys Fluent 14.0	Finite volume (2D)	RNG k–ε model	Structured (rectangles)	By open literature numerical database [128]; [129] (not specified how).	SIMPLE	Separate model	A simplified model was simulated using CFD software to investigate the effects due to different cavity widths in winter and summer conditions with opened and closed vents and considering solar radiation or not.
Effect of inclination angle of the adiabatic wall in asymmetrically heated channel on natural convection: Application to double-skin façade design [95]	2017	Vertical parallel plate channel naturally ventilated with possibility of side inclination	Different inclination angles of walls.	Ansys Fluent (version not specified)	Finite volume (2D)	No turbulence model	Structured mesh (rectangles)	By open literature experimental database [41]: thermal part: yes, dynamical part: fully.	–	Not included	Numerical study about natural laminar flow in the cavity and the influence of different inclination of sides and UHF conditions on heat and mass flow rate has been investigated.
Experimental and Numerical Investigation of Forced Convection in a Double Skin Façade [43]	2017	Mechanically ventilated DSF	Different aspect ratio and airflow rate.	Ansys Fluent 16.0	Finite volume (3D)	Realizable k-ε model	Structured mesh (rectangular cuboids)	By own experiment: thermal part: yes, dynamical part: fully.	SIMPLE	Not included	Based upon the developed CFD model, the correlation for Nusselt number is given as a function of an aspect ratio and Reynolds number. Interesting findings on thermal and hydrodynamic entrance length of mechanically induced flow are given. Flow features and geometrical characteristics of DSF that can increase fan

(*continued on next page*)

Table A.2 (*continued*)

Name	Year	Examined configuration	Examined constructional features/ quantities	Used tool	Discretization method and dimensionality	Turbulence model	Grid type	Validation	Solution algorithm	Radiation model	The description
											consumption are highlighted.
Naturally ventilated double-skin facade in modeling and experiments [90]	2017	Naturally ventilated DSF with integrated venetian blinds	Four situations where flow is differently driven by buoyancy and wind.	Open FOAM	Finite volume (2D)	SST k-ω model	Structured mesh (rectangles)	By own experiment: thermal part: yes, dynamical part: fully.	PISO	Not included (measured values used)	A simplified and CFD model has been developed in order to compare their performance in modelling mass flow rate and temperature distribution of naturally ventilated DSF. One of the rare CFD studies that analyses the influence of both wind and buoyancy on the temperature and velocity profile inside the cavity.
Design of a glazed double-façade by means of coupled CFD and building performance simulation [85]	2017	Naturally ventilated DSF	Thermal behavior of multi-storey DSF façade during summer weather.	StarCCM+	Finite volume (3D)	Standard k-ε model	Unstructured (not specified)	Not validated	Not specified	Not specified	In this paper, 3D CFD model is coupled with the BPS tool (IDA-ICE) in order to investigate the warm day cycle and its effects on the interiors.
Heat transfer analysis of an integrated double skin façade and phase change material blind system [64]	2017	Naturally ventilated DSF with integrated PCM blind system	Cross-comparison of DSF with PCM and aluminum blinds.	Ansys Fluent 14.0	Finite volume (2D)	RNG k-ε model	Hybrid mesh (rectangles + triangles)	By own experiment: thermal part: yes, dynamical part: no.	SIMPLE	The discrete ordinates (DO) model	CFD model that considers heat transfer on/ through PCM blinds has been developed. The influence of PCM blinds on the removal of excessive heat and stabilization of the flow in the cavity has been investigated.
Numerical investigation into a double skin façade system integrated with shading devices, with reference to the city of Amman, Jordan [98]	2017	Naturally ventilated DSF with integrated venetian blinds	Size, inclination angle, position, surface emissivity and surface diffuse fraction of slats and surface diffuse fraction of glass panes.	Ansys Fluent (version not specified)	Finite volume (2D)	RNG k-ε and SST k – ω model	Hybrid mesh (rectangles + triangles)	By open literature experimental database [47]: thermal part: yes, dynamical part: fully.	SIMPLE	The discrete ordinates (DO) model	The doctoral thesis includes parametric study concerning configuration and design parameters of both DSF's cavity and shading slats, in addition to boundary conditions. For the purpose of this study, a CFD-Fluent model was developed and validated.
Potential application of double skin façade incorporating aerodynamic modifications for wind energy harvesting [104]	2018	Naturally ventilated DSF	Different wind directions, different opening arrangements (recessed regions, curved walls)	ANSYS Fluent 13.0	Finite volume (3D)	SST k-ω model	Structured (rectangular cuboids)	By own experiment [106]	The pressure-based solver (not specified)	–	Experimentally validated CFD study that investigates a method for wind energy harvesting and the effect of

(*continued on next page*)

Table A.2 (*continued*)

Name	Year	Examined configuration	Examined constructional features/ quantities	Used tool	Discretization method and dimensionality	Turbulence model	Grid type	Validation	Solution algorithm	Radiation model	The description
											aerodynamic modifications: recessed regions and curved walls, on the flow characteristics inside an empty corridor-type DSF on high-rise building. Only wind as a driving force is examined.
Performance assessment of a special Double Skin Façade system for wind energy harvesting and a case study [91]	2018	Naturally ventilated DSF	Different wind intensity and incident angle.	ANSYS Fluent 13.0	Finite volume (3D)	SST k-ω model	Structured (rectangular cuboids)	By own experiment [106]	The pressure-based solver (not specified)	–	Experimentally validated CFD simulations were performed to assess the wind energy potential of corridor-type DSF placed on high-rise buildings.
Solar Heat Gain Coefficient Analysis of a Slim-Type Double Skin Window System: Using an Experimental and a Simulation Method [68]	2018	Naturally ventilated DSF (slim-type) equipped with venetian blinds	Different openings (different ventilation modes).	Star CCM+	Finite volume (3D)	Realizable k-ε model	Structured (rectangular cuboids)	By own experiment: Solar heat coefficient validated thermal part: no, dynamical part: no,	SIMPLE	The S2S (surface to surface) radiation model	Solar heat gain coefficients and the cavity temperatures are experimentally measured in order to analyze the opening influence on cooling energy needs of a special type of double skin facades (slim-type) of double skin window system with 270 mm wide cavity).
Experimental and numerical analysis of a naturally ventilated double-skin façade [60]	2018	Natural opaque DSF	Cross-comparison with standard opaque (one-skin) wall.	Ansys CFX	Finite volume (3D)	Standard k-ε model	Structured (rectangular cuboids)	By own experiment: Thermal part: yes, Dynamical part: no.	Not specified	Monte Carlo model	CFD analysis on the thermal behavior of the natural opaque DSF and its comparison with thermal behavior of standard one-skin wall.
Phase change material blind system for double skin façade integration: System development and thermal performance evaluation [65]	2019	Naturally ventilated DSF with integrated PCM blind system	Different PCM blind angles and position of shading system. Comparison with aluminum blinds.	Ansys Fluent (version not specified)	Finite volume (2D)	RNG k-ε model	Hybrid mesh (rectangles + triangles)	By own experiment: thermal part: yes, dynamical part: no.	SIMPLE	The discrete ordinates (DO) model	One of the papers in series that analyses thermal behavior of DSF with integrated PCM blinds with CFD model that is validated using a natural experiment in The Centre for Sustainable Energy Technologies (Nottingham, China).
Effective use of venetian blind in Trombe wall for	2019	Trombe wall naturally ventilated	Different incident solar radiation,	Ansys Fluent 6.3	Finite volume (2D)	k-ω turbulence model	Structured (rectangles)	By own experiment: thermal part:	SIMPLE	The S2S (surface to surface)	In this study, the thermal performance of

(*continued on next page*)

Table A.2 (*continued*)

Name	Year	Examined configuration	Examined constructional features/ quantities	Used tool	Discretization method and dimensionality	Turbulence model	Grid type	Validation	Solution algorithm	Radiation model	The description
solar space conditioning control [71]		with integrated venetian blinds	distance between blinds, slat angle, inlet width and outlet vent width for two modes: cooling and natural ventilation mode.					yes dynamical part: incomplete		radiation model	the Trombe wall with venetian blind in the cooling season was analyzed by coupling Computational Fluid Dynamics (CFD) modelling and Building Energy Simulation (BES).
Effects of radiation on turbulent natural convection in channel flows [130]	2019	Vertical parallel plate channel naturally ventilated	Different values of emissivity of the channel walls, and different relative humidity of the ambient air.	Own numerical code (Fortran)	Finite volume (3D)	No. Large Eddy Simulation (Vreman subgrid-scale model)	Structured (refinement)	Not validated	PCGS (preconditioned conjugate-gradient) solver	The discrete ordinate (DO) model	A computational study using the LES approach has been undertaken where a constant heat flux of 220 W/m^2 is imposed on one side of the vertical parallel channel in order to analyze the complex interaction of radiation with the natural flow of dry and humid air.
Investigation on thermal performance of an integrated phase change material blind system for double skin facade buildings [116]	2019	Naturally ventilated DSF with integrated PCM blinds	Cross-comparison of DSF with PCM and aluminum blinds.	Ansys Fluent (version not specified)	Finite volume (not specified)	RNG k-ε model	Not specified	By own experiment (not specified how)	SIMPLE	The discrete ordinate (DO) model	One of the papers in series that analyses thermal behavior of DSF with integrated PCM blinds and compares with conventional DSF with aluminum blinds during the hot summer period. The paper does not contain enough information about the numerical model, but it is supposed that the same model is used as in previous works of Li and Darkwa.
Effect of design parameters on thermal performance of integrated phase change material blind system for double skin façade buildings [117]	2019	Naturally ventilated DSF with integrated PCM blinds	Different angle of PCM blinds, position of PCM shading system and type of blinds (aluminum and two types of PCM)	Ansys Fluent 14.5	Finite volume (not specified)	RNG k-ε model	Not specified	By own experiment: thermal part: yes dynamical part: no	SIMPLE	The discrete ordinate (DO) model	This paper focuses on the effect of design parameters on the thermal performance of such systems by conducting a simulation study of a DSF integrated with a PCM blind with different material properties,

(*continued on next page*)

Table A.2 (*continued*)

Name	Year	Examined configuration	Examined constructional features/ quantities	Used tool	Discretization method and dimensionality	Turbulence model	Grid type	Validation	Solution algorithm	Radiation model	The description
											positions in the cavity, and tilt angles of blades.
Cooling energy performance and thermal characteristics of a naturally ventilated slim double-skin window [40]	2019	Naturally ventilated DSF (slim-type)	Three types of different outer glazing: clear, colored and low-e glass.	Star CCM+	Finite volume (3D)	RNG k-ε model	Not specified	By own experiment: thermal part: yes dynamical part: no	SIMPLE	The S2S (surface to surface) radiation model and multiband thermal radiation model	This study aims to analyze the cooling energy performance of slim-type DSF through the numerical study that investigates the influence of outer single glazing on it.
Thermal and energy performance investigation of a smart double skin facade integrating vanadium dioxide through CFD simulations [72]	2019	Naturally ventilated DSF with opaque inner side (with AlN coating)	Different air gap thicknesses.	Ansys Fluent 15.0	Finite volume (2D)	No. Unsteady Reynolds Averaged Navier Stockes equations (URANS equations)	Structured (rectangles)	By open literature experimental database [131]: thermal part: yes, dynamical part: no.	Not specified	The S2S (surface to surface) radiation model	The aim of simulations are to investigate the thermal performance of a DSF that integrates Tungsten (W) doped Vanadium dioxide (VO_2) as an optically smart material on outer glazing and a high absorbing aluminum nitride (AlN) coating on the inner facade. A parametric study was carried out in order to analyze the impact of the air cavity thickness on the thermal behavior.
Flow and heat transfer characteristics of natural convection in vertical air channels of double-skin solar façades [92]	2019	Naturally ventilated DSF with integrated PV module absorber on inner opaque side	Different channel widths and heights and input heat fluxes.	Ansys Fluent 6.3	Finite volume (3D)	Standard k-ε model	Structured (rectangular cuboids)	By open literature experimental database [132]: thermal part: yes dynamical part: yes	SIMPLE	Separate model	This study numerically investigates the flow and heat transfer process in the vertical parallel plate channel under influence of different widths and heights of the channel and imposing heat fluxes.
Simulation of the thermal performance of a geometrically complex Double-Skin Facade for hot climates: EnergyPlus vs. OpenFOAM [94]	2019	Naturally ventilated DSF	Numerical approaches comparison.	OpenFOAM	Finite volume (3D)	Standard k-ε model	Not specified	Not validated	SIMPLE	Not included (boundary conditions taken from Energy Plus)	A numerical experiment is performed in which two models of a DSF are compared; one simulated with EnergyPlus and the other with OpenFOAM CFD software. Using CFD, the aims is to better understand the thermal performance of the DSF.

(*continued on next page*)

Table A.2 (*continued*)

Name	Year	Examined configuration	Examined constructional features/ quantities	Used tool	Discretization method and dimensionality	Turbulence model	Grid type	Validation	Solution algorithm	Radiation model	The description
Experimental Validation of a Numerical Model of a Ventilated Façade with Horizontal and Vertical Open Joints [108]	2019	Naturally ventilated DSF	Opening arrangement (ventilation mode). Validation of numerical model.	Ansys Fluent (version not specified)	Finite volume (3D)	RNG k-ε turbulence model	Hybrid (tetrahedral and rectangular cuboids)	Validated with own experiment: thermal part: yes, dynamical part: full.	SIMPLE	The discrete ordinate (DO) model	This paper experimentally validates a numerical simulation model of a Ventilated Façade with Horizontal and Vertical Open Joints (OJVF).
Experimental and numerical natural convection in an asymmetrically heated double vertical façade [87]	2020	Vertical parallel plates naturally ventilated	Two cases (the constant heat flux and the constant temperature): different Rayleigh numbers and aspect ratios.	Ansys Fluent (version not specified)	Finite volume (2D)	No turbulence model (laminar).	Structured (rectangles)	By open literature experimental database [133] and by own experiment: thermal part: yes, dynamical part: no.	SIMPLE	The discrete ordinate (DO) model/No radiation model	Study on laminar flow in an asymmetrically heated open double vertical façade naturally ventilated. Turbulent quantity analysis can be useful for DSF under certain conditions.
Application of double-glazed façades with horizontal and vertical louvers to increase natural air flow in office buildings [109]	2020	Naturally ventilated DSF with integrated horizontal and vertical louvers	Two types of naturally ventilated DSFs with integrated horizontal and vertical louvers.	Ansys Fluent (version not specified)	Finite volume (2D)	RNG k-ε model	Hybrid (rectangles + triangles)	By open literature experimental database [47]: thermal part: yes, dynamical part: fully.	SIMPLE	The discrete ordinate (DO) model	Numerical simulation of airflow and heat transfer inside the cavity of the DSF and the effect of different types of solar shading systems in horizontal and vertical modes on the airflow has been investigated using the CFD technique.
Natural ventilation of double skin façade: Evaluation of wind-induced airflow in tall buildings [105]	2020	Naturally ventilated DSF (wind only)	Different wind directions and speeds at three building levels: bottom, middle and top.	Ansys Fluent 19.0	Finite volume (3D)	SST k–ω model	Structured (rectangular cuboids)	CFD validated in previous researches [106].	SIMPLE	–	A series of CFD simulations were conducted on two basic wind-induced DSF configurations considering four wind incident angles (0°, 30°, 60°, and 90°).
Simulation and experimental verification of energy saving effect of passive preheating natural ventilation double skin façade [93]	2020	Naturally ventilated DSF	Different height, position of opening, winter scenarios and orientations.	Not specified	Finite volume (3D)	Standard k-ε model	Not specified	By own experiment: thermal part: yes, dynamical part: no.	Not specified	Not specified	This paper analyzes the passive preheating and the influence of the structural parameters of the double skin facade in cold season ventilation on the preheating ventilation effect. Important information on the CFD model is missing in research.
Computational fluid dynamics assessment for the thermal	2020	Naturally ventilated DSF with integrated	Different cavity depth, opening size and louver blinds ON/OFF	Star CCM+	Finite volume (3D)	RNG k–ε turbulence model	Not specified	By open literature experimental database [47]	SIMPLE	Not specified	The impact of various configurations on the thermal

(*continued on next page*)

Table A.2 (*continued*)

Name	Year	Examined configuration	Examined constructional features/ quantities	Used tool	Discretization method and dimensionality	Turbulence model	Grid type	Validation	Solution algorithm	Radiation model	The description
performance of double-skin facades in office buildings under hot climatic condition [99]		venetian blinds						(not specified how).			performance of the DSF is evaluated under the weather situation (summer) in Saudi Arabia through CFD simulations.
Ventilation performance of a naturally ventilated double-skin façade in buildings [100]	2020	Naturally ventilated DSF	Cavity depth, size of openings, glazing area, ventilation mode, DSF location and room dimensions.	Ansys Fluent 2020R1	Finite volume (3D)	RNG k-ε model	Structured (rectangular cuboids)	By open literature experimental database[126]: thermal part: yes, dynamical part: no.	COUPLED	The discrete ordinates (DO) model	The impact of cavity depth, size of openings, glazing area, ventilation mode, DSF location and room dimensions on naturally induced flow was evaluated in this experimentally validated CFD research.

2.8 References

[1] E. Oesterle, R.-D. Lieb, M. Lutz, W. Heusler, Double-skin Facades: Integrated Planning, München: Prestel, 2001.

[2] S. Barbosa, K. Ip, Perspectives of double skin façades for naturally ventilated buildings: a review, Renew. Sustain. Energy Rev. 40 (2014) 1019–1029.

[3] M.M.S. Ahmed, A.K. Abel-Rahman, A.H.H. Ali, M. Suzuki, Double skin façade: the state of art on building energy efficiency, J. Clean Energy Technol. 4 (1) (2015) 84–89.

[4] C. Hachem-Vermette, in:" C. Hachem-Vermette (Ed.), Selected High-Performance Building Envelopes BT - Solar Buildings and Neighborhoods: Design Considerations for High Energy Performance, Springer International Publishing, Cham, 2020, pp. 67–100.

[5] M.a. Shameri, M.a. Alghoul, K. Sopian, M.F.M. Zain, O. Elayeb, Perspectives of double skin façade systems in buildings and energy saving, Renew. Sustain. Energy Rev. 15 (3) (Apr. 2011) 1468–1475.

[6] W. Pasut, M. De Carli, Evaluation of various CFD modelling strategies in predicting airflow and temperature in a naturally ventilated double skin façade, Appl. Therm. Eng. 37 (2012) 267–274.

[7] M.H. Oh, K.H. Lee, J.H. Yoon, Automated control strategies of inside slat-type blind considering visual comfort and building energy performance, Energy Build. 55 (Dec. 2012) 728–737.

[8] M.G. Gomes, A.J. Santos, A.M. Rodrigues, Solar and visible optical properties of glazing systems with Venetian blinds: numerical, experimental and blind control study, Build. Environ. 71 (2014) 47–59.

[9] M. Al Kaabi, Double Skin Façade as an Urban Heat Island Mitigation Strategy- Case Study of a Health Care Facility in Abu Dhabi, Masdar Institute of Science and Technology, 2016.

[10] H. Andoni, S. Wonorahardjo, A review on mitigation technologies for controlling urban heat island effect in housing and settlement areas, IOP Conf. Ser. Earth Environ. Sci. 152 (May 2018), 012027.

[11] A.H. Block, S.J. Livesley, N.S.G. Williams, Responding to the urban heat island: a review of the potential of green infrastructure, Vic. Cent. For Climate Chang. Adapt. Res. Melb. (2012).

[12] J. Parra, A. Guardo, E. Egusquiza, P. Alavedra, Thermal performance of ventilated double skin façades with Venetian blinds, Energies 8 (6) (2015) 4882–4898.

[13] D. Faggembauu, Heat Transfer and Fluid-Dynamics in Double and Single Skin Facades, " Universitat Politecnica de Catalunya, 2006.

[14] H. Hens, Building Physics - Heat, Air and Moisture: Fundamentals and Engineering Methods with Examples and Exercises, 2012.

[15] J.H. Ferziger, M. Peric, Computational Methods for Fluid Dynamics, 1996.

[16] V. Gavan, M. Woloszyn, F. Kuznik, J.-J. Roux, Experimental study of a mechanically ventilated double-skin façade with Venetian sun-shading device: a full-scale investigation in controlled environment, Sol. Energy 84 (2) (2010), 183–195.

[17] M. Dopudi, "Naturally Ventilated Double Skin Facade: CFD and Simplified Model for Parametric Energy Simulation, Politecnico Milano, 2017.

[18] A. De Gracia, A. Castell, L. Navarro, E. Oro, L.F. Cabeza, Numerical modelling of ventilated facades: a review, Renew. Sustain. Energy Rev. 22 (2013) 539–549.

[19] J. Zhou, Y. Chen, A review on applying ventilated double-skin facade to buildings in hot-summer and cold-winter zone in China, Renew. Sustain. Energy Rev. 14 (4) (2010) 1321–1328.

[20] G. Cattarin, et al., Empirical validation and local sensitivity analysis of a lumped- parameter thermal model of an outdoor test cell, Build. Environ., Feb. (2018).

[21] E. Catto Lucchino, F. Goia, G. Lobaccaro, G. Chaudhary, Modelling of double skin facades in whole-building energy simulation tools: a review of current practices and possibilities for future developments, Build. Simul. 12 (1) (2019) 3–27.

[22] S.S.M. Foroushani, A New Technique for Characterizing Multi-Temperature Convection with Application in Building Energy Simulation, University of Waterloo, 2017.

[23] S. Foroushani, D. Naylor, J. Wright, A new formulation for convection problems entailing multiple isothermal boundaries, Int. J. Therm. Sci. 129 (2018) 396–403.

[24] S. Foroushani, D. Naylor, J.L. Wright, Heat transfer correlations for laminar free convection in vertical channels with asymmetrically heated isothermal walls, Heat Tran. Eng. 41 (5) (2020) 418-432.
[25] S. Foroushani, J.L. Wright, D. Naylor, Turbulent free convection in a vertical channel with isothermal walls: new formulation and the resistor-network model, Comput. Therm. Sci. 11 (1–2) (2019) 131–145.
[26] S.S.M. Foroushani, J.L. Wright, D. Naylor, Asymmetric graetz problem: the analytical solution revisited, J. Thermophys. Heat Tran. 31 (1) (2017) 237–242.
[27] S.S.M. Foroushani, D. Naylor, J.L. Wright, Convective heat transfer in hydrodynamically developed laminar flow in asymmetrically heated annuli: a three-temperature problem, in: Proceedings of the 12th Intl. Conf. Heat transfer Fluid Mechanics & Thermodynamics (HEFAT2016), 2016, pp. 527–532.
[28] S. Foroushani, J.L. Wright, D. Naylor, Resistor-network formulation of multitemperature free-convection problems, J. Thermophys. Heat Tran. 31 (3) (2017) 628–633.
[29] S.S.M. Foroushani, D. Naylor, J.L. Wright, "Convective heat transfer in hydrodynamically - developed laminar flow in asymmetrically - heated Annuli: a three-temperature problem, in: Proceedings of the 12th Intl. Conf. Heat Transfer Fluid Mechanics & Thermodynamics (HEFAT2016), 2016, pp. 527–532.
[30] J.L.M. Hensen, R. Lamberts, Building Performance Simulation for Design and Operation, vol. 9780203891, 2012.
[31] J. Han, L. Lu, H. Yang, Numerical evaluation of the mixed convective heat transfer in a double-pane window integrated with see-through a-Si PV cells with low-e coatings, Appl. Energy 87 (11) (2010) 3431–3437.
[32] S. Tkachenko, V. Timchenko, G. Yeoh, J. Reizes, Effects of radiation on turbulent natural convection in channel flows, Int. J. Heat Fluid Flow 77 (2019) 122–133.
[33] X. li Xu, Z. Yang, Natural ventilation in the double skin facade with Venetian blind, Energy Build. 40 (8) (2008) 1498–1504.
[34] Z.J. Zhai, Z. Zhang, W. Zhang, Q.Y. Chen, "Evaluation of various turbulence models in predicting airflow and turbulence in enclosed environments by cfd: Part 1—summary of prevalent turbulence models, HVAC R Res. 13 (6) (2007) 853–870.
[35] J. Smagorinsky, General circulation experiments with the primitive equations: 1. The basic experiment, Mon. Weather Rev. (1963).
[36] J.W. Deardorff, A numerical study of three-dimensional turbulent channel flow at large Reynolds numbers, J. Fluid Mech. 41 (2) (1970) 453–480.
[37] G.E. Lau, G.H. Yeoh, V. Timchenko, R.K.K. Yuen, Natural convection in a PV- integrated double-skin facade using large-eddy simulation, Procedia Eng. 14 (2011) 3277–3284.
[38] O.A. Tkachenko, et al., Numerical and experimental investigation of unsteady natural convection in a non-uniformly heated vertical open-ended channel, Int. J. Therm. Sci. 99 (2016) 9–25.
[39] H. Wang, Z. John, Zhai, Advances in building simulation and computational techniques: a review between 1987 and 2014, Energy Build. 128 (2016) 319–335.
[40] H. Choi, Y. An, K. Kang, S. Yoon, T. Kim, Cooling energy performance and thermal characteristics of a naturally ventilated slim double-skin window, Appl. Therm. Eng. 160 (2019) 114113.
[41] C. Popa, D. Ospir, S. Fohanno, C. Chereches, Numerical simulation of dynamical aspects of natural convection flow in a double-skin façade, Energy Build. 50 (2012) 229–233.
[42] T. Inan, T. Bas¸aran, M.A. Ezan, Experimental and numerical investigation of natural convection in a double skin facade, Appl. Therm. Eng. 106 (2016) 1225–1235.
[43] T. Inan, T. Basaran, A. Erek, Experimental and numerical investigation of forced convection in a double skin façade, Energies 10 (9) (2017).
[44] A. Pappas, Z. Zhai, Numerical investigation on thermal performance and correlations of double skin façade with buoyancy-driven airflow, Energy Build. 40 (4) (2008) 466–475.
[45] G.K. Batchelor, Heat transfer by free convection across a closed cavity between vertical boundaries at different temperatures, Q. Appl. Math. 12 (3) (1954) 209–233.
[46] E.R.G. Eckertf, W.O. Carlson, Natural convection in an air layer enclosed between two vertical plates with different temperatures, Int. J. Heat Mass Tran. 2 (1–2) (1961) 106–110.
[47] L. Mei, et al., The influence of blinds on temperatures and air flows within ventilated double-skin facades, Proc. Clima (2007). WellBeing Indoors, 2007.

[48] O. Kalyanova, P. Heiselberg, Experimental Set-Up and Full-Scale Measurements in the 'Cube, Aalborg, 2008.
[49] W. Ding, Y. Hasemi, T. Yamada, Natural ventilation performance of a double-skin façade with a solar chimney, Energy Build. 37 (4) (2005) 411–418.
[50] F. Marques da Silva, M.G. Gomes, A.M. Rodrigues, Measuring and estimating airflow in naturally ventilated double skin facades, Build. Environ. 87 (2015) 292–301.
[51] E. Giancola, et al., Possibilities and challenges of different experimental techniques for airflow characterisation in the air cavities of façades, J. Facade Des. Eng. 6 (Aug. 2018), https://doi.org/10.7480/jfde.2018.3.2470. No 3 Spec. Issue FAÇADE 2018 – Adapt.
[52] K.J. King, Turbulent Natural Convection in Rectangular Air Cavities, Queen Mary University of London, 1989.
[53] N. Safer, "Modelisation des façades de type double-peau equipees de protections solaires : Approches multi-echelles, L'Institut National des Sciences Appliquees de Lyon, 2006.
[54] M. Bhamjee, A. Nurick, D.M. Madyira, An experimentally validated mathematical and CFD model of a supply air window: forced and natural flow, Energy Build. 57 (2013) 289–301.
[55] S.A. Kalogirou, in: E. Kalogirou (Ed.), Chapter 4 - Performance of Solar Collectors, Second, Academic Press, Boston, 2014, pp. 221–256. S. A. B. T.-S. E. E.
[56] Y. Hu, P.K. Heiselberg, H. Johra, R. Guo, Experimental and numerical study of a PCM solar air heat exchanger and its ventilation preheating effectiveness, Renew. Energy 145 (2020) 106–115.
[57] A. Jankovic, B. Lalic, Analysis of statistical methods for estimating solar radiation, Geogr. Pannonica 18 (1) (2014) 1–5.
[58] A. Hazem, M. Ameghchouche, C. Bougriou, A Numerical Analysis of the Air Ventilation Management and Assessment of the Behavior of Double Skin Facades, " Energy Build., 2015.
[59] G. Michaux, R. Greffet, P. Salagnac, J.B. Ridoret, Modelling of an airflow window and numerical investigation of its thermal performances by comparison to conventional double and triple-glazed windows, Appl. Energy 242 (2019) 27–45.
[60] L.C.O. Souza, H.A. Souza, E.F. Rodrigues, Experimental and numerical analysis of a naturally ventilated double-skin façade, Energy Build. 165 (2018) 328–339.
[61] S. Preet, M.K. Sharma, J. Mathur, A. Chowdhury, S. Mathur, Performance evaluation of photovoltaic double-skin facade with forced ventilation in the composite climate, J. Build. Eng. 32 (2020) 101733.
[62] Y. Luo, L. Zhang, Z. Liu, L. Xie, X. Wang, J. Wu, Experimental study and performance evaluation of a PV-blind embedded double skin façade in winter season, Energy 165 (2018) 326–342.
[63] C. Lee, H. Lee, M. Choi, J. Yoon, Design optimization and experimental evaluation of photovoltaic double skin facade, Energy Build. 202 (2019) 109314.
[64] Y. Li, J. Darkwa, G. Kokogiannakis, Heat transfer analysis of an integrated double skin façade and phase change material blind system, Build. Environ. 125 (2017) 111–121.
[65] Y. Li, J. Darkwa, G. Kokogiannakis, W. Su, Phase change material blind system for double skin façade integration: system development and thermal performance evaluation, Appl. Energy 252 (2019) 113376.
[66] J. Curpek, M. Cekon, J. Hraska, PCM integrated in BiPV ventilated Façade concepts: experimental test cell platform and initial full-scale measurements, IOP Conf. Ser. Earth Environ. Sci. 290 (1) (2019) 12072.
[67] H. Elarga, F. Goia, A. Zarrella, A. Dal Monte, E. Benini, Thermal and electrical performance of an integrated PV-PCM system in double skin façades: a numerical study, Sol. Energy 136 (2016) 112–124.
[68] K. Cho, D. Cho, Solar heat gain coefficient analysis of a slim-type double skin window system: using an experimental and a simulation method, Energies 11 (1) (Jan. 2018) 115.
[69] C. Zhang, W. Gang, J. Wang, X. Xu, Q. Du, Numerical and experimental study on the thermal performance improvement of a triple glazed window by utilizing low- grade exhaust air, Energy 167 (2019) 1132–1143.
[70] F. Yang, F. Yuan, F. Qian, Z. Zhuang, J. Yao, Summertime thermal and energy performance of a double-skin green facade: a case study in Shanghai, Sustain. Cities Soc. 39 (2018) 43–51.
[71] X. Hong, M.K.H. Leung, W. He, Effective use of Venetian blind in Trombe wall for solar space conditioning control, Appl. Energy 250 (Sep. 2019) 452–460.

[72] O. Iken, S. ed-D. Fertahi, M. Dlimi, R. Agounoun, I. Kadiri, K. Sbai, Thermal and energy performance investigation of a smart double skin facade integrating vanadium dioxide through CFD simulations, Energy Convers. Manag. 195 (2019) 650–671.
[73] Z. Liang, et al., Tungsten-doped vanadium dioxide thin films as smart windows with self-cleaning and energy-saving functions, J. Alloys Compd. 694 (2017) 124–131.
[74] G. Baldinelli, Double skin façades for warm climate regions: analysis of a solution with an integrated movable shading system, Build. Environ. 44 (6) (2009) 1107–1118.
[75] A. Zollner, E.R.F. Winter, R. Viskanta, Experimental studies of combined heat transfer in turbulent mixed convection fluid flows in double-skin-façades, Int. J. Heat Mass Tran. 45 (22) (2002) 4401–4408.
[76] H. Manz, A. Schaelin, H. Simmler, Airflow patterns and thermal behavior of mechanically ventilated glass double facades, Build. Environ. 39 (9) (2004) 1023–1033.
[77] I. Perez-Grande, J. Meseguer, G. Alonso, Influence of glass properties on the performance of double-glazed facades, Appl. Therm. Eng. 25 (17–18) (Dec. 2005) 3163–3175.
[78] T.E. Jiru, Y.X. Taob, F. Haghighat, Airflow and heat transfer in double skin facades, Energy Build. 43 (10) (2011) 2760–2766.
[79] F. Kuznik, T. Catalina, L. Gauzere, M. Woloszyn, J.J. Roux, Numerical modelling of combined heat transfers in a double skin faade - full-scale laboratory experiment validation, Appl. Therm. Eng. 31 (14–15) (2011) 3043–3054.
[80] A. Guardo, M. Coussirat, E. Egusquiza, P. Alavedra, R. Castilla, A CFD approach to evaluate the influence of construction and operation parameters on the performance of Active Transparent Façades in Mediterranean climates, Energy Build. 41 (5) (2009) 534–542.
[81] S. Yan, X. Li, B. Wang, W. Shi, W. Lyu, A method to describe the thermal property of pipe-embedded double-skin façade: equivalent glass window, Energy Build. 195 (2019) 33–44.
[82] J. Curpek, M. Cekon, J. Hraska, PCM integrated in BiPV ventilated façade concepts: experimental test cell platform and initial full-scale measurements, IOP Conf. Ser. Earth Environ. Sci. 290 (2019), 012072.
[83] S.P. Corgnati, M. Perino, V. Serra, Experimental assessment of the performance of an active transparent façade during actual operating conditions, Sol. Energy 81 (8) (Aug. 2007) 993–1013.
[84] D. Saelens, Energy Performance Assessment of Single Storey Multiple-Skin Facades, Catholic University of Leuven, 2011.
[85] E. Colombo, M. Zwahlen, M. Frey, J. Loux, Design of a glazed double-façade by means of coupled CFD and building performance simulation, Energy Procedia 122 (2017) 355–360.
[86] Y. Katoh, M. Miyamoto, J. Kurima, S. Kaneyasu, "Turbulent free convection heat transfer from vertical parallel Plates: effect of entrance bell-mouth shape, in: JSME Int. journal. Ser. 2, Fluids Eng. heat Transf. power, Combust. Thermophys. Prop. 34, 1991, pp. 496–501, 4.
[87] Y. Cherif, E. Sassine, S. Lassue, L. Zalewski, Experimental and numerical natural convection in an asymmetrically heated double vertical facade, Int. J. Therm. Sci. 152 (2020) 106288.
[88] A.A. Dafa'Alla, P.L. Betts, Experimental study of turbulent natural convection in a tall air cavity, Exp. Heat Tran. 9 (2) (1996) 165–194.
[89] D. Saelens, J. Carmeliet, H. Hens, Energy performance assessment of multiple- skin facades, HVAC R Res. 9 (2) (2003) 167–185.
[90] A. Dama, D. Angeli, O. Kalyanova Larsen, Naturally ventilated double-skin façade in modeling and experiments, Energy Build. 114 (2017) 17–29.
[91] S. Hassanli, K.C.S. Kwok, M. Zhao, Performance assessment of a special Double Skin Façade system for wind energy harvesting and a case study, J. Wind Eng. Ind. Aerod. 175 (2018) 292–304.
[92] T. Zhang, H. Yang, Flow and heat transfer characteristics of natural convection in vertical air channels of double-skin solar façades, Appl. Energy 242 (2019) 107–120.
[93] K. Hou, S. Li, H. Wang, Simulation and experimental verification of energy saving effect of passive preheating natural ventilation double skin façade, Energy Explor. Exploit. (Sep. 2020), 0144598720956288.

[94] S. El Ahmar, F. Battista, A. Fioravanti, Simulation of the thermal performance of a geometrically complex Double-Skin Facade for hot climates: EnergyPlus vs OpenFOAM, Build. Simul. 12 (5) (2019) 781–795.
[95] N. Kimouche, Z. Mahri, A. Abidi-Saad, C. Popa, G. Polidori, C. Maalouf, Effect of inclination angle of the adiabatic wall in asymmetrically heated channel on natural convection: application to double-skin façade design, J. Build. Eng. 12 (2017) 171–177.
[96] E. Sanchez, A. Rolando, R. Sant, L. Ayuso, Influence of natural ventilation due to buoyancy and heat transfer in the energy efficiency of a double skin facade building, Energy Sustain. Dev. 33 (2016) 139–148.
[97] B. Koo, K. Lee, Y. An, K. Lee, Solar heat gain reduction of ventilated double skin windows without a shading device, Sustainability 10 (2) (Dec. 2017) 64.
[98] I.A.E.-K.M. Amaireh, Numerical Investigation into a Double Skin Façade System Integrated with Shading Devices, with Reference to the City of Amman, University of Nottingham, Jordan, 2017.
[99] D.D. Kim, Computational fluid dynamics assessment for the thermal performance of double-skin façades in office buildings under hot climatic condition, Build. Serv. Eng. Technol. (Aug. 2020), 0143624420952962.
[100] Y. Tao, H. Zhang, L. Zhang, G. Zhang, J. Tu, L. Shi, Ventilation performance of a naturally ventilated double-skin façade in buildings, " Renew. Energy, 2020.
[101] E. Lee, S. Selkowitz, V. Bazjanac, V. Inkarojrit, C. Kohler, High-Performance Commercial Building Façades, Berkeley, 2002.
[102] D. Angeli, A. Dama, Modelling natural ventilation in double skin facade, Energy Procedia 78 (2015) 1537–1542.
[103] S. Hassanli, K. Chauhan, M. Zhao, K.C.S. Kwok, Application of through-building openings for wind energy harvesting in built environment, J. Wind Eng. Ind. Aerod. 184 (2019) 445–455.
[104] S. Hassanli, G. Hu, D.F. Fletcher, K.C.S. Kwok, Potential application of double skin façade incorporating aerodynamic modifications for wind energy harvesting, J. Wind Eng. Ind. Aerod. 174 (2018) 269–280.
[105] S. Matour, V. Garcia Hansen, R. Drogemuller, S. Omrani, S. Hassanali, Natural ventilation of double skin façade: evaluation of wind-induced airflow in tall buildings, in: 35th PLEA Conference Sustainable Architecture and Urban Design Planning: Post Carbon Cities, 2020.
[106] S. Hassanli, G. Hu, K.C.S. Kwok, D.F. Fletcher, Utilizing cavity flow within double skin façade for wind energy harvesting in buildings, J. Wind Eng. Ind. Aerod. 167 (2017) 114–127.
[107] B. Bielek, D. Szabo, M. Palko, M. Rychtarikova, Optimisation of design of air inlets in air distribution channels of a double-skin transparent façade, Slovak J. Civ. Eng. 25 (4) (2017) 1–11.
[108] M.N. Sanchez, E. Giancola, E. Blanco, S. Soutullo, M.J. Suarez, Experimental validation of a numerical model of a ventilated façade with horizontal and vertical open joints, Energies 13 (1) (Dec. 2019) 146.
[109] N. Pourshab, M.D. Tehrani, D. Toghraie, S. Rostami, Application of double-glazed façades with horizontal and vertical louvers to increase natural air flow in office buildings, Energy 200 (2020) 117486.
[110] H. El-Sadi, F. Haghighat, A. Fallahi, CFD analysis of turbulent natural ventilation in double-skin faade: thermal mass and energy efficiency, J. Energy Eng. 136 (3) (2010) 68–75.
[111] Y. Ji, M.J. Cook, V. Hanby, D.G. Infield, D.L. Loveday, L. Mei, CFD modelling of naturally ventilated double-skin facades with Venetian blinds, J. Build. Perform. Simul. 1 (3) (2008) 185–196.
[112] V.I. Hanby, et al., Nodal network and CFD simulation of airflow and heat transfer in double skin facades with blinds 29 (1) (2008) 45–59.
[113] D. Iyi, R. Hasan, R. Penlington, C. Underwood, Double skin fa??ade: modelling technique and influence of Venetian blinds on the airflow and heat transfer, Appl. Therm. Eng. 71 (1) (2014) 219–229.
[114] C. Jimenez-Xaman, et al., Solar chimneys with a phase change material for buildings: an overview using CFD and global energy balance, Energy Build. 186 (2019) 384–404.
[115] J.P. Varughese, M.M. John, Effect of emissivity of shading device and air flow inside cavity of Double Skin Facade for energy saving and Thermal Comfort in buildings: a CFD modeling, in: 2016

International Conference on Energy Efficient Technologies for Sustainability, ICEETS 2016, 2016, pp. 815–820.
[116] Y. Li, J. Darkwa, W. Su, Investigation on thermal performance of an integrated phase change material blind system for double skin façade buildings, Energy Procedia 158 (2019) 5116–5123.
[117] Y. Li, J. Darkwa, G. Kokogiannakis, W. Su, Effect of design parameters on thermal performance of integrated phase change material blind system for double skin façade buildings, Int. J. Low Carbon Technol. 14 (2) (Jun. 2019) 286–293.
[118] C. Shen, X. Li, Solar heat gain reduction of double-glazing window with cooling pipes embedded in Venetian blinds by utilizing natural cooling, Energy Build. 112 (2016) 173–183.
[119] C. Shen, X. Li, Thermal performance of double skin façade with built-in pipes utilizing evaporative cooling water in cooling season, Sol. Energy 137 (2016) 55–65.
[120] M. Coussirat, A. Guardo, E. Jou, E. Egusquiza, E. Cuerva, P. Alavedra, Performance and influence of numerical sub-models on the CFD simulation of free and forced convection in double-glazed ventilated façades, Energy Build. 40 (10) (2008) 1781–1789.
[121] R. Fuliotto, F. Cambuli, N. Mandas, N. Bacchin, G. Manara, Q. Chen, Experimental and numerical analysis of heat transfer and airflow on an interactive building facade, Energy Build. 42 (1) (Jan. 2010) 23–28.
[122] Z. Zeng, X. Li, C. Li, Y. Zhu, Modeling ventilation in naturally ventilated double- skin façade with a Venetian blind, Build. Environ. 57 (2012) 1–6.
[123] D. Brandl, T. Mach, M. Grobbauer, C. Hochenauer, Analysis of ventilation effects and the thermal behaviour of multifunctional façade elements with 3D CFD models, Energy Build. 85 (2014) 305–320.
[124] X. Hong, W. He, Z. Hu, C. Wang, J. Ji, Three-dimensional simulation on the thermal performance of a novel Trombe wall with Venetian blind structure, Energy Build. 89 (2015) 32–38.
[125] T. Basaran, T. Inan, Experimental investigation of the pressure loss through a double skin facade by using perforated plates, Energy Build. 133 (2016) 628–639.
[126] T. Inan, T. Basaran, Experimental and numerical investigation of forced convection in a double skin façade by using nodal network approach for Istanbul, Sol. Energy 183 (2019) 441–452.
[127] W. Chiu, F.J. Rixon, High resolution structural studies of complex icosahedral viruses: a brief overview, Virus Res. 82 (1–2) (2001) 9–17.
[128] R. Li, A. Pitts, Y. Li, Buoyancy-driven natural ventilation of a room with large openings, in: IBPSA 2007 - International Building Performance Simulation Association 2007, 2007, pp. 984–991.
[129] G. He, L. Shu, S. Zhang, Double skin facades in the hot summer and cold winter zone in China: cavity open or closed? Build. Simul. 4 (4) (2011) 283–291.
[130] S. Tkachenko, V. Timchenko, Yeoh, Heng Guan, J.A. Reizes, Effects of radiation on turbulent natural convection in channel flows, Int. J. Heat Fluid Flow 77 (2019) 122–133.
[131] V. Sambou, “Transferts thermiques instationnaires: vers une optimisation de parois de batiments.” Universite de Toulouse, Universite Toulouse III-Paul Sabatier, 2008.
[132] T. Yilmaz, S.M. Fraser, Turbulent natural convection in a vertical parallel-plate channel with asymmetric heating, Int. J. Heat Mass Tran. 50 (13–14) (2007) 2612–2623.
[133] B.W. Webb, D.P. Hill, High Rayleigh number laminar natural convection in an asymmetrically heated vertical channel, J. Heat Tran. 111 (3) (1989) 649–656.

3. Laboratory testbed and methods for flexible characterization of thermal and fluid dynamic behaviour of double skin facades

3.1. Abstract

Heat and mass transport in double skin façades (DSFs) are complex phenomena driven by boundary conditions and are in constant non-linear interaction with the constructional elements of the DSF. Comprehensive experimental investigations to understand these complex behaviors are usually rigid, time-consuming and expensive. In this paper, we present the concept and the features of a flexible experimental testbed that, in conjunction with optimized experimental procedures, can facilitate comprehensive investigations and performance assessment of DSFs. The testbed, which consists of an adjustable DSF mock-up placed into a climate simulator, allows many DSF configurations to be investigated in combination with a wide range of boundary conditions. Several methods for different types of experimental investigations with various levels of complexity are presented: standard metrics measurements, one-factor analysis, design of experiments and dynamic profile measurements. By providing examples and discussing the limitations, challenges and possibilities of each investigation method, the paper aims to provide an overview of different characterizations suitable to assess how different constructional features and boundary conditions affect the performance of DSFs. Experimental data collected during this study are also made available in a data repository for future independent scientific analyses of DSF thermophysical behavior or numerical models' validation.

Nomenclature

Symbols

C	Thermal conductance [$Wm^{-2}K^{-1}$]
c	Specific heat capacity [$Jkg^{-1}\,°C^{-1}$]
co	Contribution [%]
d	Depth [cm]
err	Error [depend on the quantity]
g	Solar factor, g-value [–]
h	Surface heat transfer coefficients [$Wm^{-2}K^{-1}$]
I	Solar irradiance [Wm^{-2}]
$\dot{m}$	Air mass flow rate [kgs^{-1}]
q	Heat flux density, heat flux rate [Wm^{-2}]
p	p-value [–]
t	Temperature [°C]
U	Thermal transmittance, U-vlaue [$Wm^{-2}K^{-1}$]
V	Airflow rate [m^3h^{-1}]
Δ	Difference [–]
φ	Angle [°]
γ	Dynamic insulation efficiency [–]
τ	Direct solar transmittance [–]

Subscripts

cav	refer to cavity
e	refer to efficiency
HFM	refer to heat flux meter
i	refer to inner
ic	refer to the inner half-cavity
ig	refer to the inner glazing
ii	refer to the inner side of inner glazing
in	refer to the incident
io	refer to the outer side of inner glazing
net	refer to net gain/loss
o	refer to outside
oc	refer to the outer half-cavity
oi	refer to the inner side of outer glazing
og	refer to the outer glazing
oo	refer to the outer side of outer glazing
p	refer to constant pressure
sh	shading
tr	refer to transmitted
vent	refer to convective heat gain/loss that is absorbed/released by the airflow that passes through the cavity

Acronyms

AM	Ante meridiem, before noon
ANOVA	Analysis of variance
ADC	Analog-to-digital converter
BIG	Big size of the opening
CO2	Carbon-dioxide
D	Depth
DOE	Design of experiments
DSF	Double skin facade
I–I	Indoor air curtain
ISO	International standard organization
ISR	Solar irradiance
F	Factor
FPGA	Field Programmable Gate Arrays
H	Height
HFM	Heat flow meter
L	Level
MED	Medium size of the opening
O–O	Outdoor air curtain
PIV	Particle image velocimetry
RH	Relative humidity of air
RTU	Remote terminal unit
SHGC	Solar heat gain coefficient
SHTC	Surface heat transfer coefficient
SMALL	Small size of the opening
SMI	Standard motor interface
T	Air temperature
TD	Taguchi design
VB	Venetian blinds
VPM	Velocity profile method
W	Width

3.2. Introduction

A double-skin facade (DSF) is a building envelope system that consists of an internal and external layer, usually highly transparent, with a cavity between the two skins, which is ventilated with air, and where a device for a solar and visual gain control can be installed [1]. This building envelope technology originates from the need to assure high occupant comfort [2] and effective heating, cooling, indoor air quality and daylighting control strategies [3] in the context of highly transparent building envelopes. Due to greater complexity than standard, single-skin envelope elements, finding the optimal configuration (both in terms of construction features and operational modes) for a DSF that assures the best performance across multiple domains is often rather challenging [4]. Physical processes, including transport of mass, momentum and heat/energy, are driven by the surrounding environment and are affected by the constructional features. Therefore, they are more challenging to predict in a DSF than in a single-skin facade [5], and this complexity directly impacts the reliability of the design solutions adopted for DSFs.

The complex interrelation of physical processes occurring in a DSF system can be investigated through experimental studies, thereby expanding our understanding of how constructional features

and operational modes can be fine-tuned to achieve a given performance. In addition to this direct knowledge gain, experimental characterizations represent a source of data to validate numerical models. Systematic experimental investigations and robust validations of numerical models can only be achieved if a sufficiently large range of possibilities is experimentally tested in terms of boundary conditions, construction features and operational modes – something that is difficult to achieve by testing one particular DSF configuration in a specific building or testing condition.

Many experiments have been performed so far with different levels of complexity, of which the largest number makes use of outdoor natural boundary conditions [6–23]. The major limitation of this type of experiment is that they do not allow one to set specific boundary conditions deliberately, and to isolate certain effects to focus the study on one or more particular aspects is also quite challenging in most cases. Experiments in a controlled environment can instead offer conditions that overcome these limitations and thus represent a powerful tool to systematically assess, both in-depth and in breadth, the thermo-physical behavior of DSF systems. Equipment for controlled experiments usually only allows one to perform tests in steady-state conditions, where a particular performance indicator is examined in response to a combination of controllable factors maintained at constant levels. Traditionally, due to the historical focus placed on the performance in relation to a certain thermal gradient, the majority of these experiments were performed in conditions where only the thermal environment was included in the characterization, and analyses of DSF systems have followed this trend too [24–31]. Experiments where both thermal gradient and impinging radiation (to replicate the effect of solar radiation) are controlled are much rarer [32–34] due to an increase in the complexity of the equipment required to carry out these tests. There is no evidence in the literature of experiments where all the flow drivers (incident solar radiation, temperature, and wind) are controlled simultaneously.

To increase the possibilities for systematic performance characterization and theoretical investigation of DSF systems, we have developed, in the framework of a dedicated research project [35], a flexible testbed that gives researchers an extensive range of possibilities to fill the existing knowledge gaps and provide the research community with a comprehensive experimental dataset for model validation. The testbed we have conceived is made of an adaptable DSF mock-up installed into a state-of-the-art climate simulator equipped with integrated artificial sun lamps. The features of our characterization system make it possible and (relatively) easy to investigate an extensive range of DSF configurations, operational modes and boundary conditions, making it possible to deepen the knowledge of how constructional features and operations, environmental factors and their interactions influence the thermal and fluid dynamics behavior of DSF systems.

The aim of this paper is to present the concept, design and features of the experimental set-up, to report its verification and calibration, and to demonstrate, through a series of exemplification studies, the possible investigation methods that can be adopted to address open questions about the thermal and fluid dynamics behavior of DSF facades. The array of experimental methods shown in this article aims to highlight how different methods, rather than being alternative techniques to study the same aspect, are complementary approaches that target the many ways of studying and assessing the behavior of a double skin façade. Through this, we aim to illustrate how different performance metrics that address different phenomena are necessary when studying the performance of DSFs.

In an effort to enable the whole scientific community to access experimental data for further analysis or for model validation purposes, we release together with this paper a set of experimental data collected during the first tests carried out with the use of the newly developed testbed. In this context, the paper also becomes an essential tool for understanding how to read and understand publicly released experimental data. The remainder of this paper is structured as follows. In Section 2, we present the experimental set-up, with the characteristics of the flexible mock-up, the experimental facility, hardware and software for controlling and monitoring the experiment. In Section 3, we focus on the different methods that can be employed in combination with the flexible testbed. We report therein the details about the verification and calibration of the experimental set-up, and then present four methods for the characterization of thermal and fluid-dynamics behavior of DSF, namely a method for standardized metrics measurements, the one-factor analysis, the design of the experiments (DOE) and dynamic profile measurements. In Section 4, we demonstrate the use of the testbed and the different methods by showing the results of four investigations. Though the focus of the paper is not placed on the results obtained through the different experimental runs, we briefly discuss in this section the significance of some of the findings. In Section 5, we discuss the challenges and limitations of the different experimental investigations carried out with the newly developed testbed. We also reflect on the possibilities enabled by this experimental system and on how different methods and investigations can target different ways of assessing the behavior of DSFs.

3.3. Experimental testbed

3.3.1. The flexible DSF mock-up

A new flexible testbed has been realized and designed to operate in combination with the climate simulator so the current knowledge on the thermal and fluid mechanical behavior of DSF can be expanded [3]. A mock-up is equipped with a sequence of different actuators allowing, in combination with a climate simulator, a systematic and parametric analysis of the performance of tested DSF

technology [4]. Different cavity depths ranging from 200 to 600 mm, the angle and the presence of venetian blinds and the airflow produced by the fans can be manipulated systematically. Furthermore, it is possible to control the airflow path by opening and closing the corresponding vents on the tested element. In combination with a climate simulator, a testbed offers high flexibility in testing desirable configurations and boundary conditions, both in a steady and transient state. The physical properties of DSF are monitored through more than seventy sensors for the acquisition of temperature, airflow, relative humidity, differential pressure, irradiance and many more.

DSF mock-up specifications

Test-sample is a full-scale DSF consisting of inner and outer transparent skins mounted into the aluminum frame with a thermal break (Fig. 1a). Both skins are composed of 4 mm thick double glazing with a 15 mm gap filled with a mixture of air and argon (1–9 ratio). The outer pane is clear, while the inner pane is low-E glass with a coating applied on the side in contact with the gap. The glazing area is 3.92 m^2 (W - 1.4 m X H – 2.8 m). Space between the inner and outer skin can be ventilated and contains venetian blinds as a shading device. It is possible to change its depth between 20 and 60 cm thanks to a scissor system driven by the unidirectional electrical motor (24V). The shading device is equipped with 58 slats painted in white aluminum color (RAL 9006) with estimated reflectivity between 0.5 and 0.6, length of 150 cm and width of 5 cm. Venetian blinds can be lowered and raised, and the angle of slats can be adjusted between 90^0 and near to 0^0 (closed). The DSF has four openings, two placed in the outer skin (one at the bottom and one at the top) and two placed in the inner skin (again, at the bottom and at the top). This feature makes it possible to obtain different airflow paths depending on which two of the four possible openings are kept open. Closing all four openings means maintaining the DSF in the thermal buffer state, thus insulating the ventilated cavity from both the outdoor and the indoor environment. In the experimental investigations presented in this paper as a demonstration of the test bed functionality, we have tested three airflow paths: thermal buffer (no airflow path, TB), indoor air curtain (I–I) and outdoor air curtain (O–O) ventilation modes. In the I–I airflow path, the ventilated cavity receives air from the indoor environment (usually through the bottom opening) and releases the air again to the indoor environment (usually through the top opening). In the O–O ventilation mode, outdoor air usually enters the cavity through the lower opening on the outer skin and leaves the cavity through the upper opening on the same side, thus returning to the outside environment (Fig. 1b). The flow inside the cavity can be driven mechanically by ten small fans (SanAce 60L) with dimensions of 60 × 60 × 25 mm^3 installed at the top of the cavity.

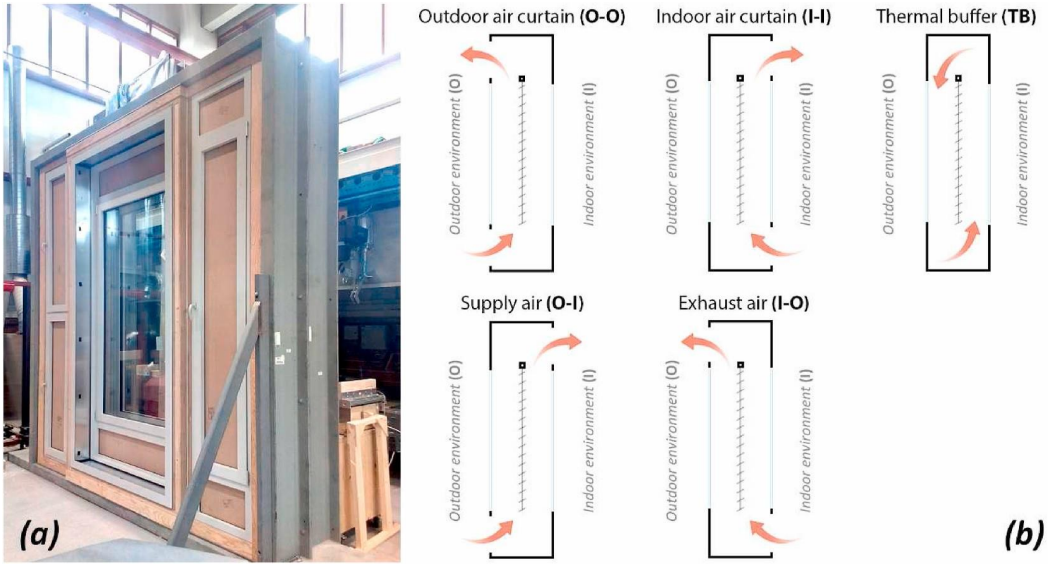

Fig. 1. ***(a)*** The façade mock-up assembled in the metal frame ready for installation in the climate simulator. At the two sides of the mock-up with an expandible cavity, two cabinets host the monitoring and control system and a ventilation section for airflow calibration. (***b)*** Possible ventilation paths allowed by the façade mock-up.

Measurement system

In order to obtain the desired information on the thermal and fluid dynamics behavior of DSFs, both thermal and velocity fields were intended to be monitored in the cavity, as well as the temperature and incident radiation distribution on the glazing surfaces. In addition to these, several other quantities were also recorded, leading to a large number of instruments (more than 70) installed in the test bed, as described in Table 1. Pyranometers were employed to measure incident solar radiation on the outer surface of DSF and the transmitted solar radiation into the indoor room. The air temperature was measured in the indoor and outdoor room at three heights, while in the central height, besides air temperature, relative humidity was measured as well. Hot- wire anemometers were placed in 12 position along three heights in the cavity so that profiles of the temperature and vertical component of velocity could be obtained (Fig. 3). Near the inlet and the outlet, the air temperature was measured in the four positions, two in the inner and two in the outer part of the cavity. Pressure difference was measured along three paths: across the inlet, across the outlet and along the cavity. Resistance temperature sensors (pt100) were placed at the four glazing surfaces to measure temperature along three heights and additionally temperatures of the frame between the openings and inner-outer and outer-inner glazing. Heat flux density through blinds and four glazing surfaces was measured, where two heat flux plates were connected in the series to determine the average heat flux that passes through inner- inner and outer-outer glazing. An ultrasonic airflow meter was placed in the airflow box to

calibrate different techniques to assess airflow rate. Five photovoltaic pyranometers were placed on the outer-outer glazing to evaluate the uniformity of incident solar radiation.

Table 1. Characteristics of the sensors used in the experimental campaign.

Sensor type	Manufacturer (model)	Signal	Outside	Bottom openings	Outer-outer	Outer-inner	Outer half-cavity	Shading	Inner half-cavity	Inner-outer	Inner-inner	Top openings	Inside	Airflow box	Quantity	Symbol	Accuracy/ uncertainty (in a considered range)
Pyranometer	DeltaOhm (LPPYRA03ACM12)	4 … 20 mA	1										1		2	1	Second class pyranometer (ISO 9060)
Air temperature and relative humidity sensor	DeltaOhm (HD48S17TV)	Digital (RS485)	1										1		2	2	RH: ±1.5 %RH for (0 … 90 %RH) t: ±0.3 °C for (0 … 70 °C)
Air temperature sensor	DeltaOhm (HD48S07TV)	Digital (RS485)	2										2		4	3	±0.3 °C for (0 … 70 °C)
Hot-wire anemometers	DeltaOhm (HD2937TC1.5)	4 … 20 mA					6		6						12	4	v: ± (0.1 m/s+3% of meas.) for (0 … 1 m/s) and t: ±0.3 °C
Air temperature sensor	DeltaOhm (HD4807TC1.5)	4 … 20 mA					4		4						8	5	±0.3 °C for (0 … 70 °C)
Differential pressure meter	DeltaOhm (HD404T1PDAZ)	4 … 20 mA or 0 … 10V		1			1		(1)			1			3	6	±1.5% of range (± 50 Pa) for (0 … 50 °C)
CO_2 concentration sensor	DeltaOhm (HD37BTC)	0 …. 10V	1												1	7	± (50 ppm +3% of meas.) for (0 … 2000 ppm) at 20 °C, 50 %RH
Airflow sensor	Lindab (Ultralink monitor FTMU)	Digital (RS485)												1	1	8	±5% of meas. or ±2.0 l/s for 200 mm diameter
Resistance temperature detector Pt100	SterlingSensors (Rubber Patch)	3 wire PT100			4	6		4		6	4				24	9	Class B (IEC 60751:2008)
Heat flux plate	Hukseflux (HFP01)	±120 mV			2	2				2	2				8	10	Calibration uncertainty: <3% In ideal conditions: ±6%
Heat flux film	greenTEG AG (gSKIN XM 26 9C)	±600 mV						2							2	11	Calibration uncertainty: ±3%
Photovoltaic pyranometer	Soluzione Solare (LM1-10V PRO)	0 …. 10V			5										5	13	Calibration uncertainity: I: ± 3.5%, t: ±1.5 °C

We implemented best-practice solutions, as available in the literature [36], to reduce to influence of solar irradiation on the measurements of temperature, heat flux and velocity (the absorption of the incident solar radiation by the sensors' surface may lead to incorrect values). For example, HFMs were protected with adhesive reflective aluminum tape from additional heating by absorbed solar radiation. Protection against irradiance and normal ventilation of the surface temperature sensors was enabled by placing them under a hollow half-cylinder with a highly reflective outer surface. A plate of high reflectivity protected the side of the hot wire-anemometers exposed to the solar simulator (Fig. 2).

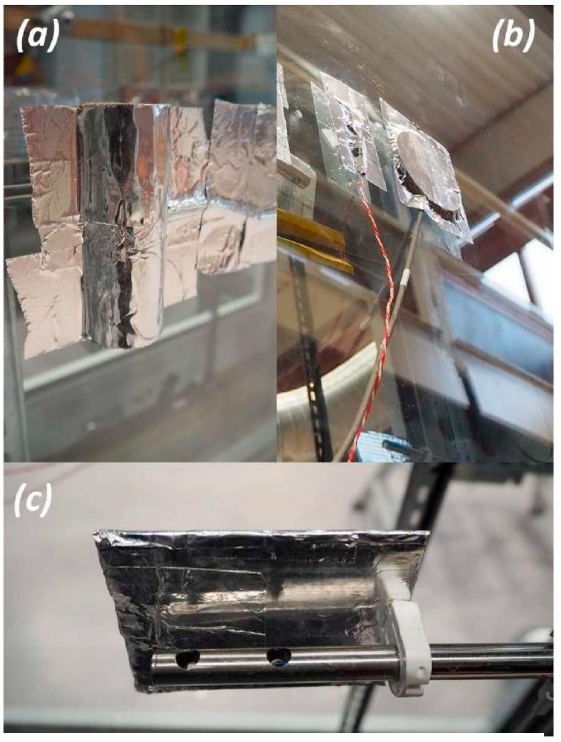

Fig. 2. Shielding of the sensors to avoid influence of solar radiation. (a) Shielding of surface temperature sensors. (b) Shielding of heat flux meters. (c) Shielding of hot-wire anemometers.

Onboard system for monitoring and control

Since many sensors were needed for monitoring, it was almost impossible to manage them manually. Instead, a system for automatic control and monitoring of the experiment was developed. A communication system was developed based on the sensor's output signal (analog voltage or current or digital RS-485). All sensors were connected to the multiplexing station composed of several acquisition cards, and 13 analog-to-digital converters (ADC) were used to combine multiple analog and digital signals into one digital signal. The multiplexing station was connected to the RS-485 port of the microcontroller – Compact Single-Board Controller (National instrument sbRIO: 9627) equipped with Field Programmable Gate Arrays (FPGA), which enabled sbRIO 9627 to work both as the source of the output signal and the receiver of the data from the sensors and ADCs.

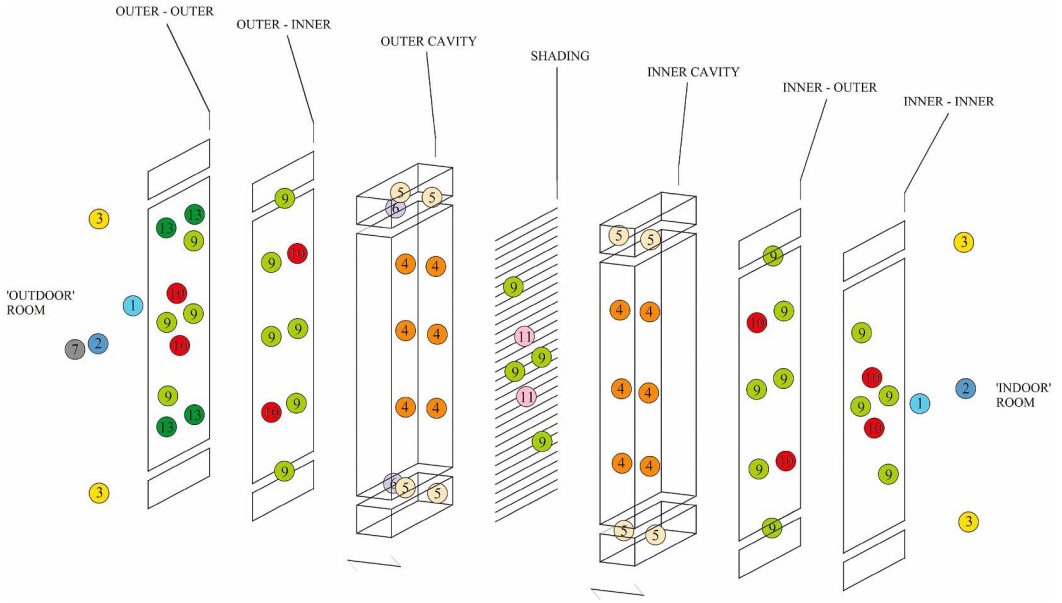

Fig. 3. Arrangement of sensors (for symbols, refer to Table 1).

Monitoring and data acquisition software deployed on the sbRIO: 9627 was developed in the LabVIEW environment. This platform contains a library of function tools based on which system for monitoring and control is developed. The Modbus library was extensively employed to control 13 ADCs used to collect analog signals from transducers and transmitters and convert them into a Modbus RTU signal. The system for monitoring and control was equipped with a graphic interface and developed to manage the measurements and main features of the test facility (cavity depth, fans rotation, shading proximity to glazing, and blind angle). The sampling data from sensors was set to the interval of 10 s, but various options were enabled to suit the data acquisition frequency for different types of tests, including averaging of values. Most of the sensors and all ADCs used the RS-485 protocol to communicate with the sbRIO 9627.

3.3.2. Climate simulator

The DSF mock-up was installed into a large metal frame that allowed the sample to be placed in the climate simulator, which is an indoor experimental facility designed to simulate indoor and outdoor conditions in terms of air temperature and humidity, rain, incident solar radiation and pressure difference. The Climate simulator has a total installed power of 40 kW and consists of two test cells; one is intended to simulate the outdoor environment and the other to simulate the indoor environment (Fig. 4a). Both rooms are insulated with 120 mm thick high density (40 kg/m^3) polyurethane foam with thermal conductivity of 0.0265 W/(mK). A test sample needs to be installed in the steel or wooden frame and placed between two rooms (Fig. 4b). Since the dimensions of the test sample can

measure up to 3.9 m in height, 3.6 in width and 0.8 in thickness, placing the frame and test sample in the required position is done using a bridge crane. The outdoor room measures 3700 × 1500 × 3240 mm^3 (W x D x H) and has a solar simulator (sun simulation system) and rain test system installed. The air temperature can be simulated in the range between − 20 and 80 ˚C with an accuracy of ±0.3 ˚C and a maximum rate of 0.5 ˚C/min. However, some limitations were experienced when particular combinations of temperature and solar irradiation were requested, as further specified further below.

Fig. 4. The climate simulator facility (a); the DSF test sample placed in the climate simulator (b) – view from the outdoor chamber with the solar simulator's lamp array on the left-hand side of the picture and the DSF mock-up on the right-hand side of the picture.

Relative humidity can be replicated in the range of 20–95% without simultaneous use of the solar simulation system and in the range between 20 and 50% otherwise. The rain test system can produce rain intensity in the range of 10–100 $dm^3/(m^2h)$ with droplet size between 15 and 35 μm. The indoor room has the same dimensions as the outdoor room and can regulate the temperature, in the range 5 and 50 ˚C with an accuracy of ±0.3 ˚C and relative humidity in the range 20 and 95% with a precision of ±3%.

The system simulating solar radiation consists of the array (3 × 3) of metal halide lamps, and it is placed on the special wall construction facility with a surface 2400 × 2400 mm^2. According to technical specifications, irradiation power is 1000 W/m^2 at a 760 mm distance from the light source with a homogeneity ±10%. It must be pointed out here that homogeneity of the incident solar radiation on the tested DSF sample within these limits is sometimes tricky to achieve, primarily due to deteriorating imperfection of the solar simulator and different ages of lamps (hours of usage). Furthermore, it is important to mention that the directionality of the emitted radiation cannot be

controlled. The array of 9 lamps, which are evenly distributed in front of the sample area, and each equipped with a reflector that focuses the radiation towards the test zone, can't be oriented. Part of the radiation that leaves the array reaches the test specimen in a relatively narrow range close to the normal angle to the specimen's surface, and another part of the radiation that leaves the array behaves as diffuse radiation, reaching the specimen without a particular direction. This feature limits the capability to study in detail the relation between radiation direction and the DSF's shading device, but still allows one to analyze the role and the impact of the shading device, and even of different degrees of opening of the shading device, in relation to the intensity of the solar radiation.

The metal halide lamps installed in the array were specially designed for accurate sun simulation and continually emitted a spectrum very close to natural sunlight. The intensity of each lamp can be controlled with a resolution of 1% in a range between 50 and 100% of the maximum electric power drawn (2500 W). That may pose a problem if one wants to replicate conditions with low solar radiation, such as winter days or a gradual increase/decrease in incident solar radiation during sunrise/sunset. The default distance between light source housing and the outer surface of the test sample is approximately 1.05 m. In the specific case of the flexible DSF mock-up, where the cavity depth can be changed by retracting the inner or outer skin, it was observed that actual solar irradiance impinging on the façade mock-up depends on the distance between the sample and simulator, and it diminishes when the distance between the façade's outer skin and the lamp's array increases. Furthermore, accurately maintaining the set-point temperature in the outdoor chamber when the solar simulator is active is not trivial, primarily when a high level of irradiance is used and very low air temperature values are set. When it is necessary to produce solar irradiance in cold conditions (>400 Wm^{-2} and <20 ˚C), the difference between the measured and programmed temperature can be over 5 ˚C. In those circumstances, a vertical temperature gradient of up to 2 ˚C directed upwards can be observed in the outdoor chamber. Furthermore, the values of the simulated solar irradiance are not entirely stable and fluctuate if the high level of radiation (>800 Wm^{-2}) is to be replicated in addition to relatively low outside air temperatures (<15 ˚C).

3.4. Methods for experimental assessment

This section presents an overview of the experimental methods that can be employed to investigate thermophysical phenomena in DSFs, given the flexibility of the designed testbed. To begin with, we provide details about the general verification of the experimental set-up and the reliability of airflow measurements, highlighting the importance of proper verification/calibration prior to experimental analyses, and show how reliable and coherent the measurements carried out with our testbed are. We also indicate the level of depth one can dive into when it comes to analyzing certain thermophysical

phenomena. Thereafter, a basic characterization methodology is illustrated, referring to principles and guidelines accepted by the scientific community for measuring standardized metrics of ventilated and non-ventilated facade systems, such as solar heat gain coefficient, thermal and solar transmittance. However, to understand the behavior of DSFs under actual conditions that foresee the ventilation in the cavity, standardized measurements are not very helpful. Therefore, it is necessary to look for more detailed and non-standardized test methods. In this context, we present three alternative methods to study the comprehensive performance of DSF: 1) one-factor analysis, 2) design of the experiments (DOE), and 3) dynamic profile measurement. One-factor analysis implies analysis where the influence of a single factor is assessed by monitoring the dependent variable response to changes in only that factor. On the other side, the design of the experiment quantifies cause-and-effect relations between multiple factors and outputs in the studied system/process using statistical tools executed over results of systematically performed series of experiments [37]. The dynamic profile method aims to assess performance under 'real' transient conditions with the idea of simulating/replicating 'typical days' where one can study the DSF.

3.4.1. Climate simulator

Although all sensors installed in the testbed were factory calibrated without further adjustments, coherence tests between measurements were performed from time to time to check the correctness of the data acquired through the system. For example, readings between different temperature sensors (three types, in total 60) were compared in thermal equilibrium when both chambers of the climate simulator had the same temperatures. The sensors whose deviations with respect to the measurements of other sensors were larger than the instrument uncertainty were replaced, or their readings were calibrated [38]. The experimental uncertainty was then assessed using the method of error propagation [39], where the uncertainty of the final value is affected by the error of each sensor/device whose readings were used to calculate that value [40].

Monitoring the fluid dynamics behavior of double-skin facades represents the most delicate part of the thermal performance assessment [41]. The complexity is reflected through the sensitivity and accuracy of experimental equipment, which by their physical presence represent perturbation in the momentum field and thus influence the measurements. In addition to this, a short path to evolve a fully developed flow and variability in driving forces make measurements even more complicated. Since most techniques are either too complex to set up, such as particle image velocimetry (PIV) [42], or have an issue evaluating variable or low airflow rates, such as pressure difference or gas tracer method [43], there is no standardized method for measuring air flow rate in DSFs. Therefore, we opted for hot-wire anemometers and the velocity profile method (VPM) to estimate the airflow

rates [44] as a trade-off between the complexity of the set-up, accuracy, desired amount of information and compatibility with the climate simulator facility that is combined with the flexible mock-up.

In order to determine the range of airflow rates in which this method can be considered reliable, it was necessary to verify the experimental set-up by comparing the reading through the VPM with one technique that could measure the bulk airflow rate so that punctual readings of velocity values and velocity profiles could be referenced to bulk airflow values. To perform this verification, a rectangular-to-round connector element was installed at the outlet so that the air leaving the cavity was collected and forced by means of a fan external to the cavity, an ultrasonic flow meter (Lindab UltraLink® Monitor) placed between the cavity and the fan. The ultrasonic flow meter (UFM) was capable of measuring low airflow rates with an uncertainty of ±2 ls^{-1} (or 7.2 m^3h^{-1}) for the given set-up. The controllable fan can force, given the set-up, an airflow in the range of 100 and 1000 m^3h^{-1}.

Values of velocity of the airflow in the cavity were recorded at three heights (¼, ½ and ¾ of DSF height), using four anemometers at each height. Velocity readings from two hot-wire anemometers installed at the first height were too discordant from the other values collected at ½ and ¾ of DSF height, so we omitted the corresponding velocity profile from the analysis as the robustness of this profile was not sufficient. At each height, two anemometers were installed close to glazing surfaces facing the cavity, the other two were placed one at each side of the shading device. The airflow rate was calculated based on the area of the velocity profile multiplied by the width of DSF, where the direction of the airflow (+ or – sign of velocity) was evaluated based on the temperature comparison with bordering surfaces. The comparison of measured airflows was made for two different cavity depths (40 and 60 cm) and several fan power consumptions (10, 15, 20, 25, 38, 63, 75, 88, and 100% of maximum power usage).

3.4.2. Measurement of standardized metrics

The climate simulator allows evaluation of the U-value using the methodology defined by the international standard ISO 9869-1 [45]. In order to determine the thermal transmittance, the heat flow meter (HFM) method was used, where the test element is exposed to steady-state conditions and the corresponding value is calculated using the simple average technique. The DSF was tested in the air-buffer ventilation mode and subjected to the temperatures of 0 °C in the 'outdoor' room and 20 °C in the 'indoor' room with no incident radiation. Simultaneously, the heat flux density was measured in two points on the inner side of the inner glazing. The average value of those two was considered representative for the calculation of the U-value of the glazed part of the DSF.

The assessment of the solar heat gain coefficient (SHGC, total solar energy transmittance, solar factor, g-value) of a full-scale test element is not standardized [36]. However, a total solar energy transmittance given by the ISO standard 9050:2003 [46] can be divided into solar transmittance and secondary heat transfer towards the inside by convection and longwave radiation [47]. Therefore, it is possible to measure it in the climate simulator by measuring an incident and transmitted solar radiation by pyranometers and the heat flux density that passes through the heat flux meter towards the interior. In this way, a small share of a heat flow that originates due to the temperature difference between inside and outside is assigned to the solar heat gains, but if the corresponding temperature difference is low, then this share is negligible. Measurement conditions were taken from the ISO standard 15099: 2003 [48], the environmental summer conditions set for a test apparatus that includes a solar simulator, climatic chamber and a metering box [49]: internal temperature of 25 °C, external temperature of 30 °C and incident solar radiation of 500 Wm^{-2}. Just like for the U-value measurements, the DSF test sample was set into the air-buffer ventilation model, while the g-value was monitored for different cavity depths and angles of venetian blinds.

Moreover, thermal conductance of both glazing and heat transfer coefficients referent for the inner and outer surfaces (SHTC) were calculated from the referent measurements of heat flux density and air temperature. We calculated the measurement uncertainty of standardized metric, which consists of two parts; the uncertainty originating from the instrument limitations [45,50,51] and the standard deviation around the mean. As with most laboratory measurements in steady-state conditions, the part of the error emerging from the instrument imprecision is dominant over the statistical part. The uncertainty propagation method was used to assess the measurement error of indirectly measured quantity [39,40].

3.4.3. One-factor analysis

An experimental testbed allows a well-established method to investigate the impact of one parameter on one or more output variables by varying only that factor [52]. This strategy is also known as the one-factor analysis or local sensitivity analysis. It is a traditional approach to experimental investigation, where one can obtain detailed insight into how a change in a particular parameter affects other variables and the system's behavior. However, this approach can be misleading in examining the overall impact of a specific parameter in complex systems whose non-linear behavior is driven by the interaction of several factors [53]. There are different possibilities to carry out a one-factor analysis, depending on the goal of the investigation and the nature of the variables involved in the process. In this paper, we present, as an example, how the change of the airflow path affects

temperature and velocity distribution in the cavity of a chosen DSF configuration during typical conditions:

- tropical summer day (t_{out} = 40 °C, I = 800 Wm^{-2}), DSF configuration (d = 60 cm, shading closed, 0°)
- tropical summer night (t_{out} = 30 °C, I = 0 Wm^{-2}), DSF configuration (d = 60 cm, shading open, 90°)
- mid-latitude warm winter day (t_{out} = 10 °C, I = 400 Wm^{-2}), DSF configuration (d = 60 cm, shading 45°)

Alternative versions of the one-factor analysis could have been to fix the airflow path and the boundary conditions, and gradually change one of the variables in the problems within the entire range of values (for example, the cavity depth or the opening size), or to change the value within a given (small) range around different baseline values. One of the challenges to bear in mind when employing this method to test small variations is that the resulting effect may be too small to be quantified with a suitable accuracy by the monitoring system. However, a change in a value too low to be detected can also be read as an important result – i.e., the independent variable has little impact on the dependent variable.

3.4.4. Design of experiments (DOE)

The DOE implies the application of statistical tools to quantify and classify relations between different variables and performance indicators in the studied process [37]. However, to obtain a good evaluation, a series of experiments need to be performed systematically. One of the efficient approaches can be factorial experimental arrays (designs). Here, the experiments are performed in a series where several factors are altered in each run, which enables the assessment of their impacts. If the array is well designed, the impact of interactions between factors can be assessed as well [54]. In the experimental campaign that lasted over several months, we tested several factorial designs and other arrays directly derived from factorial analysis to find an optimal design that will provide us with a comprehensive picture of the thermal and fluid dynamics behavior of DSFs. These arrays include full factorial, definitive screening, central composite (response surface) and multilevel Taguchi designs. In this paper, the intention is to present preliminary results of the experimental campaign and demonstrate the application of the DOE approach in the characterization of thermophysical behavior and performance of DSFs.

The array used here is the Taguchi 4Lx4F L16 array consisting of only 16 experimental runs where four different factors are discretized in four levels. Several response quantities that outline thermal

and fluid dynamics behavior of DSF were chosen: airflow rate, net heat flux density associated with the DSF, heat gain/loss rate by the airflow that passes through the cavity normalized by the surface of DSF, the average temperature of the cavity and the average temperature of the inner surface of inner glazing (mathematical description is given in Table 2). The heat gain/loss rate through the convective heat exchange of the airflow becomes part of the net heat flux density for the indoor air ventilation mode since the airflow transfers heat, in that case, between the indoor environment and the cavity. The same quantity is not part of the net heat transfer in the outdoor ventilation mode, as in that case, airflow diverts heat towards the outside. Since it uses a relatively low number of experimental runs for such a high number of factors and levels, this design only offers insight into the main effects. However, it is good enough for an initial investigation into the processes that occur in DSF. Two different ventilation modes were tested separately via this array: indoor and outdoor air curtains.

Table 2 Description of factors and response quantities.

Factors	**Symbol**	**Unit**	**Levels**			
			I	**II**	**III**	**IV**
Incident solar radiation	I	[Wm^{-2}]	0	400	600	800
Temperature difference	Δt	[°C]	–15	–5	5	15
Angle of venetian blinds	φ	[°]	OFF	0	45	90
Cavity depth	d	[cm]	20	30	40	60
Response quantities		***Unit***	***Equation***			
Net heat flux density associated with DSF	q_{net}	[Wm^{-2}]	$q_{HFM} + q_{tr} + (q_{vent})$			
The average temperature of the cavity	t_{cav}	[°C]	$\frac{\sum_{i=1}^{n} t_{cav,i}}{n}$			
Airflow rate	$\dot{V}$	[m^{3}h^{-1}]	Velocity profile method			
Heat gain/loss rate by the airflow that passes through the cavity normalized by the DSF surface	q_{vent}	[Wm^{-2}]	$\frac{\dot{m}c_p(t_{out}-t_{inl})}{A}$			
The average temperature of the inner surface of inner glazing	t_{ii}	[°C]	$\frac{\sum_{i=1}^{n} t_{ii,i}}{n}$			

3.4.5. Dynamic profile measurements

Besides measurements in the steady-state conditions, the climate simulator offers execution of the experiment in a dynamical environment where the temperature of both rooms, incident solar radiation

and relative humidity can be preprogrammed. That allows insight into the thermal performance of DSFs during typical periods (summer or winter days) by examining dynamic diurnal profiles of specific quantities. Unlike natural experiments in a real outdoor environment [13,55,56], dynamic profile measurements in a controlled environment allow the researcher to focus on the specific situation, component of the façade system or driver of the performance, or to repeat the test to better capture the behavior of the system. On the other hand, these tests are usually limited because the wind effect cannot be replicated or because the climate simulator has its limitations, especially when it comes to the incident radiation adjustment. In our case, each lamp could be controlled only in the range between 50 and 100% of the maximum power, so we could not simulate the gradual increase and decrease of the incident solar radiation in the sunrise and sunset hours. Additionally, at high radiation levels, the irradiated energy is less stable than for other levels, probably due to the high-power consumption of the climate simulator.

The chosen DSF configuration was subjected to dynamic testing, corresponding to a typically hot summer day with high irradiation levels and outdoor temperatures. The temperature oscillated as a sine wave with the crest of 35 ˚C and trough of 20 ˚C, while incident solar radiation peaked around 770 Wm^{-2} with the previously referred lack of gradual rise/fall in simulated periods of sunrise (04:51) and sunset (19:45) (Fig. 5). The tested DSF had a 20 cm wide cavity with an outdoor air curtain airflow path, where the inlet was fully opened (42 dm^2) and the outlet less opened (7 dm^2). The shading system was placed in the middle position between the two skins of the DSF with partially opened slats (45˚). The only buoyant-driven flow was examined without activation of the fans.

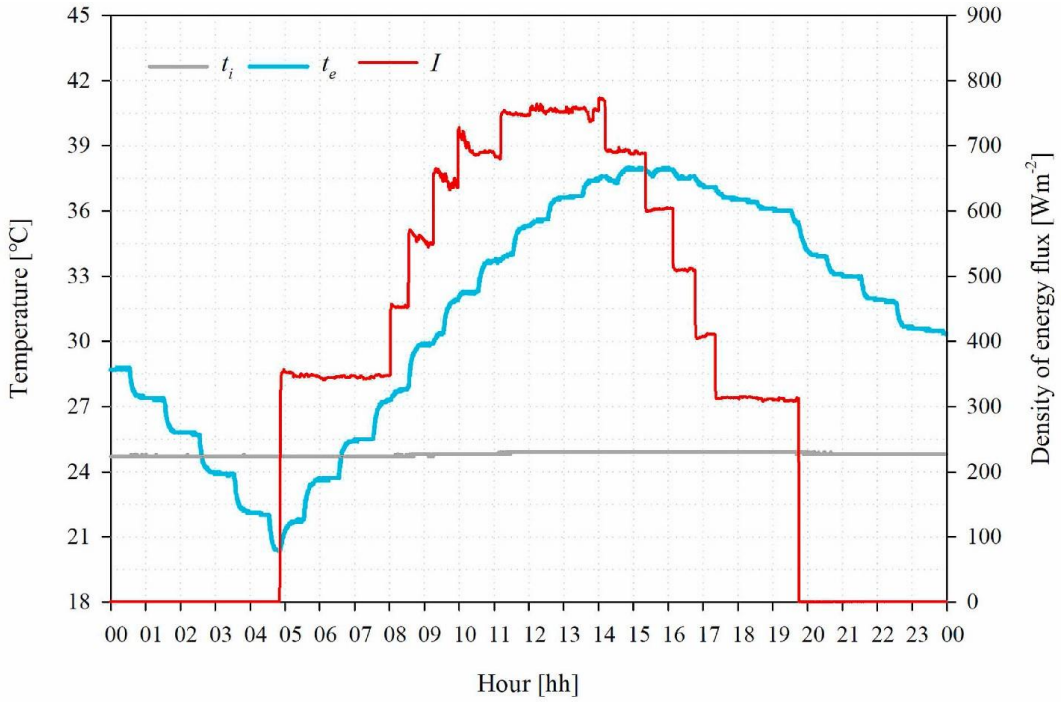

Fig. 5. Boundary conditions corresponding to a typical summer day.

3.5. Results

3.5.1. Verification of the experimental set-up and uncertainty analysis

In total, 48 measurements were performed using two different methods for various DSF configurations, for which the results of comparisons are given in Fig. 6. For low airflow rates, the velocity profile method tended to overestimate airflow rate, most likely due to the velocities in the cavity below the instrumental threshold. Overall, there were no significant differences between airflow rates assessed by the velocity profile method on the ½ and ¾ height of the DSF, except for very high airflow rates where the cavity depth was 60 cm. For these configurations, the airflow at half of the cavity height tended to be higher than at three-quarters of the cavity, most likely due to sensors in the inner half-cavity that were in the path of a stronger air flow.

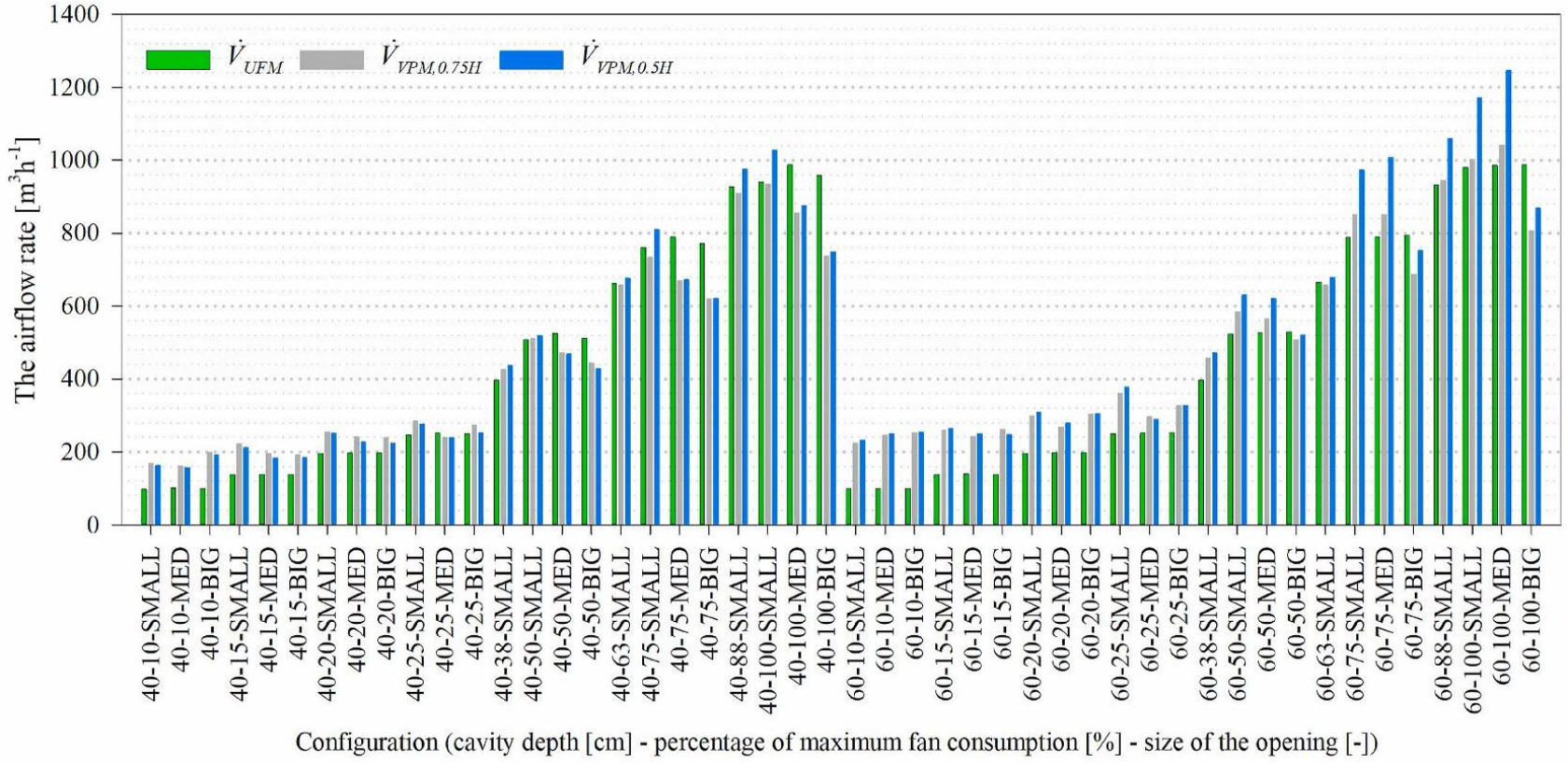

Fig. 6. The airflow measurement using ultrasonic flowmeter and velocity profile method at two different heights for different configurations of DSF.

The accuracy of the VPM in evaluating the airflow rate was assessed through comparison with measurements of the ultrasonic flow meter. The relative error was taken as the indicator quantity of the reliability with a value of ±30% as an acceptable deviation. The airflow rate was divided by the cavity cross-section area to eliminate dependence on its size. The normalized quantity can be seen as the average velocity in the cavity since the airflow was unidirectional (upward). The distribution of relative error with normalized airflow rate is shown in Fig. 7. We can conclude that the velocity profile method was relatively accurate in the range of the normalized airflow rate between 360 and 1500 mh^{-1} (0.1–0.417 ms^{-1}), and most likely the upper threshold is even higher. However, due to the capacity of the duct fan, we were not able to assess it for higher airflow rates. Therefore, only the bottom threshold for the reliability of the velocity profile method is stated. For the cavity depth of 20 cm, the lower limit was around 100 m^3h^{-1}, 40 cm, 200 m^3h^{-1}, and 60 cm, 300 m^3h^{-1}. However, in natural DSFs, attention should be paid to the threshold value of air velocity rather than air flow rate. Lower airflow rates can be reliably assessed for bidirectional flows if the absolute value of measured air velocity is greater than 0.1 ms^{-1}.

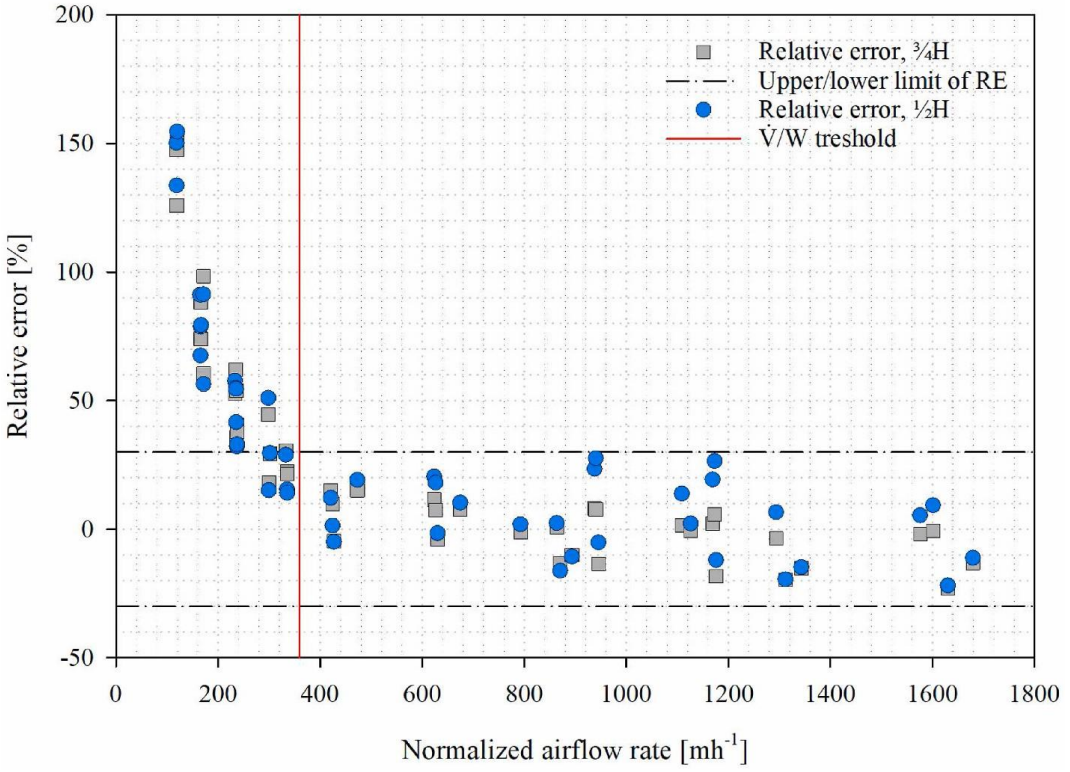

Fig. 7. Distribution of relative error with a normalized airflow rate.

3.5.2. Standardized metrics: U- and g-value

Values of thermal transmittance and solar factor were assessed for various configurations, including different cavity depths and angles of venetian blinds. Theoretical (expected) values fit well within the range of combined instrumental and measurement uncertainty (Table 3). There was a noticeable downward trend in thermal transmittance values with increasing cavity depth, as expected. Experimentally obtained values of the solar heat gain coefficient corresponded to the expected theoretical. Yet, it must be pointed out that measurement uncertainty was high, especially for the very low values of the solar factor, Table 3).

The high uncertainty is a consequence of the class of pyranometer (second) used for steady-state measurement of incident solar radiation, whereupon the main part of error originates from the uncertainty associated with the signal processing. Additionally, the assessment of the solar factor and direct solar transmittance was affected by the optical losses in the cavity, which become more pronounced as the cavity expands. As the cavity expands, the area of the lateral sides also increases, which means a larger surface that absorbs solar radiation. Therefore, a higher share of radiation is absorbed and lost for transmission, and consequently, the g-value is lower. Keeping all this in mind and compared with the test apparatus and procedure given with the standard ISO 19467, the assessment of g-value using HFM and pyranometer in a climate simulator can be considered approximate.

Indicated SHTC values characterize heat transfer during measurements of thermal transmittance, and they show weak fluctuations with DSF configuration change, which indicates the good stability of the measurement conditions. The climate simulator does not provide the ability to control the surface heat transfer coefficients (SHTC) at the borders of the test element and indoor/outdoor environments. However, similar values between them were observed, and their resemblance originates from the similar conditions in both rooms regarding convective (mainly natural) and radiative heat transfer. SHTC at the cavity interfaces showed asymmetry and weaker heat transport on the outer side of the cavity. Although both double gazing units were made of the same materials and filled with the same gas mixture (air and argon in ratio 1:9), the measured value of thermal conductance differed by a non-negligible amount. The disparity may have originated due to the different thermophysical properties (density, dynamic viscosity, and thermal conductivity) of gas mixture caused by exposure to different temperatures [58]. However, we cannot claim this with certainty since the uncertainty range around the mean values of these two quantities overlaps.

Table 3. Standard metrics measurement results (U-value, g-value, solar transmittance and heat transfer coefficients along with corresponding measurement uncertainties).

Configuration			*U-value*	*U-value error*	*g-value*	*g-value error*	τ_e	*Heat transfer coefficient*								*Conductance*			
Depth	*Shading*	*Angle*						h_{ii}	*err* h_{ii}	h_{ic}	*err* h_{ic}	h_{oc}	*err* h_{oc}	h_{oo}	*err* h_{oo}	C_{og}	*err* C_{og}	C_{ig}	*err* C_{ig}
mm	-	*0*	$Wm^{-2}K^{-1}$	$Wm^{-2}K^{-1}$	-		-	$[Wm^{-2}K^{-1}]$											
200	OFF	–	0.618	0.0572	0.346	0.0750	0.294	12.0	3.82	9.4	3.27	3.1	1.48	11.5	3.74	1.65	0.58	1.39	0.52
200	ON	0	0.617	0.0569	0.071	0.0125	0.020	12.3	3.89	8.8	2.82	2.7	1.22	11.7	3.86	1.79	0.63	1.47	0.54
200	ON	45	0.623	0.0563	0.138	0.0268	0.081	12.3	3.91	8.7	2.91	2.9	1.26	11.8	3.82	1.75	0.61	1.44	0.54
200	ON	90	0.623	0.0561	0.267	0.0563	0.215	12.3	3.89	8.9	2.97	2.9	1.28	11.9	3.86	1.75	0.62	1.45	0.54
400	OFF	–	0.608	0.0575	0.358	0.0731	0.281	11.7	3.67	9.6	3.09	2.8	1.24	12.4	4.03	1.63	0.57	1.40	0.51
400	ON	0	0.611	0.0570	0.059	0.0115	0.005	12.1	3.79	9.0	2.69	2.5	1.10	12.5	4.16	1.78	0.62	1.48	0.54
400	ON	45	0.616	0.0578	0.105	0.0202	0.059	12.1	3.77	8.9	2.91	2.6	1.14	12.4	4.07	1.76	0.62	1.44	0.53
400	ON	90	0.619	0.0559	0.223	0.0467	0.174	12.2	3.78	9.3	2.85	2.6	1.12	12.8	4.18	1.76	0.62	1.44	0.53
600	OFF	–	0.610	0.0571	0.265	0.0565	0.223	12.1	3.76	8.7	3.01	2.8	1.34	12.3	3.89	1.63	0.57	1.41	0.52
600	ON	0	0.593	0.0584	0.042	0.0114	0.007	12.6	3.89	8.1	2.71	2.4	1.15	12.0	3.86	1.64	0.57	1.42	0.52
600	ON	45	0.617	0.0575	0.085	0.0158	0.041	12.4	3.78	8.5	2.82	2.6	1.25	12.4	4.00	1.73	0.60	1.46	0.54
600	ON	90	0.611	0.0568	0.166	0.0340	0.123	12.1	3.81	9.0	2.86	2.6	1.24	12.5	3.99	1.71	0.60	1.45	0.54

3.5.3. One-factor analysis

To showcase investigations that can be classified as one-factor analysis, we provide three examples of tests where the impact of only one variable is analyzed, which is, in this case, the path of the ventilation air that crosses the DSF. The results of the investigations show the strong impact that the ventilation mode had when the conditions are those of a *hot summer day*. Shifting from outdoor to indoor air curtain mode lowered the temperature of the cavity by about 15–20 ˚C (Fig. 8a). At the same time, the net heat transfer increased more than ten times (from 30 to 385 Wm^{-2}). Furthermore, shifting from O–O to I–I ventilation mode increased the airflow rate almost three times and stabilized upward motion in the inner half-cavity (Fig. 8b, $\dot{V}$/W ~ from 260 $m^3m^{-1}h^{-1}$ to 810 $m^3m^{-1}h^{-1}$).

An example of not so relevant impact of a single factor is a change in the ventilation mode in *hot summer night* conditions. The temperature profile in the cavity remained flat, but it decreased by around 5 ˚C when changing from the O–O to the I–I ventilation mode, while the amount of heat entering the indoor environment remained quite low in both cases (Fig. 9a). The impact on the air dynamics was somewhat higher, as the airflow rate in both cases was net downward but was around eight times higher in outdoor air curtain mode (Fig. 9b, O–O: $\dot{V}$/W ~ − 390 $m^3m^{-1}h^{-1}$, I–I: $\dot{V}$/W ~ − 50 $m^3m^{-1}h^{-1}$). However, when it comes to the airflows assessed by the VPM, one should always check air velocity values and temperature differences between fluid and bordering surfaces to confirm the supposed direction of the airflow. For the same reason, we cannot claim the exact values and direction of particular streams in the flow in the given case.

As the last example of one-factor analysis, we analyzed the impact of ventilation mode in steady-state conditions corresponding to *a mid- latitude warm winter day.* One can notice that shifting from the outdoor to indoor air curtain mode increased temperatures in the cavity from around 10 to 13 ˚C (Fig. 10a), while the net heat flux density remained almost the same (O–O: q_{net} = 36.0 Wm^{-2}, I–I: q_{net} = 31.4 Wm^{-2}). In both ventilation modes, the outer half-cavity was slightly warmer than the inner due to multiple reflections and absorptions on the adjacent surfaces. Both ventilation modes were characterized by the strong upward current in the inner half-cavity with a circulatory motion in the outer half-cavity, only differing in its direction (Fig. 10b). From the given experimental data, one can envision how the naturally driven airflow is vital for removing excessive heat in the cavity ventilated by the outdoor air curtain. For the given case, a large amount of heat (q_{vent} = 166 Wm^{-2}) accumulated in the cavity was redirected to the outside by the airflow.

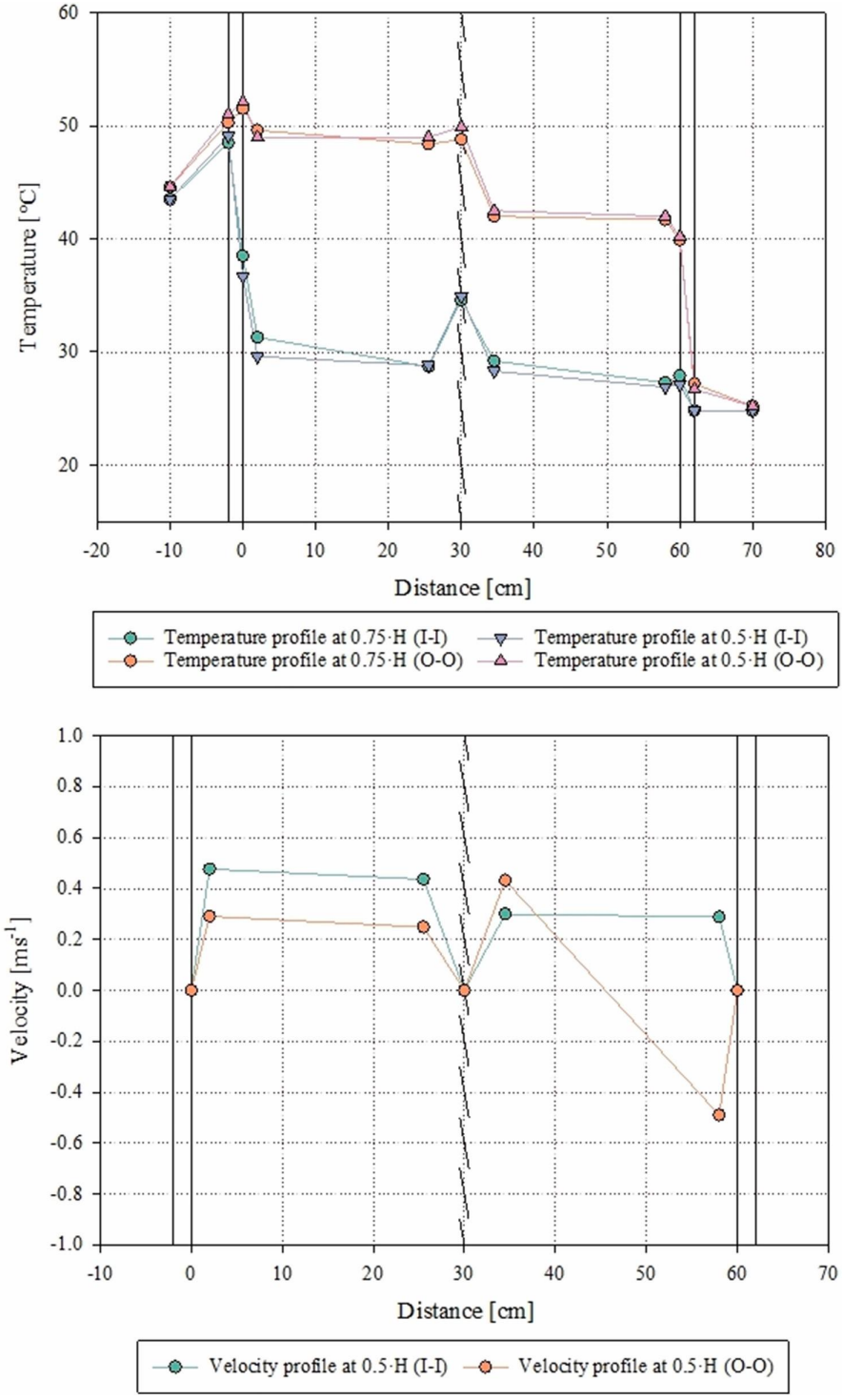

Fig. 8. a) Temperature and b) velocity profiles during a tropical summer day.

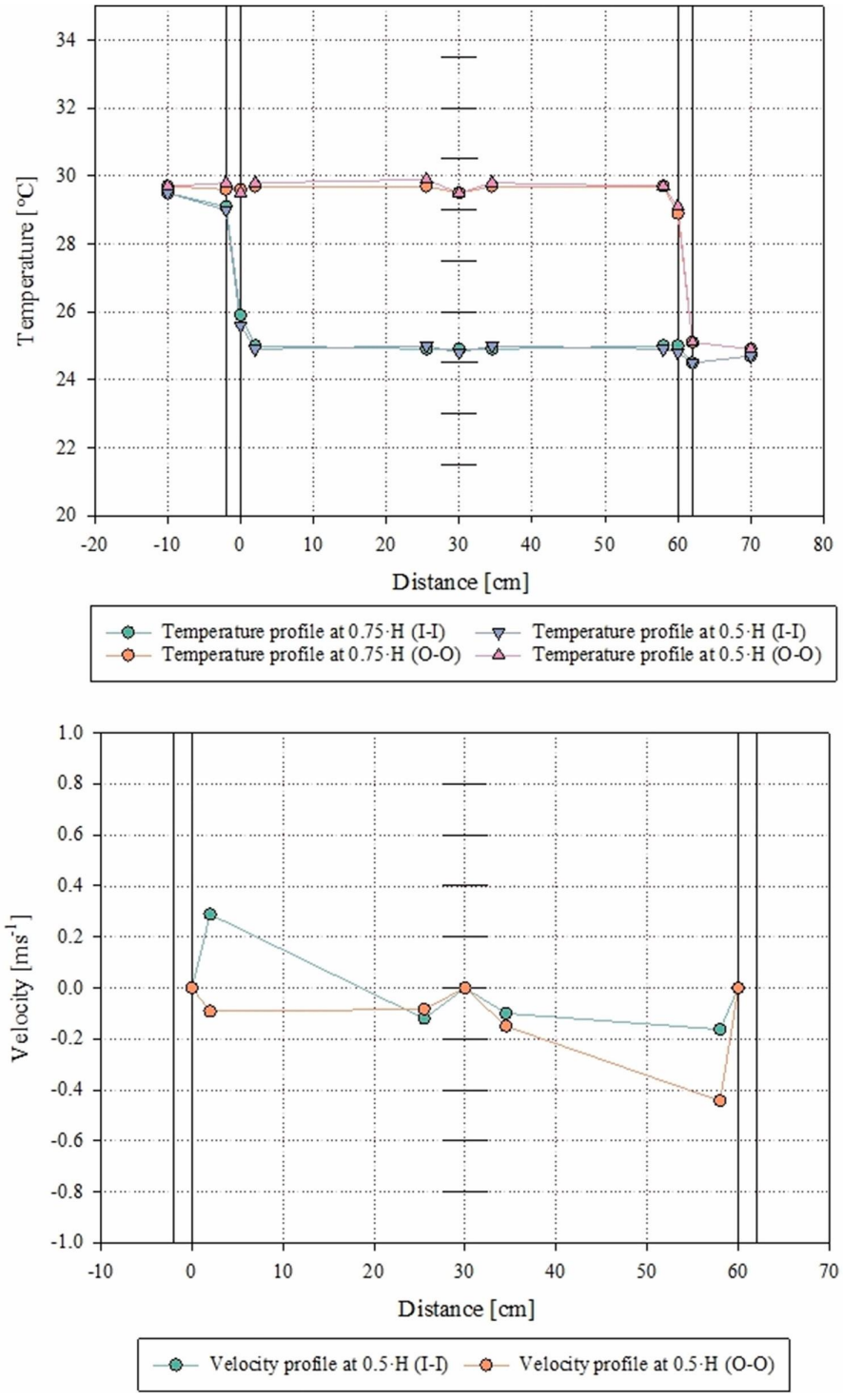

Fig. 9. a) Temperature and b) velocity profiles during a tropical summer night.

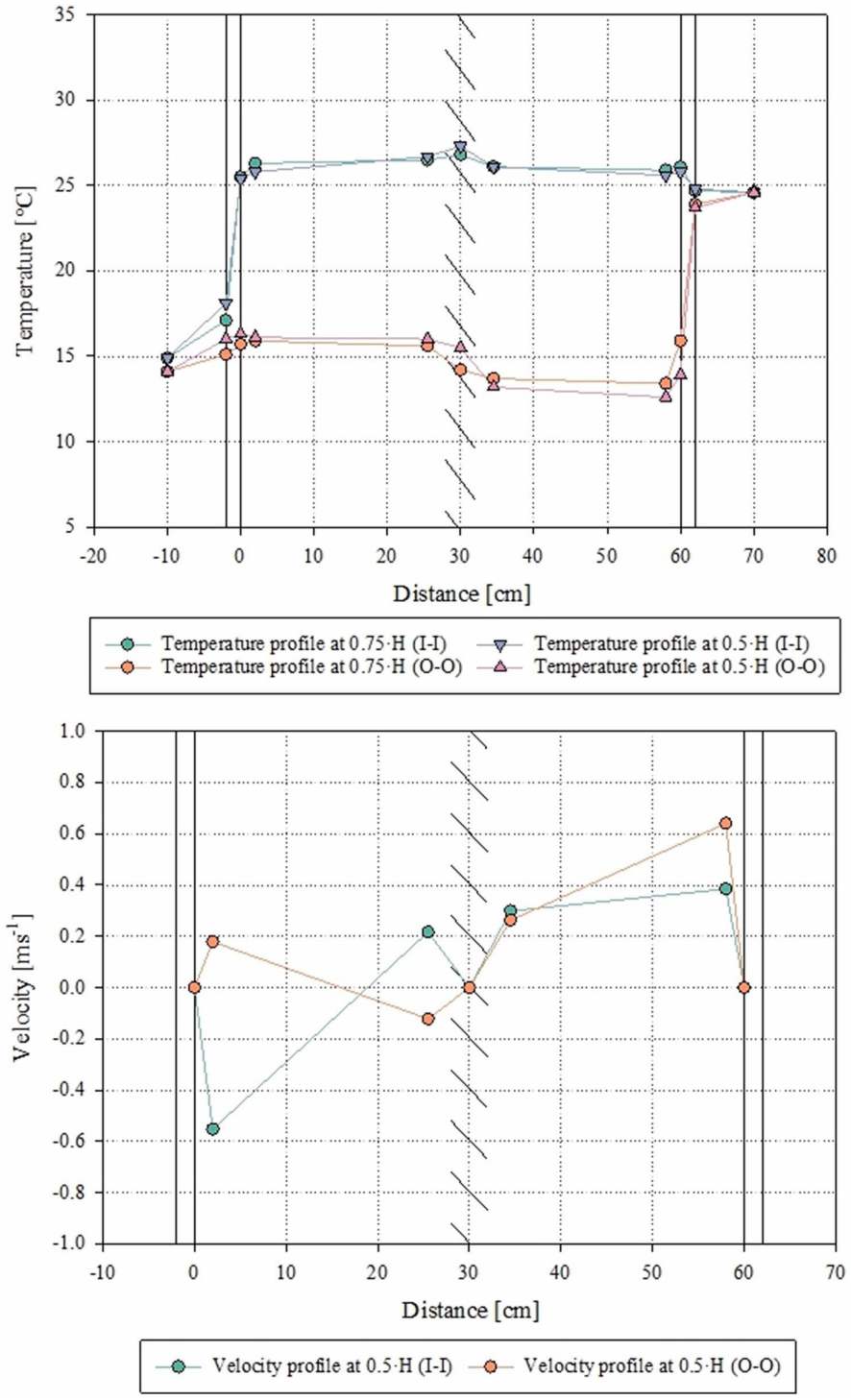

Fig. 10. a) Temperature and b) velocity profiles during a mid-latitude warm winter day.

3.5.4. Design of experiments (Taguchi 4Lx4F L16 design)

Results of the ANOVA analysis for the Taguchi design with 16 points (experimental runs) are given in Table 4 and shown in Fig. 11. Generally, analysis shows which factors drove the thermophysical behavior of DSF, and in the case of DSF with indoor air curtain ventilation mode, it was primarily the incident solar radiation. Here, we must emphasize again that this refers only to the intensity of solar radiation with directionality features proper of the solar simulator (where a certain quota of the irradiance fell in a range of angles close to 90° and another quota was due to reflected radiation that is likely to behave as the diffuse quota of solar radiation) since we could not control the direction of emitted radiation. Furthermore, one can notice that temperature difference played the second most important role in controlling heat gain/ loss by the airflow, while for the temperature of the inner side of inner glazing, it was the angle of VB.

Table 4. Contribution and statistical significance of factors (***p < 0.05***) in controlling indicators of thermal performance and dynamic behavior of fluid in the cavity obtained using a Taguchi design with 16 experiments followed by ANOVA.

Indoor air curtain	q_{net}		t_{cav}		$\dot{V}$		q_{vent}		t_{ii}	
	co [%]	p [–]	co [%]	p [–]	co [%]	p [–]	co [%]	p [–]	co [%]	p [–]
Solar irradiance	88.0	***0.004***	84.6	***0.003***	64.9	***0.003***	58.8	***0.007***	53.0	***0.033***
Temperature difference	8.2	0.1	7.0	0.088	10.5	***0.046***	28.3	***0.02***	3.2	0.580
Angle of VB	1.2	0.571	3.4	0.199	4.6	0.127	9.9	0.082	32.8	0.062
Cavity depth	1.1	0.612	3.9	0.176	19.0	***0.02***	1.4	0.526	6.8	0.347
Error	1.5	–	1.2	–	1.1	–	1.6	–	4.2	–
Outdoor air curtain	q_{net}		t_{cav}		$\dot{V}$		q_{vent}		t_{ii}	
	co [%]	p [–]	co [%]	p [–]	co [%]	p [–]	co [%]	p [–]	co [%]	p [–]
Solar irradiance	51.4	***0.05***	5.5	***0.002***	39.1	***0.006***	26.1	0.059	29.2	***0.030***
Temperature difference	1.4	0.85	94.3	***0.000***	45.4	***0.005***	60.6.	***0.019***	60.4	***0.011***
Angle of VB	34.2	0.084	0.1	0.498	11.9	***0.033***	5.1	0.352	5.9	0.211
Cavity depth	7.5	0.404	0.1	0.470	2.7	0.209	5	0.363	2.3	0.474
Error	5.5	–	0.1	–	0.9	–	3.2	–	2.1	–

The thermal behavior of DSF with the outdoor air curtain ventilation mode is more diverse in comparison to the previous one, with temperature difference becoming dominant over solar radiation in controlling it. The temperature difference was the major factor in driving all response quantities, except net heat transfer, where solar radiation and the degree of openness of venetian blinds were

dominant. The ANOVA can also indicate the structural element(s) most capable of manipulating the system performance. In the shown example, the shading device as a structural element had a large impact on the thermophysical behavior of DSF, and this influence was way greater than the cavity depth. However, there were some exceptions, such as the airflow in indoor air curtain ventilation mode, but here the conclusions related to cause-and-the- effect behavior of the airflow should be taken with caution due to the uncertainty of both the method and the sensors (check section 4.1).

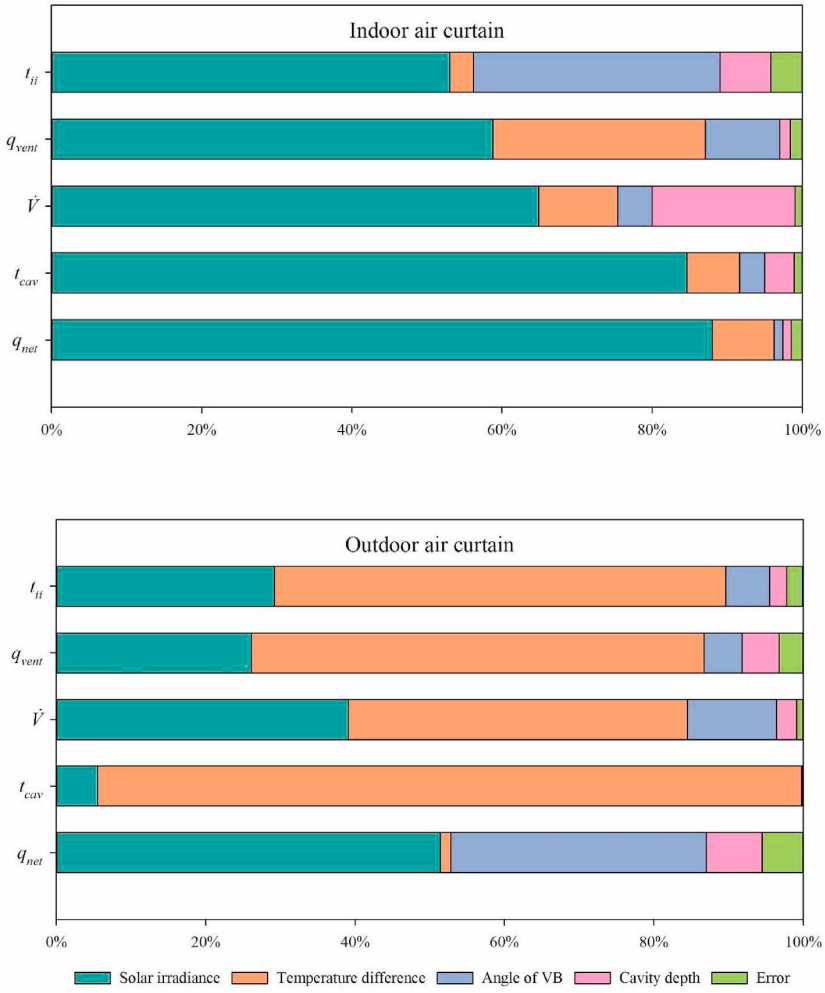

Fig. 11. Contribution of the factors to the variance of the response variables for two examined ventilation modes.

3.5.5. Dynamic profile analysis of a typical hot summer day

As the last example of investigation type, we present the analysis of temporal profiles of quantities measured during dynamical boundary conditions that were designed to represent a typical hot summer

day. The time profiles of the average temperature of the cavity (t_{cav}), shading device (t_{sh}), glazing surfaces (inner-inner t_{ii}, inner-outer t_{io}, outer-inner t_{oi}, and outer-outer t_{oo}), temperature gain/loss of the airflow in the cavity (Δt) and the airflow rate in the cavity ($\dot{V}$) are shown in Fig. 12. In the provided example, it is noticeable that the temperature gain of the airflow passing through the cavity was higher than 5 °C in the central period of the day (between 10:00 and 15:30), while before the sunset and during most of the evening, there was no increase since the temperatures of the cavity borders became almost equal to the air temperature in the cavity. One may draw important conclusions from the obtained profiles, such as for the airflow rate profile: around sunset, the airflow was unstable and oscillated between the upward and downward directions; during the daytime (between 06 and 18:30), the airflow stabilized its direction and rate with an average value around 125 m^3h^{-1} due to significantly hotter cavity borders; during the period without impinging solar radiation (nighttime between 20 and 02), airflow shifted its direction downward with a relatively stable rate of about − 125 to − 150 m^3h^{-1}.

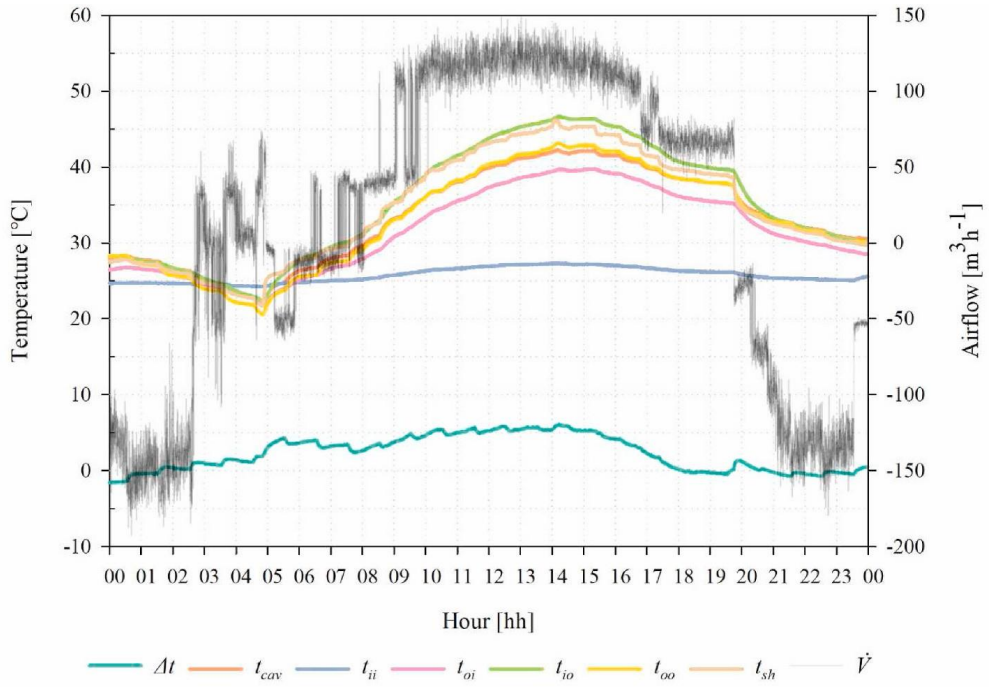

Fig. 12. Diurnal profiles of the average temperature of the cavity (t_{cav}), shading device (t_{sh}), glazing surfaces (inner-inner t_{ii}, inner-outer t_{io}, outer-inner $t_{oi,}$ and outer- outer t_{oo}), temperature gain/loss of the airflow in the cavity (Δt) and the airflow rate in the cavity ($\dot{V}$).

In the presented example from Fig. 13, one can notice how naturally induced airflow was a very useful mechanism for removing excess heat in the cavity ventilated with the outdoor air curtain mode (O–O). For example, in the period of intense solar radiation (between 10 and 15 h), almost 40% of

the heat that reached the interior was directed to the outside (see Fig. 13, dynamic insulation efficiency is around 0.4) thanks to the airflow in the cavity. As defined in the work of Corgnati et al. [17], the dynamic insulation efficiency represents the quota of the heat flux that enters through the outer surface of the facade (and which would enter the room in the case of a traditional glazed facade) that is removed by the ventilation air. The calculation of the dynamic insulation efficiency revealed a high-frequency noise originating from the airflow rate measurement. In order to eliminate this noise, the 10-min moving average was employed as a low-pass filter. From the extracted profile, one may find that in certain parts of the day, the airflow has no positive effect on the energy efficiency of DSF and that it increases net heat transfer (periods with zero value of dynamic insulation coefficient). That is evident during the hot nighttime period when the airflow is directed downward due to the colder bordering surfaces causing potentially negative (unrealistic) coefficient values. However, this effect is not so important for the considered typical day as the net heat flux density is not large in this part of the day.

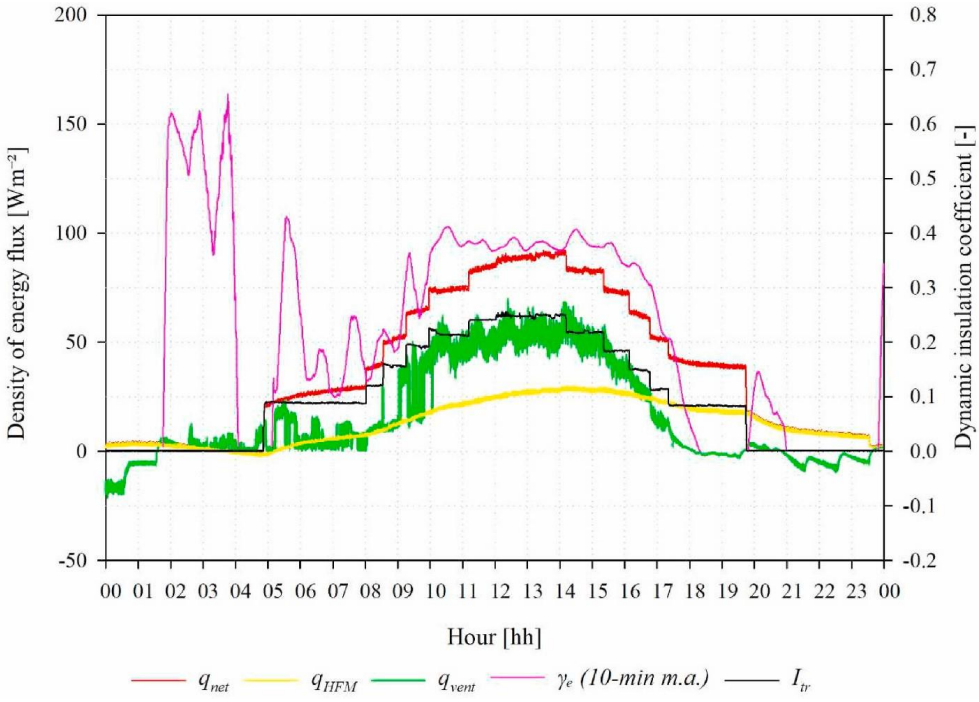

Fig. 13. Diurnal profiles of net heat flux density (q_{net}), the normalized heat rate gain/loss by the airflow (q_{vent}), heat flux density measured by HFM (q_{HFM}), transmitted solar radiation intensity (I_{tr}) and dynamic insulation efficiency (γ_e).

Another example of an interesting finding in the dynamic profile analysis is the diurnal variation of the direct solar transmittance, shown in Fig. 14. The value of this quantity steadily grew towards the end of the period with imposed solar radiation (from 0.06 to 0.14). That occurred due to the lag

between the profile of heat flux density measured by HFM and the profile of the transmitted solar radiation intensity (Fig. 14, compare maximums of q_{HFM} and I_{tr} profiles). One may notice that in the late part of the day (between 16 and 19), the heat flux density (measured by HFM) becomes equally significant as the transmitted solar radiation intensity. This effect has been seen in other experimental analyses in- field. Thus, obtaining similar results through this laboratory test shows that the developed testbed is capable of representing phenomena that are seen in systems implemented in real buildings, regardless of the limitations that the equipment presents (e.g., the limitation in replicating the full geometrical features of solar radiation).

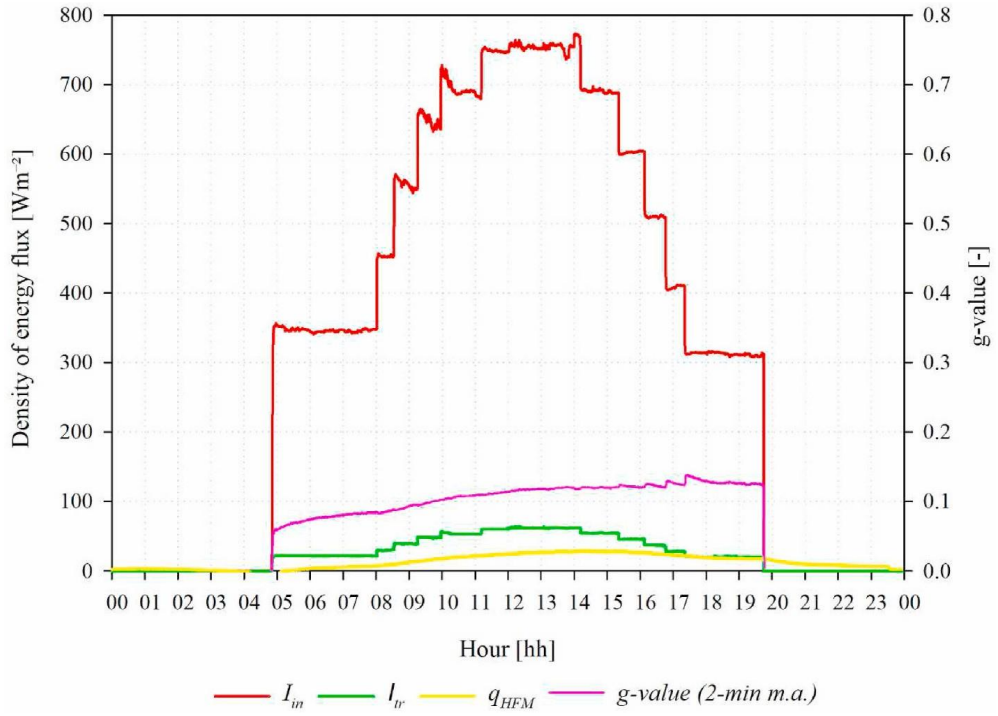

Fig. 14. Diurnal profiles of incident solar radiation intensity (I), transmitted solar radiation intensity (I_{tr}), heat flux density measured by HFM (q_{HFM}), and g-value (g).

The last example (Fig. 15) shows the profiles of airflow rate at two different heights and in two different segments of the cavity (inner and outer half-cavity). In order to smooth out high-frequency noise and increase the readability of the flow representation, a 2-min moving average was applied in the calculation of airflow rate profiles. The profiles indicate the complicated spatial structure of the flow that became even more delicate for the analysis due to its dynamical variability. However, from the shown profiles, some basic conclusions can be drawn. During the daytime, almost all mass flow occurred through the outer half-cavity, while during the nighttime, the situation reversed, and the flow became downward oriented and somewhat more intensive in the inner half-cavity. In the period before sunrise and around sunset, the flow became unstable and often changed its characteristics. The

profiles can also indicate deficiencies of measurement methods, such as VPM. For example, the airflow rate on the 2nd height resembled the airflow rate measured at the 3rd height with a similar curve profile throughout the day, except in a few hours after sunset. The discrepancy probably results from the combined effects of several sources of uncertainty: imperfections of measurement method (point measurements in the space), instrument accuracy and the developing nature of the flow.

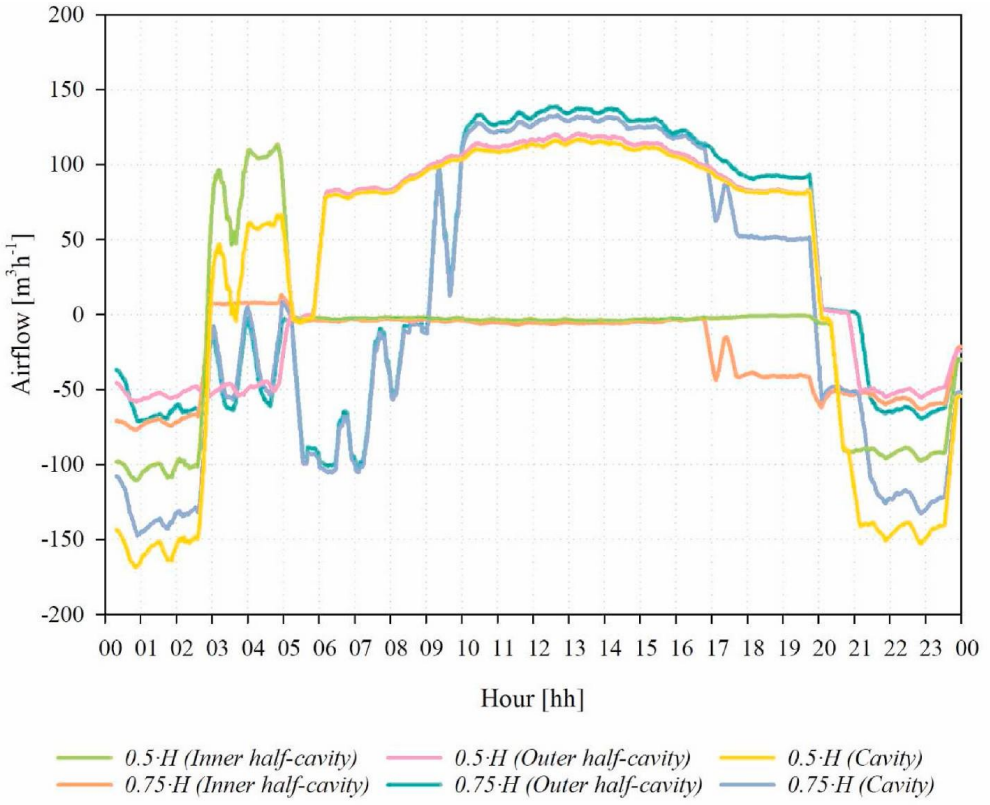

Fig. 15. Airflow rate measured in the inner and outer half-cavity at the 2nd and 3rd height.

3.6. Lessons learned, possibilities and limitations

Transport processes in DSF are highly dynamic and in constant non- linear interaction, making it very difficult to link the DSF constructive features with thermophysical behavior. The flexible testbed was developed and designed to operate in combination with the climate simulator to facilitate characterization and increase possibilities for systematic investigation of DSF systems. Several investigation approaches, including some non-standardized methods that provide a more detailed insight into thermal and fluid-dynamics system behavior, were tested. The whole campaign consisted of three equally important phases: the planning, the development of the experimental set-up and the execution of the experiment. Taught by the experience, we would like to discuss the issues we have

encountered during this course, highlight the advantages of such an experimental approach and outline possibilities in future research.

In the planning phase, it is recommended to systematically design the sensor layout and data acquisition (DAQ) system, preferably through schematic and wiring diagrams, to facilitate the physical development of the set-up and the finding of the potential problems in communication with sensors. At this stage, it is essential to design an efficient strategy for conducting the experimental campaign, taking into account the desired depth of insight, available resources and limitations of the experimental set-up.

The sensor layout should be realized in this stage so that temperature sensors and heat flux meters are shielded from direct radiation. In some situations, space for ventilation needs to be provided to sensors to avoid excessive heat accumulated by the radiative absorption of the shield. Physical support, communication and power supply lines of sensors must be placed to affect thermal and velocity fields minimally. When it comes to an experimental set-up like this, where dozens of sensors and control features need to be used, it is compulsory to develop a system for automatic control and monitoring of the experiment. The DAQ system should consist of the controller or central processing unit connected to multiple transmitters, transducers and Modbus devices via a communication network systematically organized in sections of terminal blocks for easier communication handling.

Before the experimental campaign, it is necessary to check the reliability and validity of measurements and, if needed, to calibrate sensors. The temperature sensors should be checked by setting both chambers of the climate simulator in thermal equilibrium at known temperatures, preferably below, around and over the room temperature (e.g., 5, 20, and 35 ˚C), so one may inspect uniformity between measurements over various ranges. Coherence between measurements of energy flux meters (such as heat flux meters, pyranometers, or other types of radiometers) should be inspected by placing all sensors close together and inducing stimuli of different intensities. If the experimental campaign has a long duration (several months), it is necessary to perform the sensor checks several times during this period. Alternative measurement methods also need to pass accuracy checks and calibration to detect how comprehensive an analysis they can offer.

The standard metric measurements are a quite straightforward investigation type to perform as they require one to follow (where available) the standardized procedures. However, when determining optical properties (such as g-value or direct solar transmittance), some challenges can arise from the imperfections of the equipment and the test specimen. Though it is possible to obtain some values for standardized metrics for a DSF, most of the standard metrics cannot properly characterize the thermal and especially the fluid-dynamic behavior of DSFs as these technologies presents phenomena that are far from the assumptions behind the development of some standardized metrics (such as

monotone temperature gradient or monodirectional heat flow). The one-factor analysis allows researchers to overcome the limitations set by standardized procedures and makes it possible to obtain some insight into the thermal and fluid-dynamic behavior of DSFs, though in a rather simplified way. This is because it is not possible to analyze and describe the simultaneous influence of several factors (interactions) on the variable of interest. The results of one-factor analyses can hardly be used to optimize or to predict DSF behavior fully, but they are most commonly used to analyze in depth a particular phenomenon or to obtain data for validation or calibration of numerical models. Sometimes, one-factor analyses are also used for pre-screening of important variables and key correlations between one independent variable and one dependent variable.

DOE is the most suitable way to balance accuracy, breadth and costs to obtain a complex system behavior characterization that includes the analysis of the impact of multiple factors and their interactions, including structural elements, operational modes and boundary conditions as independent variables. This investigation type requires a series of experiments in various steady-state conditions and therefore demands substantial material costs. However, the expenses can be reduced with a few practical tips. For example, it is advisable to perform the DOE in two steps if it is necessary to examine the influence of many factors. The first one is to screen out important variables affecting the performance/ behavior of the system, and the second is a more detailed analysis with a focus only on relevant factors. When it comes to DOE and its application to DSFs, we refer to our previous work for more information and the recommended course of action for performing DOE analysis, depending on the number of examined factors, the desired depth of insight and available resources [37]. Since the DOE approach requires the systematic execution of experiments, where several factors are altered during each experimental run, it is advisable to arrange the series so that factors are altered gradually between runs. The system will reach steady states faster by avoiding extreme alteration in factor values, such as the shift from bottom to peak values and vice versa. For example, priority should be given to a gradual change in ambient temperature. The system is thermally most inert to changes in chamber temperature, then in solar irradiance, and only after them in all other parameters, such as features of DSFs (e.g., blind angle, cavity depth, airflow path, or rate). Whether the system has reached a steady state can be checked conveniently and efficiently by inspection of air temperature readings in the cavity since this section of the DSF system adopts the latest stable values. In this way, an experimental campaign consisting of 15–20 runs can be shortened by several days. By applying the DOE, it is possible to describe the thermal and fluid-dynamical behavior in a wide range of conditions. This method can also be used to find optimal configurations and to build up (linearized) models that can predict the behavior of a DSF given certain boundary conditions and structural properties, even if the exact combination has not been experimentally tested.

The dynamic profile measurements imply experimental investigation in dynamic boundary conditions that usually correspond to the fluctuation of the boundary conditions in typical (design) days. Unlike the other investigation types, this method captures thermal and fluid dynamics behavior in conditions close to the real ones found when envelope systems are deployed in real buildings, and it is suitable for testing responsive façade systems. This analysis can lead to system optimization, but only in given conditions, and probably has its highest value in the joint analysis of the building technology and the control to manage its (dynamic) performance. In the case of dynamic profile measurements for a typical day, it is desirable to perform a series of measurements corresponding to several consecutive identical days to consider the effect over a longer period and to prevent initial conditions from playing a role in the results.

However, some limitations of the equipment and the applied measurement methods restrict the possibilities of thoroughly investigating the thermal and fluid dynamics behavior of DSF. For example, the climate simulator may simulate conditions that deviate from the desired one. For example, when it is necessary to maintain the low or intermediate temperature of the outdoor chamber (<25 ˚C) and at the same time to have an active solar simulator, the air conditioning system can experience problems in controlling the outdoor chamber temperature. The actual temperature is a few degrees higher than the set-point and the air is not uniformly cooled through the chamber, which results in a vertical temperature gradient up to 2 ˚C directed upwards. The reason for this is probably the combined effect of climate simulator overload and the inappropriate position of the integrated temperature sensor used to regulate the set-point temperature of the outdoor chamber.

Even though the solar simulator is calibrated to provide homogeneity of irradiance within reasonable limits (around ±10%), this property deteriorates over time due to physical changes in radiation surface, position and different aging of the lamps. Furthermore, in extreme settings where the high irradiance (>800 Wm^{-2}) is combined with low set- point temperature (<15 ˚C), the solar simulator experiences problems in maintaining time-stable irradiated power, which can fluctuate in range ±10% from the desired one. In addition to this, irradiance significantly attenuates with distance from radiation surface. The inability of the solar simulator to impose and control low radiation levels (below 250 Wm^{-2}) is a significant disadvantage that restricts reproducing particular conditions, such as low irradiance levels characteristic for a winter day or gradual increase or decrease of irradiance typical for sunrise/sunset periods. Moreover, as already pinpointed, the lamp array in the climate simulators does not offer the possibility of controlling the direction of emitted radiation. The inability to control the impinging angle represents a limitation of the solar simulator since the thermal performance (the solar reflectance and transmittance) of both the glazing and the shading device depends on the incident angle [59,60]. However, even if the system cannot allow one to obtain reliable

results on the effect of the geometry of solar radiation on the performance of the system, much information can still be obtained on the role of the different layers in the construction and how they interact with the solar radiation.

When it comes to the disadvantages of the test sample, the limited width represents a notable issue that causes optical loss, which is particularly pronounced when the cavity is maximally expanded. Therefore, slightly lower values of the solar factor and direct solar transmittance are obtained compared to those expected. Setting a constant irradiance on the outer surface of the DSF for different cavity widths is not a straightforward task since the irradiance attenuates with retraction of the outer skin of the DSF. Therefore, constant checking and readjustment of the bulb's power is advised.

Regarding the measurement methods, the VPM has shown unreliability when it comes to evaluating the low airflow rates (average velocity below 0.1 ms^{-1}). Furthermore, determining the airflow direction and especially heat transfer coefficients using temperatures of fluid and the bordering surfaces is unreliable if the temperature difference is below the instrumental error (below 0.3 or 0.5 °C). Likewise, punctual measurements cannot accurately capture the velocity profile, especially in thick cavities where the boundary layer effect is considerable. Therefore, the naturally driven airflows that usually have a complex structure with bidirectional patterns could be inappropriate for the airflow rate characterization using VPM. Alternative techniques to measure airflow in such situations, such as laser Doppler (LDV), particle image (PIV) and ultrasound velocimetry, could be employed if the scope of the investigation requires. However, complexity, technical limitations and costs associated with these techniques could make it unfeasible in the context of these studies.

In an effort to make our research freely accessible and to allow maximum usability of the collected data, all the measurements presented in this study to demonstrate the functionalities of the test bed and the applications of the different experimental methods (cft. Section 4.1, 4.3 and 4.4) have been uploaded to on an open-access repository. Data can be found at, and referenced using, the following weblink: https://d oi.org/10.5281/zenodo.5808012.

3.7. Conclusions

Thermophysical processes occurring in advanced building envelopes, such as DSF, are very intercorrelated and complicated to analyze. The experimental approach is the only way to reliable describe them, but it is rigid, time-consuming and expensive. To overcome these drawbacks and systematically study the thermal and fluid-dynamic behavior of DSFs, we have developed a flexible experimental testbed and validated its functioning with a series of experimental procedures. Different DSF configurations can be easily tested in response to various boundary conditions thanks to a purpose built DSF mock-up and a climate simulator that can recreate boundary conditions, including temperature gradient and solar irradiation. A developed system for data acquisition and control of the

experiment enables the adjustment of desired DSF configuration and environmental conditions and simultaneous monitoring of more than seventy sensors in real-time.

In the description presented in the paper, we highlighted the features of the flexible experimental testbed, its sensitivity and reliability, and discussed different types of experimental investigations with various levels of complexity: standard metrics measurements, one-factor analysis, design of experiments and dynamic profile measurements. In this manuscript, we have provided examples of each investigation type, showed the advantages and disadvantages of the different techniques, and discussed challenges and possibilities associated with them. The main take-home message that we want to convey is that complementary analyses are necessary, and depending on the scope of the investigations, one or more combinations of methods should be employed to obtain the desired knowledge of the specific performance or phenomenon. A comprehensive set of data from the measurements carried out to test and validate the testbeds and the methods has been made publicly available to the scientific community, and is especially targeted at researchers working with numerical model development, validation, and model calibration, who could benefit from the freely accessible dataset for comparison between experimental and numerical data.

By presenting some examples of different types of investigations, we have also given a preview of certain insights about the impact of structural elements, operational modes and boundary conditions on the thermal and fluid dynamics behavior of DSFs, though this was not the focus of the study. Some limitations of the testbed restrict the possibility of investigating all the possible phenomena in DSF. The impact of solar geometry and complete flow characterization are two examples of domains that cannot be fully addressed by the developed experimental equipment, though it allows obtaining some information. The preliminary findings previewed in this paper will be expanded in future studies that will focus on the specific relations between constructional features and performance in DSFs.

Though the testbed developed so far is suitable to investigate DSF systems, the same approach involving a flexible mock-up and the development of optimized experimental procedure can be applied to any advanced building envelope system to obtain a comprehensive picture of the behavior of these complex systems in the most efficient way.

Acknowledgements

The activities presented in this paper were carried out within the research project “REsponsive, INtegrated, VENTilated - REINVENT – windows”, supported by the Research Council of Norway through the research grant 262198, and the partners SINTEF, Hydro Extruded Solutions, Politecnico di Torino and Aalto University. The authors would like to thank Odne Oksavik from SINTEF Community for his support in developing the software for control and data acquisition. The technical

partner Hydro Extruded Solutions (Hydro Building Systems) is also gratefully acknowledged for its support in developing and engineering the flexible mock-up and the in-kind contribution for its construction.

3.8. References

[1] E. Oesterle, R.-D. Lieb, M. Lutz, W. Heusler, Double-skin Facades : Integrated Planning, München : Prestel, 2001.
[2] R.A. Agathokleous, S.A. Kalogirou, Double skin facades (DSF) and building integrated photovoltaics (BIPV): a review of configurations and heat transfer characteristics, Renew. Energy 89 (2016) 743–756.
[3] M.S. Siddiqui, A. Jankovic, F. Goia, Design and testing of a flexible test bed for thermal and fluid mechanic investigations of double skin façades, in: Conference Proceedings of 15th RoomVent 2020 Conference, 2021.
[4] A. Jankovic, F. Goia, D. Eckert, P. Müller, A test bed for thermal fluid dynamic analysis of double skin facade systems, IOP Conf. Ser. Mater. Sci. Eng. 609 (2019) 32006.
[5] A. Jankovic, F. Goia, Impact of double skin facade constructional features on heat transfer and fluid dynamic behaviour, Build. Environ. 196 (2021), 107796, https://doi.org/10.1016/j.buildenv.2021.107796.
[6] A. Zollner, E.R.F. Winter, R. Viskanta, Experimental studies of combined heat transfer in turbulent mixed convection fluid flows in double-skin-façades, Int. J. Heat Mass Tran. 45 (22) (2002) 4401–4408.
[7] D. Saelens. Energy performance assessment of single storey multiple-skin facades, Catholic University of Leuven, 2011.
[8] L.C.O. Souza, H.A. Souza, E.F. Rodrigues, Experimental and numerical analysis of a naturally ventilated double-skin façade, Energy Build. 165 (2018) 328–339.
[9] F. Yang, F. Yuan, F. Qian, Z. Zhuang, J. Yao, Summertime thermal and energy performance of a double-skin green facade: a case study in Shanghai, Sustain. Cities Soc. 39 (2018) 43–51.
[10] G. Michaux, R. Greffet, P. Salagnac, J.B. Ridoret, Modelling of an airflow window and numerical investigation of its thermal performances by comparison to conventional double and triple-glazed windows, Appl. Energy 242 (2019) 27–45.
[11] Y. Luo, L. Zhang, Z. Liu, L. Xie, X. Wang, J. Wu, Experimental study and performance evaluation of a PV-blind embedded double skin façade in winter season, Energy 165 (2018) 326–342.
[12] C. Zhang, W. Gang, J. Wang, X. Xu, Q. Du, Numerical and experimental study on the thermal performance improvement of a triple glazed window by utilizing low- grade exhaust air, Energy 167 (2019) 1132–1143.
[13] J. Curpek, M. Cekon, J. Hraska, PCM integrated in BiPV ventilated façade concepts: experimental test cell platform and initial full-scale measurements, IOP Conf. Ser. Earth Environ. Sci. 290 (2019) 12072.
[14] S. Preet, M.K. Sharma, J. Mathur, A. Chowdhury, S. Mathur, Performance evaluation of photovoltaic double-skin facade with forced ventilation in the composite climate, J. Build. Eng. 32 (2020) 101733.
[15] H. Choi, Y. An, K. Kang, S. Yoon, T. Kim, Cooling energy performance and thermal characteristics of a naturally ventilated slim double-skin window, Appl. Therm. Eng. 160 (2019) 114113.
[16] H. Manz, A. Schaelin, H. Simmler, Airflow patterns and thermal behavior of mechanically ventilated glass double facades, Build. Environ. 39 (9) (2004) 1023–1033.
[17] S.P. Corgnati, M. Perino, V. Serra, Experimental assessment of the performance of an active transparent façade during actual operating conditions, Sol. Energy 81 (8) (2007) 993–1013.
[18] O. Kalyanova, P. Heiselberg. Experimental Set-up and Full-scale Measurements in the 'Cube', Department of Civil Engineering, Aalborg University, Aalborg, 2008.
[19] Y. Li, J. Darkwa, G. Kokogiannakis, Heat transfer analysis of an integrated double skin façade and phase change material blind system, Build. Environ. 125 (2017) 111–121.
[20] Z. Zeng, X. Li, C. Li, Y. Zhu, Modeling ventilation in naturally ventilated double- skin façade with a Venetian blind, Build. Environ. 57 (2012) 1–6.
[21] D. Brandl, T. Mach, M. Grobbauer, C. Hochenauer, Analysis of ventilation effects and the thermal behaviour of multifunctional façade elements with 3D CFD models, Energy Build. 85 (2014) 305–320.

[22] X. Hong, M.K.H. Leung, W. He, Effective use of Venetian blind in Trombe wall for solar space conditioning control, Appl. Energy 250 (Sep. 2019) 452–460.
[23] B. Koo, K. Lee, Y. An, K. Lee, Solar heat gain reduction of ventilated double skin windows without a shading device, Sustainability 10 (2) (Dec. 2017) 64.
[24] K.J. King. Turbulent Natural Convection in Rectangular Air Cavities, Queen Mary University of London, 1989.
[25] Y. Katoh, M. Miyamoto, J. Kurima, S. Kaneyasu, Turbulent free convection heat transfer from vertical parallel plates : effect of entrance bell-mouth shape, in: JSME Int. journal. Ser. 2, Fluids Eng. heat Transf. power, Combust. Thermophys. Prop. 34, 1991, pp. 496–501, 4.
[26] M.M. Gibson, A.A. Dafa'Alla, Two-equation model for turbulent wall flow, AIAA J. 33 (8) (Aug. 1995) 1514–1518.
[27] C. Popa, D. Ospir, S. Fohanno, C. Chereches, Numerical simulation of dynamical aspects of natural convection flow in a double-skin façade, Energy Build. 50 (2012) 229–233.
[28] W. Ding, Y. Hasemi, T. Yamada, Natural ventilation performance of a double-skin façade with a solar chimney, Energy Build. 37 (4) (2005) 411–418.
[29] N. Kimouche, Z. Mahri, A. Abidi-Saad, C. Popa, G. Polidori, C. Maalouf, Effect of inclination angle of the adiabatic wall in asymmetrically heated channel on natural convection: application to double-skin façade design, J. Build. Eng. 12 (2017) 171–177.
[30] O.A. Tkachenko, et al., Numerical and experimental investigation of unsteady natural convection in a non-uniformly heated vertical open-ended channel, Int. J. Therm. Sci. 99 (2016) 9–25.
[31] Y. Cherif, E. Sassine, S. Lassue, L. Zalewski, Experimental and numerical natural convection in an asymmetrically heated double vertical facade, Int. J. Therm. Sci. 152 (2020) 106288.
[32] L. Mei, et al., The influence of blinds on temperatures and air flows within ventilated double-skin facades, in: Proc. Clima 2007, WellBeing Indoors, 2007.
[33] V. Gavan, M. Woloszyn, F. Kuznik, J.-J. Roux, Experimental study of a mechanically ventilated double-skin façade with Venetian sun-shading device: a full-scale investigation in controlled environment, Sol. Energy 84 (2) (2010) 183–195.
[34] T. Inan, T. Basaran, Experimental and numerical investigation of forced convection in a double skin façade by using nodal network approach for Istanbul, Sol. Energy 183 (2019) 441–452.
[35] "REsponsive, INtegrated, VENTilated - REINVENT - windows." Research project grant 262198 by The Research Council of Norway. Website: https://prosjektbank en.forskningsradet.no/project/FORISS/262198?Kilde=FORISS&distributio n=Ar&chart=bar&calcType=funding&Sprak=no&sortBy=score&sortOrder=des c&resultCount=30&offset=0&Fritekst=reinvent.
[36] F. Goia, V. Serra, Analysis of a non-calorimetric method for assessment of in-situ thermal transmittance and solar factor of glazed systems, Sol. Energy 166 (2018) 458–471.
[37] A. Jankovic, G. Chaudhary, F. Goia, Designing the design of experiments (DOE) – an investigation on the influence of different factorial designs on the characterization of complex systems, Energy Build. 250 (2021) 111298.
[38] C.W. Hurley, J.F. Schooley, Calibration of temperature measurement systems installed in buildings, Build. Sci. 153 (1984).
[39] J.P. Holman, Experimental Methods for Engineers, McGraw-Hill/Connect Learn Succeed, New York, N.Y., 2012.
[40] T. Bas¸aran, T. Inan, Experimental investigation of the pressure loss through a double skin facade by using perforated plates, Energy Build. 133 (2016) 628–639.
[41] E. Giancola, et al., Possibilities and challenges of different experimental techniques for airflow characterisation in the air cavities of façades, J. Facade Des. Eng. 6 (3) (Aug. 2018), https://doi.org/10.7480/jfde.2018.3.2470. Spec. Issue FAÇADE 2018 – Adapt.
[42] N. Safer, Modelisation des façades de type double-peauequi p´ees de protections solaires : approches multi-echelles, L'Institut National des Sciences Appliqu´ees de Lyon, 2006.
[43] A. Jankovic, G. Gennaro, G. Chaudhary, F. Goia, F. Favoino, Gas traces techniques for airflow characterization in double skin facades, in: RoomVent, 2020, p. 2021.

[44] O. Kalyanova, R.L. Jensen, P. Heiselberg, Measurement of air flow rate in a naturally ventilated double skin façade, in: Proceedings of Roomvent 2007: Helsinki, FINVAC ry, 2007, 13-15 June 2007.
[45] International Organization for Standardization. ISO 9869-1: 2014 Thermal Insulation, Building Elements, In-Situ Measurement of Thermal Resistance and Thermal Transmittance-Part 1: Heat Flow Meter Method, ISO, 2014.
[46] International Organization for Standardization, ISO 9050: 2003, Glass in Building—Determination of Light Transmittance, Solar Direct Transmittance, Total Solar Energy Transmittance, Ultraviolet Transmittance and Related Glazing Factors, 2003.
[47] B.P. Jelle, Solar radiation glazing factors for window panes, glass structures and electrochromic windows in buildings—measurement and calculation, Sol. Energy Mater. Sol. Cells 116 (2013) 291–323.
[48] International Organization for Standardization, ISO 15099: 2003 Thermal Performance of Windows, Doors and Shading Devices, 2003.
[49] International Organization for Standardization, ISO 19467:2017 Thermal Performance of Windows and Doors — Determination of Solar Heat Gain Coefficient Using Solar Simulator, 2017.
[50] International Organization for Standardization, ISO 9060:2018(en) Solar energy — Specification and classification of instruments for measuring hemispherical solar and direct solar radiation, 2018.
[51] J. Konings, A. Habte, Uncertainty Evaluation of Measurements with Pyranometers and Pyrheliometers, 2016.
[52] S.M. Zahraee, M. Hatami, N. Mohd Yusof, J. Mohd Rohani, F. Ziaei, Combined use of design of experiment and computer simulation for resources level determination in concrete pouring process, J. Teknol. 64 (1) (Nov. 2013).
[53] D.C. Montgomery, Design and Analysis of Experiments, John Wiley & Sons, New York, 2001.
[54] N.R. Smalheiser, in: N.R. Smalheiser (Ed.), Chapter 5 - Experimental Design: Design Strategies and Controls, Academic Press, 2017, pp. 65–85.
[55] J. Parra, A. Guardo, E. Egusquiza, P. Alavedra, Thermal performance of ventilated double skin façades with Venetian blinds, Energies 8 (6) (2015) 4882–4898.
[56] R. Fuliotto, F. Cambuli, N. Mandas, N. Bacchin, G. Manara, Q. Chen, Experimental and numerical analysis of heat transfer and airflow on an interactive building facade, Energy Build. 42 (1) (2010) 23–28.
[58] International Organization for Standardization, EN 673:1997 Glass in Building – Determination of Thermal Transmittance (U value) – Calculation Method, 1997.
[59] G. Kokogiannakis, J. Darkwa, C. Aloisio, Simulating thermochromic and heat mirror glazing systems in hot and cold climates, Energy Proc. 62 (2014) 22–31.
[60] G. Baldinelli, Double skin façades for warm climate regions: analysis of a solution with an integrated movable shading system, Build. Environ. 44 (6) (2009) 1107–1118.
[61] A. Jankovic, M.S. Siddiqui, F. Goia, An experimental data set on the thermal and fluid dynamic performance of double skin facades (DSFs) subjected to various controlled boundary conditions through the use of a climate simulator facility, 2021, https://doi.org/10.5281/zenodo.5808012.

4. Tracer gas techniques for airflow characterization in double skin facades

4.1. Abstract

Monitoring airflow rates and fluid dynamics phenomena in the ventilated cavity is a challenging aspect of the experimental assessment of the performance of double-skin facades (DSF). There are various methods to characterize the fluid-dynamics behavior of DSF, but each of these has its advantages and drawbacks. This paper presents the airflow characterization in the cavity of a double-skin façade installed in a full-scale outdoor facility through various methods, and, more specifically, it compares two tracer gas methods with the velocity traverse method. In the paper, we highlight how different characterization results can be explained by considering the features of each method, and how these differences are linked to velocity ranges and airflows in the cavity. By discussing (i) the challenges of these methods and their applicability, (ii) the requirements in terms of experimental set-up and (iii) the limitations linked to instrumentation, we aim to enhance the discussion on experimental methods for advanced building envelope characterization and contribute to a more grounded understanding of the suitability of tracer gas methods for in-field characterization of airflows in facades.

Nomenclature

Acronyms

CCM	Constant concentration method
CIM	Constant injection method
CMOS	Complementary metal-oxide-semiconductor
DM	Decay method
DVM	Direct velocity measurements
DSF	Double-skin facade
HVAC	Heating and ventilation air conditioning
LDV	Laser doppler velocimetry
PIV	Particle image velocimetry
USV	Ultrasound velocimetry
VPM	Velocity profile method
VTM	Velocity traverse method

Symbols

C	Concentration [ppm]
p	p-value [−]
t	time [s]
V	Volume [m^3]
V	Airflow rate [m^3s^{-1}]

Subscripts

b	Background
c	Cavity
tg	Tracer gas

4.2. Introduction

4.2.1. Background

Increasing the performance of building envelope systems is a long- established trend in research that aims at developing building skins that minimize energy use and maximize user comfort across different domains. This has lead to a large range of concepts and technologies in recent years [1] that are transforming the building envelope from being a problematic component of the construction to being an interesting locus of possibilities. Advanced concepts and technologies that consider the building envelope not as static but as a dynamic, active system have been developed within this research and development avenue [2]. Such an envelope should act as a living membrane that continuously changes its interactions with the indoor and outdoor environment by filtering mass and energy fluxes [3]. The most advanced dynamic building envelope components are responsive [4] and adaptive [2] building skins, and double skin facades (DSF) are a well-established concept in both research and industrial development that makes highly transparent skins highly efficient [5]. In simple terms, a DSF is a multi-layered glazed structure with an external and internal layer (the skins) and a buffer space in between (usually ventilated in different ways) that can host a solar shading device to enable continuous control of solar loads [6]. This envelope system allows a high degree of flexibility in managing the incoming thermal and visual loads, it can support the pre-heating of ventilation air, and in the most general terms, it can be operated as a dynamic interface between the outdoor and the indoor space [7]. A fully glazed facade brings the transparency often desired by architects when designing a residential or commercial building [8]. In addition, it enables balancing visual comfort, visual attractiveness, sound insulation, thermal comfort and energy savings [9]. However, DSFs are more expensive than traditional single-layer façades, and if they are not well designed and operated, the marginally increased performance is hardly able to justify their costs, or in the worst scenarios they could present a lower performance than conventional envelopes [10].

Even though the DSF is a long-established concept with many applications in real buildings, there is still much research ongoing focusing on both the optimization of the system in terms of construction features and the optimization of the control strategies and algorithms to manage the dynamic operation of DSFs dynamically operated. In this latter topic, the management of shading devices [11,12] and of the airflow in the ventilated cavity, and the interactions between these two elements interact [13,14] are key topics to ensure optimal performance of DSF. A deep understanding of how DSFs can be efficiently designed and managed depends on how well the physical processes occurring in the DSF are understood and predicted. The most reliable insight is offered by experimental

investigations [15], and many authors have performed experiments with different levels of complexity ranging from natural experiments [16–18] to those controlled with only thermal [19,20] or wind environment [21] to the experiments performed in both controlled thermal and radiative environment [15,22–24]. Data from experimental activities can also validate numerical models [25], opening up a path for design- and control optimization based on simulation.

The experimental characterization and performance assessment of a double skin façade (DSF) is a complex task, and well-established methods suitable for conventional envelope systems are often not capable of capturing the overall performance and measuring particular phenomena occurring in a DSF [26]. One of the most complex parts, if not the most complex one, concerns the determination of the airflow in the cavity, and this task is especially challenging when only naturally induced forces drive the airflow in the cavity. Various methods and techniques have been commonly adopted to monitor airflow rate, and many are standardized for the airflow estimation in HVAC ducts [27]. At the same time, there are no clearly defined procedures for measuring in DSF cavities, which are environments characterized by a higher degree of inhomogeneity compared to HVAC ducts. The methods for airflow assessment differ in the complexity and cost of the experimental set-up, accuracy, amount of information they can offer and applicability for in situ measurements. For some techniques, such as direct velocimetry, recommendations exist for more reliable set-ups that reduce the experimental error. While direct velocimetry is quite well known, and there is a clear understanding of how much this technique can offer, other methods need further research to evaluate their accuracy and applicability for airflow measurements in DSFs.

4.2.2. Research aims, objectives, and paper structure

In this paper, we present the results of a set of experimental measurements obtained to assess and compare different techniques for airflow estimation. This investigation is based on a multi-day experimental campaign of the DSF hosted in a full-scale outdoor test facility. Two gas tracer techniques, more precisely the so-called *decay method* (DM) and *constant injection method* (CIM), were tested and compared with the velocity traverse method (VTM), a well-established (and relatively simple) technique to measure the total airflow in a duct section. Both of the gas tracer techniques analyses in this paper are state-of-the-art methods that have been successfully applied for airflow measurements in HVAC systems with forced ventilation [28–30] or infiltration/exfiltration assessment in rooms and larger volumes [31, 32]. However, there is almost no research that deals with the application of gas tracer techniques for measuring airflow in DSFs, other than investigations [18,26,33,34] that employ only a constant injection method. Among these, only the research of Kalyanova [26] investigates the applicability of the constant injection method in DSFs and compares

it with other more common methods. Intending to expand knowledge about this technique and the decay method, which has not yet been employed in DSF, this research aims to identify challenges and issues related to the different experimental set-ups and measurement procedures applied to double-skin facades in actual conditions.

To do this, the methodological steps that we adopted were: to instrument (as described in more detail in the next section of the paper) a full-scale mock-up of a DSF installed on an outdoor test facility; to run several rounds of measurements with different techniques over a specific range of (assumed) airflows, and varying some controllable variables; to apply statistical analysis techniques to understand the relevance and the role of controllable and uncontrollable variables.

The experiments and the results presented in the paper give insights on: (i) how to perform the two gas tracer techniques, (ii) why they may lead to different results, as well as (iii) how the outcomes of these methods compare to the estimation of the airflow through hot-wire anemometry. Finally, it would be possible to suggest that one method may better suit a specific situation and airflow ranges in the cavity, though there are some uncertainties and limitations in the study primarily linked to the complexity of measuring a highly transient phenomenon in an in-field like installation. Aside from the measurement that resulted from the tests, which allowed us to characterize the tested façade, the outcomes of this research can be of interest to researchers who want to apply gas tracer techniques. Moreover, our research contribute to the development of standardized procedures for setting up the correct experimental set-up and carrying out measurements with the highest possible confidence.

In the following sections of the paper, we will: classify and review existing experimental techniques for airflow characterization in DSFs (Section 2); describe in detail the experimental set-up and methodology, focusing on DSF mock-up specifications, characteristics of the measurement equipment and details about the experimental design and procedures (Section 3); present the results and the comparison between gas tracer techniques and VTM, along with the details on correlation analysis, discuss the challenges and possibilities of these methods, and argue which methods are suitable for airflow characterization in different situations (Section 4); draw conclusive remarks of our study (Section 5).

4.3 Experimental techniques for airflow characterization

Experimental investigation of airflow varies by complexity and the depth of the insight it offers, and, generally, it can be divided into three categories/groups: bulk airflow measurements, direct velocity measurements (DVM) and non-intrusive velocity measurements methods, such as ultrasound measurement of velocity (USV), particle image (PIV) or laser doppler velocimetry (LDV) [35]. A short introduction to these three families of available methods is provided for the sake of completeness

even if, as previously mentioned, we will focus in this paper on bulk airflow measurements through tracer gas and on direct velocity measurements, and we will not explore other techniques because of some intrinsic limitation they present for in-field application.
In particular, the last two categories (PIV and LDV) can provide turbulent quantity analysis, offering a large amount of information about the flow, but at the same time, they are very complex to realize in terms of the experimental design and sensitivity [36] and are almost entirely limited to laboratory environments, while their in-field application is almost inoperable and difficult to carry out.

4.3.1. Direct velocity measurements

A method that uses the direct velocity measurements acquired by hot-wire, hot-sphere or vane anemometers represents the most applied method for airflow estimation in DSF, especially when it comes to in- field measurements. The experimental set-up may vary in complexity and in the amount of information it can offer, from the most basic one, where only one anemometer is used, to the most advanced such as the velocity profile method (VPM) [8,21,22,33,37]. In a VPM, several anemometers are placed along one or more heights inside the cavity, indicating in such a way the spatial distribution of the airflow. Spatial discretisation of such information needs to be balanced with the measurement accuracy since the sensors' probes, cable, and physical support represent obstacles to the flow. Besides the reduced flexibility of the experimental set-up, the main disadvantages of this method are the limited amount of information about the spatial structure of the flow provided by the punctual measurements, the issues with the determination of the airflow direction [38] and the inadequate accuracy for the lowest velocity ranges. Regardless of these limitations, studies have shown that this technique offers the best balance between complexity, set-up cost, accuracy, amount of provided information and applicability in in-field conditions.

4.3.2. Non-intrusive techniques

Non-intrusive techniques, such as laser Doppler (LDV), particle image (PIV) and ultrasound (USV) velocimetry, employ optical/acoustics methods for the determination of the airflow in the cavity. LDV assesses the velocity in fluid flow in a non-intrusive way by recording the Doppler (frequency) shift between emitted and reflected laser beams. The PIV technique obtains instantaneous velocity fields by recording images of particles at successive times, the velocity of the fluid is determined by the characteristics of the light scattered from fine particles illuminated by monochromatic light. USV is based on either measuring frequency shift or the difference in the transit time between two oppositely emitted ultrasonic pulses. USV techniques show the promising possibility for long-term airflow monitoring in DSFs, but further research is needed to fully understand their applicability [31],

especially in relation to the range of velocity that can be accurately measured by USV sensors. Many non-intrusive techniques such as those based on LDV and PIV are characterized by excellent accuracy, but they are at the same time limited by laboratory-restricted instrumentation, cost, complexity and sensitivity of the experimental set-up [36,39,40], therefore their application for in-field continuous measurements in buildings is unfeasible.

4.3.3. Bulk airflow method

Bulk airflow methods are based either on measuring the pressure difference along the airflow path in a DSF cavity (pressure difference method) or on monitoring the concentration of a tracer gas inside the cavity (trace gas techniques) [41]. The first method needs calibration, usually performed in the laboratory, to determine the empirical relation between the airflow rate and the measured pressure difference. Once it is calibrated, then it is relatively easy to set up the experiment in field settings. Still, care should be taken when choosing the representative sampling point for external pressure since it is susceptible to wind-induced turbulence [37]. The method shows excellent accuracy in estimating the mechanical flow in laboratory conditions, yet further research is needed to assess its applicability for real (dynamical) environments and naturally ventilated DSFs.

Tracer gas techniques are well-known methods to measure airflow rate in rooms and larger volumes. The following tracer gas techniques are the most commonly adopted: constant injection (CIM), constant concentration (CCM) and the decay method (DM). Sulfur hexafluoride (SF_6) or carbon dioxide (CO_2) are often used as a tracer gas, with the latter used more often as a preferred marker due to its low cost, faster response of CO_2 sensors and being a less harmful greenhouse gas with 23,500 times lower global warming potential (GWP) than SF_6 [42]. In DM, a particular concentration is achieved at the beginning of the experiment $C(t_1)$, whereafter the time (t_2-t_1) required for the tracer gas to descend close to the background reference level $C(t_2)$ is measured [43], based on which the average airflow rate $\dot{V}$ is assessed:

$$\bar{\dot{V}} = \frac{V}{t_2 - t_1} log_e \frac{C(t_1)}{C(t_2)} \quad (1)$$

where V represent volume of DSF cavity.

In a CIM, a fixed and known amount of tracer gas $\dot{V}_{tg}$ is steadily injected while the fluctuating concentration $C_c(t)$ is measured downstream so one can estimate the airflow rate $\dot{V}(t)$ [29]:

$$\dot{V}(t) = 10^6 \frac{\dot{V}_{tg}}{C_c(t) - C_b} \quad (2)$$

Background concentration C_b needs to be assessed as well, and if it is expressed in *ppm*, then a coefficient 10^6 *ppm* should be used in the equation. In a CCM, instead of injecting a fixed amount of tracer gas, a variable quantity is infused $\dot{V}_{tg}$ (t) so that constant concentration C_c is achieved downstream or in the volume where the measurement is carried out [44]:

$$\dot{V}(t) = 10^6 \frac{\dot{V}_{tg}(t)}{C_c - C_b} \quad (3)$$

In their review, Remion and colleagues [45] concluded that the gas tracer techniques do not interfere with the flow and that they better account for infiltration/exfiltration flows compared to conventional airflow measurement methods [46]. However, if not met, some limiting requirements, such as the assumption of gas tracer homogeneity and the flow steadiness during measurements, lead to increased uncertainties [47]. In addition, tracer gas techniques are intended for short-time characterization, and they are not suitable for continuous monitoring. Applications are primarily seen in ducts (with forced ventilation) and not commonly in DSF cavities [21,22]. Therefore, there are no clear guidelines on the experimental set-up, such as the preferred position and the number of emission and sampling points in the DSF cavity [47]. Furthermore, the assumption of non-interfering with the flow/driving forces is questionable as the tubes releasing gas and sensors measuring concentration need to be inserted into the duct/cavity. As such, they represent obstruction to the flow when the cavity is not very large realtive to the space occupied by the experimental set-up. Other sources of inaccuracies, such as drainage of emitted tracer gas near the opening, can result in too high airflow rates [41]. Also, injection of a significant amount of tracer gas could affect the fluid dynamics in the duct/cavity since the CO_2 or SF_6 have different gas properties than air [48].

4.4 Experimental set-up and methodology

4.4.1. Experimental test-rig

We performed the airflow characterization presented in this paper using a full-scale mock-up of a DSF installed in the outdoor test TWINS test facility [49]. The test facility has dimensions of (3.5 m (l) x 1.6 m (w) x 3 m (h)), and for this experimental campaign it hosted a DSF of (1.5 m (w) x 2.8 m (h)) which consised of 2 skins, made up of 2 double glazing units (1.22 m × 2.0 m, U-value = 1.2 W/m^{2}K, g-value = 0.47), separated by an air cavity (250 mm) (Fig. 1). The DSF was oriented nearly perfectly toward the south. It had four axial vertical fans (maximum flow of 220 m^3/h each) placed at 2.6 m from the bottom, though only a small fraction of the maximum theoretical flow rate can be achieved under real operative conditions. The cavity hosted a roller blind to control solar gain.

Different airflow paths between outdoor and indoor environments could be tested by operating the vents (1.5 m × 0.3 m).

Fig. 1. An experimental set-up consisting of CO_2-supply instrumentation, the DSF test sample, the automatic weather station (left) and the view from the inside of the cell (right).

The DSF module was equipped with the following sensors used for the airflow characterization: four air velocity and temperature transducers at two different heights inside the cavity (1 and 2 m height from the bottom of the cavity), five CO_2 concentration sensors (based on CMOS technology) that were previously calibrated in the laboratory against a gas tracer analyzer and could also measure temperature and relative humidity, and the outdoor anemometer to monitor both wind speed and direction in the horizontal plane (Fig. 1). Hot-wire anemometers could measure air velocity in four different ranges, but according to prevailing measurement conditions, we opted for the lowest output range (0.05 ~ 1 m/s) with the instrumental error of ±(0.1 m/s + 3%). The outdoor anemometer was located left of the DSF (Fig. 1). One CO_2 sensor was placed outside the DSF to measure the background CO_2 level and four were distributed in the cavity. The measurement sampling rate was 20 s (coherent with the CO_2 response time of the sensor) and CO_2 concentration was kept within the range of values read by the sensor. The following set-up was built to supply the CO_2 inside the cavity: a CO_2 tank equipped with a valve was placed outside the test facility; an asameter was located downstream of the tank and a gas flow meter was used to measure and control the injected CO_2 flow (Fig. 1).

4.4.2. Experimental procedures

For the CIM, a constant CO_2 flow was injected at the bottom of the cavity (8 pipes near the inlet vents). The CO_2 sensors were located in the upper part of the cavity to measure the CO_2 concentration

at the exhaust. The control valve regulated the amount of the injected CO_2, which depended on the configuration. It was necessary to intensify the volumetric flow of injected CO_2 with the enhancement of the fan speed and DSF openings (Fig. 2) in order to keep a large enough difference between the background CO_2 concentration and the CO_2 concentration in the cavity. However, there was a slight increase in average CO_2 level in the cavity as configurations shifted from left to right, as shown in Fig. 2.

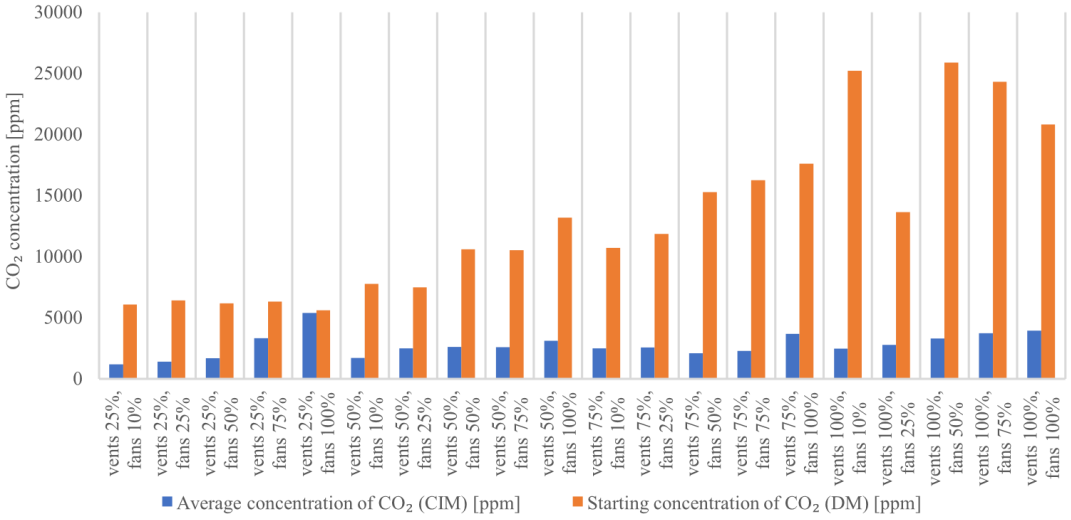

Fig. 2. The starting and the average CO_2 concentration in the cavity.

In the DM, four source pipes were set per side at two different heights and the CO_2 sensors were placed near the air velocity transmitters (Fig. 3). The CO_2 was injected at different cavity heights to reach the target CO_2 concentration (with all vents closed) and bottom fans were installed and used to ensure the perfect mixing of the CO_2 in the cavity (Fig. 1 right). When the target CO_2 concentration was reached, the bottom fans were switched off and the vents and top (main) fans were operated according to the tested configuration. Then, the time required for the CO_2 concentration to drop close to the background level was measured. It was necessary to inject higher volumes of CO_2 for configurations with larger openings to maintain a sufficient decay time in order to ensure a robust measurement. For example, the starting concentration needed to be between 20,000 and 25,000 ppm for the configurations with large openings (100%) to have a decay time of at least *100 s* (Fig. 3). However, as described in more detail in the next section, such a large CO_2 amount in the cavity affected the air mixture and may have changed its dynamics. As the volume of injected CO_2 normalized per volume of DSF cavity increased, the difference between it and the average concentration in the cavity increased too, meaning that one part was either directly lost to the outside or descended to the lower parts of the cavity below the level of the sensors.

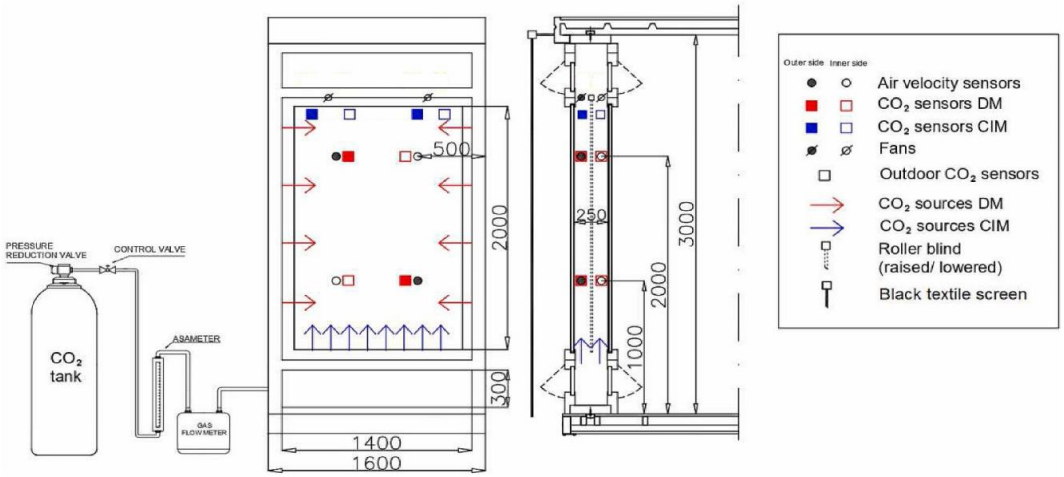

Fig. 3. Schematic representation of experimental set-up for different airflow characterization methods.

An attempt was made to minimize the influence of sudden changes of external factors by placing a black textile screen in front of the DSF and keeping the facility's door open. The screen was hung parallel to the outer surface of DSF at a distance of around 40 cm from the surface. The textile screen was also placed in front of both openings, shielding them from the direct effect of the wind. Here, it is important to highlight that due to the geometry of the openings (each realized by means of a top-hang, outward opening sash - see the schematic representation in Fig. 3), the presence of the screen did not obstruct the flow through the openings, but only shielded them from direct wind strikes. The black textile screen protected the DSF during both CIM and DM measurements.

Consequently, the wind influence was reduced to a certain extent, and the thermal gradient was kept to a minimal level compared to conditions one may experience in a DSF under real operations. Temperature differences between indoor (inside the test cell) and outdoor ranged between 5.0 and 7.4 ˚C, with an average value of 5.9 ˚C during CIM and 6.4 ˚C during DM measurements. The solar irradiance on the DSF's vertical surface ranged between 0 and 30.4 Wm^{-2}, with an average value of around 3 Wm^{-2} during CIM and 16 Wm^{-2} during DM measurements. Our goal in implementing these settings was to make the flow in the cavity as homogeneous and steady-state as possible by making it driven by the fan to the largest extent. By completely controlling boundary conditions, we could eliminate sudden and abrupt changes in external factors that may undermine the assumption of homogeneity and steady-state conditions in the cavity. Therefore, one of the assumptions underpinning this study was that the velocity profile was symmetrical and directed upward, which allowed us to calculate the airflow rate using the velocity traverse method (VTM) more easily.

The airflow rate was calculated in three ways by multiplying the cross-sectional area of the cavity and the average velocity (obtained from two sensors) for the corresponding height. The first two ways

involved correction of measured velocity by the factor k [27,50], while the third assumed that measured velocity corresponded to average velocity in the cavity. Comparing three approaches with the high-precise airflow measurements of the ultrasonic flow meter in the laboratory showed us that the third approach was most suitable for the airflow calculation in the specified conditions [54]. EN ISO 12569:2012 [31] and EN 12599:2012 [28] provided the basis for calculating the airflow for the DM and the CIM, respectively.

Different DSF cavity configurations were tested multiple times, comparing DM and CIM bulk airflow estimations with airflow assessment via the VTM. Twenty-three different configurations of DSF were tested with both DM and CIM by varying vent opening (25, 50, 75 and 100%), fan speeds (10, 25, 50, 75, and 100%) and roller blind's position (displaced and retracted). Only one airflow path was investigated in this experimental study for both the CIM and DM, i.e., the outdoor air curtain mode. In this ventilation mode, the outdoor air enters the cavity, and when it leaves the cavity, it is released again towards the outdoor environment. The DSF is therefore isolated from the test cell's indoor air, and outdoor air cannot enter the indoor space behind the DSF by going through the DSF's cavity.

The sampling of all the different physical quantities was performed every 20 s, which was the declared time constant of the employed CO_2 concentration sensors, while the duration of each experimental run depended on the characteristics of the chosen method. In CIM, the data acquisition period of each measurement run was 3 min, while for the DM, the duration depended on the decay time, which was between 600 and 100 s.

4.5 Results and discussion

4.5.1. Airflow assessment analysis

Both DM and CIM were tested and compared to the VTM, with DM showing a larger offset than CIM. In two cases with the raised roller blind, the estimated airflow value obtained through CIM exceeded the range of combined instrumental and measurement uncertainty added to the value obtained by VTM (Fig. 4). In almost all cases (12 out of 15), the airflow was overestimated compared to VTM, with an average relative error of 52%. However, VTM can not be considered a benchmark for evaluating other methods for the lowest airflow range due to the large instrumental error (indicated with vertical error bars) and low threshold value (0.05 ms^{-1}) of velocity sensors. Alternatively, if we consider cases where VTM can be regarded as reliable (marked with blue and gray columns), the relative offset to VTM is 31%. Therefore, CIM can be considered relatively successful in airflow estimation for the average velocity range in the cavity of over 0.1 ms^{-1} (Fig. 7., dots over the black line). A positive correlation coefficient (0.71) between airflows obtained by the VTM and CIM

confirmed the expected monotonic function between airflow and the opening size. As mentioned in experimental procedures, the injected CO_2 amount depended on the tested configuration. Experience in the experimental campaigns taught us that targeting levels below 2000 ppm can result in an unrealistic overestimation of the airflow or even in negative values because the CO_2 concentration in the cavity can get too close to or even fall below the background level. The upper limit of 5000 ppm proved to be high enough to prevent sudden drops to background levels, while at the same time low enough not to modify air mixture and dynamics.

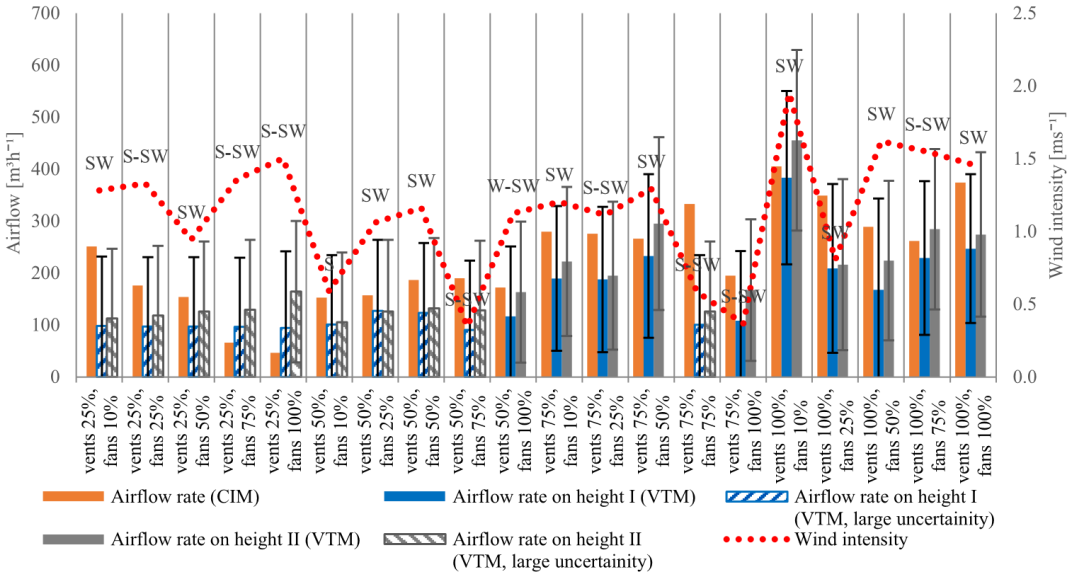

Fig. 4. Comparison of CIM and VTM for different tested configurations (raised roller blind).

DM and VTM showed a worse agreement. In nine cases, the assessment of DM was within the range of combined instrumental and measurement uncertainty of the VTM. The airflow derived by the VTM was considerably higher than obtained with DM (green bars in Fig. 5). However, due to the higher pressure drops caused by the small openings (25%) that led to lower airflow rates, velocity values below the instrumental threshold value were most likely present in those cases. Furthermore, considering the trend between VTM and openings in a reliable range (full colored bars in Fig. 5), it is probable that lower airflows than measured by VTM characterize smaller openings. Weighing the monotonic function between opening size and airflow assessed by DM, DM may be more suitable for low airflow assessment than VTM. As opposed to CIM, with an average relative error of 64%, the airflow in all cases by DM was underestimated compared to VTM. DM showed better agreement with VTM regarding monotonic function between airflow and size of the opening area and fans' speed (correlation coefficient between airflow values obtained by VTM and DM is 0.78).

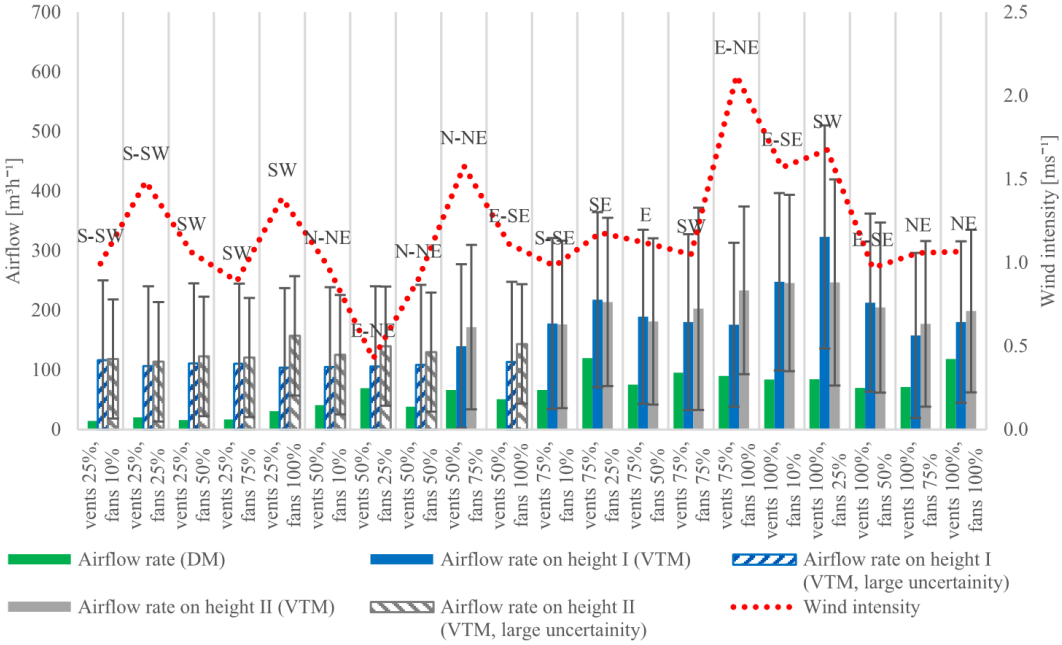

Fig. 5. Comparison of DM and VTM for different tested configurations (raised roller blind).

For the case where the roller blind was lowered, both gas tracer techniques underestimated the airflow rate compared to the VTM, except CIM for the configuration with 75% opened vent and 100% turned on fans (Fig. 6). With an average relative error of 23%, CIM showed better agreement with VPM, while in the case of DM, the error is 51%. The general conclusion is that the estimation of the airflow rate via DM and CIM was more accurate when the roller blind is lowered than when it is not. One may think this originates from the tested configurations and the associated higher airflows, where there is generally better agreement between methods. However, it might be caused by the presence of the roller blind making the flow more structured in each half-cavity. For the cases with lowered roller blind, the airflow estimated by VTM was higher in the inner cavity than in the outer, which might be caused by the slightly higher inner glazing temperature that led to the accelerated upward motion in the inner cavity. In contrast, colder outer glazing reduced the flow in the outer cavity. A similar phenomenon can be seen with the DIM and CM methods, which indicate that gas tracer techniques can also provide hints about the airflow's spatial structure, although these techniques rely on the assumption of even distribution of the tracer gas particles in the measurement volume.

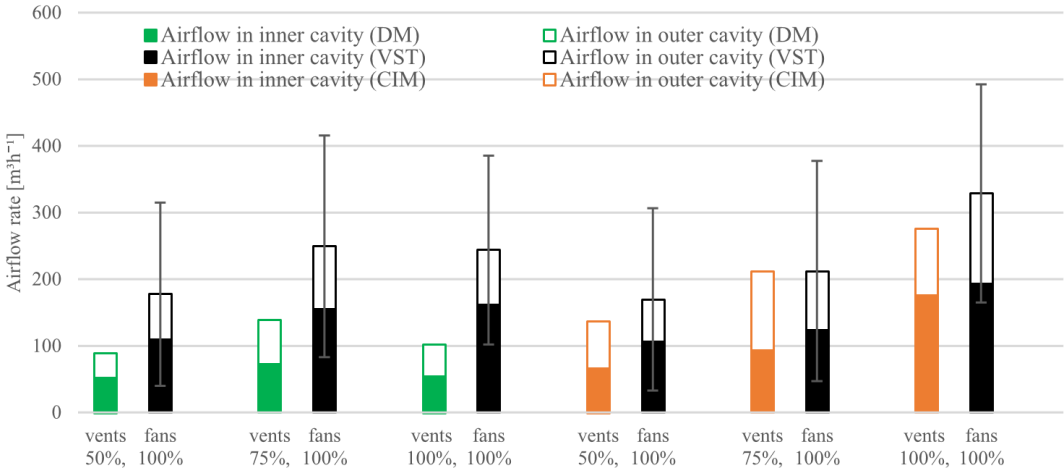

Fig. 6. Comparison of DM and CIM with VTM for different tested configurations (lowered roller blind).

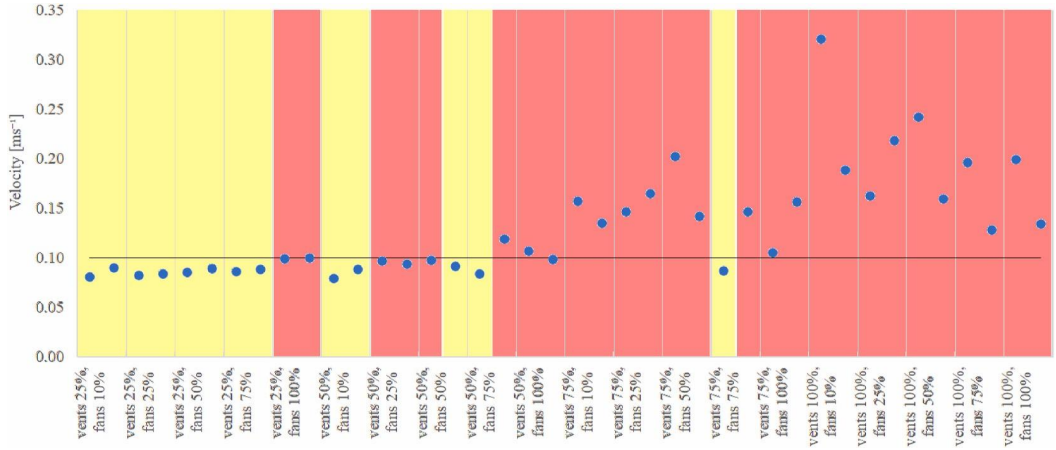

Fig. 7. Average velocity in the cavity and the assumed flow regime.

In both methods, it was noticed that measurements of certain CO_2 sensors deviated from the other. For example, in CIM, a CO_2 sensor installed at 2nd height in the inner cavity registered high fluctuations in CO_2 level, which led to the assessment of unrealistically extreme or even negative airflow rates. These fluctuations are most likely associated with sudden and sporadic direct penetrations of the wind (which has a lower CO_2 concentration), leading to violation of the good mixing assumption in the cavity. In DM, the decay curve for certain sensors showed different shapes and decay times, indicating non-uniform dispersion of injected CO_2 in the cavity. While one can think that differences in sensors' readings might be due to different devices being used, it is important to recall that all the sensors were calibrated in the laboratory before the experimental campaign. We can thus assume with a high degree of confidence that (substantially) different readings are meaningful and are not attributable to the sensor's performance difference. Therefore, care should be taken to select the sampling and injection point positions. It is recommended to use several sensors for

measuring CO_2 concentration and to conduct run pretests to find the most suitable positions and eliminate discrepancies between measurements. Furthermore, the CO_2 injection points in the DM method need to be distributed evenly along several heights to distribute CO_2 uniformly in the cavity.

4.5.2. Correlation analysis

To understand which factors influenced the airflow measurements and which controlled the airflow generation in the cavity, we ran a regression and correlation analysis using Pearson's correlation coefficient with a confidence level of 95% as a measure of dependence between variables. The results of the correlation analysis are shown in Table 1, and they refer to configurations with raised roller blinds. The temperature difference between the indoor and outdoor environment and the solar irradiance on the outer surface of the DSF were taken as factors that induce thermally buoyant flow, while the wind intensity and the opening size were taken as drivers of the wind-induced natural flow. Fans' speed was taken as an indicator of mechanical flow in the DSF cavity.

Table 1. Correlation analysis between airflow rates measured by different methods and various factors.

		Wind-induced natural flow		**Mechanical flow**	**Thermally-induced natural flow**	
		Wind intensity	**Opening size**	**Fan speed**	**Temperature difference**	**Solar irradiance**
Airflow rate	*VTM during CIM*	0.60	0.75	−0.16	−0.01	0.80
	VTM during DM	0.48	0.85	−0.09	0.10	−0.33
	CIM	0.19	0.82	−0.27	0.10	0.54
	DM	0.21	0.83	0.13	0.51	−0.42

The results of correlation analysis showed that opening size and wind intensity had a positive correlation with airflow rates measured by all methods. That was especially true for the opening size, where a very strong/strong positive correlation was found with the airflow rates measured by all methods. VTM displayed a moderate/strong positive correlation between airflow rate and wind intensity, while CIM and DM saw there a weak positive correlation. Other quantities did not show such a directed dependence for all considered methods.

The regression analysis performance for airflows measured by VPM with velocities over 0.1 ms^{-1} showed that statistically significant factors ($p < 0.05$) in the generation of the airflow were the opening

size (*p=0.008*) and the wind intensity (*p=0.006*). A regression model with the coefficient of determination of 0.71 excluded fan speed (*p=0.087*), temperature difference (*p=0.093*) and vertical solar irradiance (*p=0.926*) as statistically significant influencing factors. Based on both analyses, we can conclude that the airflow was to the greatest extent induced by the wind, where the opening, as expected, played a major role in controlling the rate. Also as expected, the correlation analysis showed that increasing the opening size and wind intensity lead to amplification of airflow. However, the influence of wind seems to have had a dominant role in controlling the flow rate even though dedicated expedients were implemented during the experiment to suppress the wind influence. This fact made it more complicated to ensure that the flow was homogeneous and under steady-state conditions. By setting the black textile screen, we may have significantly blocked the direct wind penetration in the cavity through the openings, especially for the smaller sizes (25 and 50%). However, it seemed that we could not completely eliminate associated turbulence and pressure field modifications caused by the wind. These caused air movement in and out the cavity, depending on wind intensity and direction. It was expected that the wind would increase pressure on the windward side of the test cell, while there would be a decrease on the leeward and lateral sides [51–53], with the addition that the presence of a black textile screen most likely reduced the influence of the wind from the clear southern direction. If we consider airflows assessed by VPM with velocities over 0.1 ms^{-1} on Figs. 4 and 5, it seems that winds with SW and S-SW directions amplified the airflow, while easterly winds suppressed the flow, which was in line with expectations [51–53]. However, due to the unknown wind's 3D behavior, along with instrumental limitations in measuring air speed values below 0.1 ms^{-1} and the complexity of weighing wind direction in statistical analysis, it was impossible to mathematically prove that wind direction amplified or hindered the airflow. Considering this, we can not claim that wind direction affected the measurements in a significant way, though it is very reasonable to assume that wind direction could have influenced the airflow in the cavity, even if its influence was probably not in the same range of magnitude as the wind intensity and the opening size. The wind is an uncontrollable variable in this type of experiment, and because of this feature, the only way to deal with it is to measure it as accurately as possible and to use statistical tools (in combination with repeated measurement runs) to infer its contribution.

Through the series of experimental settings adopted in the tests, we made the buoyant flow significantly low, especially for the medium and big size openings (75 and 100%). For these configurations, sudden wind strikes might have caused instabilities in the assumed "steady" state and oscillations in the CO_2 concentration, leading to airflow overestimation by CIM (the airflow estimated by this method is inversely proportional to the difference between CO_2 concentration in the cavity and the background level). Conversely, the decay time decreased with increasing airflow, which in

turn depended on the vent opening percentage. To ensure sufficient decay time for larger openings (75 and 100%), high CO_2 concentration needed to be injected in the cavity (10,000–35,000 ppm), which might have caused its subsidence and resistance to upward air motion due to higher molar mass of CO_2.

Air velocities below and around the instrument threshold were most likely present in configurations with very small and some small openings (25 and 50%). Hot-wire anemometers determined these velocities with large uncertainty (Fig. 7, dots below black line). Consequently, we can assume that the correlation analysis related to VTM most likely did not outline the actual drivers and characteristics of the flow for these configurations. Here, the flow could be more driven by the thermal effects and the fan, and the correlation analysis related to the DM could characterize the flow better. Furthermore, we can assume that the DM can be a suitable measurement technique in cases with very low airflows (average velocity below 0.1 ms^{-1}). In those configurations (very small and small openings), the air behaves similarly and leaks slowly, just like in building spaces, where this method has found its successful application. However, more research and comparison with more precise measurement techniques, such as ultrasonic flow measurements, are needed to prove this.

The analysis of the measured velocities for the case with raised roller blind also revealed that flow was turbulent for almost all the configurations (Fig. 7, red area), except for the least opened vents (25%), where its nature cannot be judged due to too low velocities. Corresponding configurations where the flow could be laminar or transitional are indicated with yellow color in Fig. 7, while turbulent ones are marked red.

4.5.3. Limitations

Our study highlighted how some variables could be tricky to control regardless of the many efforts put in place to have the highest possible control over the experimental domain. In this context, statistical tools that can allocate the variance of the response variable to different factors represent a valuable technique for better process understanding and interpretation of data obtained from in-field experiments. Furthermore, repeated measurements can provide more data for better applications of statistical tools. However, this type of analysis can also show some limitations, as in our case, we could not quantify the influence of wind direction due to accumulated uncertainties. Therefore, we could not associate and quantify certain adverse effects with wind direction, though it seems reasonable to assume that direction is a variable that can be of influence.

Looking back at the entire experience gained in this investigation, we can say that gas tracer techniques present limitations in assessing the airflow rate for in-field or in-field-like experiments

due to the rather complex experimental set-up, at least compared to other methods as the VTM. We also need to consider that they have shown a relatively high uncertainty, not far better than the simpler methods may offer. Using CO_2 as a tracer gas is a more environmentally friendly solution than other tracer gas, yet it is not free from impacting the environment. Alternative promising techniques suitable for continuous measurements, such as methods based on the orifice plate or ultrasonic measurements, could be further developed and compared to tracer gas methods in future studies to expand the analysis of the reliability of the different techniques for different measurement ranges.

Though one of the original goals of the investigation was to define clear best-practice procedures and guidelines for this type of experimental activity, we need to consider that this goal could not be fully developed based on the experiments we could carry out at this stage, as we realized that we would have needed to develop a more comprehensive experimental campaign that included DSFs of different dimensions, ventilation modes, weather conditions, and further variables that are outside the possibilities that we currently have. We nevertheless hope that our reflections on these techniques and the sharing of our experience with this particular set of measurements will help other researchers in carrying out their experiments and that, cumulatively, a more robust set of guidelines for tracer gas techniques applied to ventilated facades can be developed in the long run.

4.6 Conclusion

The outcomes of this study, which aimed at investigating how gas tracer techniques can be performed for in-field or in-field-like experiments and at assessing their performance in such context against a reference method (VTM), can be summarised according to the following points: dosing of the tracer gas, points of injection of the tracer gas, points for a sampling of the tracer gas, the overall performance of the techniques, and their applicabilities.

CO_2 dosing - In order to prevent unrealistic airflow estimation, CIM requires that the average CO_2 concentration in the cavity is several times higher than the background level (five or more times) with a reasonable upper limit of 5000 ppm that limits modification of air mixture and its dynamics. For the same reason, the initial CO_2 concentration in the DM should generally not exceed 10,000 ppm.

Injection points - Using several injection points in the cavity is desirable in both methods. In CIM, the CO_2 sources need to be placed at one height level nearby and above the inlet to allow the longest possible mixing path, whereby attention should be paid to avoid CO_2 'wash-out' effect. Injection points in DM should be distributed along several heights between inlet and outlet in both half-cavities to evenly disperse CO_2 along the airflow path. If a uniform distribution can not be achieved, an additional fan can be installed to mix more thoroughly CO_2 right before the start of decay time measurement while the cavity is still closed.

Sampling points – It is recommended that CO_2 sensors in CIM are placed evenly in the cavity at one height level close to the outlet, assuring that measurements are not influenced by outside air. Sampling points in DM should be distributed uniformly in the cavity volume so one may extract volumetric average values and check the homogeneity of CO_2 distribution.

Performance of the tracer gas techniques – Both techniques showed significant offsets compared to the velocity traverse method (VTM). CIM tends to overestimate the airflow, most likely due to the sudden drops in CO_2 concentration linked to the wind strikes and sudden and sporadic penetration of CO_2-depleted air in the cavity. DM tends to underestimate the airflow, which may arise from slow subsidence of highly concentrated CO_2, causing a longer time of CO_2 extraction. However, CIM showed acceptable agreement with VTM for configuration with higher airflow rates (air velocities over 0.1 ms^{-1}), while DM showed potential to be one of the few methods, if not the only one, available to estimate very low airflow rates.

Applicability of the techniques to in-field measurements - Both techniques have shown considerable limitations regarding airflow rate assessment in a field or in-field-like experiments due to the complex experimental set-up and relatively high uncertainty. For example, DM proved unsuitable for DSF configurations with large airflow rates where a significant volume of CO_2 needs to be injected to achieve a sufficiently long decay time, while CIM showed to be more sensitive to wind influences arising from the equation where the airflow is inversely proportional to the difference in CO_2 concentration. In this context of in- field experiments, statistical tools are essential elements to process data and reach sound conclusions. Repeated measurements are also a suitable strategy to obtain enough data, enabling more robust statistical processing of the collected measurements.

4.7 References

[1] A.S. Eugenia Gasparri, Arianna Brambilla, Gabriele Lobaccaro, Francesco Goia, Annalisa Andaloro (Eds.), Rethinking Building Skins – Transformative Technologies and Research Trajectories, Woodhead Publishing Series in Civil and Structural Engineering, 2021.

[2] R.C.G.M. Loonen, M. Tr˘cka, D. Costola, J.L.M. Hensen, Climate adaptive building´ shells: state-of-the-art and future challenges, Renew. Sustain. Energy Rev. 25 (2013) 483–493.

[3] M. Perino, V. Serra, Switching from static to adaptable and dynamic building envelopes: a paradigm shift for the energy efficiency in buildings, J. Facade Des. Eng. 3 (2015) 143–163.

[4] E. Taveres-Cachat, S. Grynning, J. Thomsen, S. Selkowitz, Responsive building envelope concepts in zero emission neighborhoods and smart cities - a roadmap to implementation, Build. Environ. 149 (2019) 446–457.

[5] W. Streicher, et al., On the typology, costs, energy performance, environmental quality and operational characteristics of double skin facades in European buildings, Adv. Build. Energy Res. 1 (2007) 1–28.

[6] E. Oesterle, R.-D. Lieb, M. Lutz, W. Heusler, Double-skin facades : *integrated planning*, München : Prestel (2001).

[7] M.M.S. Ahmed, A.K. Abel-Rahman, A.H.H. Ali, M. Suzuki, Double skin façade: the state of art on building energy efficiency, J. Clean. Energy. Technol. 4 (1) (2015) 84–89.

[8] F. Kuznik, T. Catalina, L. Gauzere, M. Woloszyn, J.J. Roux, Numerical modelling of combined heat transfers in a double skin faade - full-scale laboratory experiment validation, Appl. Therm. Eng. 31 (14–15) (2011) 3043–3054.
[9] M.A. Shameri, M.A. Alghoul, K. Sopian, M.F.M. Zain, O. Elayeb, Perspectives of double skin façade systems in buildings and energy saving, Renew. Sustain. Energy Rev. 15 (3) (2011) 1468–1475.
[10] A. Ghaffarianhoseini, A. Ghaffarianhoseini, U. Berardi, J. Tookey, D.H.W. Li, S. Kariminia, Exploring the advantages and challenges of double-skin façades (DSFs), Renew. Sustain. Energy Rev. 60 (2016) 1052–1065.
[11] M.H. Oh, K.H. Lee, J.H. Yoon, Automated control strategies of inside slat-type blind considering visual comfort and building energy performance, Energy Build. 55 (Dec. 2012) 728–737.
[12] M.G. Gomes, A.J. Santos, A.M. Rodrigues, Solar and visible optical properties of glazing systems with Venetian blinds: numerical, experimental and blind control study, Build. Environ. 71 (2014) 47–59. Complete.
[13] C.-S. Park, G. Augenbroe, N. Sadegh, M. Thitisawat, T. Messadi, Real-time optimization of a double-skin façade based on lumped modeling and occupant preference, Build. Environ. 39 (8) (2004) 939–948.
[14] S.-H. Yoon, C.-S. Park, G. Augenbroe, On-line parameter estimation and optimal control strategy of a double-skin system, Build. Environ. 46 (5) (2011) 1141–1150.
[15] V. Gavan, M. Woloszyn, F. Kuznik, J.-J. Roux, Experimental study of a mechanically ventilated double-skin façade with Venetian sun-shading device: a full-scale investigation in controlled environment, Sol. Energy 84 (2) (2010) 183–195.
[16] A. Zollner, E.R.F. Winter, R. Viskanta, Experimental studies of combined heat transfer in turbulent mixed convection fluid flows in double-skin-façades, Int. J. Heat Mass Tran. 45 (22) (2002) 4401–4408.
[17] H. Manz, A. Schaelin, H. Simmler, Airflow patterns and thermal behavior of mechanically ventilated glass double facades, Build. Environ. 39 (9) (2004) 1023–1033.
[18] D. Saelens, Energy Performance Assessment of Single Storey Multiple-Skin Facades, Catholic University of Leuven, 2011.
[19] T. Inan, T. Bas¸aran, M.A. Ezan, Experimental and numerical investigation of natural convection in a double skin facade, Appl. Therm. Eng. 106 (2016) 1225–1235.
[20] T. Inan, T. Basaran, A. Erek, Experimental and numerical investigation of forced convection in a double skin façade, Energies 10 (2017) 9.
[21] S. Hassanli, G. Hu, K.C.S. Kwok, D.F. Fletcher, Utilizing cavity flow within double skin façade for wind energy harvesting in buildings, J. Wind Eng. Ind. Aerod. 167 (2017) 114–127.
[22] L. Mei, D. Loveday, D. Infield, V. Hanby, M. Cook, Y. Ji, M. Holmes, J. Bates, The influence of blinds on temperatures and air flows within ventilated double-skin facades, Proc. Clima 2007 WellBeing Indoors (2007). http://usir.salford.ac.uk/id /eprint/15870/1/Clima_2007_B02E1606.pdf.
[23] T. Inan, T. Basaran, Experimental and numerical investigation of forced convection in a double skin façade by using nodal network approach for Istanbul. Sol, Energy 183 (2019) 441–452.
[24] T. Bas¸aran, T. Inan, Experimental investigation of the pressure loss through a double skin facade by using perforated plates, Energy Build. 133 (2016) 628–639.
[25] G. Gennaro, F. Fabio, F. Goia, G. De Michele, M. Perino, Calibration of DSF model for real-time control, in: Journal of Physics: Conference Series, 2069, IBPC, 2021, 012027.
[26] O. Kalyanova, Double-skin Facade: Modelling and Experimental Investigations of Thermal Performance, 2008.
[27] International Organization for Standardization, EN 16211:2015 Ventilation for Buildings - Measurement of Air Flows on Site - Methods, 2015.
[28] International Organization for Standardization, ISO 12599-2012 Ventilation for Buildings - Test Procedures and Measurement Methods to Hand over Air Conditioning and Ventilation Systems, 2012.
[29] International Organization for Standardization, ISO 16956:2015 Thermal Performance in the Built Environment — Determination of Air Flow Rate in Building Applications by Field Measuring Methods, 2015.
[30] S.B. Riffat, Comparison of tracer-gas techniques for measuring air flow in a duct, J. Inst. Energy 63 (1990) 18–21.

[31] International Organization for Standardization, ISO 12569: 2017 Thermal Performance of Buildings and Materials - Determination of Specific Airflowrate in Buildings - Tracer Gas Dilution Method, 2017.
[32] D. Laussmann, in: D.H.E.N. Mazzeo (Ed.), Air Change Measurements Using Tracer Gases: Methods and Results. Significance of Air Change for Indoor Air Quality, IntechOpen, Rijeka, 2011, p. 14.
[33] S.P. Corgnati, M. Perino, V. Serra, Experimental assessment of the performance of an active transparent façade during actual operating conditions, Sol. Energy 81 (8) (2007) 993–1013.
[34] L.C.O. Souza, H.A. Souza, E.F. Rodrigues, Experimental and numerical analysis of a naturally ventilated double-skin façade, Energy Build. 165 (2018) 328–339.
[35] E. Giancola, et al., Possibilities and challenges of different experimental techniques for airflow characterisation in the air cavities of façades, J. Facade Des. Eng. 6 (3) (Aug. 2018), https://doi.org/10.7480/jfde.2018.3.2470. Spec. Issue FAÇADE 2018 – Adapt.
[36] N. Safer, Mod´elisation des façades de type double-peau ´equip´ees de protections solaires : approches multi-´echelles, L'Institut National des Sciences Appliqu´ees de Lyon (2006).
[37] O. Kalyanova, P. Heiselberg, Experimental Set-Up and Full-Scale Measurements in the 'Cube, Aalborg University, 2008. Aalborg.
[38] R.L. Jensen, O. Kalyanova, C.-E. Hyldgård, On the use of hot-sphere anemometers in a highly transient flow in a double-skin façade, in: Proceedings of Roomvent 2007: Helsinki 13-15 June 2007, FINVAC ry, 2007.
[39] K.J. King, Turbulent Natural Convection in Rectangular Air Cavities, Queen Mary University of London, 1989.
[40] M. Bhamjee, A. Nurick, D.M. Madyira, An experimentally validated mathematical and CFD model of a supply air window: forced and natural flow, Energy Build. 57 (2013), 289–301.
[41] O. Kalyanova, R.L. Jensen, P. Heiselberg, Measurement of air flow rate in a naturally ventilated double skin façade, in: Proceedings of Roomvent 2007: Helsinki 13-15 June 2007, FINVAC ry, 2007.
[42] G. Myhre, D. Shindell, J. Pongratz, Anthropogenic and Natural Radiative Forcing. Climate Change 2013: The Physical Science Basis. Contribution of Working Group I to the Fifth Assessment Report of the Intergovernmental Panel on Climate Change [Stocker, T.F., D. Qin, G.-K. Plattner, M. Tignor, S.K. Allen, J. Boschung, A. Nauels, Y. Xia, V. Bex and P.M. Midgley (eds.)]., Cambridge University Press, Cambridge, United Kingdom and New York, NY, USA, 2014.
[43] D. Etheridge, M. Sandberg, Building Ventilation: Theory and Measurement, Wiley, 1997.
[44] H. Poirazis, Double skin façades for office buildings, Report EBD (2004).
[45] G. Remion, B. Moujalled, M. El Mankibi, Review of tracer gas-based methods for the characterization of natural ventilation performance: comparative analysis of their accuracy, Build. Environ. 160 (2019), 106180.
[46] N. Nikolopoulos, A. Nikolopoulos, T.S. Larsen, K.-S.P. Nikas, Experimental and numerical investigation of the tracer gas methodology in the case of a naturally cross-ventilated building, Build. Environ. 56 (2012) 379–388.
[47] F. Marques da Silva, M.G. Gomes, A.M. Rodrigues, Measuring and estimating airflow in naturally ventilated double skin facades, Build. Environ. 87 (2015) 292–301.
[48] A. Jankovic, F. Goia, Impact of double skin facade constructional features on heat transfer and fluid dynamic behaviour, Build. Environ. 196 (2021), 107796.
[49] V. Serra, F. Zanghirella, M. Perino, Experimental evaluation of a climate façade: energy efficiency and thermal comfort performance, Energy Build. 42 (1) (2010) 50–62.
[50] R.R. Rothfus, D.H. Archer, I.C. Klimas, K.G. Sikchi, Simplified flow calculations for tubes and parallel plates, AIChE J. 3 (2) (1957) 208–212.
[51] H.C. Lim, M. Ohba, Interference effects of three consecutive wall-mounted cubes placed in deep turbulent boundary layer, J. Fluid Mech. 756 (2014) 165–190.
[52] J. Zheng, Q. Tao, L. Li, "Wind pressure coefficient on a multi-storey building with external shading louvers, Appl. Sci. 10 (2020) 3. https://doi.org/10.3390/app 10031128, 1128.
[53] R. Jin, et al., "Numerical investigation of wind-driven natural ventilation performance in a multi-storey hospital by coupling indoor and outdoor airflow, Indoor Built Environ. 25 (8) (2015) 1226–1247.

[54] A. Jankovic, M.S. Siddiqui, F. Goia, Laboratory testbed and methods for flexible characterization of thermal and fluid dynamic behaviour of double skin facades, Building and Environment 210 (2022), 108700. In press, https://doi.org/10.1016/ j.buildenv.2021.108700.

5. Designing the design of experiments (DOE) – An investigation on the influence of different factorial designs on the characterization of complex systems

5.1. Abstract

Although a general set of guidelines and procedures for performing the design of experiments (DOE) exists, the literature lacks a recommended course of action for finding and selecting the optimal design of experiments among a large range of possible designs. This research tries to fill this gap by comprehensively testing more than thirty different DOEs through nearly half a million simulated experimental runs. The performance of various DOEs in the characterization of the thermal behaviour of a double skin façade (DSF) is assessed by comparing the outcomes of the different designs and using the full factorial design (FFD) as the ground truth. Besides the finding for the specific case study used in this investigation, this research allowed us to obtain some broad conclusions on the behaviour of different DOEs, which are summarized and translated into recommendations and a general decision tree chart for selecting the suitable DOE(s). The outcomes of this study help researchers and designers to apply DOEs that consider the extent of nonlinearity and interaction of factors in the investigated process in order to select the most successful and the most efficient designs for the specific process characterization.

Graphical abstract

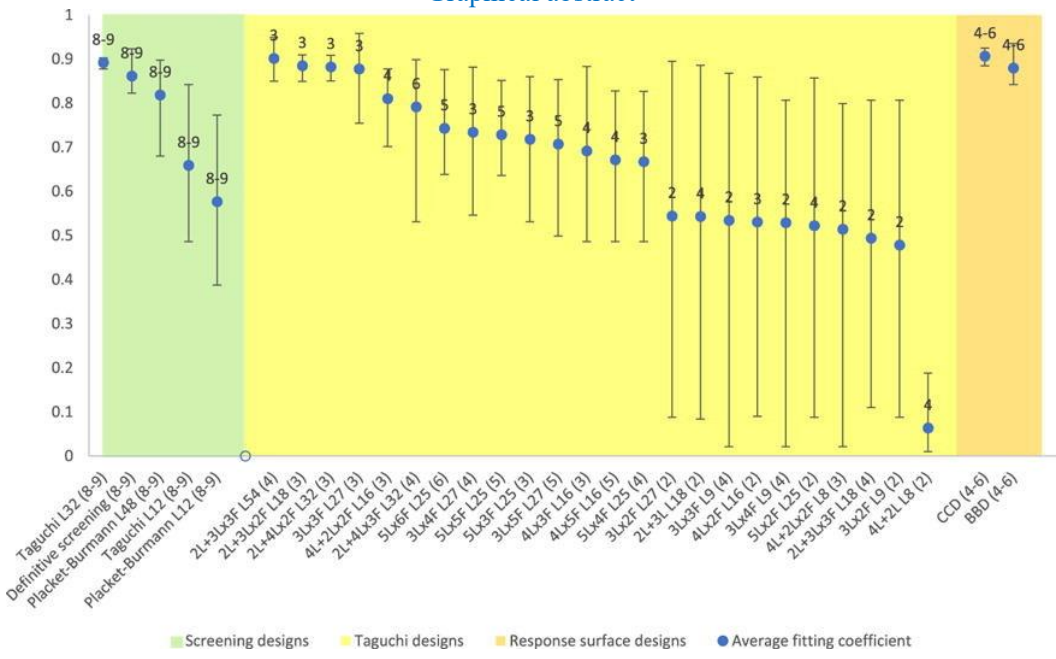

5.2. Introduction

Although developed primarily for agricultural purposes by British statistician Sir Ronald Fischer in the 1920s [1], the design of experiment (DOE) as a statistical method has been widely applied in different fields of science and industry, especially to support the design, development, and optimization of products and processes [2]. The design of experiments includes a series of applied statistics tools used to systematically classify and quantify cause-and-effect relations between variables and outputs in the studied process or phenomenon, which may result (if that is the aim) in finding the settings and conditions under which the process becomes optimized.

Well-established, general guidelines and procedures are available to support the implementation of DOE methods [3]. These steps include defining the objectives and response variables, determining factors, levels, experimental design type and experiment execution. Variables in the DOE such as the number of factors, levels, and the logic to select them usually depend on the type of investigation (screening, characterization, or optimization), the process type and the available resources. However, there is a multitude of different DOEs that can theoretically match the type of investigation, and therefore it is not straightforward to identify which design provides the best possible insight using the least resources. In general terms, a good experimental design ensures the validity of the given insight. However, good and excellent DOEs differ in efficiency, i.e., the ratio between extracted information from the examined process and the invested resources. Unfortunately, there is very little information in the literature that investigates and explains what types of procedures and steps need to be taken to find the optimal DOE among all the possible alternative options which have been developed and proposed.

The knowledge gap on how to select optimal DOEs became evident in our planning of the experiments in a controlled environment on a mock-up of an advanced fenestration system based on a double-skin façade (DSF) concept. This lack of recommended procedures in the literature, not only for the specific case of building envelope systems or even buildings but also in more general terms, motivated us to plunge into the search for answers to the following research questions: to what extent and why do different design of experiments give different results? And, further: what are the recommended steps to be followed to find optimal design(s) of experiments for given research?

We tackled this problem through a case study, where an advanced façade system was examined. The aim was to identify general guidelines that can facilitate finding one or more optimal designs of an experiment for different types of problems or processes, thus going beyond the specific case used in our investigation. Through the use of building performance simulation, we compared and analyzed a wide variety of fractional factorial designs to find one or more optimal methods for our specific case.

More than 400 000 simulation runs were performed to assess 30 different DOEs. The use of simulation tools to support the design of experiments is not a novel concept [5]. However, in this study, we used the possibility given by simulating a huge number of cases as a strategy to explore how it is possible to find optimal DOEs. As a secondary effect of this research strategy, we also showed how simulation tools could support the selection of the best DOEs and, at the same time, serve as good preparation for physical experiments.

Nowadays, researchers primarily select the DOE based on the assumed importance of the factors and the desired number of experimental runs [4–6]. If the aim is in-depth characterization, not knowing the nature of the complex process can lead to the wrong selection of experimental design and false conclusions about the importance of different factors, the extent and the type of nonlinearity within the process. A better understanding of what is the optimal or the best DOE(s) is important to assure that such a powerful investigation technique is properly used. Therefore, the results of this study can help researchers who need to find the optimal design for an experiment, using as few resources as possible and discovering as many details as possible about the process.

The remainder of this paper is organized as follows. In the following Section 2, we provide the reader with a background on DOEs and linked statistical tools. In the last part of this section, we also present a brief review of studies where simulation tools were employed to support experimental design. In Section 3 (Methodology), we give an overview of the general flow of the research, with details on: the specific case study, the numerical model implemented in software for building performance simulation, the description of the selected factors, the response variables, tested experimental designs, analysis of variance (ANOVA) and data analysis methodology for comparing various designs. In the fourth section, Results and Discussion, we present the outcome of our investigation of the case study based on the statistical analysis of variance performed on full factorial design (FFD) and its comparison with other DOEs. There, we summarize the performance of the different DOEs from the case study and provide a generalized flow-chart to facilitate selecting the appropriate DOE. Finally, in the fifth section, Conclusions, we recall the main lessons learned from the paper.

5.3. Background

5.3.1. Overview of the main DOEs

Each DOE can be seen as being composed of a series of steps: the planning, the execution of the experiment, and the analysis of the collected experimental data using various statistical methods in order to draw valid and objective conclusions [7]. Each DOE starts with selecting the system/process and recognizing the investigation problem. The problem statement leads to establishing the objectives

based on which the performance indicator (response variable) needs to be defined. The response variable should represent a quantitative measure of system behavior. As an essential step in the whole process, the factors affecting the performance indicator and how they are discretized, the number of experimental runs, and a suitable array need to be defined in the second stage [8]. The third stage covers the performance of the experiment according to the designed array and collection of data.

The last step includes data analysis using statistical tools (ANOVA and associated statistical methods) and interpretation of results, leading to a better understanding of system behavior or its optimization.

In order to examine the impact of several factors and interactions among them on the response quantity [9], experiments need to be performed systematically using factorial experiments (so-called factorial experimental designs/arrays), where several factors are altered during each experimental run.

A factorial experiment whose design consists of all possible combinations of the chosen factors and levels is called full factorial design (FFD). Effects of all factors (main effects) and interactions among them are considered in this design [8], making it a potent tool that, compared to other experimental designs, provides the most comprehensive insight into the system's behavior. If all factors k has the same number of levels n, the total number of runs is equal to n^k. By increasing the number of factors and levels, the number of experimental runs grows hugely. For classical experiments, this brings high costs and time consumption. However, due to enormous diversity in combinations, the response quantity variance can be explained, decomposed and attributed to all possible causes, thereby providing in that way an almost-realistic depiction of the process. The nature of the FFD means that its results can be considered good references to discuss other designs' performance in the characterization.

Besides FFD, there is a wide variety of factorial designs, and they differ in the insight they offer. The depth of the characterization depends on the resolution level of the design, which identifies the order of confounding the main effects and their interactions [10]. Resolution designs below III levels are not helpful, because, by definition, I level design consists of only one experimental run, while in II level, main effects are mutually confounded [11]. The most common types are III, IV, and V level designs [12]. Third-level resolution designs assess only the impact of factors, but these main effects are confounded with two-factor interactions. Fourth-level resolution designs consider main effects, and they are not aliased with two-factor interactions, but two-factor interactions are confounded with each other. In fifth-level resolution designs, the main effects are not aliased with each other or two-factor interactions, and two-factor interactions are not aliased with each other. However, higher-order interactions may originate a background noise in lower-order terms.

Selecting the ‘‘right” design means identifying the best way to sample the domain of possibilities. There is a wide variety of factorial designs. Some are used to screen out important variables (III

resolution), others to characterize processes (IV-V resolution) and a third type to optimize them (>IV resolution). Some designs, such as definitive screening or designs associated with response surface methodology (RSM), have been derived from factorial designs and can be considered partial factorial designs that include points (runs) that are not covered by standard factorial designs. In the following text, the main characteristics of experimental designs that have been studied in this research are presented. In our study we selected designs that are most often employed for characterization, both in science and industry. For the sake of completeness, we need also to recall that other types of designs, such as reliability, optimal custom, mixture, and split-plot designs can also be adopted [13–16]. However, they are employed either for purpose other than characterization or for the experiments that require special conditions, which is not of particular interest to our research.

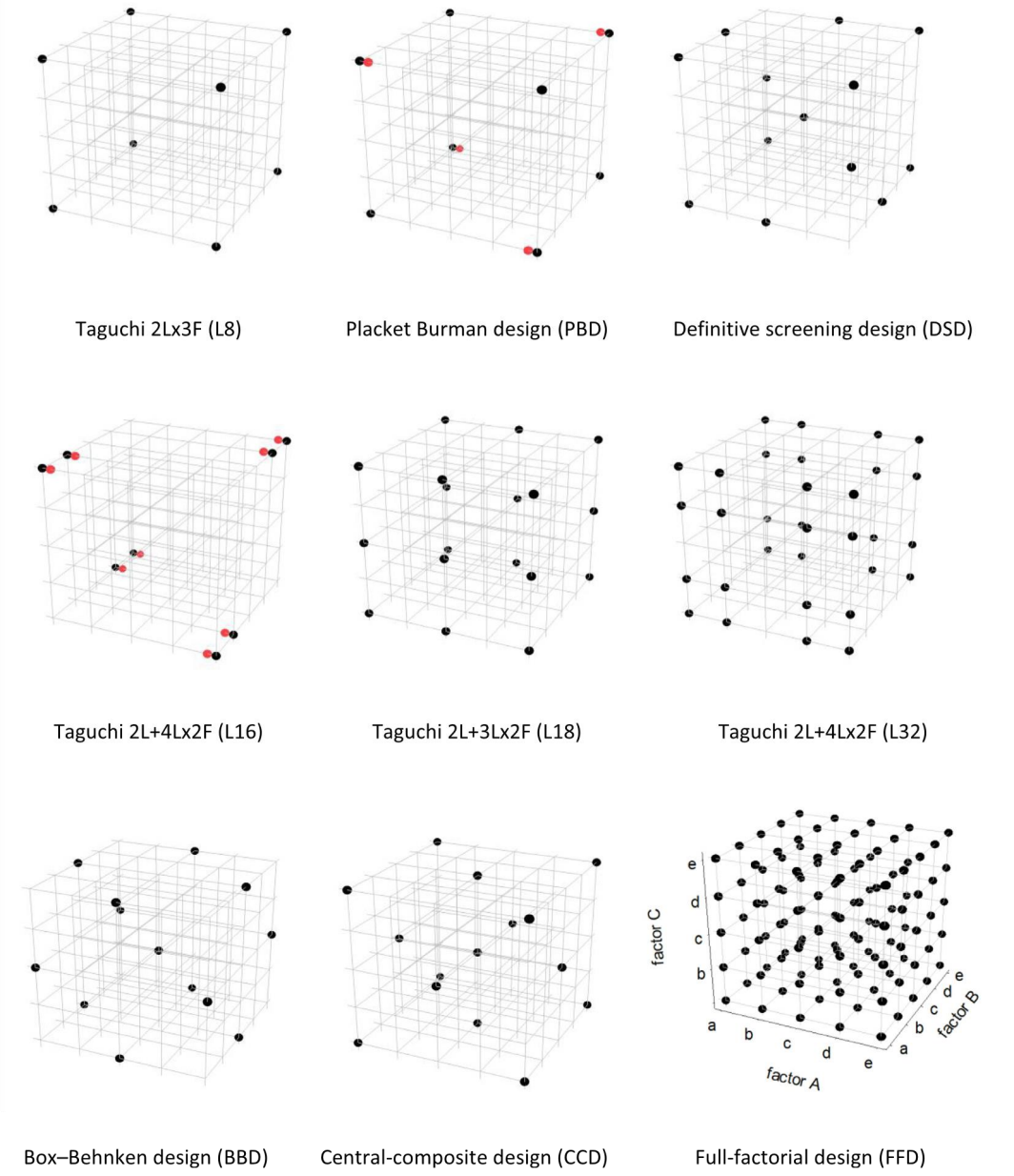

Fig. 1. Various designs for the three-factor model. The intersections of the lines represent the possible combinations of the three factors, while the black dots on some of these intersections represent the combinations to be investigated with that design. Red dots are tests repeated on some combinations to reach the minimum number of tests according to the specific design. In full-factorial design, all the possible combinations are explored.

The difference between various designs can be visualized, for example, assuming a problem with three factors (A, B, C), each discretized in five levels (a, b, c, d, e), as in Fig. 1.

Definitive screening design (DSD), unlike other screening designs, introduces the third (middle) level for continuous factors. At the same time, it lowers the number of required experimental runs to 2 k + 1 (k – number of factors) [17], which can be very suitable when some process is affected by a large number of factors [18]. This design can estimate two-factor interactions using a low number of experimental runs, which is impossible in other screening methods. For the characterization of complex processes affected by a high number of factors and interactions, DSD could be a suitable choice for screening and even characterization.

R.L. Plackett and J.P. Burman developed Placket-Burmann design (PBD) in 1946. Up to now, it represents one of the most applied screening methods [19,20] for recognition of the most significant factors among a large number of variables. Classic PBD is a third-level resolution design that offers insight into only the main (first-order) effects [21]. However, folding this design increases the number of experimental runs and resolution levels (to 4th), thus enabling the determination of two-factor interactions [22]. Both classic and folded PBD are studied in this research.

Taguchi design (TD). Despite its divided reception in the scientific community [23], Taguchi design, due to its practicality, became the most commonly applied experimental design, both in industry and science [18]. Its strength lies in effective orthogonal matrices where factor levels are distributed in a balanced way, reducing the required number of experimental runs [24]. Most orthogonal arrays are focused only on the main effects, but some designs allow the estimation of specific interactions. Given the practicality of TD, most of the experimental designs examined in this research are Taguchi's. Some of the designs are suitable for screening (two-level TD), while others are more suitable for more in-depth characterization and optimization.

Designs associated with Response Surface Methodology (RSM). These class of designs were developed in 1951 by Box and Wilson [25]. Over time, two main groups of designs have evolved: central-composite and Box-Behnken designs (CCD and BBD). They offer an understanding of the system behavior (reveal a type of connection between factor and response) and its optimization at the same time. CCD is usually applied after narrowing down important factors by some screening methods. It consists of central and axial points beside cube points, allowing insight into a curvature of response and estimation of higher-order effects [26]. BBD is similar to CCD but requires fewer experimental runs and does not contain points at the vertices of the cube (low/high points), which can be very useful for physical experimentation since extreme points are sometimes expensive or difficult to test [27]. For this reason, compared to standard CCD, BBD design contains regions of lower prediction quality [28]. Although RSMs are primarily oriented toward optimizing the system, we decided to include RSMs in the study since they offer an assessment of higher-order terms (quadratic or cubic), which is not possible with the other methods.

5.3.2. Statistical tools

Parallel to selecting representative runs that can sample the domain of exploration effectively, dedicated methods need to be employed to post-process the results of the experiment. In this way, qualitative and quantitative information on the impact of the different independent variables on the dependent variable is obtained. The analysis of variance (ANOVA) is an analytical and statistical procedure that determines if there are differences between group means in a sample and whether these differences exist only due to randomness or can be attributed to a specific cause. When it comes to DOE, the sample represents a series of experimental runs determined by design (i.e., L32, the sample of 32 experimental runs). In contrast, groups within a sample are a set of runs associated with a particular level/factor/interaction. By comparing group means and variation among them, ANOVA decomposes the total variance and attributes it to all the different causes, thus quantifying the effects of various predictors (factors and interactions) on the dependent variable.

While ANOVA evaluates the impact of various factors, interactions and randomness on the response quantity [29], regression analysis, on the other hand, builds a quantitative relationship between them in the form of a regression equation (model), most often using the least-squares method [30]. The coefficient of determination indicates how well an estimated regression equation explains the variance of the response variable. The RSM allows this regression model to be expanded even further to fit a polynomial function that includes cross-product terms that may be raised up to any power [31]. However, since the structure of the RSM model is only adapted to fit the low-degree Taylor series so it can perform well for the localized region, the class of lower-degree polynomials (up to three) is most often used. Sometimes, built models contain too many predictors, which may be impractical for predictive purposes, if that is the aim. In that case, a delicate balance between the complexity of the model (number of factors) and how well it predicts the response can be found through factor selection procedures. The most commonly adopted strategies to do so are forward entry, backward elimination, and stepwise selection procedures [35]. In an effort to keep this article concise, we cannot report here all the details about the calculation procedures of the ANOVA and the associated statistical methods, but the readers who want to obtain more information can find a synthetic descriptions of these aspects in Appendix A.

5.3.3. Applications of DOE methods in simulation studies for building physics problems

The use of simulations is becoming a commonly exploited strategy to support the optimization of the experimental runs in various fields of engineering and technology. At the same time, the use of methods for experimental design in computer simulations is an increasingly popular approach. These

trends can be considered two sides of the same coin: in both cases the goal is to minimize the resources necessary to understand a certain phenomenon – whether through experiments or through simulations. Accurate numerical simulations (such as CFD simulations) can be costly, time-consuming and require expensive software and computing equipment, and are therefore limited in their applicability. The utilization of DOE investigation methods provides a rationale to limit the number of accurate numerical simulations without losing the reliability of the overall picture obtained by the simulation runs. Furthermore, applying DOEs to simulations allows one to realize surrogate models that show an acceptable prediction accuracy and can be used in a fast and effortless way to explore large domains. DOE-based high-fidelity simulations can provide researchers with general trends and a high-level understanding of the relationships between variables used to optimize experimental runs. While a relatively large number of factors, levels and ‘‘experimental” runs can be oftentimes explored through DOEs implemented in simulations, high-quality experiments can be used to investigate in more depth particular regions or subdomains for a given problem that is identified after a simulation based pre-screening.

In some cases, simulations could also be the only possibility when physical experimentation is not available or where material saving in terms of labor costs and time is significant [32]. For the purposes of robust parameter design, noise factors can be more easily controlled in simulations compared to experiments, while also experimental variation (noise, error) is absent due to deterministic nature of simulations [33]. In a simulation-based DOE there is no need for randomization, replication of experimental runs, and division of runs into experimental blocks. This is due to the deterministic nature of simulations [34], consistency of input quantities and the ability to control noise (uncontrollable) factors. However, replication can be useful in folding designs where it is needed to increase the design’s resolution. However, simulation based DOE cannot be considered the perfect solution and should be used with caution. In addition to the common problems of physical experiments (selection of factors, levels, and optimal design), the final result of simulation-based DOE also depends on the simulations’ accuracy, i.e., the physics captured by the numerical representation of the mathematical model. If the simulation quality is not sufficient and therefore not reliable, then any DOE application makes no sense. Alternatively, using a perfect model/simulation that exactly replicates reality (if it exists) is useless as, in that case, everything is already known about the phenomenon/process. Yet, adopting the DOE approach in building performance simulation can be considered an effective strategy to combine detailed, computationally extensive simulations with the exploration of a large domain as an alternative approach to using other methods like parametric analysis and optimization.

There are, however, relatively few applications of simulationbased DOE in building energy performance research. Sadeghifam et al. [35] examined the influence of various building components and interior temperature on cooling energy loads of buildings in tropical areas using EnergyPlus simulations. Full factorial design with four factors and two-level resolution was applied and replicated three times to account for higher-order interactions. ANOVA analysis showed that the main effects were dominant (82.7 %), among which the ceiling had the most substantial influence. Jaffal [36] developed a simple polynomial function using DOE and regression analysis, which estimated the annual energy demand of a low energy building based on its envelope parameters. Simulations were done in TRNSYS. A total of 11 parameters with the two-level resolution were used: U-values of vertical walls, floor, windows, roof, the linear transmission coefficient of the thermal bridges, solar heat gains through north, east, south, and west windows, infiltration, and ventilation rates. Several different experimental designs were applied for three different climates (continental, oceanic and Mediterranean) to find optimal function: Taguchi's L12 and L20, a face-centered composite design with 35 runs, and four D-optimum designs (L68, L80, L136, and L160). Overall, the full quadratic model (D160) showed the best performance and lowest error.

Delgram [37] used EnergyPlus as a simulation tool and OFAT (one-factor-at-time) as an experimental design to assess the impact of building orientation, optical characteristics and size of windows, overhang system, and envelope thermal characteristics on building energy demand and annual lightning of a typical room for four different climate types in Iran. Variance-based sensitivity analysis showed window size as a prevailing parameter for building energy demand and glazing visible transmittance for annual lightning [37]. The Box–Behnken experimental design with 28 simulations performed in EnergyPlus was used to optimize an integrated daylighting and HVAC system [38]. Shen [27] compared full factorial (FFD), central composite rotation (CCRD), optimal (OPD), Box–Behnken (BBD) and space-filling design (SFD) to find the optimal design in the sense of a balance between accuracy and number of experimental runs. The aim was to find a regression model to assess ventilation rate from three factors with two-level resolution: sidewall opening size, outdoor wind speed and direction. For simulations, the CFD numerical model was used, and the SFD proved to be the most accurate, while the BBD was the most efficient.

In conclusion, it is possible to see that DOE methods have been used in combination with building performance simulation to investigate an array of different problems. However, in this area, as in many other areas of engineering and technology, there is a lack of guidelines and suggestions about how different designs can influence the results of an analysis based on the application of these methods. This knowledge-gap is addressed in this study through using simulation as a platform to investigate the implications of employing different DOEs (either in pure experiments or in simulation-

based analyses) for a specific case study (a double-skin façade), which we believe can well represent the complexity of many building science problems.

5.4. Methodology

The research methodology in this study is based on the objectives as listed below.

I) To select a problem and identify the independent variables and the dependent variable(s) which will be the target of the study.
II) To develop a numerical representation of the problem to be able to carry out simulations.
III) To identify a number of DOEs that can be utilized to study the selected problem.
IV) To apply a series of DOEs, and of the full factorial case, by using numerical simulations.
V) To post-process simulation data and execute the data analysis according to the relevant methods and tools on both the DOEs and on the full factorial case.
VI) To assess through comparison what information is obtained and what is the quality of such information from the different DOEs, using as the ‘‘ground truth” the results that are obtained by the full factorial design.
VII) To develop a series of guidelines for making the selection of the DOE a more grounded choice, supported by evidence collected both though the review of the literature in the field and the lessons-learned of this study.

The central assumption behind the overall methodological approach of this investigation is that it is possible to know the ‘‘true” behavior of a system when such a system is investigated through the full factorial design. In other words, the execution of the full factorial design allows us to ‘‘fully” know the impact of every single permutation (i.e. combining all the different levels and all the different independent variables) on the response variable. In this way, we obtain the representation of the entire complexity of the system, and by comparing this with the representations produced by another design (with a lower number of experiments compared to the full factorial design), we can assess how good the latter factorial design is in returning the ‘‘real” behavior of the system.

5.4.1. Case study

The case study selected for this research is a mechanically ventilated double-skin façade (DSF), where both constructional and operational features are selected as independent variables, and the global thermal performance corresponds to the response quantity, as explained more in detail at the end of this section. DSFs are advanced envelope systems where thermophysical, fluid mechanical and

optical phenomena that regulate the overall performance are highly dynamic and in constant interaction with different structural elements. Methods based on DOEs seem to be suitable tools to unveil the complex and intertwined interactions between different driving forces in DSFs. The impact of the different construction and operational features on how DSFs behave is still, in large aspects, incompletely evaluated and represents a current knowledge gap when it comes to assessing the performance of these envelope systems [51]. In the context of this study on DOE methods, the intrinsically articulated and multi-domain characteristics of a DSF make it suitable for use as a comprehensive yet relatively simple case technology to investigate the impact of the DOE formulation on the characterization of a certain performance.

The physical–mathematical modeling of such a building system is not a straightforward task [39], and for the sake of this investigation, a model of the DSF was implemented in the simulation environment EnergyPlus by making use of the in-build function ‘‘airflow window” [40]. This routine allows the users to specify different features of a DSF, together with the usual construction characteristics, and to model the five possible ventilation modes the airflow window can take: indoor air curtain (I-I), outdoor air curtain (O-O), air supply (O-I), exhaust (I-O), and air buffer mode (AB).

The DSF is incorporated in a virtual cubicle where only one surface (where the DSF is modeled) is exposed to the outdoor conditions, while all other surfaces are set as adiabatic and with a fixed temperature equal to indoor air temperature. The nature of this study required systematic experimental procedures in controlled conditions (i.e., fixed values of indoor and outdoor air temperature and solar irradiance). Therefore, dedicated settings were implemented to ensure the right conditions to replicate steadystate simulations.

The model of DSF simulated in this study has a transparent frontal area of dimensions 1.4 m (W) 2.8 m (H), with a cavity depth that can range from 20 to 60 cm. A venetian blinds system with 50 mm blinds is positioned at the center of the ventilated cavity between the inner and outer skin. The thermal and optical properties of glazing and venetian blinds of the case study DSF are summarised in Table 1.

Table 1. Thermal and optical properties of glazing and venetian blinds implemented in EnergyPlus

	Inner/outer glazing			*The front side of the slat*			*The back side of the slat*		
	Type 1	Type 2	Type 3	Type 1	Type 2	Type 3	Type 1	Type 2	Type 3
Total thickness [cm]	1	1	2.3	0.23	0.23	0.23	0.23	0.23	0.23
Solar transmittance [-]	0.83	0.59	0.43	0.03	0.03	0.03	0.03	0.03	0.03
Front side solar reflectance [-]	0.08	0.27	0.26	0.36	0.59	0.83	-	-	-
Back side solar reflectance [-]	0	0	0	-	-	-	0.36	0.59	0.83
Front side IR emissivity [-]	0.9	0.9	0.9	0.9	0.9	0.9	0.9	0.9	0.9
Back side IR emissivity [-]	0.9	0.9	0.9	0.9	0.9	0.9	0.9	0.9	0.9
Conductivity [$Wm^{-1}K^{-1}$]	0.3	0.3	0.3	205	205	205	205	205	205

When it comes to the independent variables that can influence the global thermal performance of the facade, the following factors were chosen:

- the temperature difference between indoor and outdoor air [ºC] (discretized in 5 levels)
- incident solar irradiance on the vertical plan [Wm^{-2}] (discretized in 5 levels)
- slat angle of venetian blinds [] (discretized in 5 levels)
- airflow rate [m^2s^{-1}] (discretized in 3 levels)
- cavity depth [cm] (discretized in 3 levels)
- optical and thermal properties of the inner and outer glazing [-] (discretized in 3 levels/types), and
- optical properties of front and back surface of blinds [-] (discretized in 3 levels each).

In the simulation runs, the indoor temperature was kept constant at 20 ºC while wind influence was excluded from this research. Three types of inner/outer glazing and front/back surface of venetian blinds were taken into consideration, and their characteristics are given, together with information on the different levels for the independent variables, in Table 2.

Table 2. Factors and corresponding levels for FFD

	Level I	*Level II*	*Level III*	*Level IV*	*Level V*
Temperature difference [^{0}C] (DBT)	-20	-10	0	10	20
Incident solar radiation [Wm^{-2}] (ISR)	0	200	400	600	800
Slat angle of blinds [^{0}] (SA)	OFF	90	60	30	0
Airflow rate [m^2s^{-1}] (AR)	0	0.04	0.08		
Cavity depth [cm] (CD)	20	40	60		
Inner glazing [see Table 1] (IG)	LOW	MED	HIGH		
Outer glazing [see Table 1] (OG)	LOW	MED	HIGH		
The front side of the slat [see Table 1] (FSR)	LOW	MED	HIGH		
The back side of the slat [see Table 1] (BSR)	LOW	MED	HIGH		

The dependent variable, i.e., the response quantity in this study, was the global thermal performance of the DSF, which is constituted by the total heat gain density associated with examined DSF element according to the general equation:

$$q_{net} = q_{sol,SW} + q_{sol,LW} + q_{conv} + q_{vent} + q_{ent} \quad (1)$$

where the intensity of transmitted solar irradiance through the element is given by $q_{sol,SW}$, longwave irradiance exchanged between the inner glazing and the interior environment by $q_{sol,\,LW}$, and the heat flux density transferred by convection between the interior surface of the glazing and indoor environment by q_{conv}; q_{vent} indicates the convective gain or loss due to the airflow that passes through the cavity, and q_{ent} gives the contribution necessary to compensate the convective heat gain or loss

due to infiltration to assure the air mass balance in those configurations where mass exchange occurs between inside and outside.

All quantities are normalized per unit area, and they are given with the next equations:

$$q_{sol,SW} = \tau \cdot I \tag{2}$$

$$q_{sol,LW} + q_{conv} = (h_{conv} + h_{rad}) \cdot (t_i - t_{is}) \tag{3}$$

Transmitted solar irradiance depends on the optical properties of glazing and shading (s – solar transmissivity of the DSF system). Convective and infrared heat exchanged between surface and indoor air is dependent on its temperature difference (t_i-t_{is}) and emissivity of glazing that faces an indoor environment. There are various empirical formulas for convective and radiative heat transfer coefficients (h_c and h_r) implemented in EnergyPlus, and the following algorithms were adopted in this study: TARP and DOE-2. Convective heat exchange between indoor air and airflow that passes the cavity and enters the indoor environment is given with q_{vent}, in equation (1):

$$q_{vent} = \dot{m} c_p (t_{gap} - t_i) \tag{4}$$

Where ṁ represents air mass flow rate, c_p specific heat capacity at constant pressure, and t_{gap} temperature of air that enters the interior from the gap. Convective heat exchange is equal to zero due to the absence of interaction with indoor air in O-O, AB, and I-O ventilation mode. The last term in Eq. (1) represents energy that needs to be added or subtracted from the air infiltrated from the outside in order to bring its temperature to the interior one:

$$q_{ent} = \dot{m} c_p (t_o - t_i) \tag{5}$$

The infiltrated air from the outside replaces the air ventilated through the DSF cavity to the outside environment. In this way, the air balance is maintained. As might be expected, this quantity is different from zero only for exhaust ventilation mode.

5.4.2. Tested DOEs

Full factorial design (FFD) considers the highest number of factors and levels, which results in by far the largest number of experimental runs. Such diversity in combinations means that ANOVA results for this design can be considered a benchmark for other designs' performance in process characterization. The following factors and corresponding levels were chosen for four ventilation modes (O-O, I-I, O-I, I-O):

The total number of simulations was 91,125 simulations for each ventilation mode, except AB, where the number of factors was reduced to 8 (no airflow rate), leading to a lower number of simulations (30,375). Considering all five ventilation modes, the total number of simulations was nearly 400,000.

Screening designs - Definitive screening (L17/L21), PlackettBurman (L12), folded Plackett-Burman (L48) and two two-level Taguchi designs (L12 and L32) were tested as screening designs. Levels in the screening designs were chosen to correspond to high and low levels from FFD, while the same number of factors was considered. DSD introduces an additional intermediate level between high and low for continuous factors, making the characterization deeper. In order to suit the structure of this design, five factors whose physical properties are continuous were arbitrarily discretized. Therefore, level II (MED) was defined as the intermediate level for the factors: inner and outer glazing type and the front and backside of the slat. For the slat angle of the blinds, open blinds (90, level II) were taken to represent the intermediate level that is found between low (0) and high (OFF) levels. Here it is useful to highlight that although some of the factors in the problem we analyze may appear to be categorical (like the glazing type, or the shading position), they are simply technological implementations of continuous factors, as the fundamental equations that describe the relations between independent and dependent variable make use of continuous factors (which are the thermal and radiative properties of the different layers in the DSF). For example, in this case the slat angle of venetian blinds can be described with the direct solar transmissivity of a layer placed in the middle of the DSF (the shading system), whose value goes between zero or close to zero (fully closed) and one (no shading system). In DSD, AB ventilation mode has a lower number of experimental runs (L17) than other ventilation modes (L21) because it contains fewer factors (8 compared to 9).

Taguchi multilevel designs - Twenty-three different Taguchi multilevel designs were tested in five different ventilation modes, resulting in 115 designs and 2480 experimental runs. Arrays differ in the number of experimental runs (8–54) and considered factors (2–6), leading to some being able to assess the main effects (F), while others can evaluate both main effects and interaction (F&I). The values for the levels in Taguchi designs are chosen to correspond to those of FFD. Unlike screening designs, Taguchi multilevel and RS designs do not consider all factors, so it was necessary to define base levels for factors not included in designs. Base levels were set to ‘mid’ levels or in a state where the related element is not present and cannot influence heat transfer (Table 3). Factors included in Taguchi multilevel designs were selected based on the magnitude of their contribution seen by the ANOVA applied on FFD.

Table 3. Base levels of factors that were not included in Taguchi's multilevel design

Factors	*Temperature [°C]*	*Incident solar radiation [Wm^{-2}]*	*Slat angle [°/-]*	*Airflow rate [m^2s^{-1}]*	*Cavity depth [cm]*	*Inner glazing [-]*	*Outer glazing [-]*	*Inner blinds [-]*	*Outer blinds [-]*
Base	20	0	OFF	0	40	MED	MED	MED	MED

Designs associated with RSM - Central composite and BoxBehnken designs (CCD and BBD) were chosen as representative cases of designs associated with RSM. The number of experimental runs in these cases grows significantly if categorical runs exist. Though some of the factors in this investigation may seem to be categorical at first sight (e.g. the glazing type), because the underlying physics is based on continuous physical properties and functions, there was no need to treat such factors as categorical. This makes it possible to limit the numbers of runs to 25–45 for CCD, depending on the number of factors included in the design (four to six). For Box-Behnken design, the number of experimental runs goes from 24 to 48, depending on the number of factors considered (four to six factors). The RSDs include only those factors that ANOVA and FFD see with a percentage of contribution greater than 1% (including interactions). Factors not included in RSDs are tuned to their base levels, just like for the Taguchi multilevel designs. The face-centered type of CCD was selected with an alpha value of one so that the axial points fall into the interest range and correspond to low and high levels of FFD. The type of glazing, blind's radiative properties and shading system state were chosen to suit the corresponding axial and center points required by the CCD and BBD. Due to the deterministic nature of the simulations, one center point, along with no replication and randomization of runs, was selected as the preferred settings for both designs.

Since a large number of simulation runs were carried out in this study (i.e., nearly 400,000 for the FFD and around 3500 for the whole set of investigated DOEs) through the use of EnergyPlus, the simulation workflow, including inputting data, running simulations, reading output and classifying data, had to be automatized. A template input file for EnergyPlus was created as the first step in the workflow, and through a dedicated custom-made Python script, individual input data files were then authomatically created for each simulation (hence changing the independent variables). Another Python script was then used to run all the group EnergyPlus simulations and post-process the simulation's output data. The output data for all simulations were then collected in a single CSV file, later used for further analysis.

5.4.3. Data analysis

Simulation outputs from both the FFD and the different factorial designs of the investigated DOEs were processed by applying ANOVA to identify the nature of the process and the cause-andeffect relationships between the variables. ANOVA quantified the impact of factors, and factors' interactions, on the response variables and estimated the amount of the variance that cannot be explained and attributed to the factors and their interactions. However, that means that ANOVA of the FFD also contained a certain amount of unexplainable variance. To consider full factorial analysis highly successful, the amount of unattributable part of variance needs to be negligibly small, or in other words, the coefficient of determination needs to be very high (R^2 0.95–1.00). An additional condition that ensures that variance is explained only by significant factors is that the values of the adjusted coefficient of determination and of the predicted coefficient of determination are similar to the value of the standard coefficient of determination R^2.

To assess how well each (simpler) factorial design matched the information extracted from the full factorial design for a given factor and interaction, and to have such an assessment carried out in a quantitative way, we introduced in this study a new metric called fitting coefficient ([]). This indicator was conceived as a one-value number that provides a comprehensive assessment of the ‘‘distance" between the output information of a certain design and the correspondent information in the full factorial design, as well as the assessment of the match between the unexplained variance in the FFD and the certain design. This coefficient is calculated for each specific factor and interaction and can assume values between 0 and 1, where 0 means that the particular design does not detect any statistically significant dependence of the response variable on factors, while the FFD explains all the variance (tested model fails, FFD succeeds). Some designs are able to estimate the contributions of each individual factor, but if they do not leave any degrees of freedom for the calculation of the error, they are not able to assess whether these contributions are statistically significant. Therefore, these designs are considered unsuccessful in characterization. A value equal to 1 means that the compared design provides an identical picture as FFD and that at the same time, FFD can explain all variance (both tested model and FFD succeed) in a statistically significant way. The mathematical formulation of the fitting coefficient is given in Equation 6, where $SS_{F\&I}/SS_{T,FFD}$ is the contribution of the specific factor/interaction in a full factorial design, and $SS_{F\&I}/SS_{T,D}$ is the corresponding contribution in tested design. Furthermore, $SS_{E,FFD}/SS_{T,FFD}$ represents the extent of randomness (unpredictability) in the process seen by ANOVA in the full factorial design, while $SS_{E,D}/SS_{T,D}$ represent same for the tested design. A total number of factors and interactions is given with max, and depends on the FFD. For the considered case, this number is equal to 45.

$$f = 1 - \frac{\sum_{F\&I=1}^{max} \left| \frac{SS_{F\&I,FFD}}{SS_{T,FFD}} - \frac{SS_{F\&I,D}}{SS_{T,D}} \right| + \left| \frac{SS_{E,FFD}}{SS_{T,FFD}} - \frac{SS_{E,D}}{SS_{T,D}} \right|}{2} \quad [-] \qquad (6)$$

For each design applied to a particular ventilation mode, the fitting coefficient f was systematically calculated. Since there are five possible ventilation modes, the range of variation of the fitting coefficient was identified for each design and the average value of the fitting coefficient f calculated using all possible modes. These two quantities (the range of f and the average f) were used to classify the performance of the different DOEs against the FFD.

In FFD, a second order fixed-effects model in FFD was adopted, and this showed excellent coefficients of determination. We did not consider it necessary to employ higher-order fixed-effect models because this would have been harder to physically interpret (if physical interpretations were even possible) and, in the end, to compare with lower resolution designs. The existence of statistically significant higher interactions in the fixed-effect model may indeed not have an obvious physical interpretation, but can only mean that any optimization must simultaneously take into account pairs, three or more n-tuples of factors. In CCD and BBD we adopted a full quadratic polynomial model and both the contribution of first-order and the contribution second-order cross-product were considered when assessing the contribution of each factor

5.5. Results and Discussion

5.5.1. ANOVA for full factorial design and factors' influence

The analysis of variance for the FFD revealed the functional dependence of total thermal gain. It showed that the DSF's behaviour can be represented in a very satisfying way with a model that includes only the main effects and interactions (Table 4). The addition of higher-order terms (quadratic, triple interactions, or cubic) complicates the model and reduces the coefficients of determination (adjusted and predicted). Each ventilation mode was assessed independently, and separate ANOVAs were carried out for each of the five ventilation modes. It was impossible to produce one FFD that encompassed all the ventilation modes since the air buffer (AB) mode does not have the same number of factors. Furthermore, when the four ventilation modes were analyzed together, a less satisfactory result (R^2 = 86.6 %, Error = 13.4 %) was achieved compared to FFDs for separate ventilation modes and corresponding, independent ANOVA.

Table 4. Contribution of all factors and interactions for five ventilation modes.

	Contribution [%]				
Ventilation modes	I-I	I-O	O-I	O-O	AB
Model R^2	98.46	99.73	99.59	97.90	99.02
Model R^2 (predicted)	98.45	99.73	99.59	97.89	99.01
Model R^2 (adjusted)	98.46	99.73	99.59	97.90	99.01
Linear	91.23	65.01	68.49	81.00	90.34
2-Way Interactions	7.23	34.72	31.10	16.90	8.68
Error	1.54	0.27	0.41	2.10	0.98
DBT	1.36	52.89	48.12	2.03	0.81
ISR	79.21	7.69	18.03	51.60	75.73
SA	4.06	2.47	1.04	16.38	9.17
AR	3.48	1.10	0.54	5.27	–
CD	0.01	0.00	0.00	0.00	Not sign.
IG	0.57	0.30	0.14	2.03	2.17
OG	2.04	0.55	0.50	3.65	2.22
FSR	0.47	0.00	0.10	0.03	0.23
BSR	0.04	0.00	0.01	0.02	0.00
DBT*ISR	Not sign.	0.00	0.01	0.01	0.00
DBT*SA	Not sign.	0.00	0.00	0.00	Not sign.
DBT*AR	0.11	32.22	29.48	0.11	Not sign.
DBT*CD	0.00	Not sign.	0.00	Not sign.	Not sign.
DBT*IG	0.00	0.00	0.00	0.08	0.02
DBT*OG	0.05	0.00	0.00	0.01	0.01
DBT*FSR	Not sign.	Not sign.	0.00	Not sign.	Not sign.
DBT*BSR	Not sign.	Not sign.	0.00	Not sign.	Not sign.
ISR*SA	2.05	1.24	0.53	8.27	4.58
ISR*AR	1.71	0.41	0.30	2.79	–
ISR*CD	0.00	0.00	0.00	0.00	Not sign.
ISR*IG	0.29	0.15	0.08	1.02	1.12
ISR*OG	1.04	0.28	0.26	1.84	1.10
ISR*FSR	0.24	0.00	0.05	0.01	0.11
ISR*BSR	0.02	0.00	0.00	0.01	0.00
SA*AR	0.19	0.05	0.04	0.28	–
SA*CD	Not sign.	Not sign.	0.00	Not sign.	Not sign.
SA*IG	0.14	0.06	0.03	0.43	0.22
SA*OG	0.59	0.21	0.15	1.41	1.11
SA*FSR	0.43	0.01	0.09	0.10	0.28
SA*BSR	0.05	0.00	0.01	0.01	0.01
AR*CD	0.00	0.00	0.00	0.00	–
AR*IG	0.12	0.01	0.03	0.04	–
AR*OG	0.03	0.04	0.01	0.25	–
AR*FSR	0.05	0.01	0.01	0.06	–
AR*BSR	0.01	0.00	0.00	0.02	–
CD*IG	0.00	Not sign.	Not sign.	Not sign.	Not sign.
CD*OG	0.00	Not sign.	0.00	Not sign.	Not sign.
CD*FSR	Not sign.	Not sign.	Not sign.	Not sign.	Not sign.
CD*BSR	Not sign.	Not sign.	Not sign.	Not sign.	Not sign.
IG*OG	0.04	0.02	0.01	0.13	0.09
IG*FSR	0.00	0.00	0.00	0.00	0.01
IG*BSR	0.00	0.00	0.00	0.00	0.00
OG*FSR	0.06	0.00	0.01	0.00	0.02
OG*BSR	0.01	0.00	0.00	0.00	0.00
FSR*BSR	0.00	0.00	0.00	0.00	Not sign.
Total	100.00	100.00	100.00	100.00	100.00

The ANOVA analysis showed that 2-way interactions contributed considerably to a global heat transfer for outdoor air curtain (16.90 %), exhaust air (34.72 %) and supply air (31.10 %) ventilation

modes. In contrast, the influence of interaction was much less relevant for the other two modes. Among the main factors, the cavity depth was the least influential variable, and for the air buffer mode, it was not even significant in the control of the heat transfer. Regarding the indoor air curtain mode, the incident solar irradiance had by far the greatest impact on the global heat transfer (79.21 %), followed by the slat angle (4.06 %) and the airflow rate (3.48 %). The low impact of temperature difference on global heat transfer performance can be explained by the lack of interaction between indoor and outdoor air. Regarding exhaust air mode, the temperature difference emerged, instead, as the most critical factor (52.89 %), followed by the 2-way interaction between temperature difference and airflow rate (32.22 %) and incident solar irradiance (7.69 %). The importance of the first two factors originated from the enthalpy flow rate, which was directly dependent on temperature difference and the rate of air extraction through the cavity (equation 5).

The general picture for supply ventilation mode is similar to exhaust mode; the highest impact was caused by the temperature difference (48.12 %), followed by interaction between temperature difference and airflow rate (29.48 %) and incident solar irradiance (18.03 %). The influence of solar radiation is amplified here, possibly due to the shading heated by the radiation, which in turn warms up air delivered from the outside through the cavity. The outdoor air curtain mode showed the most diverse situation, where five factors and interactions contributed more than 3 %: incident solar irradiance (51.60 %), slat angle (16.38 %), the interaction between incident solar irradiance and slat angle (8.27 %), airflow rate (5.27 %), and type of outdoor glazing (3.65 %). In addition to this, there was an influence of six other factors and interactions larger than 1 %. This order in contributions of factors probably comes from the absence of direct interaction between inner and outer air. Outer glazing and airflow through ventilation effects additionally control the heat transfer. The analysis of variance for the air buffer mode did not recognize cavity depth as a significant variable. Here, incident solar irradiance played the most crucial role by far (75.73 %), followed by the slat angle (9.17 %) and interaction between them (4.58 %). Air acts as an insulator, decreases the heat flow due to transmission, and reduces the impact of temperature difference in this way.

The graphical representation of ANOVA results is given in Fig. 2, where the effects of the six most influential factors are shown. The average values of global heat gain density for each ventilation mode, i.e., the grand mean of all runs associated with a particular mode, are presented with horizontal dashed lines. This quantity can be interpreted as the overall (bulk) efficiency or capability of each ventilation mode in damping the net heat transfer across the whole domain of boundary conditions utilized as independent variables in the factorial designs. The highest value (169.5 Wm^2) characterizes indoor air curtain, while the lowest (95.8 Wm^2) characterizes exhaust air mode. The average values of the levels for certain factors are denoted with circles. For example, in supply ventilation mode, an

average value for level 5 (20 °C) of temperature difference is 429.0 Wm^2, and this is denoted with the highest blue circle on the first graph. A greater range of average values of levels for some particular factor (vertical extent of solid lines on the figures below) means at the same time a greater impact of that quantity on the thermal metric [41]. For example, based on the graphs below, temperature difference and incident solar irradiance were the dominant factors in exhaust and supply ventilation modes Fig. 3.

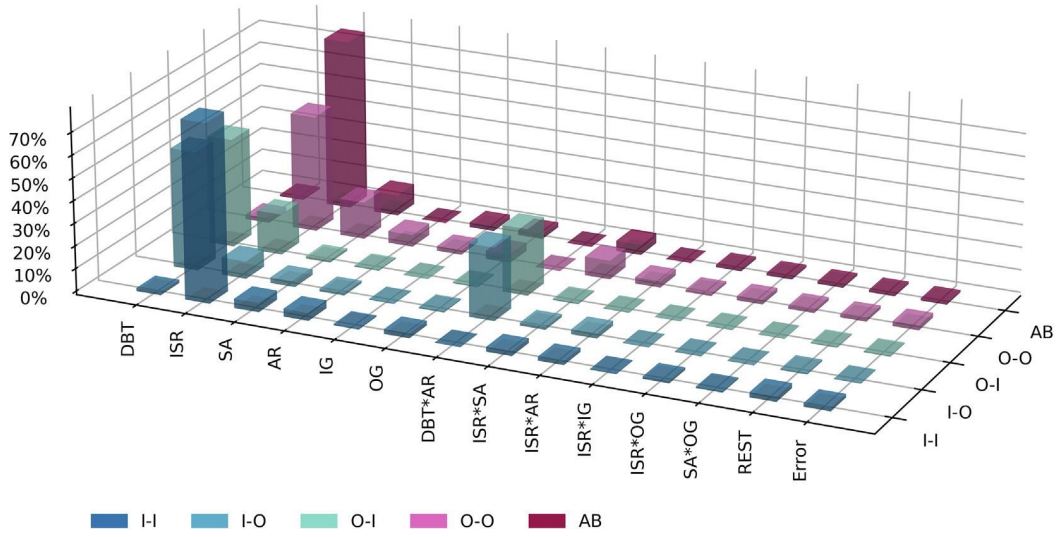

Fig. 2. Contribution of the most relevant factors and interactions for different ventilation modes.

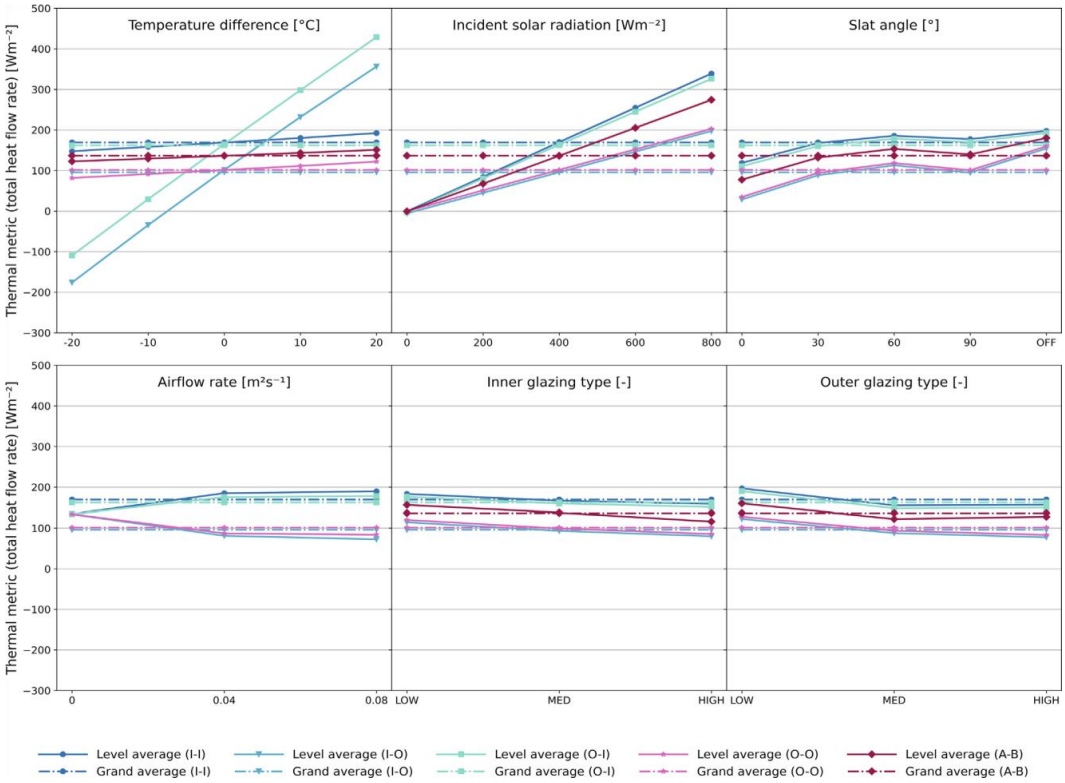

Fig. 3. Results of analysis of variance ANOVA.

However, some other interesting conclusions can be drawn from the presented graphs; for example, overall net heat transfer increased by increasing the airflow rate for indoor air curtain and supply ventilation mode. For outdoor air curtain and exhaust mode, the situation is the opposite. Consequently, it seems that airflow in some modes makes DSF more efficient and, in others, less efficient. It is also visible that increasing the angle of venetian blinds from 0 to 60 generally promoted net heat transfer. However, the maximum of transfer occured for the angle between 60 and 90, due to the fact that the simulations were carried out assuming fully diffuse radiation, which is conventionally modeled in many software tools for building performance simulations as corresponding to direct radiation with an impinging angle on the surface between 60 and 70. Interestingly, the preferred type of inner glazing for reducing overall heat transfer was the one with high transmittance for all ventilation modes. However, when it comes to the outer glazing, the type with medium transmittance was preferred for all ventilation modes, except for outdoor air curtain and supply mode.

5.5.2. Screening designs

The detailed information on the results of the ANOVA of screening designs is given in Table 5. The fourth column indicates whether a design can assess only the main effects (F), or if it is capable of evaluating both the influence of factors and interactions (F&I). In the fifth column, the recommended selection procedure is indicated, and when both methods are specified (forward / backward), the final result is the same regardless of choice. When ‘‘NO” is displayed, it is not recommended to apply any of the selection procedures, while ‘‘-‘‘ means that the ANOVA model fails to recognize any statistically significant dependence on the factors (both with the application and no application of selection procedures). The alpha value (critical p-value) for both forward and backward selection procedures is set to 0.05, indicating a high probability that the considered variable is significant. The sixth column shows the range of values for the fitting coefficient from the lowest to the highest. The average fitting coefficient is obtained as the mean value of fitting coefficients for five ventilation modes.

Table 5. Values of fitting coefficients for various definitive screening designs.

Designs	Number of runs	Number of factors	Factors & Interactions	Recommended selection procedure	Fitting coefficient (range)	Fitting coefficient (average)
Taguchi (L32)	32	8/9	F&I	Backward	0.88–0.90	0.89
Definitive screening	17/21	8/9	F&I	Backward mainly	0.82–0.92	0.86
Placket-Burmann 48	48	8/9	F&I	Forward mainly	0.68–0.90	0.82
Taguchi (L12)	12	8/9	F	Forward/backward	0.49–0.84	0.66
Placket-Burmann 12	12	8/9	F	Forward/backward	0.39–0.77	0.58

The analysis shows that Taguchi’s (L32) design gave the best results overall among all tested screening designs. The definitive screening design can be regarded as the most efficient since it had roughly 30% fewer experiments than Taguchi’s L32 array. It is not recommended to use screening designs with fewer experimental runs (Placket Burman and Taguchi L12) since doing so means that only the main effects can be assessed. However, adding interactions does not necessarily mean greater accuracy, i.e., the folded Plackett-Burmann design did not show considerably higher accuracy than III level resolution designs, despite a higher number of experimental runs (48).

The performance of the two best designs in screening out important variables is worth analyzing even more deeply. In the Table 6 we can see a number of factors and interactions whose contribution is higher than a certain percentage (1, 5, or 10 %) in the FFD. It is also shown how many factors and interactions were recognized in DSD and TD L32 designs with an appropriate success rate. If we

consider factors whose contribution is higher than 10 %, then these three designs filter out the same factors. The same stands for factors whose contribution is higher than 5 %, except in outdoor air curtain ventilation mode, where three out four factors are recognized. If we consider how good screening designs recognize factors and interactions with a higher share than 1%, then DSD has an average success rate of 57 %, while TD L32 has 78 %.

Despite this, DSD and TD L32 showed very good performance in filtering out important variables and consequently can facilitate finding the optimal design. In contrast, screening designs that do not include interactions should not be used to filter out important variables as they show poor performance even in recognizing factors that have a contribution of more than 10%.

Table 6. Performance of definitive screening and Taguchi L32 designs in filtering out important variables.

	> 1 %					***> 5 %***					***> 10 %***				
	I-I	*O-O*	*I-O*	*O-I*	*AB*	*I-I*	*O-O*	*I-O*	*O-I*	*AB*	*I-I*	*O-O*	*I-O*	*O-I*	*AB*
	Number of factors (-)														
FFD	8	11	6	4	8	1	4	3	3	3	1	2	2	3	1
DSD	5	5	4	3	3	1	3	3	3	3	1	2	2	3	1
T L32	5	8	5	4	6	1	3	3	3	3	1	2	2	3	1
	Success rate (%)														
DSD	62.5	45.5	66.7	75.0	37.5	100	75.0	100	100	100	100	100	100	100	100
T L32	62.5	72.7	83.3	100	75.0	100	75.0	100	100	100	100	100	100	100	100

5.5.3. Taguchi multilevel designs

As shown in Table 7, Taguchi's multilevel designs 2L + 3Lx3F (L54), 2L + 4Lx2F (L32), 2L + 3Lx2F (L18), and 3Lx3F (L27) showed the highest accuracy with an average value of the fitting coefficient equal to or higher than 0.88. The second and third designs had a low range of fitting coefficient values, which means that they performed very well for all ventilation modes. However, 3Lx3F (L27) design had a broader range of values, and for some ventilation modes, such as outdoor air curtain and air buffer, the value of the fitting coefficient was around 0.75. The most efficient design is 2L + 3Lx2F (L18), which used only 18 experimental runs and allows the input of three factors. The design 2L + 3Lx3F (L54) is very accurate but cannot be considered among the most efficient ones, as it used a large number of experimental runs. The analysis of the results for different Taguchi multilevel arrays shows how, in general terms, it is not recommendable to use designs with too low a number of experimental runs. It is desirable that a total number of runs is higher than the sum of degrees of freedom for factors and first-order interactions (Appendix A, Tables A.1 and A2) so that design can recognize the basic extent of nonlinearity. However, having many experimental runs is, in itself, not an assurance of good performance. For example, the designs 5Lx2F (L27) and 3Lx2F (L27) were inaccurate in characterizing the role of the factors in the system compared to the full factorial design,

although they had fewer experimental runs than some other more successful DOE arrays. Here, the number of the factors that were taken into consideration plays a crucial role in why these designs fail. The average value of the fitting coefficient for designs that could only assess the main factors' influence was 0.55. Those arrays that can evaluate both factors and interactions instead showed a fitting coefficient of 0.78. For non-linear processes, such as the heat transfer phenomena in DSF, it is essential to consider designs that will assess both factors and interactions.

Table 7. Fitting coefficient values for various Taguchi's multilevel designs.

Designs	Number of runs	Number of factors	F/F&I	Recommended selection procedure	Fitting coefficient (range)	Fitting coefficient (average)
2L + 3Lx3F (L54)	54	4	F + I	No	0.85–0.95	0.90
2L + 3Lx2F (L18)	18	3	F&I	Backward	0.85–0.91	0.88
2L + 4Lx2F (L32)	32	3	F&I	Backward	0.85–0.91	0.88
3Lx3F (L27)	27	3	F&I	Backward	0.75–0.96	0.88
4L + 2Lx2F (L16)	16	3	F&I	Backward	0.70–0.88	0.81
2L + 4Lx3F (L32)	32	4	F&I	Backward mainly	0.53–0.90	0.79
5Lx6F (L25)	25	6	F	Backward mainly	0.64–0.88	0.74
3Lx4F (L27)	27	4	F + I	Forward mainly	0.55–0.88	0.73
5Lx5F (L25)	25	5	F	Backward mainly	0.64–0.85	0.73
5Lx3F (L25)	25	3	F	Backward mainly	0.53–0.86	0.72
3Lx5F (L27)	27	5	F&I	Forward	0.50–0.85	0.71
4Lx3F (L16)	16	3	F	Backward	0.49–0.88	0.69
4Lx5F (L16)	16	5	F	Backward mainly	0.49–0.83	0.67
5Lx4F (L25)	25	4	F	Forward / backward	0.49–0.83	0.67
3Lx2F (L27)	27	2	F + I	No	0.09–0.90	0.54
2L + 3L (L18)	18	2	F + I	No	0.08–0.89	0.54
3Lx3F (L9)	9	3	F	Backward mainly	0.02–0.87	0.53
3Lx4F (L9)	9	4	F	Forward	0.02–0.81	0.53
4Lx2F (L16)	16	2	F	Forward	0.09–0.86	0.53
5Lx2F (L25)	25	2	F	Forward	0.09–0.86	0.52
4L + 2Lx2F (L8)	8	3	F	Backward mainly	0.02–0.80	0.51
3Lx2F (L9)	9	2	F	Forward	0.09–0.90	0.5
2L + 3Lx3F (L18)	18	4	F + I	Forward	0.11–0.81	0.49
4L + 2L (L8)	8	2	F	–	0.01–0.19	0.06

5.5.4. Designs associated with RSM

The CCD (Table 8) shows excellent results with the highest average fitting coefficient of 0.91. However, the number of experimental runs was relatively high for some ventilation modes (45 for outdoor air curtain). When there were five or fewer factors, the total number of experimental runs was lowered to a value considered more acceptable (<27). A similar picture is seen for BoxBehnken design, which has the advantage of not using too many extreme levels simultaneously. However, it

has a slightly higher number of experimental runs and a broader range of fitting coefficient values with a lower average value.

Table 8. Fitting coefficient values for RSM designs.

Designs	Number of runs	Number of factors	F/F&I	Selection procedure	Fitting coefficient (range)	Fitting coefficient (average)
Central composite	25–45	4–6	F&I	Backward	0.89–0.92	0.91
Box-Behnken design	24–48	4–6	F&I	Backward	0.84–0.93	0.88

5.6. Summary of the DOEs performance assessment

Fig. 4 represents a graphical summary of the DOEs performance assessment, where the values of fitting coefficients for each ventilation mode and tested design are given. The ventilation modes are indicated with different colors, while the tested designs are determined by the corresponding radial directions on which the values of the fitting coefficient for five different ventilation modes lie. Among the screening designs, the Taguchi (L32) and the definitive screening designs proved to be the best ones. The former showed very good performance for all ventilation modes (low fitting coefficient range) and the slightly higher average value of the fitting coefficient. Screening designs are recommended as the initial step when the nature of the process is unknown or where the number of possible factors that may affect the response quantity is high. In this way, by performing screening designs, the important parameters can be filtered out. From the previous analysis, both DSD and Taguchi L32 have proved to be reliable in filtering out the factors that most contribute to the variation of response quantity while pointing to the possible existence of higher-order terms.

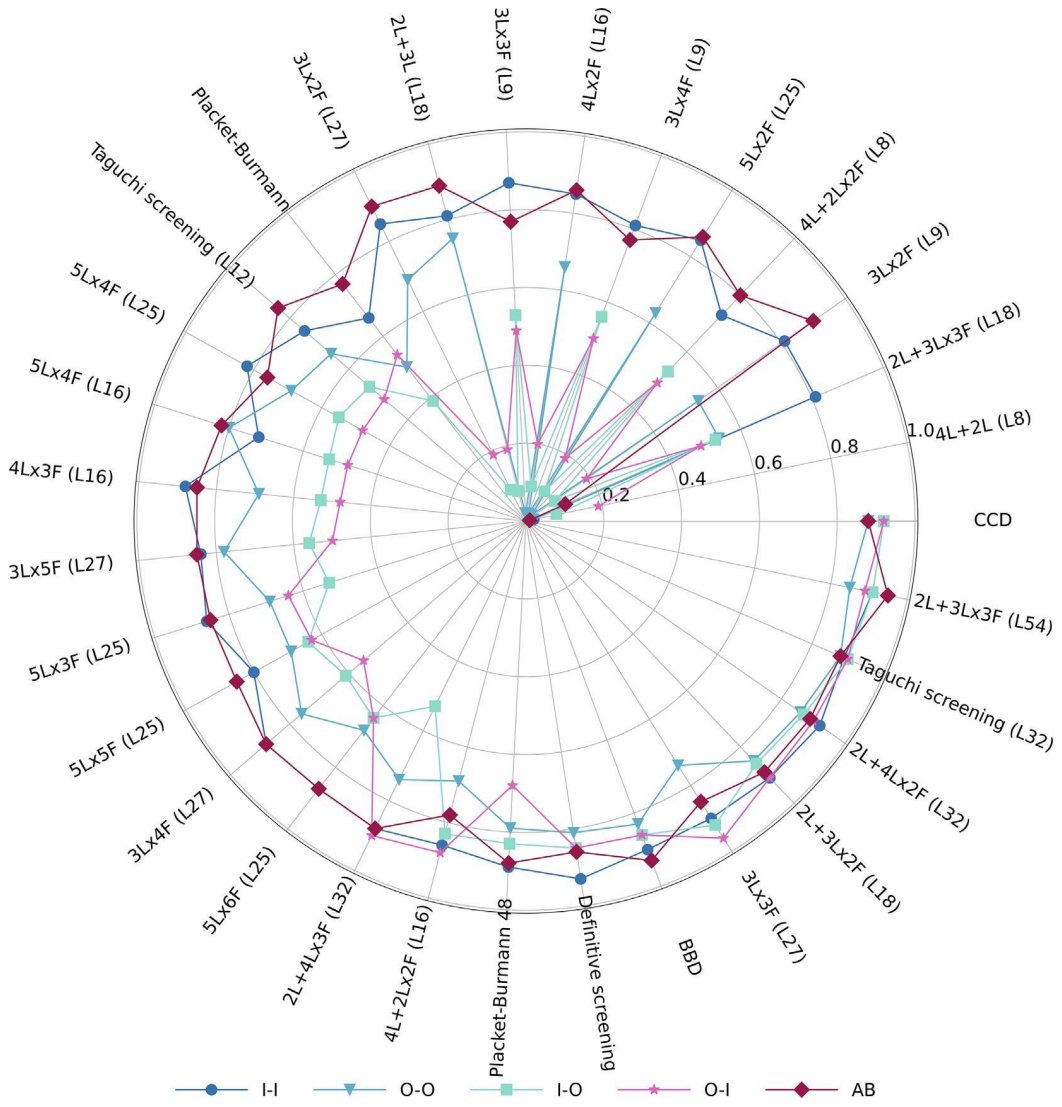

Fig. 4. Fitting coefficient values of all tested designs, where for each one, five different values are indicated in the radial direction (representing five different ventilation modes). Satisfactory designs, such as CCD, Taguchi L32, 2L + 3Lx2F (L18), or BBD, have high fitting coefficient values for all the ventilation modes, i.e., the points representing these values are close to the circumference, and they are characterized by a small extent in the radial direction. In such designs, there is a balance between the number of experimental runs (moderate), factors (moderate or high), and levels (low or moderate), and ANOVA can unveil the strong statistical significance of both factors and interactions.

Unlike screening, Taguchi multilevel designs tend to use fewer experimental runs, but they do not allow one to include a high number of factors. In this analysis, three designs showed very good performance: 2L + 4Lx2F (L32), 3Lx3F (L27), and 2L + 3Lx2F (L18), where the last one had the highest efficiency in comparison to all other tested designs. Taguchi multilevel designs are recommended when one is sure that a complex process is affected by few(er) factors. At the same

time, the possibility to carry out experimental runs is very limited. This type of design allows one to have higher discretization for factors that are assumed to be more important than others, not only when it comes to their direct impact but also their interactions with other factors. In this way, a better insight into the nature of interaction can be obtained compared to what screening designs offer with their two-level approach. However, one should be careful not to choose the design that is overloaded with levels as a sufficient number of degrees of freedom may not be secured for assessment of interactions.

Finally, CCD showed the best performance among all tested designs, while BBD appeared somewhat less consistent with FFD than CCD. However, BBD could be a suitable choice if it is hard or expensive to replicate conditions where several factors are set at extreme levels. If the experiment is limited with runs, the highest number of considered factors is five for CCD and four for BBD.

5.7. General guidelines for the selection of optimal DOEs

Based on the information available in the literature and the results of the investigation presented in this study on the specific case of a DSF, we tried to define some general guidelines to help researchers and designers select optimal DOEs that go beyond the considered case. Since every investigation is different, it is impossible and meaningless to define a ranking for more or less efficient DOEs in general terms. Instead, the recommendations we report here provide a general approach to have a more thoughtful and grounded selection process when adopting a DOE-based approach. Furthermore, this strategy refers to resource-limited experiments that aim to investigate complex processes/systems characterized by a certain amount of nonlinearity, which we usually encounter in many processes in nature and building physics.

We summarize and visualize the different steps and checks that we recommend in order to carry out to select suitable options for DOEs in Fig. 5.

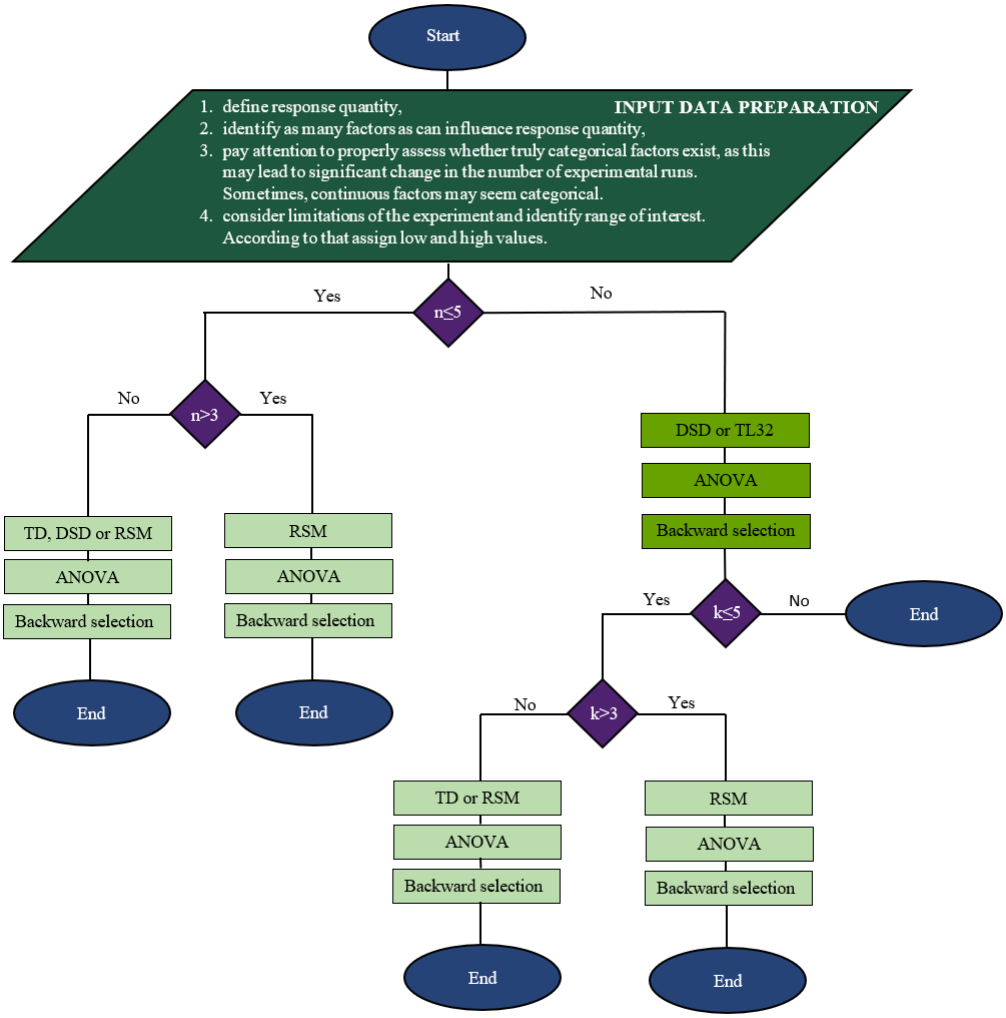

Fig. 5. Recommended decision tree to support the selection of DOEs to investigate a given process. The total number of factors (n) and the number of important factors (k) are used to determine the suitable DOEs for different cases.

The essential step in the recommended approach is the proper preparation of input data. In order to make the results of an experiment more general and applicable, it is recommended to identify as many factors as possible that can influence response quantity. They must be mutually independent so that a change in one factor does not induce a change in another factor (not to be confused with interactions). The input data preparation also includes the assignment of low- and high-level values to each factor. These values should be selected based on the range of interest. However, the physical experiment's limitations should be considered since the extreme values may sometimes be complicated to replicate, primarily when several factors with extreme values are run simultaneously.

Care should be taken in analyzing the problem to properly assess whether truly categorical factors exist, and this can sometime be tricky to assess in building science problems at first sight. Technology in the building industry usually promotes discrete product classification, such as components with sets or combinations of predetermined mechanical, thermal, or optical characteristics. These elements may seem to be only described in the form of categorical factors, which can increase the numbers of simulations/tests in some DOEs. While some properties/ products can indeed only be described in the form of categories in opposition to continuous factors (such as the ventilation path in the case presented in this article), many variables that can appear at first glance as categorical are, from a physics perspective, continuous. Here, the researcher's experience with the underlying physics and phenomena described in the problem is of fundamental importance to understand the ''true" nature of the factor's physical properties behind the technological implementations.

In the next step (Fig. 5), the total number of factors n determines whether it is necessary to filter important factors. If the total number of considered factors is six or more, then filtering important factors k is recommended (Fig. 5). DSD or Taguchi L32 designs are favored designs for screening, where the factors with a contribution higher than 1–2 % (both through individual action or through interaction) should be considered important factors. The CCD design is recommended when the number of considered factors has dropped to five or less. If it is difficult to perform an experiment when several factors simultaneously have extreme values, BBD could be a more suitable design than CCD. In the RSDs, the extreme levels (one that corresponds to the axial points) should be chosen to conform to the limits of the interest range so that the ''classic" low / high levels fall inside the interest domain if alpha is higher than one.

However, besides RSDs, Taguchi multilevel or DSD can be optimal if only two or three factors are considered. Here, special care should be taken to leave a sufficient number of degrees of freedom for the error, especially with the Taguchi multilevel designs. If the array is designed so that it leaves no degrees of freedom for the error, then it will not be able to evaluate statistical significance of individual contributions. Attention should also be paid to the magnitude of the error. A very large error (>20%) means that ANOVA fails to explain a large part of variance and that either an experiment has not been performed well, or that inappropriate design, factors or even processes are chosen for the analysis. In general, errors greater than 5% for a limited number of experimental runs make it very difficult to argue for a strong statistical significance ($p < 0.05$) of the factors and their interactions. To retain a sufficiently high resolution and enable the assessment of the influence of higher-order terms (interactions), it is not recommended to overload design with too many levels. Taguchi

multilevel designs containing at most three or four levels have shown remarkable performances. A backward selection procedure is recommended if the aim is to include only significant terms and reduce the model's complexity so it can be used for prediction. If there are enough resources, it is always wise to compare the analysis of variance obtained by two different designs to ascertain the validity of the obtained characterization picture. This is not so far-fetched considering that the individual design points are common to different types of DOE arrays. DOE is applicable to experiments in a controlled environment, where the factors can be systematically manipulated. However, DOE can be applied to natural experiments, such as time-series data, as long as the response quantity is not inert to factor values changes.

5.8. Conclusions

Through the results of an extensive simulation study, we have investigated how different design of experiments (DOEs) can lead to the different characterization of the same phenomenon and how the optimal design(s) can be selected to obtain the best possible characterization of the process using the fewest possible experimental runs. In the specific case study used in this research (investigating the thermal behaviour of a double skin façade as a function of its constructional and operational features), the RSM (Response Surface Methodology) with central composite design showed the best performance in the characterization with the average value of the fitting coefficient of 0.90. The number of experimental runs differed for this design, based on the total number of factors that influence more considerable (>1%) response quantity. This number went from 25 experiments for exhaust air, supply air, and air buffer, through 27 for indoor air curtain, to 45 for outdoor air curtain ventilation mode. However, the most efficient design that best balanced the number of experimental runs and accuracy is the Taguchi L18 array 2L + 3Lx2F. This array considered only two factors with three levels and one factor with two levels using 18 experimental runs, but it could explain almost 80 % of the total variance. Some of the Taguchi designs surprisingly failed in characterization, so one should be very careful when choosing the appropriate design.

Based on the central study results, general guidelines that go beyond the considered case are established. These guidelines recommend procedures for preparing input data for various types of experimental designs. They encompass the definition and interpretation of factors along with assigning level values and ranges. Depending on the initial number of factors, screening procedures can be used to filter out the most significant factors. The extent of nonlinearity in the process determines the resolution of optimal design. If the higher-order terms are significant, some of the RSM designs are advisable. On the other side, if only the main effects and interactions influence response quantity, then some Taguchi design of lower resolution is sufficient (resolution IV).

However, during the selection of optimal design, one must carefully consider the physical experiment's limitations, such as time and material resources and the ability to perform experiments under extreme conditions. The selected design should secure a comprehensive picture of interactions using as few resources as possible during the physical experiment.

5.9. Appendix A

Let's consider a general case where the impact of three factors A, B, and C, containing a certain number of levels (a, b, c, respectively), needs to be assessed. The response variable may not be dependent only on factors in a linear way, as interactions between them can also have an effect. For example, one factor's influence can be affected by the other factor's level. The mathematical procedure starts with the calculation of the total sum of squares SS_T, which equals a sum of squared differences between each run x_{ijkl} and grand mean $\bar{x}$. This quantity can be partitioned into several components: the sum of squares for the factors (SS_A, SS_B, and SS_C), the sum of squares for the interactions (SS_{AB}, SS_{AC}, SS_{BC}, and SS_{ABC}), and the error sum of squares (SS_E). Squared difference between group ($\bar{x}_i$; $\bar{x}_j$; $\bar{x}_k$) and grand mean, multiplied by the number of the runs within the group, represent the sum of squares for that factor [42]. A similar definition can be derived for the interaction sum of squares. On the other side, the error sum of squares (SS_E) is the sum of squared differences between individual runs and group means. This term indicates the extent of randomness, and if it is large, then there is less probability that factors or interactions influence response quantity in a statistically significant way.

To conclude whether the main effects or interactions exist, the F-ratio for these elements needs to be calculated. This number represents the ratio between the group and the error variance, where variance can be defined as a particular sum of squares divided by its degree of freedom (DOF), where DOF is dependent on the number of levels (a,b and c). The calculated value of F-ratio is compared with the critical F value determined from statistical tables. If it is higher than critical, then there is evidence that at least two levels of a factor differently affect the response variable (i.e., factor significantly affects response variable) or that interaction between factors exists [43]. The following Table A1 summarizes the concepts, procedures and equations adopting the terminology mentioned above.

Table A1. Terminology in the three-factor ANOVA.

Source of variation	Degrees of freedom	Sum of squares	Mean square	F-ratio
Factor A	$df_A = a - 1$	$SS_A = nbc \sum_{i=1}^{a} (\bar{x}_i - \bar{x})^2$	$MS_A = \frac{SS_A}{df_A}$	$F_A = \frac{MS_A}{MS_E}$
Factor B	$df_B = b - 1$	$SS_B = nac \sum_{j=1}^{b} (\bar{x}_j - \bar{x})^2$	$MS_B = \frac{SS_B}{df_B}$	$F_B = \frac{MS_B}{MS_E}$
Factor C	$df_C = c - 1$	$SS_C = nab \sum_{k=1}^{c} (\bar{x}_k - \bar{x})^2$	$MS_C = \frac{SS_C}{df_C}$	$F_C = \frac{MS_C}{MS_E}$
Interaction AB	$df_{AB} = (a-1)(b-1)$	$SS_{AB} = nc \sum_{j=1}^{b} \sum_{i=1}^{a} (\bar{x}_{ij} - \bar{x}_i - \bar{x}_j + \bar{x})^2$	$MS_{AB} = \frac{SS_{AB}}{df_{AB}}$	$F_{AB} = \frac{MS_{AB}}{MS_E}$
Interaction AC	$df_{AC} = (a-1)(c-1)$	$SS_{AC} = nb \sum_{k=1}^{c} \sum_{i=1}^{a} (\bar{x}_{ik} - \bar{x}_i - \bar{x}_k + \bar{x})^2$	$MS_{AC} = \frac{SS_{AC}}{df_{AC}}$	$F_{AC} = \frac{MS_{AC}}{MS_E}$
Interaction BC	$df_{BC} = (b-1)(c-1)$	$SS_{BC} = na \sum_{k=1}^{c} \sum_{j=1}^{b} (\bar{x}_{jk} - \bar{x}_j - \bar{x}_k + \bar{x})^2$	$MS_{BC} = \frac{SS_{BC}}{df_{BC}}$	$F_{BC} = \frac{MS_{BC}}{MS_E}$
Interaction ABC	$df_{ABC} = (a-1)(b-1)(c-1)$	$SS_{ABC} = n \sum_{k=1}^{c} \sum_{j=1}^{b} \sum_{i=1}^{a} (\bar{x}_{ijk} - \bar{x}_{ij} - \bar{x}_{ik} - \bar{x}_{jk} + \bar{x}_i + \bar{x}_j + \bar{x}_k - \bar{x})^2$	$MS_{ABC} = \frac{SS_{ABC}}{df_{ABC}}$	$F_{ABC} = \frac{MS_{ABC}}{MS_E}$
Error	$df_E = n - abc$	$SS_E = \sum_{l=1}^{n} \sum_{k=1}^{c} \sum_{j=1}^{b} \sum_{i=1}^{a} (x_{ijkl} - \bar{x}_{ijk})$	$MS_E = \frac{SS_E}{df_E}$	
Total	$d_T = n - 1$	$SS_T = \sum_{l=1}^{n} \sum_{k=1}^{c} \sum_{j=1}^{b} \sum_{i=1}^{a} (x_{ijkl} - \bar{x})$	$MS_T = \frac{SS_T}{df_T}$	

A general three-factor model that accounts for interactions can be written through regression analysis in the following form:

$$x_{ijkl} = \mu + \alpha_i + \beta_j + \gamma_k + (\alpha\beta)_{ij} + (\alpha\gamma)_{ik} + (\beta\gamma)_{jk} + (\alpha\beta\gamma)_{ijk} + e_{ijkl} \quad (1)$$

where μ represents the overall mean response (or intercept grand mean), a number that is constant regardless of the level settings, e_{ijkl} is the residual term (error), which represents the effect of all other factors that are not considered in the model [44]. The main effects (i.e., factor A at level i, factor B at level j and factor C at level

k) are given in Table A2 with terms α_i, β_j and γ_k, while interactions (between A and B, A and C, B and C and A, B, and C) are given with $(\alpha\beta)_{ij}$, $(\alpha\gamma)_{ik}$, $(\beta\mu)_{jk}$ and $(\alpha\beta\gamma)_{ijk}$, respectively:

Table A2. Three-factor model and its terms.

3-factor model terms				
Main effects	$\mu = \bar{x}$	$\alpha_i = \bar{x}_i - \bar{x}$	$\beta_j = \bar{x}_j - \bar{x}$	$\gamma_k = \bar{x}_k - \bar{x}$
2-way Interactions	$(\alpha\beta)_{ij} = \bar{x}_{ij} - \bar{x}_i - \bar{x}_j + \bar{x}$	$(\alpha\gamma)_{ik} = \bar{x}_{ik} - \bar{x}_i - \bar{x}_k + \bar{x}$	$(\beta\gamma)_{jk} = \bar{x}_{jk} - \bar{x}_j - \bar{x}_k + \bar{x}$	
3-way interaction and the error term	$(\alpha\beta\gamma)_{ijk} = \bar{x}_{ijk} - \bar{x}_{ij} - \bar{x}_{ik} - \bar{x}_{jk} + \bar{x}_i + \bar{x}_j + \bar{x}_k - \bar{x}$			$e_{ijkl} = x_{ijkl} - \bar{x}_{ijk}$

The selection of the factors to be included in the regression model as predictors of the response quantity is done via the variable selection procedures (e.g. forward entry, backward elimination, and stepwise selection procedures [45]). Forward entry starts with the null model and gradually adds one factor at a time from the most to the least significant until the previously specified criterion (critical p-value, F-ratio) is not met or until all factors are included in the model. This method is recommended when the number of factors under consideration is larger than the number of experimental runs. The backward elimination criterion starts the full model. It gradually removes one factor at a time, from the least to the most significant, until the previously specified criterion (critical p-value, F-ratio) is not met or until all factors are excluded from the model. Generally, backward elimination is preferred over forward entry because it is less negatively affected by the collinearity of the model's factors, except when the number of experimental runs is low [46]. The stepwise selection criterion combines forward and backward, so it adds one factor at a time and recalculates the significance of all the factors considered in the model up to this step [47]. If a nonsignificant factor is found, then it is eliminated from the model. This selection procedure requires two specified criteria, one for the entry of the factor and the other for its elimination, where the first one needs to be greater than the second.

There is a close connection between RSM and regression analysis [48]. While regression analysis seeks an empirical relationship between the response variable and its affecting factors, RSM represents supplementary techniques including planning, model testing procedures and optimization employed ahead of, during and after regression analysis [49]. Response surface modeling is based on the assumption that response function (surface) can be approximated by a Taylor series expansion and that the surface is curved around the optimum. To describe such response adequately, cross product terms need to be incorporated [50]. The response function can be approximated by polynomials of order higher than three, but if the experimental region is not too broad, lower-degree polynomials (at most three) can successfully approximate the response function.

5.10. References

[1] J. Antony, ‘‘1 - Introduction to Industrial Experimentation,” J. B. T.-D. of E. for E. and S. (Second E. Antony, Ed. Oxford: Elsevier, 2014, pp. 1–6.

[2] B. Durakovic, Design of experiments application, concepts, examples: State of the art, Period. Eng. Nat. Sci. 5 (3) (Dec. 2017) 421–439.

[3] D.C. Montgomery, Design and analysis of experiments, John Wiley & Sons, New York, 2001.

[4] A. Alafaghani, A. Qattawi, Investigating the effect of fused deposition modeling processing parameters using Taguchi design of experiment method, J. Manuf. Process. 36 (2018) 164–174.

[5] F. Kolivand, R. Rahmannejad, Estimation of geotechnical parameters using Taguchi’s design of experiment (DOE) and back analysis methods based on field measurement data, Bull. Eng. Geol. Environ. 77 (4) (2018) 1763–1779.

[6] C. Shen, L. Wang, W. Cao, L. Qian, Investigation of the effect of molding variables on sink marks of plastic injection molded parts using taguchi DOE Technique, Polym. Plast. Technol. Eng. 46 (3) (Mar. 2007) 219–225.

[7] S.M. Zahraee, M. Hatami, N. Mohd Yusof, J. Mohd Rohani, F. Ziaei, Combined use of design of experiment and computer simulation for resources level determination in concrete pouring process, J. Teknol. 64 (1) (2013) Nov.

[8] M.A. Farooq, H. Nóvoa, A. Araújo, S.M.O. Tavares, An innovative approach for planning and execution of pre-experimental runs for Design of Experiments, Eur. Res. Manag. Bus. Econ. 22 (3) (2016) 155–161.

[9] N.R. Smalheiser, in: Chapter 5 - Experimental Design: Design Strategies and Controls, Academic Press, 2017, pp. 65–85.

[10] W.J. Kolarik, Creating quality: concepts, systems, strategies, and tools, McGraw-Hill New York, 1995.

[11] G. Box, J. Hunter, W. Hunter, ‘‘Chapter 6 Fractional Factorial Designs”, in Statistics for experimenters design, innovation, and discovery, 2nd ed., WileyInterscience, Hoboken, New Jersey, 2005, pp. 235–271.

[12] J. Antony, in: 2 - Fundamentals of Design of Experiments, Elsevier, Oxford, 2014, pp. 7–17.

[13] B. Jones, K. Allen-Moyer, and P. Goos, ‘‘A-optimal versus D-optimal design of screening experiments,” J. Qual. Technol., pp. 1–14, May 2020.

[14] L. Eriksson, E. Johansson, C. Wikström, Mixture design—design generation, PLS analysis, and model usage, Chemom. Intell. Lab. Syst. 43 (1) (1998) 1–24.

[15] K.K. Choi, B.D. Youn, R.-J. Yang, Moving least square method for reliabilitybased design optimization, Proc. 4th World Cong. Struct. Multidiscip. Optim. (2001).

[16] B. Jones, C.J. Nachtsheim, Split-Plot Designs: What, Why, and How, J. Qual. Technol. 41 (4) (Oct. 2009) 340–361.

[17] W. Libbrecht et al., Optimization of soft templated mesoporous carbon synthesis using Definitive Screening Design, Chem. Eng. J. 259 (2015) 126– 134.

[18] L. Ilzarbe, M.J. Álvarez, E. Viles, M. Tanco, Practical applications of design of experiments in the field of engineering: a bibliographical review, Qual. Reliab. Eng. Int. 24 (4) (2008) 417–428.

[19] S.K. Ahuja, G.M. Ferreira, A.R. Moreira, Application of Plackett-Burman design and response surface methodology to achieve exponential growth for aggregated shipworm bacterium, Biotechnol. Bioeng. 85 (6) (2004) 666–675.

[20] J. Zhou et al., Optimization of phenol degradation by Candida tropicalis Z-04 using Plackett-Burman design and response surface methodology, J. Environ. Sci. 23 (1) (2011) 22–30.

[21] K. Vanaja, R.H. Shobha Rani, Design of Experiments: Concept and applications of plackett burman design, Clin. Res. Regul. Aff., Jan. 24 (1) (2007) 1–23.

[22] A. Miller, R.R. Sitter, Using the Folded-Over 12-Run Plackett—Burman Design to Consider Interactions, Technometrics 43 (1) (2001) 44–55.

[23] G. Box, S. Bisgaard, C. Fung, An explanation and critique of taguchi’s contributions to quality engineering, Qual. Reliab. Eng. Int. 4 (2) (1988) 123– 131.

[24] K.N. Ballantyne, R.A. van Oorschot, R.J. Mitchell, Reduce optimisation time and effort: Taguchi experimental design methods, Forensic Sci. Int. Genet. Suppl. Ser. 1 (1) (2008) 7–8.
[25] G.E.P. Box, K.B. Wilson, On the experimental attainment of optimum conditions, J. R. Stat. Soc. Ser. B 13 (1) (Sep. 1951) 1–45.
[26] S. Karimifard, M.R. Alavi Moghaddam, Application of response surface methodology in physicochemical removal of dyes from wastewater: A critical review, Sci. Total Environ. 640–641 (2018) 772–797.
[27] X. Shen, G. Zhang, B. Bjerg, Assessments of experimental designs in response surface modelling process: Estimating ventilation rate in naturally ventilated livestock buildings, Energy Build. 62 (2013) 570–580.
[28] W.F. Guthrie, NIST/SEMATECH e-Handbook of Statistical Methods (NIST Handbook 151), Natl. Inst. Stand. Technol. (2020).
[29] H.C.J. Hoefsloot, D.J. Vis, J.A. Westerhuis, A.K. Smilde, J.J. Jansen, in: 2.23 Multiset Data Analysis: ANOVA Simultaneous Component Analysis and Related Methods, Elsevier, Oxford, 2009, pp. 453–472.
[30] S. Weisberg, ‘‘Linear Hypothesis: Regression (Basics),” N. J. Smelser and P. B. B. T.-I. E. of the S. & B. S. Baltes, Eds. Oxford: Pergamon, 2001, pp. 8884–8888.
[31] K. M. Carley, N. Y. Kamneva, and R. J, ‘‘Response surface methodology,” in CASOS Techn. Rep. CMU ISRI-04-136, Pittsburgh: Carnegie Mellon University, 2004.
[32] D.R. Gunasegaram, D.J. Farnsworth, T.T. Nguyen, Identification of critical factors affecting shrinkage porosity in permanent mold casting using numerical simulations based on design of experiments, J. Mater. Process. Technol. 209 (3) (2009) 1209–1219.
[33] I. Lorscheid, B.-O. Heine, M. Meyer, Opening the ‘black Box’ of Simulations: Increased Transparency and Effective Communication through the Systematic Design of Experiments, Comput. Math. Organ. Theory 18 (1) (2012) 22–62.
[34] A. Giunta, S. Wojtkiewicz, M. Eldred, Overview of Modern Design of Experiments Methods for Computational Simulations (Invited), American Institute of Aeronautics and Astronautics, 2003.
[35] A.N. Sadeghifam, S.M. Zahraee, M.M. Meynagh, I. Kiani, Combined use of design of experiment and dynamic building simulation in assessment of energy efficiency in tropical residential buildings, Energy Build. 86 (2015) 525–533.
[36] I. Jaffal, C. Inard, C. Ghiaus, Fast method to predict building heating demand based on the design of experiments, Energy Build. 41 (6) (2009) 669–677.
[37] N. Delgarm, B. Sajadi, K. Azarbad, S. Delgarm, Sensitivity analysis of building energy performance: A simulation-based approach using OFAT and variancebased sensitivity analysis methods, J. Build. Eng. 15 (2018) 181–193.
[38] W. Kim, Y. Jeon, Y. Kim, Simulation-based optimization of an integrated daylighting and HVAC system using the design of experiments method, Appl. Energy 162 (2016) 666–674.
[39] E. Catto Lucchino, F. Goia, G. Lobaccaro, G. Chaudhary, Modelling of double skin facades in whole-building energy simulation tools: A review of current practices and possibilities for future developments, Build. Simul. 12 (1) (2019) 3–27.
[40] A. Gelesz, E. Catto Lucchino, F. Goia, V. Serra, A. Reith, Characteristics that matter in a climate façade: A sensitivity analysis with building energy simulation tools, Energy Build. 229 (2020) 110467.
[41] A. Jankovic, F. Goia, A simulation study on the performance of double skin façade through experimental design methods and analysis of variance, IOP Conf. Ser. Mater. Sci. Eng. 609 (2019) 62003.
[42] J. Berk and S. Berk, ‘‘Chapter 11 - ANOVA, Taguchi, and Other Design of Experiments Techniques: Finding needles in haystacks...,” J. Berk and S. B. T.Q. M. for the T. S. Berk, Eds. Woburn: Butterworth-Heinemann, 2000, pp. 106– 123.
[43] B. Bowerman et al., Experimental Design and Analysis of Variance, in: In Business Statistics and Analytics in Practice, 3rd ed.,., McGraw Hill, 2003, pp. 399–443.
[44] B. R. Clarke, ‘‘Helmert Matrices and Orthogonal Relationships,” Linear Models: The Theory and Application of Analysis of Variance. pp. 77–112, 18-Jul-2008.

[45] A. M. McIntosh, M. Sharpe, and S. M. Lawrie, ‘‘9 - Research methods, statistics and evidence-based practice,” E. C. Johnstone, D. C. Owens, S. M. Lawrie, A. M. McIntosh, and M. B. T.-C. to P. S. (Eighth E. Sharpe, Eds. St. Louis: Churchill Livingstone, 2010, pp. 157–198.
[46] D.C. Montgomery, E.A. Peck, G.G. Vinning, Variable Selection and Model Building, in: Introduction to Linear Regression Analysi, 5th ed.,., Wiley, 2012, pp. 327–372.
[47] L. J. Hintze, ‘‘Stepwise Regression,” in NCSS User’s Guide III: Regression and Curve Fitting, Kaysville, Utah, pp. 311-1,311-10.
[48] R.H. Myers, D.C. Montgomery, C.M. Anderson-Cook, Response surface methodology : process and product optimization using designed experiments, Wiley, Hoboken, 2019.
[49] A.I. Khuri, J.A. Cornell, Response Surfaces : Second Edition, Routledge, Boca Raton, 2018.
[50] R. B. T.-D. H. in S. and T. Carlson, Ed., ‘‘Chapter 12 Response surface methods,” in Design and Optimization in Organic Synthesis, vol. 8, Elsevier, 1992, pp. 249–324
[51] Aleksandar Jankovic, Francesco Goia, Impact of double skin facade constructional features on heat transfer and fluid dynamic behaviour, Building and Environment 196 (2021), https://doi.org/10.1016/j.buildenv.2021.107796 107796.

6. Characterization of a naturally ventilated double-skin façade through the design of experiments (DOE) methodology in a controlled environment

6.1. Abstract

The two-fold aim of this study was to compare and reflect on the impact of different experimental designs on the characterization of a complex façade system, and to understand the role of constructional elements and boundary conditions on the thermal and fluid dynamic behavior of a double-skin facade (DSF), focusing on the controllability of these phenomena during the operation of the DSF.

We employed and compared four experimental designs capable of assessing factors' interactions and non-linear behaviors typical of dynamic façades. Experimental data were obtained using a full-scale DSF mock-up, installed in a climate simulator, which was operated in outdoor air curtain mode under boundary conditions typical of the summer season. Similarities and differences between characterizations obtained through different experimental designs enabled us to analyse the impact of different experimental designs and to identify the features that affect the DSF's performance.

The results demonstrated that the design of experiments methodology could be successfully employed to study the behavior of complex facades. Using more than one experimental design allowed us to obtain a robust picture of the behavior of a naturally ventilated façade. Relevant factors and interactions were also identified and linked to phenomena that determine how the DSF behaves under typical summer conditions.

Nomenclature

Acronyms

2-FI	2-factor interaction model
ANOVA	Analysis of variance
BIG	Big size of the opening
CCD	Central composite design
DBT	Temperature difference
DOE	Design of experiment
DSD	Definitive screening design
DSF	Double skin facade
F	Factor
FFD	Full factorial design
H	Height
ISR	Solar irradiance
L	Level
MID	Mid-size of the opening
OFF	Raised venetian blinds (no shading)
OS	Opening size
RQ	Research question
RSD	Response surface design
SA	Slat angle
SMALL	The small size of the opening
TD	Taguchi design
W	Width

Symbols

c	Contribution [%]
f	Fitting coefficient [–]
k	Number of factors [–]
q	Heat flux density [Wm^{-2}]
SS	Sum of squares [same as for the response quantity]
t	Temperature [℃]
v	Velocity [ms^{-1}]
V	Airflow rate [m^3h^{-1}]

Subscripts

cav	refer to cavity
D	refer to the compared design
E	refer to error
$F\&I$	refer to factor or interaction
net	refer to net
RD	refer to referent design
s	refer to indoor surface
T	refer to total
$vent$	refer to ventilated

6.2. Introduction

6.2.1. Background

Thermal and energy performance of double-skin facades (DSFs) are linked to non-linear behaviors driven by the boundary conditions and controlled by the structural elements and operational modes. As opposed to the influence of a single factor, the combined effects of multiple factors, such as the simultaneous balance between different driving forces or the interaction of different constructional features, are challenging to understand and are rarely analyzed [1]. The design of experiments (DOE) represents an efficient and reliable method, based on well-established statistics theories [2], to systematically quantify and classify impacts of factors and their interactions in complex systems, as a DSF is. Each DOE begins with the problem statement, followed by establishing the objectives, which then determine the performance indicator (response quantity) and affecting factors to be studied [3]. A crucial step in the whole course is the selection of one (or more) suitable experimental design (also called an array) [4]. Experiments are executed according to the designed array once the experimental design(s) is chosen [5]. In the final stage, the analysis of variance (ANOVA) and other associated statistical methods are used to analyze the collected data to understand the impact of each factor (and sometimes their interactions, too) on the response quantity(s) [6].

There are few examples of DOE methodology in building energy or thermal performance research, and most focus primarily on numerical experiments (simulations) [7]. Some research activities use impact analysis to obtain performance characterization [8,9], while others employ DOE for

optimization [10,11]. There are also examples where building simulations were paired with the DOE approach to find the optimal experimental design [12,13] and to develop a simple surrogate model [14].

Adopting the DOE method implies systematically altering several factors across experiental runs [12,15] with the aim of obtaining a full characterization with the least possible amount of experimental tests. The choice of experimental design(s) is not trivial, as not all those available are well-suited to characterize a given phenomenon. Depending on the nature of the studied process, some arrays may be too shallow to recognize the full complexity of the process. Consequently, they can provide incorrect or partially incorrect conclusions on the importance of particular factors and the extent of non-linearity within the process. Therefore, the experimental design(s) need to be well chosen to consider all non-linearities and the interaction of factors in the investigated process. For complex behavior dictated by several factors in a nonlinear way, such as the thermal and fluid-dynamical behavior of a DSF, the use of experimental designs that can assess interactions (so-called arrays with resolution >IV [16]) is mandatory as they are the only ones capable of considering the how two or more factors in combination affect the response quantity. However, the complexity and comprehensiveness of experimental designs often need to be carefully balanced against the costs and duration of the experimental runs. In short, the struggle is to find the most comprehensive system characterization using the fewest resources possible.

In a previous study where we employed extensive simulations to create the dataset for analyses, we investigated how the DOE could be applied to a complex system such as a mechanically ventilated DSF [12] for a complete characterization of its performance. We compared more than 30 different arrays to define guidelines for finding an optimal experimental design that would give the most comprehensive picture of the process, including all non-linearities, using the fewest resources possible.

Building on that theoretical, simulation-based investigation, we have now examined how well the characterization of the DSF performance can be carried out using real experiments in a laboratory setting, following the guidelines we have developed, through the application of some of the most promising experimental designs. This examination has allowed us to obtain a comprehensive picture of the thermophysical and fluid dynamic behavior of a naturally ventilated DSF.

6.3. Research aims, research questions, and audience

The study we present in this paper aims, at first, to examine how a laboratory characterization based on a certain experimental design may differ from another based on a different experimental array. We

also hypothesize that by comparing the results obtained with more experimental designs, one can obtain robust knowledge about the behavior of the tested DSF, which is the second aim of this paper. The research questions that drove the development of this study were:

RQ1) Do different experimental designs give the same characterization picture, and what features should an experimental design have to characterize the complex systems/processes of a DSF adequately?

RQ2) What is the thermophysical and fluid dynamics behavior of a naturally ventilated DSF under summertime conditions?

RQ3) What factors and their interactions effect (and how) the heat transfer and air dynamics in a DSF?

By answering the research questions, we also aim to validate the approach previously developed with the assistance of simulations on selecting suitable arrays and deepen our understanding of the complex DSF behavior in terms of its thermal and fluid-dynamics processes. We employ a flexible experimental testbed that we have previously developed [17]. This experimental facility makes it possible to carry out thermal and fluid mechanical characterization on DSF configurations in a laboratory setting. The experimental testbed consists of a flexible mock-up with operable features (such as cavity depth, venetian blinds angle, airflow path, airflow rate, opening size), a climate simulator, and a real-time control system experiment and data acquisition.

The results of this study can guide experimental researchers investigating the overall behavior of a complex system/phenomena/process in a wide range of conditions to find the most efficient way to reach their goals. Moreover, the results of the experimental campaign (with almost fifty different configurations of a DSF tested in response to various boundary conditions) are made publicly available for the scientific community for future independent research and calibration and validation of numerical models. Furthermore, by carrying out the study on a particular type of DSF, the results of this study also contribute to deepening the knowledge of the thermal and fluid mechanical behavior of naturally ventilated DSFs.

The contents of the papers are organized as follows. After this brief introduction, we describe, in the section ‘‘Methods and materials,” the overall research design and objectives; we provide general information on the DOE methodology, and more specifically, its application to the case study DSF. In the ‘‘Results and discussion” section, we present and compare the characterization outcomes for the different experimental designs. Based on the common features, we draw overall conclusions on the thermal and fluid dynamics behavior of DSF. Finally, in the ‘‘Conclusion” section, we summarize the outcomes related to the impact of different experimental designs, and we set our findings of the

thermophysical and fluid mechanic behavior of a DSF in the context of the current knowledge in this domain.

6.4. Materials and methods

6.4.1. Research design and research objectives

In this research, we used the design of experiment (DOE) methodology to study, in a laboratory setting, the behavior of double-skin facades (DSFs), with a two-fold aim: to compare and reflect on the impact of different experimental designs (i.e., whether or not they provide the same outcomes), and to understand the role of construction elements and boundary conditions on the overall thermal and fluid-dynamics phenomena in DSF (i.e., how different features in a DSF impact on its performance). The methodological approach we adopted in this investigation was broken down in a series of steps that are described by the following research objectives:

1) To identify a suitable case study (i.e., a DSF configuration), representative boundary conditions, and a set of performance parameters that describe the behavior of the DSF to be characterized.
2) To select several experimental designs based on previously defined guidelines that could be suitable to characterize the performance of the DSF.
3) To carry out a series of experimental runs, based on the arrays identified in the previous step, using a flexible DSF mock-up installed in a climate simulator.
4) To analyze the data collected during the various experimental runs by adopting the DOE methodology, in order:
    a. to compare the characterizations obtained through different arrays in both a quantitative and qualitative way – to be able to answer RQ1.
    b. to identify common patterns in the characterizations obtained with different arrays that can allow one to describe with a good degree of confidence the overall thermal and fluid-dynamical behavior of the DSF –to be able to answer RQ2.
    c. to analyze the impact of the different factors and their interactions in determining the DSF behavior – to be able to answer RQ3.
5) To synthesize the conclusions and main implications of the study in regards to:
    a. the use of different experimental designs in the characterization of a complex system such as a DSF;
    b. the impact of operational features and boundary conditions on the performance of a DSF

6.4.2. The design of experiment (DOE) methodology

The performance of a DSF (and, in general, of a complex system) may depend on many factors (either constructional features, operational features, or boundary conditions) and their multiple interactions. It is practically impossible, in most cases, to investigate all the possible combinations of such factors with real experiments, as this would require unlimited resources in terms of time and costs. The DOE methodology mitigates these limitations because it reduces the number of experiments to be carried out so that the obtained characterization picture is as close as possible to the one acquired by running all the possible combinations. The selection of an experimental design (or array) is at the heart of the DOE methodology, and one has the possibility to choose among a large number of possible arrays, built by using different logics and different statistical theories. In this investigation, we selected four classes of experimental designs that are most often employed for characterization in different engineering fields [18]. The classes of experimental design we decided to employ in this study are synthetized below, and the selection of the exact design features within each class was based on the experience gained and the guidelines developed in a previous study [12].

Taguchi design (TD) has become the most applied experimental design in science and industry [19,18] even though it shows some limitations [20] because of its high flexibility in combining factors with different levels using few experimental runs [21]. The resolution of TDs varies from the most simple ones intended for screening to more complex ones designed for in-depth characterization.

Definitive screening design (DSD) is intended for screening in combination with two-factor interaction assessment. The advantage of this array is that it lowers the required experimental runs to $2k + 1$ (k number of factors) [22]. Its application comes in handy for the processes driven by many factors or in situations where it is desired to filter the most important ones.

Full-factorial design (FFD) contains all possible combinations of the factors and corresponding levels and can provide a more profound characterization picture than any other experimental design [4]. Since it considers all possible combinations, the number of experimental runs grows significantly with the increase of factors or levels.

Central-composite design (CDC) offers a comprehensive understanding, and it is most commonly applied for optimizing system performance, when the number of factors is narrowed by some screening method to five or lower. CCD can assess higher-order terms and the curvature in the response of the output quantity [23].

After performing the experimental runs using the selected array (s), the collected data are post-processed using regression analysis and the analysis of variance (ANOVA). The regression analysis

builds a model that describes the cause-effect link most often using the least-square method [24], while the ANOVA evaluates the constructed model and quantifies the influence of factors and interactions on the output variable by decomposing total variance [25].

6.4.3. Case study DSF and experimental set-up specifications

In the context of this study, we decided to select one representative DSF configuration, i.e., a naturally ventilated DSF operating in the so-called ‘‘outdoor air curtain” mode. In this system, the ventilated cavity of the DSF receives air from the outdoor and releases air back to the outdoor. This configuration aims to reduce the solar gain through the glazing by combining the use of an in-cavity shading device (in the case study, a venetian blinds system) and ventilation airflow to remove heat from the cavity (see, e.g. [26]). This type of façade may thus operate by modulating the free cross-sectional area of the inlet/outlet sections – to control the naturally driven airflow – and by deploying the shading device (and titling the blinds) – to reduce the direct solar transmission through the façade. This operational mode and control possibility is of particular interest in the cooling season since this configuration is one of the most adopted for improving the thermal performance during this period [27], as fully glazed envelopes usually show poorer performance [28]. Congruent with this configuration, the boundary conditions (as described more in detail in the next section) were chosen to represent situations where such DSF mode would be most helpful, i.e., conditions typical of the summer period. The characterization of the performance of such a DSF under the selected boundary conditions was carried out through a full-scale DSF mock-up installed into a climate simulator (Figs. 1 and 2). The DSF test sample was made of inner and outer double glazing incorporated into the aluminum frame. Both were composed of two glass panes with dimensions 1.4 m (W) 2.8 m (H), and the gap between the panes was filled with a mixture of air and argon (4–15–4 mm) [17].

The measurement system consists of more than 70 sensors to measure the temperature of the surrounding environment, the air in the cavity and surface of different facade segments, incident and transmitted solar radiation, air velocity in the cavity, pressure difference, and heat flux density [17]. A dedicated system for control and monitoring of the experiment was developed in the LabView environment to monitor a large number of measurements in real-time. The characteristics of sensors that measured the physical quantities used for the assessment of the performance indicators (response variables) are given in Table 1.

The climate simulator is an indoor experimental facility with two chambers intended to replicate the indoor and outdoor environment surrounding a building envelope element. The test element needs to be installed into a large metal frame and placed between two chambers. The integrated sun simulator can replicate solar irradiance in the approximate range between 250 Wm^{-2} and just over 1000 Wm^{-2}

by using an array of nine metal halide lamps. In the study presented in this paper, we controlled the cells' air temperature values and the irradiance provided by the solar simulator. The climate simulator is not capable of reproducing the effect of the dynamic pressure of wind, and hence when the airflow in the DSF's cavity was activated due to the boundary conditions, this could only be attributed to the stack effect generated in the DSF's cavity. Therefore, no other pressure source than the one thermally induced was involved in this process.

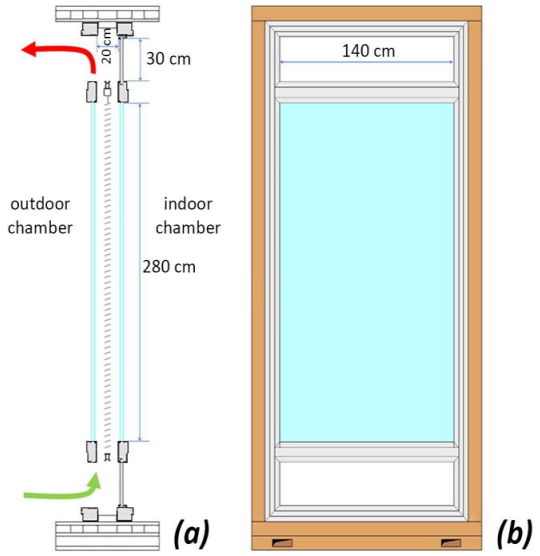

Fig. 1. Schematic representation of the DSF a) vertical section, b) front view.

We must also point out here that due to the limitations of the climate simulator, we were not able to fully replicate desired conditions in some experimental runs. For example, the air conditioning system experiences problems controlling the temperature of the outdoor chamber when the solar simulator is active. For irradiation levels of 350 Wm^{-2}, the actual temperature is 2–3 ºC, while for 700 $Wm^{-2,}$ it is 4–5 ºC higher than the projected one. Furthermore, the air is not uniformly cooled through the chamber, which results in a vertical temperature gradient up to 2 ºC directed upwards. The reader who is interested in obtaining more details on both the flexible DSF mock-up and the climate simulator can find this information, which is not reported here in the complete form for the sake of brevity, in a previous paper [17].

6.4.4. Applications of the DOE methodology in the context of this study

Relevant independent variables (factors) and dependent variables (response variables) were identified considering the degree of freedom allowed by the experimental set-up and a set of interesting quantities that could be used to study the performance of the DSF. These variables and their levels are summarized in Tables 2 and 3.

The air temperature in the outdoor cell of the climate simulator was considered an important variable, and therefore different levels were adopted, while the indoor temperature was set to the constant value of 25 °C, which corresponds to a realistic indoor air temperature setpoint during the cooling period. The combination of a variable outdoor air temperature level and a fixed indoor air temperature level led to a variable temperature difference between the outdoor and the indoor environment (in the range 10 °C to + 10 °C), which we considered a relevant factor in the performance of a DSF and therefore it was investigated. In addition to this factor, solar irradiance level on the vertical plane was chosen as the second boundary condition variable, with the range 0 W/ m^2 to 700 W/m^2.

The flexible mock-up allowed a large range of configurations to be tested, and in the experimental run presented in this study, the following features of the DSF were changed: the angle (0, 45 and 90) of white-aluminum colored venetian blinds with a solar reflectivity in the range of 0.5 to 0.6; the free cross-sectional area of the openings at the top and at the bottom of the DSF (for each opening, between 7 dm^2 and 42 dm^2, which corresponds to 500 and 3000 cm^2/m of facade width, respectively). Considering that the focus of this study was on the operational phase of a DSF (i.e. when design decisions have already been taken and the performance is driven by how the façade is controlled), the choice of varying the only two variables that can be modified under operation seemed a fully logical choice. Furthermore, these two variables also have an impact on other domains than the thermal one (e.g. shading devices influence the light transmission through the facade, inlet/outlet opening influence the sound transmission through the façade) and their operations might therefore be based on more complex logics than just the thermophysical performance of the DSF. Undestanding what impact they have on the thermophysical performance is therefore also important in light of constructing control strategies for a dynamic DSF that trade-off against performance across different domains (e.g. when an optimized thermal performance needs to be combined with sound insulation requirements or with daylight exploitation targets).

We must emphasize that other design factors, such as the optical properties of glazing or slats, can have a significant impact on the thermal performance of DSF [29–31,12]. However, in the context of our study, we treated these as invariable elements and used a constant configuration. The selected types of glazing was, to some extent, not conventional, and a short explanation of the reason for this choice might be beneficial.

DSF are oftentimes realized with a combination of a single-glass skin and a double/triple-glazing skin. For this study we instead opted for a double glazing unit for both the skins. The reason is that we wanted to enhance the thermal decoupling of the cavity and the inner and outer environment. In this way the intrinsic flexibility that a DSF has, i.e. to remove/store heat in the cavity thanks to the

cavity airflow, can be better investigated due to lower transmission loss through the two skins compared to a conventional DSF configuration.

Fig. 2. Experimental set-up: (a) the climate simulator with the façade installed between the two chambers (and visible as the metal frame between the two blue cells); (b) frontal view of the DSF mock-up installed in the frame for insertion in the climate simulator facility; (c) and (d) sensors installation on the mock-up. (For interpretation of the references to color in this figure legend, the reader is referred to the web version of this article.).

Table 1. Characteristics of the sensors used in the characterization of the DSF.

Sensor type	***Measured quantity***	***Accuracy***
Pyranometer	Incident and transmitted solar irradiance	Class 2 (ISO 9060)
Hot-wire anemometer and temperature sensor	Speed and temperature of the air in the cavity	v: ± (0.1 m/s + 3 % of measured) for (0…1 m/s) and t: ±0.3 ºC
Air temperature sensor	The temperature of the air near the inlet and outlet	± 0.3 °C for range (0…70 ºC)
Resistance temperature detector Pt100	The surface temperature of glazing and shading	Class B (from ±0.37 °C at -10 °C to ±0.70 °C at 80 °C)
Heat flux plate	Heat flux density through glazing	Calibration uncertainty: ± 3 %

Table 2. Factors and corresponding levels

Factors	Symbol	Unit	Levels		
			Low	Mid	High
Solar irradiance	ISR	[Wm^{-2}]	0	350	700
Temperature difference	DBT	[℃]	−10	0	10
Venetian blind angle	SA	[°]	0	45	90
Inlet/outlet free cross-sectional area (Opening size)	OS	[cm^2m^{-1}]	500	1500	3000

Another fixed construction feature that may have an impact on the extendibility of the results presented in this study is the cavity depth. Narrow cavities have recently gained preference (especially in single-floor DSFs) for a series of reasons [32–34], among them lower costs and volume, and

because of this trend we opted in this investigation to fix the cavity depth to 20 cm. In addition to being a representative configuration from a market perspective, our previous studies have also shown that for the single-floor DSFs with cavity depths in the range of 20–60 cm, this feature plays a less relevant role compared to other factors in shaping the performance of a DSF [12,17]. While, in general, the cavity size (and the relative position of the shading, i.e. closer or further away from one of the two skins) can impact on the heat exchange between the shading and the glazing, we have seen that for the situation where there is a sufficient cavity depth that ensures a certain distance between the shading and the glazing, the size of the cavity and the exact position of the shading does not have a great impact. Therefore, the missing exploration of the impact of the cavity depth as an independent parameter does not represent, in our opinion, a relevant shortcoming in this study, particulary when considering that this parameter cannot be varied under operations of a DSF.

Several response quantities may be chosen to outline the thermal and fluid dynamics behavior of a DSF, and we decided to include the following in our study: the net heat flux density, the average temperature of the cavity, airflow rate, heat gain/loss rate by the airflow that passes through the cavity normalized by the DSF surface (hereafter referred to as heat gain/loss rate by the airflow), and the average surface temperature of the inner glazing. Net heat flux density represents the sum of heat flux density measured by the heat flux meter installed on the inner side of the inner glazing (q_{HFM}) and transmitted solar radiation to the interior registered by the inside pyranometer (q_{TR}). The average cavity temperature is determined based on the 12-point measurements of hot wire anemometers. The same instruments were used to assess velocity profiles and airflow rate at two heights, based on which the airflow rate is evaluated. Heat gain/loss rate by the airflow represents the heat rate absorbed or released by the airflow that passes through the cavity normalized by the DSF surface, and it is calculated based on the evaluated airflow rate and measured heating/cooling of the airflow when passing through the cavity (t_{out}-t_{inl}). The indoor surface glazing temperature represents the average temperature of the inner surface of the inner glazing measured by the surface temperature sensors.

The uncertainty of the measurements of the response quantity was assessed using the method of error propagation [35] and expressed in a range of values, from the lowest to highest error, since the error may depend on the exact conditions of the tests, and more than 50 experimental runs were done. Experimental uncertainty consists of two parts: the uncertainty originating from the instrument limitations and the error arising from the variability of the measured quantity (standard deviation). As is always the case with steady-state measurements under well-controlled conditions, the first part is dominant over the statistical error. This effect can be clearly seen in the temperature measurement results, where the experimental error belongs almost entirely to instrumental inaccuracy, though this also indicates the strictly maintained steady-state conditions in the climate chambers. It is also

important to note that the airflow and heat gain/loss rateby the airflow are characterized by the high uncertainty due to the inaccuracy of hot-wire anemometers.

Table 3 - Response quantities and corresponding uncertainties.

Response quantity	*Symbol*	*Unit*	*Equation*	*Uncertainty range*
Net heat flux density associated with the DSF	q_{net}	[Wm^{-2}]	$q_{HFM} + q_{TR}$	0.3~9.9
The average cavity temperature	t_{cav}	[°C]	$\bar{t}_{cav}$	0.30~0.32
The airflow rate	$\dot{V}$	[m^3h^{-1}]	Velocity profile method	101~122
Heat gain/loss rate by the airflow that passes through cavity normalized by the DSF surface	q_{vent}	[Wm^{-2}]	$\dot{m}c_p(t_{out} - t_{inl})$	3~116
The indoor surface glazing temperature	t_s	[°C]	$\bar{t}_s$	0.50~0.50

As previously mentioned, we selected four classes of experimental designs that are most often employed in engineering, where the exact features within each class were decided based on the guidelines for finding the optimal design developed in one of our previous researches [12]. The number and type of the factors and their low and high values were chosen based on the problem statement and objectives, while the complex nature of DSF behavior predetermined the minimum resolution (IV) of the design. Limitations regarding the resource demand of the physical experiments in the controlled environment dictated the maximum number of experimental runs, which in our opinion should not exceed 30. Therefore, we identified four experimental designs capable of assessing the influence of both factors and their interactions using a reasonable number of experimental runs: Taguchi (3Lx4F), definitive screening, 2-level full-factorial, and face-centered central-composite design. All the experimental designs were configured to cover the exact same range of variations (min value – max value) for the four factors under investigation so that they can be considered fully equivalent arrays when it comes to the domain of exploration.

The Taguchi design adopted is a fourth-order resolution design that considers not-aliased main effects and confounded two-factor interactions. It takes into account four factors with three levels using 27 experimental runs (Table 4). In comparison to this, the definitive screening design (DSD) uses just half as many experimental runs (13 runs), and it was therefore interesting to investigate its performance considering its resource efficiency. The chosen full-factorial design analyzes four factors with only two levels (low and high). In this way, the array offers, on the one hand, relatively high efficiency by having only 16 experimental runs, but on the other hand, it shows a limitation in the depth of the characterization. Our previous research [12] revealed that the face-centered type of central-composite design (CCD ($\alpha = 1$)) had the best results among 30 tested experimental designs when four or five factors governed the system behavior. Therefore, we opted for the same type of array, with 25 experimental runs, and considered four factors characterized only by the central and

cube points. The critical p-value for recognizing the statistical significance of factor/interactions in the analysis of variance and the factor selection procedures was set to 0.05 for all the designs, indicating a high probability that the considered variable is significant.

It must be emphasized here that different designs may have common points, i.e., identical configurations tested under the same conditions. This was the case in our study, where the four selected experimental designs had a series of coincident experimental runs.

Table 4 - Characteristics of chosen experimental designs.

Experimental designs	Number of runs	Number of factors	Number of levels	Model
Taguchi (3Lx4F)	27	4	3	2-FI
Definitive screening design	13	4	2/3	Quadratic
Full factorial design	16	4	2	2-FI
Central composite design	25	4	2/3	Quadratic

Since the experiments were performed in a controlled environment, where the experimental variation (noise, error) is minimal, these ‘‘repeated” experimental runs were performed only once and not separately for each different design. Therefore, the total number of experimental runs actually carried out to acquire data for all the four experimental designs was 49 instead of 81, thereby significantly reducing resource consumption. Just as is the case here, if there are enough resources, it is always wise to compare the results obtained from the ANOVA performed on two or more different experimental designs to confirm the validity of the obtained characterization picture.

In Table 5, it is possible to see, for each experimental design, the number of experimental runs that are unique and the number of those that are shared with each of the other experimental designs. We indicate the unique points along the top-left/bottom-right diagonal of the table, while shared points between different arrays are noted in the intersection of different designs. For example, FFD does not contain unique points since all other designs are derived from this array, while it shares 6 runs with TD, 4 runs with DSD, and the whole set of 16 runs of the FFD is also included in the CCD. The value in brackets refers to the percentage of runs shared between two experimental designs in cross-section of a row and column, and it measures how ‘‘unique” each experimental design is compared to the others (the lower the percentage, the more unique).

6.4.5. Data analysis

Upon performing the entire sequence of experimental runs that constitutes all the four experimental designs, the analysis of variance (ANOVA) was performed for each different experimental design with the aim of:.

1) comparing the characterization pictures obtained from different arrays,

2) obtaining a general picture of the performance of the façade, and

3) understanding the role of the factors and their interactions.

Table 5. - Unique points and shared points for different combinations of experimental designs. Unique points can be read along the main diagonal of the table (i.e., unique points for TD(3Lx4F) are 16, for DSD are 6, for FFD 0, and for CCD 5), while in all the other cells the number of shared points between the two designs can be read, with the percentage indicated between brackets.

Experimental designs	Number of runs	TD (3L×4F)	DSD	FFD	CCD
TD (3Lx4F)	27	16 (59%)	3 (11%)	6 (22%)	9 (33%)
DSD	13	3 (23%)	6 (46%)	4 (31%)	5 (38%)
FFD	16	6 (38%)	4 (25%)	0 (–)	16 (100%)
CCD	25	9 (36%)	5 (20%)	16 (64%)	5 (20%)

The overall thermal and fluid dynamic behavior was represented through assessed contributions of each factor and interaction on the variability of the different performance indicators. This quantity was calculated based on the ANOVA procedure, where the sum of squares for the factor or interaction ($SS_{F\&I}$) of interest is divided by the total sum of squares SS_T:

$$c_{F\&I} = \frac{SS_{F\&I}}{SS_T} 100 \qquad [\%]$$

where F&I is a particular factor A, B, C, D... or interaction between AB, AC, AD..., ABC, ABD...

In order to identify and quantify the similarity between two characterizations obtained with different experimental designs, we have employed a comparison method based on the fitting coefficient f, which we introduced in our previous study [12]:

$$f = 1 - \frac{\sum_{F\&I} |c_{F\&I,RD} - c_{F\&I,D}| + \left| \frac{SS_{E,RD}}{SS_{T,RD}} - \frac{SS_{E,D}}{SS_{T,D}} \right|}{2} \qquad [-]$$

The coefficient measures how much the contributions of factors/interactions ($c_{F\&I}$) and randomness (SS_E/SS_T) differ between two designs (RD – referent and D – design to be compared). The value of f varies from 0 to 1, where one corresponds to the absolute identity between the two characterizations, while zero indicates complete disagreement between the two characterizations.

Factorial and interaction plots were used to understand how factors and their interactions affect the behavior of DSF. The main effects (factorial) plot shows the mean response of dependent quantity for each factor level connected by a line, while the interaction plot shows how the relationship between the response variable and a factor depends on the value of a second factor. More information on this, as well as on the ANOVA calculation procedures and method for comparison of designs, one can be found in one of our previous research studies [12].

6.5. Results and discussion

6.5.1. Performance of the different experimental designs

The comparison of the different experimental designs showed an excellent agreement in terms of the characterizations of the thermal performance, carried out using the net heat flux density Q_{net}, the average temperature of the cavity t_{cav}, and the indoor surface glazing temperature t_s. All experimental designs estimated almost equal shares in the total variance with low error (Fig. 3). Only the response of the indoor surface glazing temperature fitted from DSD deviated slightly from the corresponding response obtained from FFD and CCD, but even in these cases, the match between the different designs can be considered very good (Table 6). There were also differences in whether certain designs see particular factors or interactions as statistically significant, but the contribution of these variables was very small to substantially influence the thermophysical behavior of DSF (Fig. 3). The factors' impact was dominant in influencing the cavity and indoor surface glazing temperature, and therefore linear models containing only main effects would be suitable to describe the response of these quantities. However, that was not the case with net heat flux density, where the influence of interaction between irradiance and slat angle was nearly dominant as the individual influence of factors. Therefore, models containing higher-order terms are needed to adequately fit this quantity's response.

As opposed to the thermal, fluid dynamic characterization showed more significant discrepancies, especially regarding the airflow rate assessment. For example, there were notable differences in impact assessment of different factors between the FFD and other experimental designs (Table 6). Compared to other designs, the FFD recognized the different contributions of the solar irradiance and temperature difference and did not see the statistical significance of the slat angle (Fig. 3). Most likely since twopoint designs cannot fit the non-linear response of output quantity (in this case, the airflow rate $\dot{V}$), as explained more in detail in 3.3. Every experimental design led to a simple linear model that contained only the main effects to fit the response of the airflow rate (Fig. 3). This result may raise some questions knowing that the underlying nature of the airflow is, in general, non-linear. Since all the arrays had errors higher than 5 %, it was challenging to recognize the statistical significance of non-linear terms. One may question if this result derives from the phenomenon being mostly linear in the range of investigation, or from the levels used in the investigations not being suitable, or from some other reason. Since the levels/sample points have shown to be suitable for the other indicators, there are no particular reasons to hypothesize that they were not suitable for unveiling the behavior of the airflow rate. We rather understood the large error as linked to the high measurement uncertainty in the airflow rate measurement since hot-wire anemometers could not register velocities below 0.1

ms^{1}. Additionally, uncertainty was also associated with determining the airflow direction when the temperature difference between the fluid and the interface was less than 0.5 °C. As a result, the airflow variations below a certain threshold could not be registered by the hotwire anemometers, resulting in a low resolution for the characterization of this phenomenon, regardless of the employed experimental design.

The resemblance between different experimental designs regarding heat gain/release by the airflow Q_{vent} ranged from very good to excellent, which was slightly worse compared to thermal performance quantities, but better than for the airflow rate (Table 6). All four experimental designs recognized the same factors/interactions as the most relevant, and these were the two boundary conditions (temperature difference and solar irradiance). Errors were more acceptable than in the case of the airflow rate but still considerably high (>5%) for some experimental designs, such as TD and DSD (Fig. 7). Due to the considerable error in those designs, the slat angle and opening size (free cross-sectional area) were not recognized as statistically significant in controlling heat absorbed/released through the airflow for a tested range of configurations and boundary conditions. The uncertainty associated with the threshold of hot-wire anemometers was most likely felt here, but to a lesser extent, as the variance of this quantity was less influenced by the low-velocity variations (check equation, Table 3). Like the net heat flux density, the response of the heat gain/release by the airflow is fitted best by a model containing higher-order terms. The interaction between solar irradiance and the temperature difference plays an important role in controlling this quantity response.

Generally speaking, it is possible to see that the differences between the four experimental designs were minor, and this indicates that all of the selected designs could sample the most representative points within the domain. More importantly, the fact that different experimental designs returned a very robust picture about the role of the different factors can be understood as a confirmation that the outputs of the analysis truly described (minus any experimental error) the thermal and fluid-dynamics behavior of the DSF. Based on this conclusion, we could therefore determine with a good degree of confidence which factors and interactions were significant and to what extent they controlled the heat transfer and the fluid flow in the DSF.

The comparison of the ANOVA performed on the different experimental designs showed that the experimental design must be capable of assessing the impact of higher-order terms to adequately characterize the behavior typical of dynamic facades. In addition to this, it is highly desirable to use designs that allows factors to have more than two levels so that the fitted model (such as quadratic) can capture curvature in the response of the dependent variable. However, it is important to emphasize that the success of the DOE characterization depends to a great extent on the uncertainties associated with the experimental campaign, even if a suitable experimental design is chosen. In a case where the

variability of the response quantity was measured or determined in a less accurate way because of the challenge to measure a physical quantity (such as it was the case for air velocities below 0.1 ms^{1}) or because of the use of a less reliable measurement method, the experimental uncertainty propagates throughout the ANOVA results, and the results coming from this process will, in the end, be less reliable. Furthermore, a large error can be caused if unsuitable factors are introduced into the analysis (e.g., interdependent factors) or desired boundary conditions are not met in the experimental procedure.

Table 6. – Fitting coefficient values between four different experimental designs

	The fitting coefficient [-]					
	TD vs DSD	***TD vs FFD***	***TD vs CCD***	***DSD vs FFD***	***DSD vs CCD***	***FFD vs CCD***
Q_{net}	0.96	0.95	0.95	0.95	0.97	0.98
t_{cav}	0.97	0.96	0.97	0.94	0.95	0.99
t_s	0.92	0.97	0.97	0.89	0.90	0.99
q	0.91	0.78	0.88	0.73	0.82	0.79
Q_{vent}	0.90	0.89	0.92	0.92	0.88	0.95

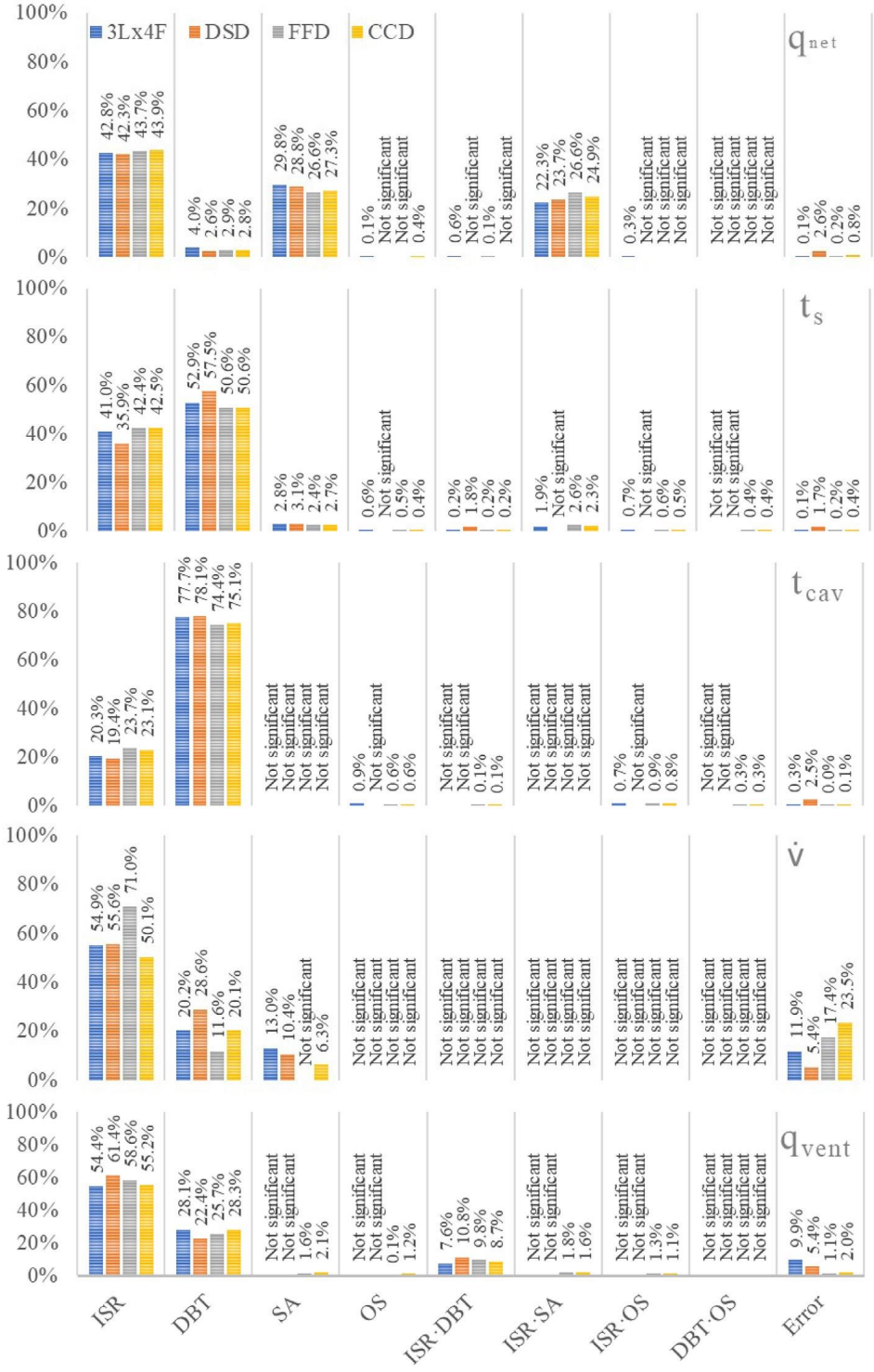

Fig. 3. Comparison of characterization of thermal and fluid-dynamic behavior of DSF obtained by different experimental designs

6.5.2. Overall thermal and fluid-dynamic behavior of a naturally ventilated DSF

The net heat flux density of the DSF in outdoor air curtain ventilation mode was shown to be controlled almost entirely by solar irradiance and the venetian blinds, where the interactions among these two also played an essential role. Therefore, the position of the blinds in response to the incoming solar radiation clearly showed potential in controlling the heat transfer in the DSF, and hence in control of the energy efficiency of DSFs. The ANOVA results confirmed the expected prevalence of heat transfer induced by incoming solar radiation over the transmission driven by the temperature difference between indoor and outdoor environments. Therefore, the impact of solar irradiance was shown to impact the dependent variable with a weight far greater than temperature difference.

The temperature at the indoor-facing surface of the inner skin can be used as a proxy for potential thermal discomfort issues, as it impacts the mean radiant temperature of the indoor space and may contribute to local discomfort phenomena (such as radiant asymmetry). The surface temperature is almost entirely regulated by solar irradiance and the temperature difference solely, while the slat angle and the size of the opening have negligible influence. Most likely, the high insulation glazing properties decouple the cavity from the indoor surface when it comes to heat transfer. Therefore, control of accumulated heat and the airflow in the cavity by changing the slat angle and size of the opening has a minor effect on the temperature of the indoor facing surface of the glazing.

Since the air inside the cavity was in direct contact with (i.e., originated from) the outdoor air, the ANOVA indicates that the average temperature of the cavity was highly impacted by the temperature difference, more precisely by the outdoor air temperature (as the indoor air temperature was kept constant). The influence of solar irradiance was also noticeable, and similarly, as for the previous indicator, the boundary conditions were the only ones that regulated the air temperature in the cavity. The results of the ANOVA did not identify the slat angle as a significant factor that impacted the cavity air temperature, and the free cross-sectional area was also shown to be negligible. That may seem contrary to our preconceptions, but we must point out that the configuration with active shading was tested by changing only the blind angle. The shading device itself certainly influenced the temperature of the cavity by absorbing incoming solar radiation but changing only the blind angle on an already lowered shading device did not have a significant effect as it redistributed accumulated heat in the cavity while average temperature did not change significantly. Moreover, the high reflectivity of the venetian blinds with white aluminum color most likely reduced the heat accumulation and air temperature increase in the cavity. From a control perspective, this means that neither changing the angle of venetian blinds nor the percentage of the inlet and outlet opening vents

(in the tested range) seemed to be an effective way to control this quantity. However, we need here to highlight that the analysis was carried out by combining boundary conditions and control features, and the results showed that boundary conditions have a much greater impact on the dependent variable(s). This effect might ‘‘hide”, in the ANOVA, the effect of the control features, which could still be nonnegligible given a specific set of boundary conditions. Parametric experiments where only the control variable (i.e. slat angles of the blinds or free cross sectional area of the inlet/outlet) is changed and boundary conditions are kept constant could possibly to identify the effect of each control variable given a certain solicitation.

The airflow generated in the DSF’s cavity was generated only due to the stack effect, as this could be the only driving force to activate a flow (considering that the climate simulator could not replicate, for example, the effect of the wind). Hence, we considered the heat transfer due to temperature difference across the DSF’s domain and the heat gain due to solar irradiance as the two reasons for a temperature stratification within the DSF’s cavity. The ANOVA analysis showed that the airflow in the cavity was triggered more by the solar irradiance than the temperature difference, which was something we had expected. The first factor, especially in the summer period, provides the DSF with higher heat gain and thus generates larger temperature differences between the air in the cavity and the surrounding boundaries, thereby contributing to stronger natural convection. Changing the slat angle modified the amount of absorbed radiation and consequently the temperature difference to the surrounding air and thus most likely affected natural airflow in the cavity. The smallest size of the opening was probably big enough to create pressure drops comparable to the one generated by the largest size, so the effect of changing aperture size was not significant. We can hypothesize that further reducing the inlet/outlet opening size (hence the free cross sectional areas) would reduce airflow, which would be felt more significantly since the DSF would gradually switch to another operational mode (air buffer).

Heat gain/loss associated with the airflow plays a vital role in the thermal load relief of a DSF ventilated by the outdoor air curtain means in the summer. As mentioned, the solar irradiance generated a stronger heat gain/release by the airflow than the temperature difference, though the former factor also played an important role since the cavity was in direct contact with the outdoor air. The solar radiation prevalence comes from the fact that the radiative processes are largely responsible for the accumulation of the heat in the cavity and the generation of the airflow rate. Similar to the cavity temperature, it is expected that installing the venetian blinds induces heat absorption/release by the airflow and its diversion toward the outside. However, changing only the slat angle on an already deployed shading device did not play a significant role. Since the ANOVA results showed that the opening size did not significantly affect the airflow in the cavity, it was expected that the

impact of the same factor was not recognized as statistically significant for the heat absorbed/released by the airflow.

Summing up, the results of the characterization showed that the thermal performance of the tested configuration in the summer period was governed primarily by the boundary conditions, and to a lesser extent, by the slat angle of venetian blind as a structural/operational parameter. That was especially true for indoor surface glazing and cavity temperatures, where the temperature difference played a dominant role. These variables could hardly be controlled by changing the slat angle or the size of the vent opening. On the contrary, by modifying the reflected, absorbed and transmitted solar radiation, the shading device angle was crucial in controlling net heat flux density. Since the inlet/outlet opening size did not significantly affect the airflow generation in the cavity, its influence on other response quantities was not recognized by the results of the ANOVA. The airflow in the cavity was induced by the solar radiation more than the temperature difference, while the slat angle helped control its rate, but to a limited extent. The predominance of solar irradiance compared to the temperature difference was also notable in heat gain/release by the airflow, but unlike the airflow rate, changing the slat angle had a negligible impact on this response quantity.

From this picture it seems that some response variables could not be significantly modified through construction variables (the slat angle and the size of the vent opening), at least compared to natural drivers (boundary conditions) in the given range of boundary conditions and tested configurations. Here, again, we can propose as a reasonable explanation for this evidence that larger variations of these response quantities are possible at the design stage, where optical and thermal properties of the glazing and the shading device can be selected over a large range of possibilities, but once these are fixed, the variation allowed by the operational factors are limited. Of course, such results may depend on the choice we made for the specific test case (in terms of glazing types and shading type, especially when it comes to their optical properties), though the selected configuration for the unchangeable factors was done bearing in mind a realistic case scenario.

6.5.3. Assessment of main effects and interaction effects

Factor impact analysis

The different designs generally identified a linear response of net heat flux density to all factors, and thus we can conclude that experimental designs that use only two points can be almost as successful in modeling the response of the net heat flux density as those that use more than two points. On average, the increase in solar irradiance led to a rise in neat heat transfer, while opening the blinds led to an increased transmitted solar radiation and thus to an amplified net heat flux density – two results that are not surprising (Fig. 4 – 1a). The impact of the temperature difference was not as strong as the

solar irradiance and slat angle when it comes to the net heat flux density (Fig. 4 – 1b). However, this factor showed similar linear behavior as the two previously mentioned parameters, where lower temperatures (than those inside the interior) suppressed the net heat flux density, while the higher ones induced it (Fig. 4 – 1c). The response of the output quantity to changes in the free cross-sectional areas of the inlet/outlet (vents' opening size) showed certain features of non-linearity, where the middle-sized point had the most optimal outcome in reducing net heat flux density (Fig. 4 – 1d). However, just a small error would be made if the effects of non-linearity were neglected since it was shown that the cross-sectional area did not strongly influence either the airflow or the heat absorbed/released by it in the ventilated cavity.

The way factors affected the indoor surface glazing and cavity temperature was similar to the net heat flux density, where on average, the increase in solar radiation and temperature difference led to a linear rise of considered response quantities (Fig. 4 – 2a, 2b, 3a, and 3b). CCD recognized a certain extent of non-linearity in cavity temperature response to temperature difference and opening size (2b and 2d), but these effects were negligible. The same is notable for the indoor surface glazing temperature response to alteration in the slat angle and the opening size (3c and 3d).

As expected, solar radiation and temperature difference induced the airflow in the cavity, while thermal equilibrium and conditions with no radiation tended to diminish it (Fig. 4 – 4a and 4b). All designs except FFD point to the considerable nonlinear response of the airflow rate to changes in temperature difference, which must be taken into account to obtain the correct characterization picture (Fig. 4 – 4b). FFD does not account for this non-linearity, and therefore the weaker effect of temperature difference on airflow rate was approximately two times greater than for the other three designs (Fig. 3). The airflow rate response fitted from the FFD might erroneously indicate that the airflow rate weakens as the outdoor temperature rises. On the contrary, RS, DS, and Taguchi 3Lx4F designs imply that the absence of a temperature difference dampened the airflow in the cavity, which is much more physically grounded. The gradual closure of the venetian blinds led to an increase in the airflow rates, which is expected as the temperature difference between slats and surrounding fluid also increases, leading to the intensification of natural convection (Fig. 4 – 4c). Due to the high error, none of the models saw opening size as the significant factor in controlling airflow rate (Fig. 4 – 4d). As stated before, the inability of designs to adequately fit airflow rate response originates from the limitations of the measurement technique and the underlying non-linear nature of air dynamics in the cavity.

In general, there was a linear response of heat gain/loss rateby the airflow to changes in solar irradiance and the temperature difference (Fig. 4 – 5a and 5b). However, it is interesting that solar radiation and outdoor temperature exerted opposite effects on the heat gain/release by the airflow

(Fig. 4 – 5a and 5b). Generally, the amount of absorbed heat by the airflow decreased with increasing outdoor temperature, which is different from the concave-shaped response of the airflow rate with a minimum at medium temperature (0 °C temperature difference). Therefore, we can conclude that the amount of heat removed by the airflow toward the outside decreases as the ambient temperature increases. The CCD indicated particular non-linearity in response to the slat angle and opening size, implying that the highest quantity of removed heat (by the airflow) corresponds to the closed blind and mid-size opening (Fig. 4 – 5c and 5d).

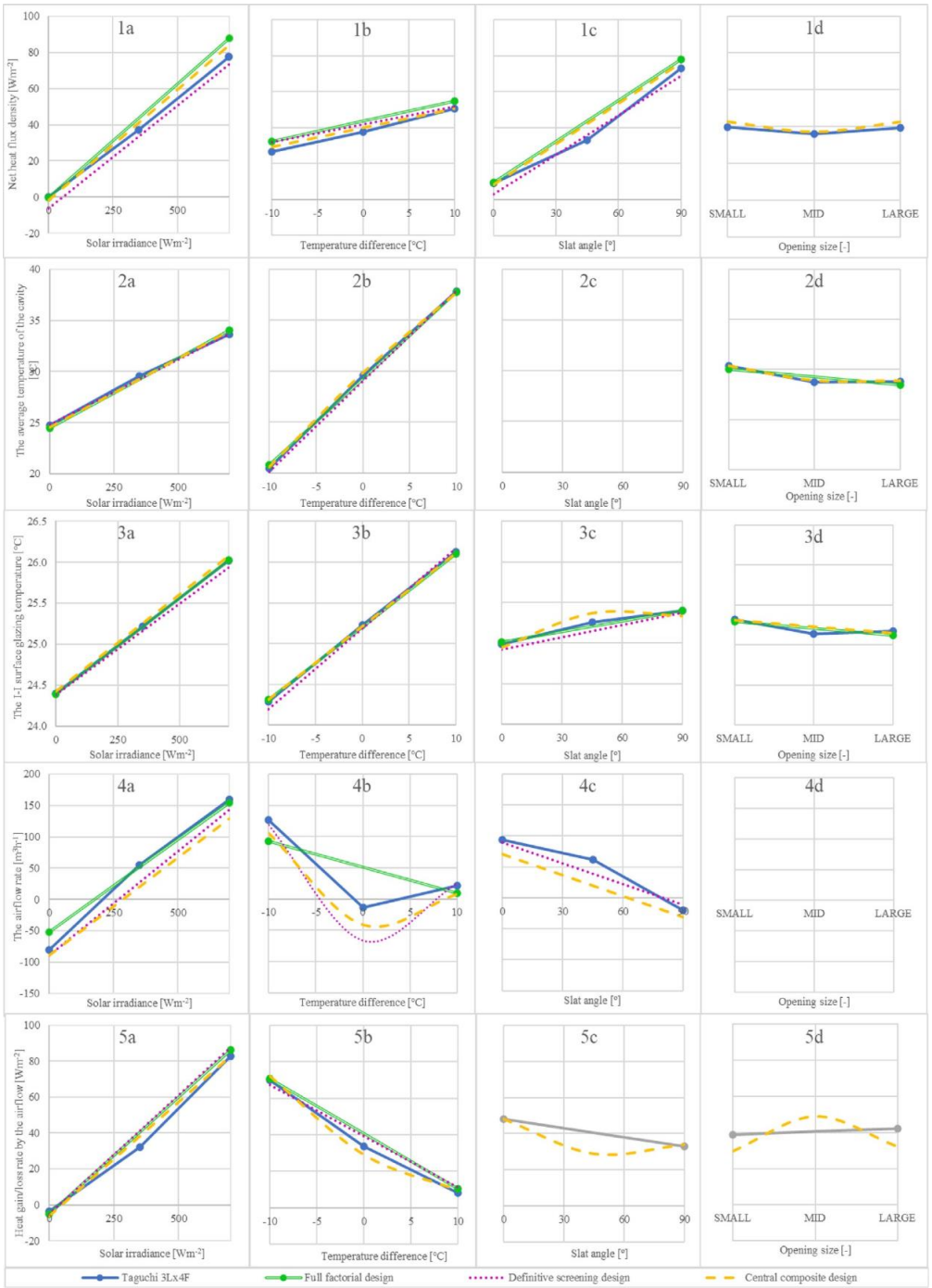

Fig. 4. Analysis of the influence of factors on neat heat transfer, the average air temperature of the cavity, the indoor surface glazing temperature, the airflow rate, and heat gain/loss rate by the airflow (from top to bottom, respectively). The responses to statistically non-significant factors seen by various experimental designs resulted in an empty chart (see graphs 2c and 4d) or a chart that with an almost flat profile (see graphs 1d, 2d, 5c, and 5d). The responses fitted by the quadrature models (DSD and RASD) do not contain markers, unlike those fitted from the 2-FI models (TD and FFD).

Factors impact analysis showed that the heat transfer and natural convection gradually intensified while temperatures of construction DSF elements linearly rose with the increase of solar irradiance. Similarly, an increase in outdoor temperature led to a linear rise of both indoor glazing surface and cavity temperature and net heat flux density. In contrast, the amount of heat removed from the cavity by the airflow decreased linearly as the temperature difference increased from negative to positive. Non-linear, concave-shaped airflow response to temperature difference was recorded without clearly defined minimum, but with notable feature indicating largest airflows for negative temperature differences. Opening venetian blinds (0 to 90º) led to the rise of the heat entering the indoor environment and the temperature of the indoor glazing surface. In contrast, the same act caused attenuation of the airflow and the amount of heat removed by it from the cavity, although to quite a bounded extent for the latter response quantity. Although the vent opening size had shown a very limited range of influence, some traces of its action on response quantities could be glimpsed in the factorial plots. The CCD recognized that the mid-size opening had the most optimal impact on the net heat flux density reduction and the amount of heat removed from the cavity by the airflow. Furthermore, reducing the opening size led to the increased temperatures of the indoor glazing surface and the air in the cavity.

Interaction impact analysis

The main effects described the airflow rate and cavity temperature response, while for all other response quantities, interactions were needed to characterize the thermophysical behavior of the DSF correctly. Therefore, interactions played a significant role in controlling processes in the DSF, and hence, the main effects could not be interpreted without considering them. Since many statistically significant interactions were not decisive in controlling DSF performance, we will consider only those with the highest contribution share. The analysis outcome showed that the interaction between solar irradiance and the slat angle (in regulating net heat flux density) and the interaction between solar irradiance and temperature difference (in controlling heat gain/release by the airflow in the cavity) were the significant interactions to consider.

The net heat flux density response to a combination of solar irradiance and the slat angle, fitted from Taguchi 3Lx4F and FF designs, is shown in Fig. 5. The plot indicates the importance of the slat angle in controlling net heat flux density when there is a non-null value of solar irradiance. Shifting the angle from 90 (open position) to 0 reduced, on average, the net heat transfer by seven times while changing from 45 to 0 (closed position) resulted in a reduction by around three times. Furthermore, combining a medium level of solar irradiance (350 Wm^{-2}) and open slats produced approximately the

same net heat flux density as for high solar radiance level (700 Wm^{-2}) and 45º opened blinds. The interaction plot does not differ significantly between FFD and Taguchi 3Lx4F designs for opened and closed blinds. However, we could not achieve insight into the combined effect of halfclosed blind and solar irradiance relying only on the FFD.

Fig. 6 shows the interaction effect between solar irradiance and temperature difference on heat gain/loss brought by the airflow in the cavity, where a negligible heat gain/release by the airflow in the absence of solar irradiance is notable. When the outside air temperature was colder than the indoor air temperature combined with a medium or a high solar of solar irradiance (>350 Wm^{-2}), the airflow absorbed large quantities of heat accumulated in the cavity. The amount of heat removed from the cavity and transported towards the outdoor environment decreased as the outside temperature rose. The combination of medium solar irradiance (350 Wm^{-2}) and the medium and high outdoor air temperature (from 25 °C to 35 °C) emphasized this effect. Following the same situation as the previous case, it is impossible to obtain insight into the combined effect of a null temperature difference and solar irradiance with FFD due to the limitations characterizing this design. Finally, we can conclude that ventilating a DSF with an outdoor air curtain is not recommended during hot periods (35 °C) combined with no or medium radiation levels (350 Wm^{-2}) since the airflow removed no heat, or the heat was even released to the boundaries of the cavity. The interaction plots obtained from the CCD and DSD indicated similar features as those retrieved from Taguchi and FFD, so we decided to omit the former to make the graphics easier to read.

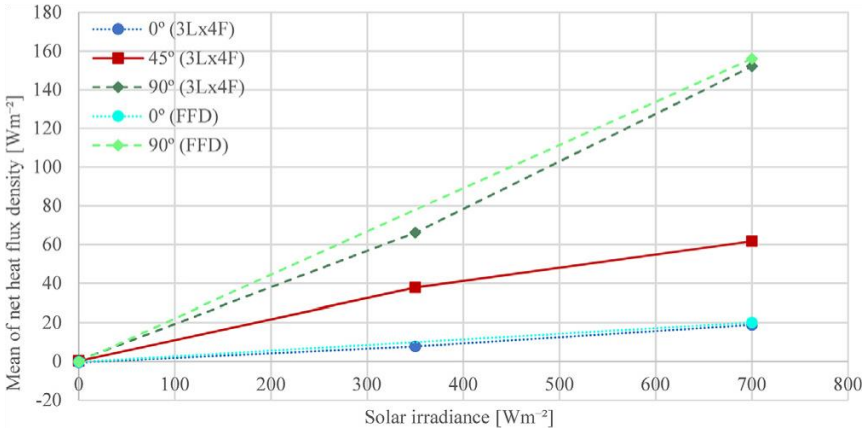

Fig. 5. Effects of interaction between solar irradiance and the slat angle on net heat flux density

Interaction effects can be analyzed from the contour and surface plots for experimental designs that use quadratic models, such as DSD and CCD. The fitted response of net heat flux density as a function of solar irradiance and the slat angle can be seen in Fig. 7a (for DSD) and 6b (for CCD). In each chart, the surfaces parametrically depict the net heat flux density response to solar irradiance and the slat angle as a function of constant values of the other statistically significant factors. In Fig. 7a

(concerning DSD) surfaces represent net heat flux density response to solar irradiance and slat angle as a function of constant temperature difference, while in Fig. 7b (concerning CCD), surfaces depict the same response as a function of combined constant temperature difference and opening size.

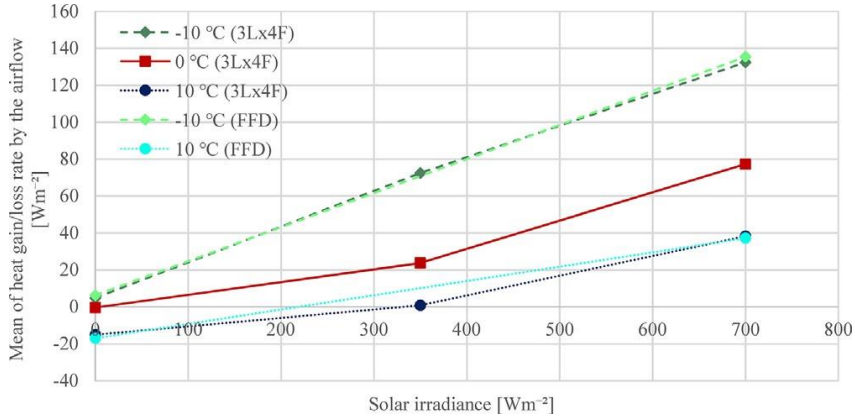

Fig. 6. Effects of interaction between solar irradiance and the slat angle on heat gain/loss rate by the airflow.

In Fig. 7a and 7b, one can see that the slat angle played the dominant role in controlling the net heat flux density by blocking solar radiation from being transmitted in the interior. For example, having closed slats substantially limited the effect of alteration in solar irradiance. By closing the venetian blinds (from 90 to 0º), the reduction factor for a net heat transfer increased multiple times, depending on the value of solar irradiance. The thickness of the stacked surfaces in Fig. 7a, 7b, and 8b indicates the variations range of the response quantity caused by the significant factors held at the constant level. Considering this, it is visible from Fig. 7a that the temperature difference had a considerably weaker impact on the net heat flux density than solar irradiance or the slat angle. Similar is notable in Fig. 7b for the combined influence of temperature difference and the opening size. Parallel surfaces visible in Fig. 7a and 7b point to the type of interaction between the solar irradiance and the slat angle, which is the same for any temperature difference (Fig. 7a) or any combination of the temperature difference and the opening size (Fig. 7b).

Fig. 8a and 8b depict the heat gain/release (by the airflow) response to the temperature difference and the solar irradiance fitted from DSD and CCD. Both figures indicate similar behavior, with the DSD showing only one surface since no statistical significance other than solar irradiance and temperature difference was recognized. In addition to two dominant factors, the quadratic model fitted from CCD recognized the statistical significance of the slat angle and the opening size. Therefore, in Fig. 8b concerning CCD, surfaces represent the response of the heat gain/release by the airflow to the temperature difference and the solar irradiance as a function of combined constant slat angle and the opening size. From the given figure, one can detect the optimal configuration for heat removal by the airflow from the cavity in certain environmental conditions. For example, in situations that

correspond to high solar irradiance and outdoor temperature difference (700 Wm^{-2}, 35 °C), closed blinds and mid-size openings produced six times higher heat removal by the airflow than the combination of opened blinds and small opening size. For conditions that suit high solar irradiance and low outdoor temperature, that effect is less amplified (700 Wm^{-2}, 15 °C), with an increase of around 50%. Unlike in Fig. 7a and 7b, surfaces intersect, which means that the temperature difference interacted with solar irradiance in different ways for different combinations of the slat angle and the opening size. Like the interaction plots, surface plots indicate the negative effect of the outdoor air curtain ventilation mode in periods without solar irradiance and with high outdoor temperature. The highest amount of diverted heat towards the outside was for a combination of high radiation and cold outside temperature. Under these conditions, the enthalpic gain of the ventilation airflow was about 2.5 to 3.5 times greater than in the case of both high outside air temperature and a high level of solar irradiance.

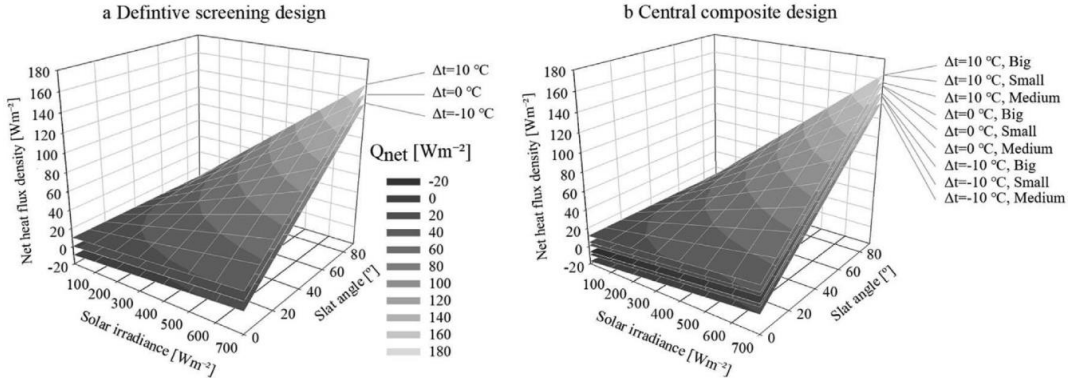

Fig. 7. The surface plot of the net heat flux density response to solar irradiance and the slat angle fitted from the DSD (left) and CCD (right).

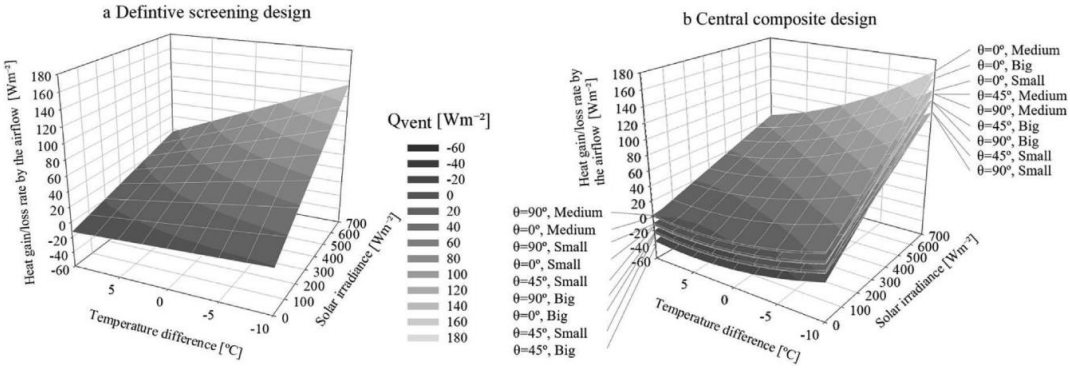

Fig. 8. The response of heat gain/release rate by the airflow to the temperature difference and the solar irradiance fitted from the DSD (left) and CCD (right).

Interactions played a significant role in controlling DSF performance, especially when it comes to the net heat flux density and the amount of heat absorbed/released by the airflow passing through the cavity. The solar radiation impact on the heat entering the indoor environment was significantly reduced with closed blinds. For high radiation levels, shutting the blind from completely open to closed led to a reduction of net heat flux density up to seven times. The highest heat amount removed by the airflow from the cavity was present in replicated conditions of high solar irradiance and cold outdoor temperature (15 °C). In situations corresponding to the absence of solar irradiance and high outdoor temperature (35 °C), the airflow passing through the cavity released the heat to the surrounding boundaries, while in the same thermal conditions and with medium solar irradiance level, the airflow hardly removed any heat from the cavity.

6.6. Conclusions

The application of DOE methodology in building energy and thermal performance research is not a novel concept, but almost all studies involve simulations rather than physical experiments. With this research we aimed to contribute to the knowledge on how to apply DOE methodology successfully to experiments in a controlled environment and choose an optimal experimental design suitable for the characterization of complex systems.

In our analysis we employed and compared four experimental designs able to assess higher-order terms and non-linear behaviors typical of a DSF. The depictions of thermal behavior obtained from different experimental designs resemble each other excellently, while the somewhat weaker agreement between arrays was found for the fluid dynamics. However, even in this case, the resemblance was satisfactory, which enabled us to deduce which factors affect, and in what way, heat transfer and air dynamics in the cavity.

We can conclude what characteristics an array needs to have to provide a sufficient characterization picture of the cause-andeffect relationships between variables in the complex process of a DSFs, and by extension, in other complex processes seen in building science:.

- Experimental design needs to adequately estimate the impact of higher-order terms in order to characterize the behavior of complex systems, such as dynamic facades, adequately. The main effects in such systems can not be interpreted without considering interactions.
- Designs should be able to assess the non-linear response of the output quantity. Therefore, arrays should either fit a quadratic model or have a minimum of three points so that 2FI-models can recognize deflection in the response.
- The unexplained variance needs to be as low as possible, preferably less than 5%, so the statistical significance of interactions and weaker terms can be recognized. If we suppose

optimal experimental design is chosen for characterization, an error larger than 5 % indicates possible irregularities in planning or performing the experiment. For example, the experimenter can select the factors that are not mutually independent, or in the experimenting phase, there may be problems in maintaining the desired boundary conditions. Furthermore, a high error can be caused by the limitations (inaccuracies) of the used instrumentations or the unreliability of the experimental method, where all these experimental uncertainties will propagate to the results of the ANOVA.

- If there are enough resources, it is always wise to compare the results obtained from the ANOVA performed on two or more different experimental designs to confirm the validity of the obtained characterization picture. That is often feasible since many experimental designs share common points and the total number of experimental runs for two different array may be less than the sum of the experimental run for each individual array.

In addition to comparing the performance of different experimental designs, this research aimed at deepening the understanding of the behavior and the quantification of the thermopysical phenomena (and to what extent they can be controlled) in naturally ventilated DSFs, operating in outdoor air curtain mode, under typical summer conditions. The characterization of these processes was performed using a climate simulator system and an on-purpose developed façade mock-up. Construction and operational features of both the climate simulator and the mock-up may have impacted the results and limited their full extendibility to in-field cases. It is therefore necessary to consider the following aspects while going through the conclusions of our study.

The climate simulator was able to replicate the conditions in which the airflow in the cavity was driven only by the buoyancy, and thus the effect of the wind as an environmental factor is not considered. Most likely, the DSF performance will depend to a greater extent on the inlet/outlet opening size if the effects of wind are taken into consideration as an additional driving factor.

From a measurement perspective, it should be emphasized that the characterization of fluid-dynamic behavior through quantities such as the airflow rate or heat gain/loss by the airflow contained a considerable amount of uncertainty accumulated through the limitations of the velocity profile method and inaccuracy of hotwire anemometers. The nature of the test facilty, however, makes it complicated to select alternative techniques for monitoring the airflow, and other options that are (at least on the paper) more promising than the velocity profile method for low airflow rates (e.g. [36]), might not be suitable for this test setting.

The tested facade mock-up was a single-story DSF, which we considered representative of current trends in the construction of adaptive facades that prefer compact prefabricated elements. However, there are other types, such as the shaft-box or multistory DSF, where stronger buoyancy effects may

result in a different picture when it comes to the processes assessed in this study. Moreover, some of the factors that influence the global performance of a DSF, such as the optical characteristics of glazing or shading, were not treated as variables in this study, but we adopted fixed elements that we considered suitable to study the problem of the control of a DSF under (peak) summer-time boundary conditions.

In focusing our study on control variables (opening size of the inlet/outlet section; tilt angle of the venetian blind), it was easy to set the range for the venetian blinds (from fully closed to fully open), while a much greater degree of freedom was left in choosing the range for the opening size. The results of the impact of the free cross-sectional area on the controllability of some phenomena might therefore be linked to the selected range for this variable, and different (notably, smaller) values of the free cross-sectional area might have led to a different picture (i.e. that this variable too could play a more relevant role when one can modulate the free cross-sectional area down to 100 to 200 cm^2/m of facade width).

Based on the outcomes of the characterizations obtained from different experimental designs, we can draw the following conclusions for our specific façade mock-up, which we believe are realistically extendable to a larger range of single-story naturally ventilated DSFs.

- Boundary conditions are central regulators of the thermal and airflow behavior of a DSF, and the range in which DSF behavior can be impacted by adjusting the operational features (i.e., the shading devices and the free cross-sectional area) can be very limited for some performance parameters (i.e., convective gains of the airflow in the cavity, the indoor glazing surface, and cavity temperatures).
- However, certain aspects of energy performance can be efficiently controlled by manipulating the features of the DSF, such as net heat flux density through the control of the slat angle. Finding the optimal position of the lamellae in response to solar irradiance is beneficial to optimize the energy efficiency of a DSF, as transmitted solar radiation represents, on average, the largest share in the net heat flow.
- Buoyant flow in the cavity with installed venetian blinds is driven far more by the solar irradiance (absorption of solar radiation by the DSF components) than by the temperature difference between outdoor and indoor environments.
- The highest airflow rates are observed for the combination of high solar irradiance and negative air temperature difference (colder outdoor temperature compared to the internal one).
- The slat angle can control the airflow to a limited extent, where the gradual closing of blinds leads to intensifying the mass flow rate in the cavity.

- The highest amount of heat removed by the airflow from the cavity is found in conditions corresponding to high radiation levels and outdoor air temperatures lower than internal ones. We can conclude that the amount of accumulated heat in the cavity diverted toward the outside by the outdoor air curtain is reduced with increasing outdoor temperature and decreasing solar irradiance, making it a ventilation mode with a moderate or litttle effect in periods like hot nights or hot cloudy days.

Similar conclusions about the importance of venetian blind slat angle in controlling heat entering the indoor environment have been obtained as in the studies [37–39] with a similar reduction factor for closed slats [37]. Experimental and CFD investigations [38,40,41] found likewise that gradual closure of the blind leads to the enchantment of naturally induced airflow and heat removed from the cavity. Unlike most research that evaluates the individual (parametric) influence of constructional features in clearly defined conditions, this study addressed the different configurations' influence in a range of boundary conditions typical for the most critical period for DSF performance. As such, a broader view was given of the extent to which the thermal and fluid dynamic behavior of a DSF can actually be controlled under summer conditions.

As a final note, in an effort to make our research data freely accessible and to allow maximum usability of the collected experimental characterisations, all the measurements presented in this study have been uploaded to on an open-access repository. Data can be found at, and referenced using, the following weblink: https://doi.org/10.5281/zenodo.6187723 [42].

6.7. References

[1] A. Jankovic, F. Goia, Impact of double skin facade constructional features on heat transfer and fluid dynamic behaviour, Build. Environ. 196 (2021) 107796.

[2] J. Antony, 2 – Fundamentals of Design of Experiments, J. B. T.-D. of E. for E. and S. (Second E. Antony, Ed. Oxford: Elsevier, 2014, pp. 7–17.

[3] J.K. Telford, A brief introduction to design of experiments, Johns Hopkins Apl Tech. Dig. 27 (2007) 224–232.

[4] M.A. Farooq, H. Nóvoa, A. Araújo, S.M.O. Tavares, An innovative approach for planning and execution of pre-experimental runs for Design of Experiments, Eur. Res. Manag. Bus. Econ. 22 (3) (2016) 155–161.

[5] C.F.J. Wu, M.S. Hamada, A systematic approach to the planning and implementation of experiments, in: Experiments: planning, analysis, and optimization, 2nd ed., John Wiley & Sons, New Jersey, 2009, pp. 4–8.

[6] H. Guo, A. Mettas, Design of experiments and data analysis, in: 2010 Reliability and Maintainability Symposium, 2010, pp. 1–11.

[7] N. Delgarm, B. Sajadi, K. Azarbad, S. Delgarm, Sensitivity analysis of building energy performance: a simulation-based approach using OFAT and variancebased sensitivity analysis methods, J. Build. Eng. 15 (2018) 181–193.

[8] A.N. Sadeghifam, S.M. Zahraee, M.M. Meynagh, I. Kiani, Combined use of design of experiment and dynamic building simulation in assessment of energy efficiency in tropical residential buildings, Energy Build. 86 (2015) 525–533.
[9] A. Schlueter, P. Geyer, Linking BIM and Design of Experiments to balance architectural and technical design factors for energy performance, Autom. Constr. 86 (2018) 33–43.
[10] W. Kim, Y. Jeon, Y. Kim, Simulation-based optimization of an integrated daylighting and HVAC system using the design of experiments method, Appl. Energy 162 (2016) 666–674.
[11] R. Evins, P. Pointer, R. Vaidyanathan, S. Burgess, A case study exploring regulated energy use in domestic buildings using design-of-experiments and multi-objective optimisation, Build. Environ. 54 (2012) 126–136.
[12] A. Jankovic, G. Chaudhary, F. Goia, Designing the design of experiments (DOE) – An investigation on the influence of different factorial designs on the characterization of complex systems, Energy Build. 250 (2021) 111298.
[13] X. Shen, G. Zhang, B. Bjerg, Assessments of experimental designs in response surface modelling process: estimating ventilation rate in naturally ventilated livestock buildings, Energy Build. 62 (2013) 570–580.
[14] I. Jaffal, C. Inard, C. Ghiaus, Fast method to predict building heating demand based on the design of experiments, Energy Build. 41 (6) (2009) 669–677.
[15] N.R. Smalheiser, Chapter 5 – Experimental Design: Design Strategies and Controls, N. R. B. T.-D. L. Smalheiser, Ed. Academic Press, 2017, pp. 65–85.
[16] B.H. Margolin, Resolution IV fractional factorial designs, J. R. Stat. Soc. Ser. B 31 (3) (1969) 514–523.
[17] A. Jankovic, M.S. Siddiqui, F. Goia, Laboratory testbed and methods for flexible characterization of thermal and fluid dynamic behaviour of double skin facades, Build. Environ. 210 (2022) 108700.
[18] L. Ilzarbe, M.J. Álvarez, E. Viles, M. Tanco, Practical applications of design of experiments in the field of engineering: a bibliographical review, Qual. Reliab. Eng. Int. 24 (4) (Jun. 2008) 417–428.
[19] B. Durakovic, Design of experiments application, concepts, examples: state of the art, Period. Eng. Nat. Sci. 5 (3) (2017) 421–439.
[20] G. Box, S. Bisgaard, C. Fung, An explanation and critique of taguchi's contributions to quality engineering, Qual. Reliab. Eng. Int. 4 (2) (1988) 123– 131.
[21] K.N. Ballantyne, R.A. van Oorschot, R.J. Mitchell, Reduce optimisation time and effort: Taguchi experimental design methods, Forensic Sci. Int. Genet. Suppl. Ser. 1 (1) (2008) 7–8.
[22] W. Libbrecht, F. Deruyck, H. Poelman, A.n. Verberckmoes, J. Thybaut, J. De Clercq, P. Van Der Voort, Optimization of soft templated mesoporous carbon synthesis using Definitive Screening Design, Chem. Eng. J. 259 (2015) 126– 134.
[23] S. Karimifard, M.R. Alavi Moghaddam, Application of response surface methodology in physicochemical removal of dyes from wastewater: a critical review, Sci. Total Environ. 640–641 (2018) 772–797.
[24] D.C. Montgomery, The regression approach to the analysis of variance, in: Design and analysis of experiments, 9th ed., John Wiley & Sons, New York, 2017, pp. 119–123.
[25] H.C.J. Hoefsloot, D.J. Vis, J.A. Westerhuis, A.K. Smilde, J.J. Jansen, in: 2.23 Multiset Data Analysis: ANOVA Simultaneous Component Analysis and Related Methods, Elsevier, Oxford, 2009, pp. 453–472.
[26] F. Favoino, Assessing the performance of an advanced integrated facade by means of simulation: The ACTRESS facade case study, J. Facade Des. Eng. 3 (2) (2015) 105–127.
[27] T. Hong, J. Kim, J. Lee, C. Koo, H. S. Park, Assessment of seasonal energy efficiency strategies of a double skin façade in a monsoon climate region, Energies, 6 (9). 2013.
[28] I.-A.-E.-K.-M. Amaireh, Numerical investigation into a double skin façade system integrated with shading devices, with reference to the city of Amman, University of Nottingham, Jordan, 2017.

[29] A. Guardo, M. Coussirat, E. Egusquiza, P. Alavedra, R. Castilla, A CFD approach to evaluate the influence of construction and operation parameters on the performance of Active Transparent Façades in Mediterranean climates, Energy Build. 41 (5) (2009) 534–542.
[30] H. Choi, Y. An, K. Kang, S. Yoon, T. Kim, Cooling energy performance and thermal characteristics of a naturally ventilated slim double-skin window, Appl. Therm. Eng. 160 (2019) 114113.
[31] J.P. Varughese, M.M. John, Effect of emissivity of shading device and air flow inside cavity of Double Skin Facade for energy saving and Thermal Comfort in buildings: A CFD modeling, in: 2016 International Conference on Energy Efficient Technologies for Sustainability, ICEETS 2016, 2016, pp. 815–820.
[32] G. He, L. Shu, S. Zhang, Double skin facades in the hot summer and cold winter zone in China: cavity open or closed?, Build Simul. 4 (4) (2011) 283–291.
[33] N. Safer, M. Woloszyn, J.J. Roux, Three-dimensional simulation with a CFD tool of the airflow phenomena in single floor double-skin facade equipped with a venetian blind, Sol. Energy 79 (2) (2005) 193–203.
[34] A. Hazem, M. Ameghchouche, C. Bougriou, A numerical analysis of the air ventilation management and assessment of the behavior of double skin facades, Energy Build. 102 (2015) 225–236.
[35] J.P. Holman, Uncertainty Analysis and Propagation of Uncertainty, in: Experimental Methods for Engineers, 8th ed., McGraw-Hill/Connect Learn Succeed, New York, N.Y., 2012, pp. 63–72.
[36] A. Jankovic, G. Gennaro, G. Chaudhary, F. Goia, F. Favoino, Tracer gas techniques for airflow characterization in double skin facades, Build. Environ. 212 (2022) 108803.
[37] D. Iyi, R. Hasan, R. Penlington, C. Underwood, Double skin façade: Modelling technique and influence of venetian blinds on the airflow and heat transfer, Appl. Therm. Eng. 71 (1) (2014) 219–229.
[38] Y. Ji, M.J. Cook, V. Hanby, D.G. Infield, D.L. Loveday, L. Mei, CFD modelling of naturally ventilated double-skin facades with venetian blinds, J. Build. Perform. Simul. 1 (3) (2008) 185–196.
[39] X. Hong, M.K.H. Leung, W. He, Effective use of venetian blind in Trombe wall for solar space conditioning control, Appl. Energy 250 (Sep. 2019) 452–460.
[40] V.I. Hanby et al., Nodal network and CFD simulation of airflow and heat transfer in double skin facades with blinds, Build. Serv. Eng. Res. Technol. 29 (1) (2008) 45–59.
[41] L. Mei et al., The influence of blinds on temperatures and air flows within ventilated double-skin facades, in: Proceedings of Clima 2007 WellBeing Indoors, 2007, p. 1606.
[42] A. Jankovic, F. Goia, An experimental data set for the analysis of the thermophysical behavior of a single-story naturally ventilated double-skin façade (DSF) under summer boundary conditions, 2022. [Online]. Available:10.5281/zenodo.6187723.

7. Control of heat transfer in single-story mechanically ventilated double skin facades

7.1. Abstract

This paper investigates how effective the ventilation rate and the configuration of the venetian blinds are in managing the heat transfer in mechanically ventilated double-skin façades (DSFs). In particular, it explores and quantifies how these two operational variables influence the preheating and delivery of fresh air when a DSF is operated in supply-air mode and removing excess heat accumulated in the DSF cavity when operated in outdoor air curtain mode.

We employed for this experimental study a full-scale mock-up of a single-story DSF in combination with a climate simulator that replicates indoor and outdoor boundary conditions, including the simulation of solar irradiance. We chose two sets of boundary conditions to study the behavior of the DSF under two representative cases of temperature fields and solar irradiation for the summer and the winter. A series of experimental runs using a steady-state regime were then performed where the mechanically-induced airflow rate and the state of the cavity venetian blinds were altered. The study results showed that venetian blinds' configuration was far more dominant than the mechanically induced flow rate in controlling the net heat transfer during the summer season, while the opposite behaviour was seen for the removal from the cavity of the solar heat through the airflow. Regarding the behaviour of the façade under winter and mid-season operation mode (preheating of the supply air), it was observed that the mechanical ventilation rate was the dominant variable in controlling the net heat transfer. Low ventilation rates (in the range of ~7 ÷ ~80 m^3h^{-1} per linear meter of façade) were needed to deliver sufficient fresh air supply (0.4 - 5 ACH) for a reference room area behind the facade and to provide suitable control over the net heat transfer with sufficiently preheated air flow rate.

Acronyms

ACH	Air change per hour
ANOVA	Analysis of variance
DOE	Design of experiments
DSF	Double skin facade
FFD	Full factorial design
HVAC	Heating, ventilation, and air conditioning
OFF	Not present blinds
RQ	Research question
RSM	Response surface methodology
SHTC	Surface heat transfer coefficient

UFM	Ultrasonic flow meter
VPM	Velocity profile method

Nomenclature

Symbols

A	Area	[m^2]
c	Specific heat capacity	[$Jkg^{-1}\,{}^oC^{-1}$]
g	Solar factor, g-value	[-]
I	Solar irradiance	[Wm^{-2}]
$\dot{m}$	Air mass flow rate	[kgs^{-1}]
q	Heat flux density, heat flux rate	[Wm^{-2}]
t	Temperature	[^oC]
U	Thermal transmittance, U-value	[$Wm^{-2}K^{-1}$]
$\dot{V}$	Airflow rate / Normalised airflow rate	[m^3h^{-1}] ; [$m^3h^{-1}m^{-1}$]
γ	Dynamic insulation efficiency	[-]
η	Preheating efficiency	[-]

Subscripts

cav	refer to cavity
e	refer to exterior/outside
exc	refer to gained/released heat by the airflow passing through cavity
exh	refer to the exhaust
hfm	refer to heat flux meter
i	refer to inside
ii	refer to the inner side of inner glazing
in	refer to the incident
inl	refer to the inlet
net	refer to net gain/loss
p	refer to constant pressure
tr	refer to transmitted
vent	refer to convective heat exchange between the indoor environment and freshly supplied air

7.2. Introduction

7.2.1. Background

Double skin facades (DSFs) are well-established (mostly) transparent envelope systems that employ a ventilated cavity to either prevent or reduce the solar-induced cooling load or to exploit solar energy for a passive solar heating purpose [1].

Following the definition of the mechanical ventilation given by the EN 12792 standard [2], mechanically ventilated DSFs are envelope systems whose cavities are ventilated by powered components, most often fans, that generate the airflow. In this case, we can assume that most, if not

all, of the airflow rate through the DSF's cavity are not induced by naturally-driven mechanisms. The fan-induced airflow rate can thus be considered an independent variable that can be employed to influence the performance of the DSF.

The mechanical ventilation of the cavity offers higher flexibility than a naturally ventilated DSF, which largely depends on stochastic and unpredictable external conditions. Natural ventilation of the DSF's cavity is a solution that requires fewer components and possibly lowers maintenance, making it a suitable option when one wants to reduce electrical energy use for air movement. However, relying on natural cavity ventilation can be tricky as thermal buoyancy is sometimes dominant in generating the airflow [3] while other times it is driven by wind [4][5], and very often, neither of these two factors can generate significant airflow [6]. The predictability of the naturally-induced airflow is far from trivial, making the control of a DSF much more challenging. The mechanically induced airflow can, if properly managed, positively impact the thermal and energy performance of a DSF. In the summer period, it can remove any excess heat accumulated in the cavity [7], while in winter or mid-season, the cavity and the mechanical air flow rate can be used for preheating fresh air.

The influence of mechanical ventilation and its combined effects with other construction elements on the thermal performance of DSFs has been the subject of interest in a number of studies that have shaped our current understanding of the performance of such systems under different operational conditions modes.

Mechanical ventilation can be beneficial in warm periods by reducing solar energy absorbed by a DSF, removing excess heat accumulated in the cavity, and lowering solar heat gains into the interior [8][9]. In such cases, an outdoor air curtain ventilation method is effective, where air enters from outside and passes through the cavity, absorbs heat, and increases in temperature. Finally, it leaves the channel through an outward-facing opening, redirecting a certain amount of the heat accumulated in the cavity toward the outside. Dynamic insulation efficiency has proved to be a good indicator of how much ventilation (in this case, mechanical) can off-load DSF from excess heat accumulated in the cavity [10]. Mechanical airflow lowers the temperature of DSF structural elements by absorbing heat and thus reduces exchanged long-wave radiation [11]. However, sometimes in hot and sunny conditions, even high mechanically induced airflow rates cannot prevent overheating of structural elements. For example, in the case of the upper-crossed lateral ventilation scheme, the dynamic insulation efficiency is independent of the ventilation rate when there are venetian blinds in the cavity with almost closed slats (> 75º) [11]. When mechanical ventilation cannot prevent overheating, the operating costs of the fan become significant [12], such as in the case of a DSF with internal double glazing and an outer clear glass pane that is ventilated with an outdoor air curtain. In such cases,

attention must be paid to passive ways to avoid overheating, such as adjusting the shading device or airflow path according to preferences [10].

Electrical energy use due to fans can also be increased due to other factors, such as a sharp-edged opening that behaves as an obstacle to the flow and creates recirculation zones near the inlet [13]. Reduction of width opening lowers the average velocity within the cavity and thus may affect fan consumption [14]. Increased turbulence can also lead to pressure drops [15]. The shading device also influences mechanical airflow in the cavity by forming two channels, and if the flow is driven by the fans only, higher velocities will be encountered in the larger channel [16]. However, velocity distribution can be quite different when the flow is additionally driven by the thermal or wind effects [17]. The blind position in terms of distance to the glazing impacts air velocity and surface heat transfer coefficient (SHTC) more than the slat angle [17]. In the cavity with the installed venetian blinds, the airflow has highly complicated three-dimensional patterns, while the mean thermal field can be considered two-dimensional in a vertical plane perpendicular to the glazing [18]. Forced flow through the DSF cavity is mainly in the thermally and hydrodynamically developing phase, meaning that it is characterized by higher SHTC than if it is fully developed [13].

One of the main advantages of DSFs compared to traditional single-skin envelopes in terms of thermal and energy performance is provided in the winter, as they can deliver a sufficient amount of preheated, fresh air by utilizing the greenhouse effect in the cavity [19]. In such configurations, the cold air enters the channel from the outdoors, warms up and rises, and if the greenhouse effect is pronounced, leaves the cavity to the interior sufficiently heated. For the narrow cavities (~10 cm), single float glass on the inner side leads to more intensive preheating than if double glazing is installed [20]. Also, the higher absorptivity of single-layer internal glazing will lead to greater heat exchange between the forced airflow and the glass and, consequently, to greater preheating [21]. Preheating can be enough to enable heat recovery and supply a sufficient amount of fresh air, which is very important for indoor air quality [19][22]. However, some studies show preheating is not enough for most of the heating season, although in this study, a DSF is used as the exhaust outlet of the heating, ventilation, and air conditioning (HVAC) system, where the air is drawn from the interior of the room. [10].

7.2.2. Research question, significance, and structure of the paper

Previous studies have generally shown the significance of mechanical ventilation in relation to the supply of fresh air and the removal of excess heat from the cavity. However, only indications related to these positive effects are given, while a complete picture is missing of how effective mechanically-ventilated DSFs can be in utilizing the collected heat for a wide range of airflow rates and boundary

conditions. Also, the interaction of mechanical ventilation with other construction elements, such as the glazing or shading device, and its effects on the thermal performance of a DSF appear to be under-researched. The reason is that mechanically ventilated DSFs are less researched than naturally ventilated ones; approximately only one-fifth of DSF research, whether numerical or experimental, deals with configurations where the airflow is driven and maintained by one or more fans. Due to the complex nature of flow patterns and difficult predictability of behavior, naturally ventilated DSFs have been the subject of greater interest to the research community than mechanically ventilated DSFs.

Therefore, in the research presented in this paper, we systematically examined the possibilities of mechanical ventilation in utilizing the heat collected in the cavity, especially in relation to the shading device, as this is the most influential structural element in governing the thermal behavior of DSF [23]. Two primary applications were considered based on their typical (expected) use, i.e., outdoor air curtains during the cooling season and supply air during the heating season. The preheating efficiency and the ability of DSF to release excess heat in these configurations have been previously tested. However, the novelty in this research is related to a detailed analysis of the mechanical ventilation impacts in a large range (from very low to very high rates) and its interaction with venetian blinds, as the effects of these two parameters may not be trivial. The results of this study can be significant for researchers dealing with the optimization of DSFs through seeking the optimal combination of mechanical ventilation rate and the shading setup for various purposes, such as the delivery and preheating of fresh air or reliving excess heat from the cavity. As described in more detail in the following sections, we selected a particular structure for the two glazed skins of our experimental mock-up that aimed at maximizing the exploitation the solar energy by a DSF through the cavity ventilation, but we are confident that the obtained response curves for performance indicators that we obtained for our specific case study should show very similar functional dependence for all other DSFs of this type (single-story mechanical DSF with venetian blinds) and similar conditions to those that were tested. The research questions that motivated us to perform the study are:

RQ1) What is the impact of mechanically induced ventilation rate and venetian blinds on the thermal behavior of single-story DSF in typical conditions for warm winter and summer.

RQ2) In what way does mechanical ventilation interact with venetian blinds when it comes to the utilization of accumulated heat in a cavity?

Beyond the introduction section of the paper (where we have scoped the research, summarised the current state of knowledge, and specified the study's goal in the form of research questions), there are

three additional sections where methods, results, and take-home lessons are presented. Section 2 will briefly describe the experimental testbed and climate simulator, experimental design and boundary conditions, performance indicators, data analysis, and processing. The results are presented through a) quantification of the overall impact of mechanical ventilation and venetian blinds on the thermal behavior of the DSF and b) the combined effect of these two factors on the utilization of the accumulated heat in the cavity. The last section closes the research with conclusive remarks, lists the limitations, and discusses possibilities for future research.

7.3. Methodology

This research assessed the thermophysical behavior of a mechanically ventilated DSF by deliberate variation of mechanical ventilation rate and venetian blind configuration in response to boundary conditions replicated by a climate simulator. The following methodological approach was devised to achieve this, which can be broken down into the several steps described by the following objectives:

1) To develop and equip an experimental testbed suitable for such investigation;
2) To select the appropriate experimental design and boundary conditions;
3) To identify performance indicators and carry out a series of experimental runs;
4) To analyze and post-process data in order to:
    a) quantify the impact of mechanical ventilation and venetian blind configuration on the thermal behavior of single-story DSF in typical winter and summer conditions;
    b) assess the combined effect of these two factors on the utilization of the cavity heat.

An experimental testbed developed in the previous research was upgraded and later employed for a series of experimental tests in a climate simulator. Basic information on the tested DSF configuration can be found in the subsection below, but a more detailed description of the experimental testbed is provided in a corresponding publication [24].

7.3.1. The experimental setup

The experimental testbed

A full-scale DSF mock-up equipped with more than 70 sensors and a system for monitoring and controlling the experiment was employed for systematic investigation in a climate simulator. A series of experiments involved altering only mechanical ventilation rate and venetian blind setup, while all other construction features were held constant. A 200 mm cavity separates the inner and outer glazing

of the test element with installed venetian blinds colored in white aluminum with an estimated reflectivity between 0.5 and 0.6 [25]. The same glazing covers both sides of the test element, and it consists of 4 mm thick double glazing separated by the 15 mm gap filled 90 % with Argon and 10 % with air. A cavity is connected through the upper opening with a system of ducts (radius of 20 cm) with a fan capable of generating an airflow rate up to 1000 m^3h^{-1} (Figure 1). The fan causes a pressure difference that forces the air to enter the cavity from the lower opening on the outer side of the DSF (air is drawn from the outdoor chamber). After passing through the cavity, the air exits through the upper opening and reaches the fan through connected ducts. Finally, it is discharged into the inner or outer chamber, depending on the desire (Figures 1 and 2b). The fan is an impeller (a rotor placed in a duct) with curved blades that can produce a maximum flow rate of 271 ls^{-1} (976 m^3h^{-1}). The nominal flow rate of the fan is 0.115 m^3s^{-1} (414 m^3h^{-1}), while the nominal external pressure is 397 Pa. For the developed experimental setup, the highest airflow rates that the fan could produce at maximum power measured by the ultrasonic flow meter were in the range of ~865 - ~890 m^3h^{-1}.

Fig. 1. – The DSF draws air from the lower opening and transfers it through the cavity to the upper opening. Further, the ventilation system attached to the upper vent takes the air first to the ultrasonic flow meter and then to the fan located in the vertical duct placed in the DSF's side section. Finally, the air is expelled to the outside or inside as needed.

The airflow rate in the cavity was assessed by the velocity profile method (VPM) and ultrasonic flow meter (UFM). Twelve hot wire anemometers were arranged along three heights (¼, ½, and ¾ of glazing height) to measure the velocity of the air (Figure 2a). The values of the airflow rates were obtained from the second and third heights, while the values from the first level were discarded due to the dissonant readings from two hot-wire anemometers, which were likely to be poorly performing sensors. The final value was obtained by averaging the values from these two heights. Measurements

with the ultrasonic flow meter were performed in the duct that was connected with the cavity through the upper opening and ventilation system (Figure 2b). Target irradiance value on the façade was measured using one spectrally flat, class B pyranometer [26] placed at the center of the glazed area of the DSF. However, the solar irradiance distribution on the outer DSF surface was also assessed using five photovoltaic pyranometers evenly distributed to obtain a more detailed picture of actual values at different surface points (Figure 2b). Though less accurate, these photovoltaic pyranometers were verified against the thermopile and showed a deviation of up to 4.5 %.

Although over 70 sensors were mounted on the DSF mock-up, Figure 2 shows only the most important ones used in this experimental campaign for clarity and readability. The temperature of the glass pane facing the indoor chamber was measured at three heights, the same as the hot-wire anemometers, using four surface temperature sensors. Two heat flux meters were placed on the same glass pane to measure the heat flux density toward/from the interior space, where the representative value for the whole DSF glazing was obtained by averaging these two values. The air temperature near the inlet was measured using four air temperature sensors. The air temperature near the upper opening, to which the ventilation system was connected, was measured in the same way. However, due to unexpectedly low readings, temperature measurements obtained from the hot-wire anemometers located on the 3rd height were taken as more representative for calculating airflow heating in the cavity in this study. The cause for these low readings was most likely air infiltration in places where the ventilation system is attached to the upper opening and due to the features of the façade mock-up that made it a flexible platform to test many DSF's configurations (which might differ from a "real," fixed-configuration DSF with properly fully insulated inlet/outlet section). Another reason could be the possible existence of a recirculation zone at the channel outlet [27]. This pattern might cause the mixing of the colder air from the opaque upper part of the cavity.

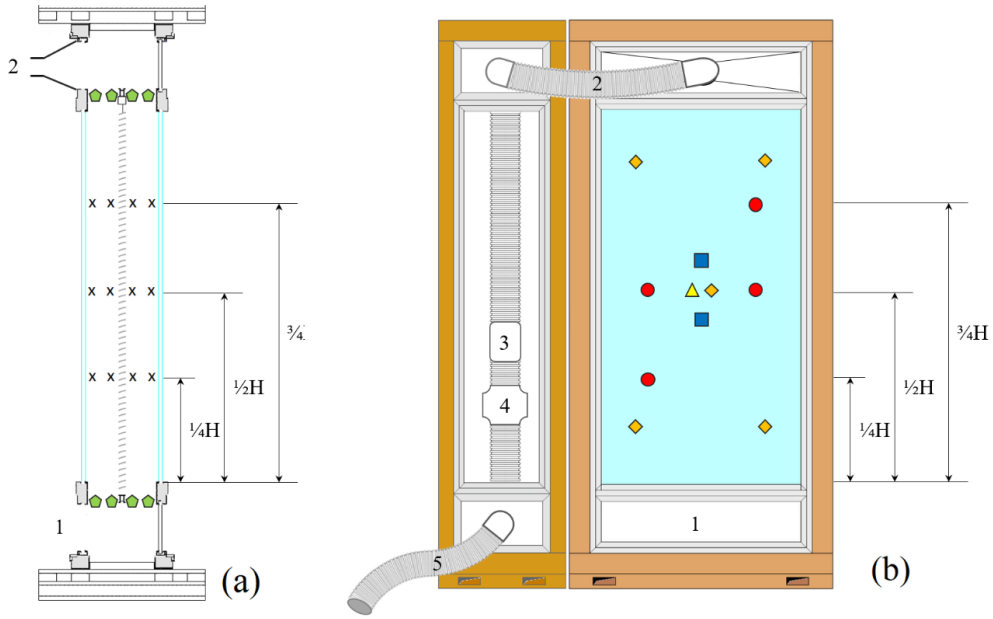

Fig. 2. – a) Layout of sensors in the cavity, b) Layout of sensors placed on the indoor glazing, and a sketch of the ventilation system attached to the DSF.

Labels meaning: X – hot wire anemometers, ⬠ - air temperature sensor, ☐ – heat flux meter, △ – thermopile pyranometer, ◇ – photovoltaic pyranometer, ◯ - surface temperature sensors, 1 – inlet, 2 – ventilation system attached to the upper opening, 3 – ultrasonic flow meter, 4 – fan, 5 -exhaust.

The climate simulator

The climate simulator facility consists of two chambers intended to replicate indoor and outdoor conditions in terms of temperature and humidity. The outdoor chamber contains a solar simulator that can emit radiation intensity up to 1000 Wm^{-2}. The equipped DSF mock-up is placed between two sections and subjected to different boundary conditions in two chambers. Due to the proximity between the test element and the solar simulator and the inability of the air conditioning system to cool the air in the outer chamber uniformly, the setpoint temperature in the outdoor chamber and air temperature measured near the tested element differed by 2-3 °C. The air temperature in the indoor section was maintained with a stable value at the desired level.

As will be explained in more detail later, the lamps' power was adjusted to irradiate the central part of the DSF with 300 Wm^{-2} (winter/mid-season) and 500 Wm^{-2} (summer). The intensity of the radiated energy was stable over time in each of the two sets (winter/mid-season and summer) of experimental runs, with small fluctuations between experimental runs in which different DSF configurations were changed (venetian setup and mechanical ventilation rate). Readings from the thermopile pyranometer

in the center point were 500 and 304 Wm^{-2}, while the 5-point averages detected by the photovoltaic pyranometers were 436 and 270 Wm^{-2}, which indicates the inhomogeneity of solar irradiance on the outer surface of the DSF. The inhomogeneous distribution of the solar irradiance on the DSF's outer surface was observed with a somewhat more pronounced inequality in the replicated conditions corresponding to the winter period (Figure 3 left). Irregularities are likely to originate from the different hours of usage of light sources, which causes the lamps to change the power emitted with time and by a lower accuracy (of some lamps) in returning the desired radiative flux when a particularly low partial load is adopted. It is possible to see this effect by comparing homogeneity in the case of summer conditions and winter conditions.

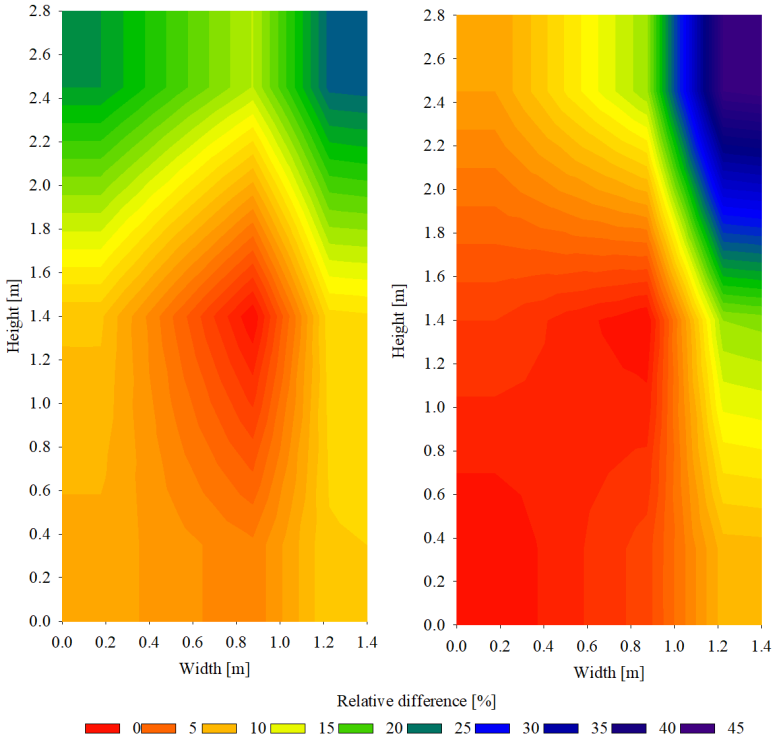

Fig. 3. – Distribution of the relative deviation of the solar irradiance measured on the DSF surface in relation to the values measured in the central part for the summer (left) and winter period (right).

Measurement of the airflow rate

Since both methods for airflow assessment (VPM and UFM) had drawbacks, a combined profile of airflow rate was used to calculate indicators of fluid-dynamics behavior. The UFM measurements were used to fit the lowest part of the airflow rate profile (up to 15% of maximum fan power), while the values obtained by the VPM were used for the upper part so that each of the two methods was considered in the range where it delivered the best performance and was free from intrinsic (sensor

limitations) or extrinsic (installation limitations) shortcomings. In order to obtain a unique and smooth profile with no clear transition between UFM and VPM measurements, discrete measurements were fitted to a third-order polynomial function (Figure 4). The measured airflow rates were normalized by the facade width (1.4 m), and thus ventilation rate will be presented later in the paper.

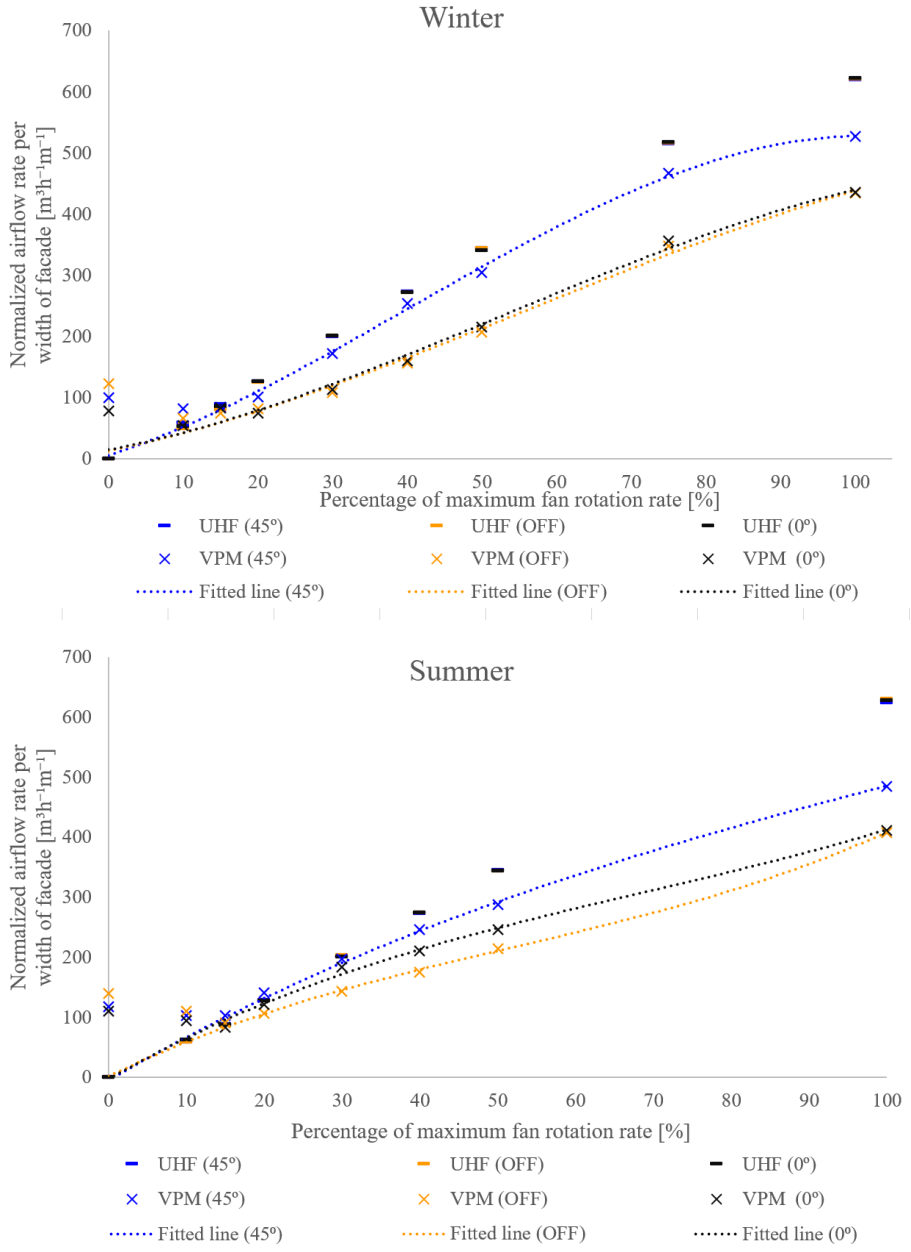

Fig. 4. – The normalized airflow rates per width of the façade measured by the UFM and the VPM method. The figure shows the airflow rate profile obtained by fitting the measurements obtained by the UFM and the VPM method.

Due to the lower threshold limit, the VPM has problems determining the lowest airflow rates and their direction if the temperature differences are minor or mechanical and natural ventilation is present simultaneously [28]. Therefore, the ultrasonic flow meter measurements were more appropriate to measure the airflow rate profile corresponding to the lowest fan rotation rates. Due to a greater pressure difference and insufficiently good sealing, higher rotation rates likely increased infiltration through joints of the ventilation system (especially the connection to the upper opening), even if measures were put in place to limit possible infiltrations along the airflow path. For that reason, the ultrasonic flow meter registered higher mass flow rates than the velocity profile method (Figure 4). Thus, the values calculated by the VPM were more appropriate to measure the actual mass flow in the DSF cavity without overestimating it due to infiltrations that might have happened at connection points in the ducts outside the façade. Since the temperature difference is not a reliable indicator of airflow direction when both mechanical and natural ventilation is present, the absolute velocity values were used to calculate the airflow rates using the VPM. The assumption was that mechanical ventilation prevailed over the natural for the higher fan rotation rates (>15 % of the maximum fan rotation) and that all airstreams in the cavity were directed upward.

When the façade was tested with no mechanical ventilation, the naturally induced airflow was not strong enough to overcome the pressure drop created by the ventilation system attached to the upper DSF opening. As a result, the ultrasonic flowmeter did not register any significant airflow rate in conditions where the mechanical ventilation was off. However, the sensors measured the velocities even higher than in certain situations with mechanical ventilation, but the airflow was most likely circulatory in such cases. The gradual increase in fan rotation first caused a decrease in the velocity of the streams initially directed downwards up to the point of changing their direction. Further increase in rotation rate led to steady growth in airspeed. The moment when all currents in the cavity became directed upwards, i.e., when mechanical ventilation prevailed over other circulation paths likely induced by natural phenomena, can be recognized on the graph as the minima in the airflow rates obtained by the VPM method.

The airflow rate profile corresponding to 45º opened venetian blinds shows a certain offset compared to the other two profiles determined by VPM. Having higher airflow rates at a 45º blind angle than in the case without venetians could be expected, as the natural ventilation increases with the closure of the blinds [25]. Therefore, it can be inferred that there was a superposition of natural and mechanical ventilation, which resulted in higher total ventilation rates for the case when the blinds are half-open than in the case without venetian blinds. However, having higher airflow rates than in the case of closed blinds was not expected. That may have originated from the combined effect arising from the punctual measurements of VPM and the nature of the flow. The difference between profiles was

evident for the higher airflow rates, where the flow was almost certainly turbulent. Most likely, the drag of partially inclined slats made the flow more turbulent and the velocity profile flatter, resulting in the higher velocity measurements in points close to the channel's borders.

7.3.2. Experimental design and tested boundary conditions

This experimental campaign focused on understanding the influence of structural factors in clearly defined conditions, and therefore this study did not include an assessment of the effect of environmental factors on the thermophysical behavior of the DSF. The flexible mock-up allowed testing a large range of configurations through modifications of the venetian blind setup and mechanical ventilation rate. Venetian blinds were placed in three configurations: closed (0º), half-opened (45º), and not present (OFF), while the mechanical ventilation rate was controlled through a percentage of maximum fan power. Since the focus was on a more detailed analysis of the impact of mechanical ventilation, a higher-than-usual number of levels were selected for this factor (0, 10, 15, 20, 30, 40, 50, 75, and 100%). Therefore, experimental designs such as Taguchi, definite screening, and arrays related to the response surface methodology (RSM) were dropped [29], and full factorial design (FFD) was selected as appropriate. In an FFD, a series of experiments encompass all possible combinations of chosen factors and levels, consisting in this case of 27 experimental runs. However, for summer boundary conditions, due to technical limitations, a level corresponding to 75 % of maximum fan power consumption was omitted from the analysis, and therefore that series consists of 24 experimental runs. According to our assumptions, which were later confirmed in the results, this point was not important from the aspect of analysis since, for the highest air flow rates, the indicators of thermal behavior did not change significantly.

Table 1. – Selected factors, levels and boundary conditions

Factors	Levels								
Fan rate [%]	0	10	15	20	30	40	50	(75)	100
The venetian blind setup [º]	OFF (not present)				45		0		
Tested boundary conditions	Temperature [°C]				Solar irradiance [Wm^{-2}]				
Summer	30				500				
Mid-season/Winter	10				300				

In a previous study [25], the design of experiments (DOE) methodology was employed to assess the thermophysical behavior of a DSF for a wide range of summer boundary conditions. In this way, apart from the influence of structural elements, the impact of environmental parameters was quantified. However, by choosing a wide range of boundary conditions, a wide range of variations of behavioral indicators was obtained as well, thus including a large number of situations in which the impact of construction elements on response quantities was either not necessary or it was negligible.

In this way, the impression was that the influence of the construction features was modest, but actually, it was masked by the impact of environmental parameters. Therefore, in this experimental campaign, the effect of environmental parameters was not examined in order to gain a better insight into the influence of construction elements on the thermal and fluid-dynamic behavior of DSF. Fixed boundary conditions were selected for 'problematic' situations where the intervention of construction elements is needed to influence the thermophysical behavior of the DSF.

For the analysis of the utilization of excess heat accumulated in the cavity and prevention of DSF overheating, boundary conditions corresponding to g-value measurement were selected [30], which are more or less typical for summer conditions. Those were outdoor and indoor temperatures, 30 °C and 25 °C, respectively, and solar irradiance of 500 Wm^{-2}. Such conditions correspond to the warm summer day, where a lot of heat accumulates in the cavity due to not enough strong naturally-generated airflow capable of removing this excess heat [25]. In this way, a better insight into the effect of mechanical ventilation and its interaction with shading as the most influential structural element can be obtained for situations when natural ventilation cannot expel excess heat from the cavity.

For the analysis of air preheating in the DSF cavity, the boundary conditions corresponding to typical situations for air preheating (cold outdoor air and low-to-moderate solar irradiance) were selected. Due to the limitations of the climate simulator, we went to the limit of its capabilities: the lowest possible temperature during the active solar simulator and the minimum achievable solar irradiance. These were around 10 °C and 300 Wm^{-2}, respectively, while for the indoor environment, a temperature of 25 °C was selected in order to establish a greater temperature difference between interior and exterior. We believe that the selection of higher internal temperature compared to the typical 20 °C for residential buildings or 17 °C for office spaces during the heating period did not affect the functional dependence of performance indicators on construction features. After all, it is neither the internal nor the external temperature but the temperature difference that drives physical processes, such as heat and mass transfer.

7.3.3. Performance indicators

The following quantities were chosen for performance indicators of thermal and fluid-dynamics behavior: net heat flux density (q_{net}), dynamic insulation efficiency (ε), air preheating efficiency (η), average cavity temperature ($\bar{t}_{cav}$), g-value (solar factor, solar heat gain coefficient, total solar energy transmittance), the indoor surface glazing temperature ($\bar{t}_{ii}$), and the heat gain rate by the airflow (q_{exc}). Net heat flux density represents the sum of measured heat flux density by the heat flux meter and

transmitted solar radiation intensity measured by the pyranometer set behind the inner glazing in the indoor chamber. In the case when the air is delivered from the outside to the interior through the cavity, this quantity is supplemented by the convective heat exchange between the indoor environment and freshly supplied air (q_{vent}). It represents the heat flux density that needs to be absorbed or released by the imported air in order to bring itself into thermal equilibrium with the indoor environment. Dynamic insulation efficiency [10] represents the portion of the heat flux entering the cavity from the outer side that is removed and directed back by the airflow toward the outside. This quantity is a very important indicator of the ability of a DSF to relieve its cavity from excess heat by ventilation in hot periods.

The preheating efficiency represents the ratio of two temperature differences, where the one in the numerator represents the difference between the temperature of the air delivered to the indoor space and the exterior temperature. The denominator indicates the difference between the air temperatures in the indoor and outdoor space. The preheating efficiency measures the capability of the DSF to preheat the ventilation airflow rate during the cold season [31].

Table 2. – Description of performance indicators

Performance indicator	Unit	Equation
Net heat flux density	[Wm^{-2}]	$q_{net} = q_{hfm} + I_{tr} + \frac{\dot{m}c_p(t_{exh} - t_i)}{A}$
Dynamic insulation efficiency	[-]	$\gamma = \frac{\dot{m}c_p(t_{exh} - t_{inl})}{q_{hfm}A + q_{tr}A + \dot{m}c_p(t_{exh} - t_{inl})}$
Air preheating efficiency	[-]	$\eta = \frac{t_{exh} - t_e}{t_i - t_e}$
Average cavity temperature	[°C]	$\bar{t}_{cav} = \frac{\sum_{n=1}^{12} t_{cav,n}}{12}$
g-value	[-]	$g = \frac{q_{net}}{I_{in}} = \frac{q_{hfm} + I_{tr}}{I_{in}}$
The indoor surface glazing temperature	[°C]	$\bar{t}_{ii} = \frac{\sum_{n=1}^{4} t_{ii,n}}{4}$
The heat gain rate by the airflow normalized by the DSF surface	[Wm^{-2}]	$q_{exc} = \frac{\dot{m}c_p(t_{exh} - t_{inl})}{A}$

The average cavity temperature was obtained from temperature measurements of 12 hot-wire anemometers. Solar factor (g-value) was evaluated based on the ratio between the measured net heat flux density and the incident solar radiation on the outer side of the DSF. The indoor surface glazing temperature represents the temperature of the inner glazing surface facing the indoor environment, and it is calculated as the average of four-point measurements. Heat gain rate by the airflow represents the heat rate absorbed by the airflow passing through the cavity normalized by the DSF surface. It is

calculated based on the evaluated airflow rate and measured temperature gain of the airflow through the cavity.

For calculation of ventilation rates to check the requirements given by the standard EN 16798 [32][33] in terms of indoor air quality and delivery of sufficient quantities of fresh air, we assumed an office of a certain depth behind the DSF. The adopted dimensions of the room were 1.5 m x 5 m x 3 m, with a floor area of 7.5 m^2. According to the EN 16798 standard [33], the floor area occupied by one person in the single and landscape office is 10 m^2 and 15 m^2, respectively. Therefore, it was assumed that only one person occupies the space located behind the DSF. Minimum ventilation rates per person for offices (single and landscape) range from 2.5 to 10 $ls^{-1}person^{-1}$, depending on the environmental quality category (from low to high). If these values are converted into more familiar forms of ventilation rates, then they will amount to 9 – 36 m^3h^{-1} (expressed in cubic meters per hour), ~7 – ~26 $m^3m^{-1}h^{-1}$ (normalized by the glazing width), and 0.4 – 1.6 ACH (air changes per hour).

7.3.4. Data analysis and processing

After performing a series of experimental runs according to the FFD, the experimental data were collected, and the analysis of variance (ANOVA) was performed over two data sets, which referred to two typical situations (winter/mid-season and summer). The influence of mechanical ventilation rate and venetian blind configuration on the thermal and fluid-dynamics behavior was represented through contributions of each factor on the variance of the behavioral/performance indicator. The contributions of mechanical ventilation rate and venetian blind setup (c_{MV} and c_{VB}) were calculated as the ratio of the sum of squares for these factors (SS_{MV} or SS_{VB}) and the total sum of squares (SS_T):

$$c_{MV} = \frac{SS_{MV}}{SS_T} 100 \qquad \text{and} \qquad c_{VB} = \frac{SS_{VB}}{SS_T} 100$$

where subscripts MV and VB refer to mechanical ventilation rate and venetian blinds setup/configuration, respectively.

An FFD with only two factors cannot assess the statistical significance of the interaction between these factors. One option would be to fold the FFD, i.e., duplicate the pattern of this design and carry out an experimental campaign twice, but since it would require extensive material resources, it was abandoned. Another option, requiring fewer resources, was to use some of the designs related to the response surface methodology or a folded Taguchi design. However, such an approach would require that the number of levels corresponding to the mechanical ventilation rate be reduced to 3 or 4, potentially losing more detailed insight into the effects of this factor. Nevertheless, the combined effect of mechanical ventilation rate and venetian blind setup was assessed directly from the graphs showing the dependence of the performance indicators upon these two factors. In order to obtain the

dependence curve, a linear change was assumed between the points at which the response quantity was sampled according to the FFD pattern.

7.4. Results

7.4.1. Overall thermal and fluid-dynamics behavior of a mechanically ventilated DSF in specified conditions

In the tested winter conditions, the mechanical ventilation rate had prevalence over the venetian blinds in controlling the indicators of thermophysical behavior of the DSF, except for the solar heat gain coefficient (g-value). The amount of heat that the air supplied by mechanical ventilation was exchanging with the internal environment represented the dominant component in net heat transfer. Therefore, the mechanical ventilation by controlling the amount of delivered air also controlled the net heat transfer. The forced air flow rate dictated the convective heat exchange between the air passing through the cavity and the surrounding borders and thus significantly affected the amount of heat absorbed by the airflow. The effect of the shading device was limited, most likely due to the low thermal capacity and high reflectivity of the blinds. A combination of several factors most likely led to the reduced impact of the venetian blinds on the indoor surface glazing temperature. The amount of the absorbed radiation on the indoor-facing glass pane was quite limited due to three glass panes in front reducing the available radiation for absorption. Additionally, the low absorption coefficient of these glass panes (low-E) further decreased the amount of absorbed radiation, and thus its variations arising from the venetian blind setup. Consequently, the temperature of the indoor glazing was influenced more by the heat transferred by the mechanical ventilation than by the absorption of solar irradiance that the venetian blinds could control. Similarly, like for the heat gain rate by the airflow, mechanical ventilation rate was dominant in controlling the preheating efficiency. As expected, the shading device, through the control of transmitted solar radiation, took over the role of the dominant factor in the regulation of solar heat gain coefficient.

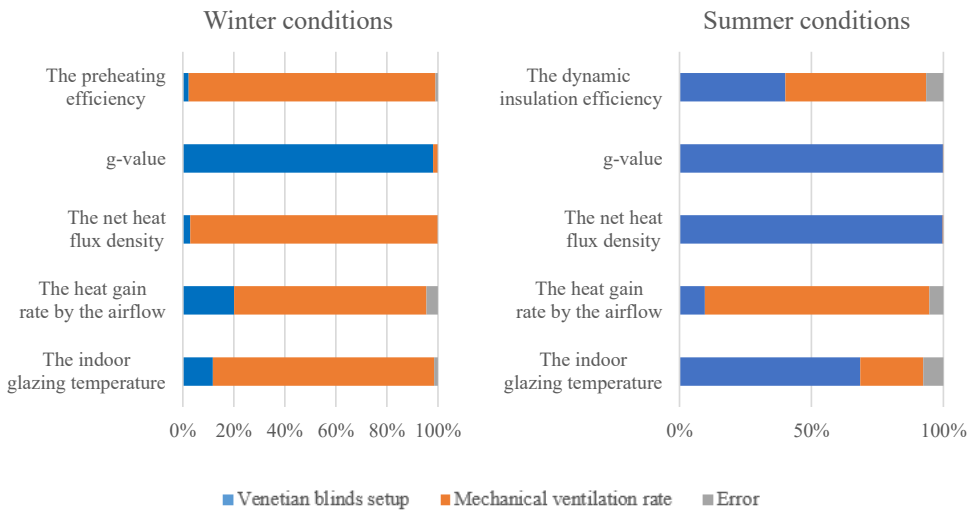

Fig. 5. - The overall thermal and fluid-dynamic behavior of the mechanically-ventilated DSF in winter (left) and summer (right) conditions.

Unlike in the previous case, venetian blinds were more dominant than mechanical ventilation in controlling the thermophysical behavior of the DSF, except for heat gain by the airflow in the cavity and the dynamic insulation efficiency. Since, in this configuration, the indoor air was isolated from the outdoor, the largest share of the net heat transfer belonged to the transmitted radiation, which is why the impact of venetian blinds was far more pronounced. It is to be expected that the identical causes (low thermal capacity of blinds and high reflectivity) as in the previous case made mechanical ventilation significantly more effective than the shading device in managing the heat gain rate by the airflow. Both factors were almost equally important in driving the dynamic insulation efficiency. Compared to the winter conditions, the higher solar irradiance led to a more prominent role of venetian blinds in controlling the indoor glazing surface temperature. As expected, the value of the solar heat gain coefficient was managed efficiently with the shading device, while the influence of mechanical ventilation was minimal. A somewhat higher value of unexplained variance in both the dynamic insulation efficiency and the indoor glazing temperature indicates the possible need for the addition of nonlinear terms to describe these quantities' behavior adequately.

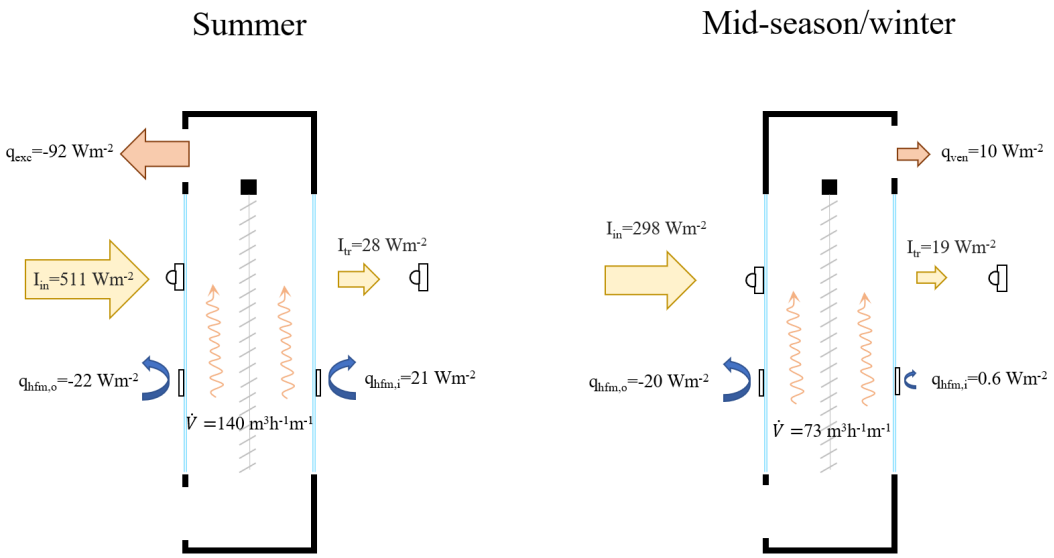

Fig. 6. – Energy flow diagram in summer and mid-season/winter conditions (I_{in} and I_{tr} – incident and transmitted solar irradiance measured by the thermopile pyranometer, $q_{hfm,i}$ and $q_{hfm,o}$ – heat flux density measured by the heat flow meter installed on the indoor and outdoor glazing, $\dot{V}$ – airflow rate normalized by the glazing width, q_{exc} – heat flux rate absorbed and removed by the airflow rate passing through the cavity and q_{vent} – heat flux rate exchanged between the supplied fresh air and the indoor environment.

7.4.2. The combined effect of the mechanical ventilation and venetian blinds

Low mechanical ventilation rates (7 ~ 80 m^{3}m^{-1}h^{-1}) were enough to provide fresh air (0.4 ~ 5 ACH) and sufficiently preheat the air (Figure 7 left). Any further increase in the airflow rate from these low values would significantly decrease the net heat transfer and cause the requirement for a large amount of energy for heating to maintain the interior temperature at 25 °C. For the same reason, preheating efficiency was around 1.0 only for lower airflow rates, with a drastic reduction for higher rates. The mechanical ventilation could not even provide sufficiently heated air from the cavity if venetian blinds were raised, while its presence caused an increase in the preheating efficiency. In the considered boundary conditions, preheating efficiency was the highest when the blinds were semi-opened, except in a short interval for the lowest airflow rates, where the fully closed blinds led to the most intensive preheating. Figure 7 (right) shows the values of the preheating efficiency for a supply air temperature setpoint of 17 °C. The dependence curves do not change significantly and retain their basic characteristics as do the curves related to the setpoint temperature of 25 °C. When comparing the three shading configurations, with the slats entirely shut, the lowest ventilation rates (60 m^{3}h^{-1} m^{-1}) were required to reach a negative value for the net heat transfer, while in the absence of the blinds, it remained positive for airflow rates as high as about 80 m^{3}h^{-1}m^{-1}).

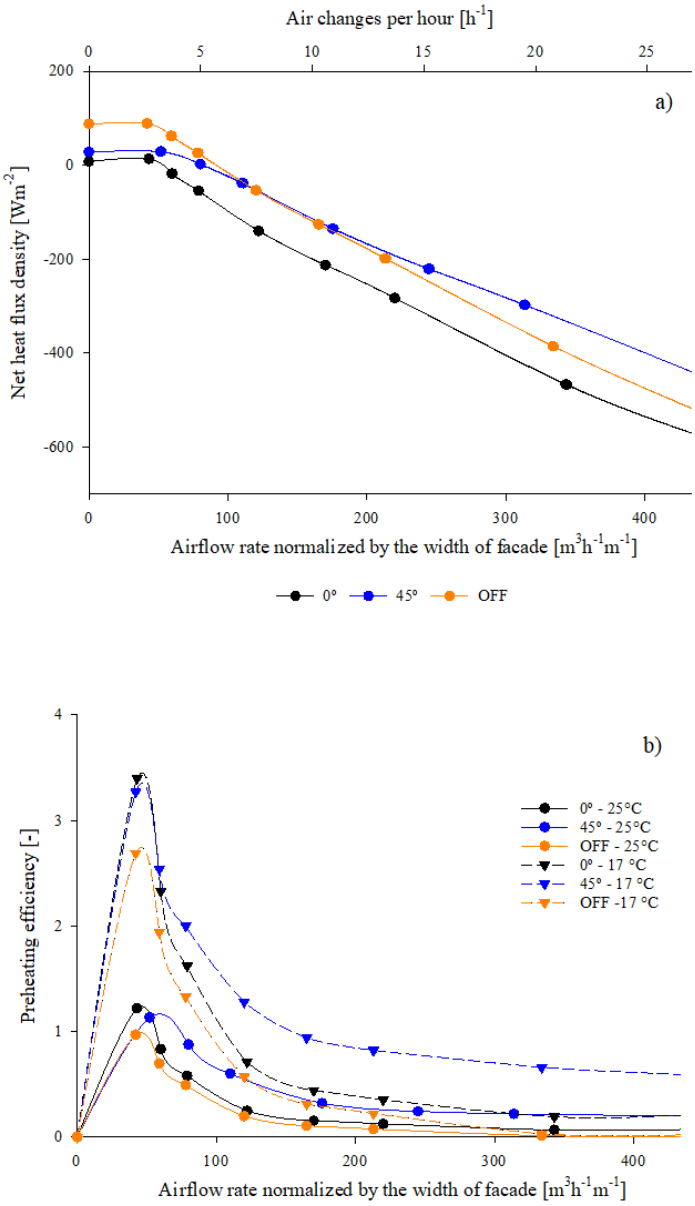

Fig. 7. – The combined effect of mechanical ventilation rate and venetian blind set up on a) the net heat transfer and b) preheating efficiency (right) in the considered winter conditions.

In considered winter conditions, the highest amount of absorbed heat by the airflow was found for low mechanical ventilation rates (50 - 80 $m^3m^{-1}h^{-1}$), where further increase first led to a slight decrease and then to stagnation of the absorbed heat (Figure 8a). The slats in a semi-opened position (45º) transferred more heat to the airflow than completely closed slats, most likely due to increased turbulence and amplified heat transfer between slats and fluid. For low airflow rates (up to 60 $m^3m^{-1}h^{-1}$), airflow temperatures at the outlet of the cavity were more than ten °C higher than the outside

air temperature. The curves describing the heat absorbed by the airflow in summer conditions are very much like those corresponding to the winter conditions, with similar values of the absorbed heat (Figure 8b). The only difference was a somewhat more gradual increase in the heat absorbed by the airflow with the rise in the ventilation rate. The presence of blinds increased the amount of heat transferred to the airflow, but unlike in the tested winter conditions, there was no significant difference between the slats semi- or completely closed. In the case of lowered venetian blinds and airflow rates up to 100 $m^3m^{-1}h^{-1}$, airflow temperatures at the cavity outlet were over 40 °C, indicating the potential of the DSF as a "solar collector," thereby allowing the excess heat accumulated in the cavity to be used for various purposes. The presence of mechanical ventilation did not always decrease the airflow temperature at the cavity outlet, as seen from the example when the venetian blinds were not lowered. For low ventilation rates (~40 $m^3m^{-1}h^{-1}$), the air temperature near the exhaust is around 4 to 5 °C higher than when the fan is not active.

a)

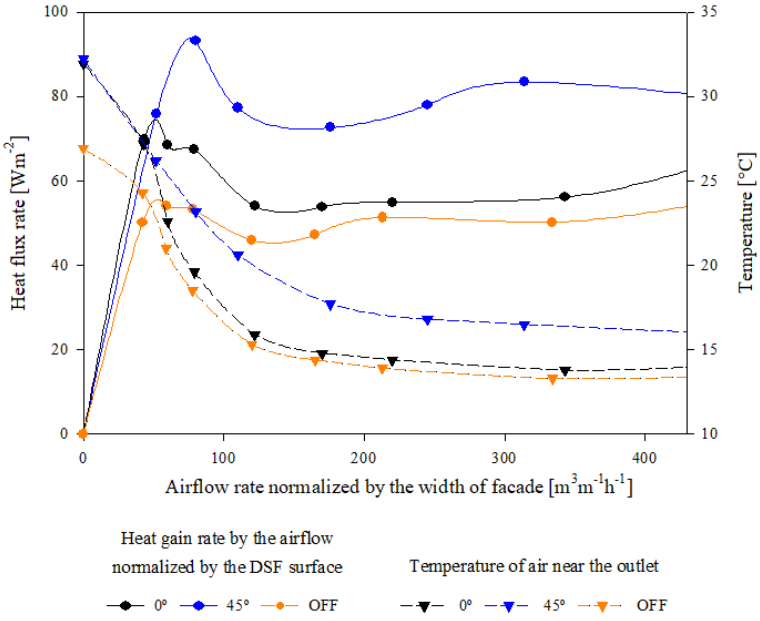

b)

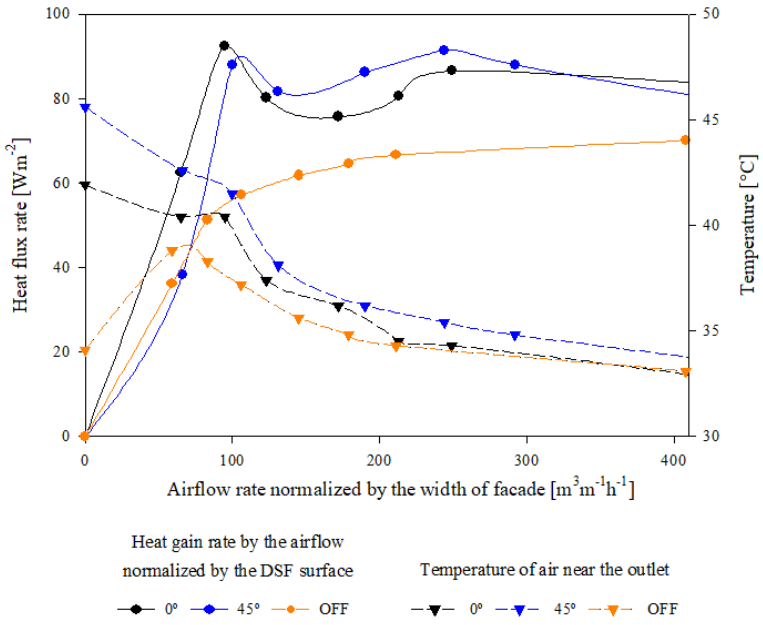

Fig. 8. - The combined effect of mechanical ventilation rate and venetian blind setup on the normalized heat gain rate by the airflow and temperature of the airflow near an outlet in a) the winter and b) summer conditions.

In the tested configuration, typical for a summer period where the indoor environment was decoupled from the outdoor, the blinds dominated the net heat transfer entirely. The effect of mechanical ventilation was minimal, as seen in Figure 9b, where the net heat flux density curves are practically horizontal. As expected, the largest amounts of heat directed inwards were in the case of open slats and the least in the case of the closed. Unlike the net heat transfer, the mechanical ventilation significantly affected dynamic insulation efficiency up to a certain point (100 ~ 150 m^2h^{-1}), corresponding to low ventilation rates, after which further increase did not lead to any significant change (Figure 9a). The influence of venetian blinds on the dynamic insulation efficiency was also substantial, where the closure of the blinds led to an increase in the dynamic insulation efficiency.

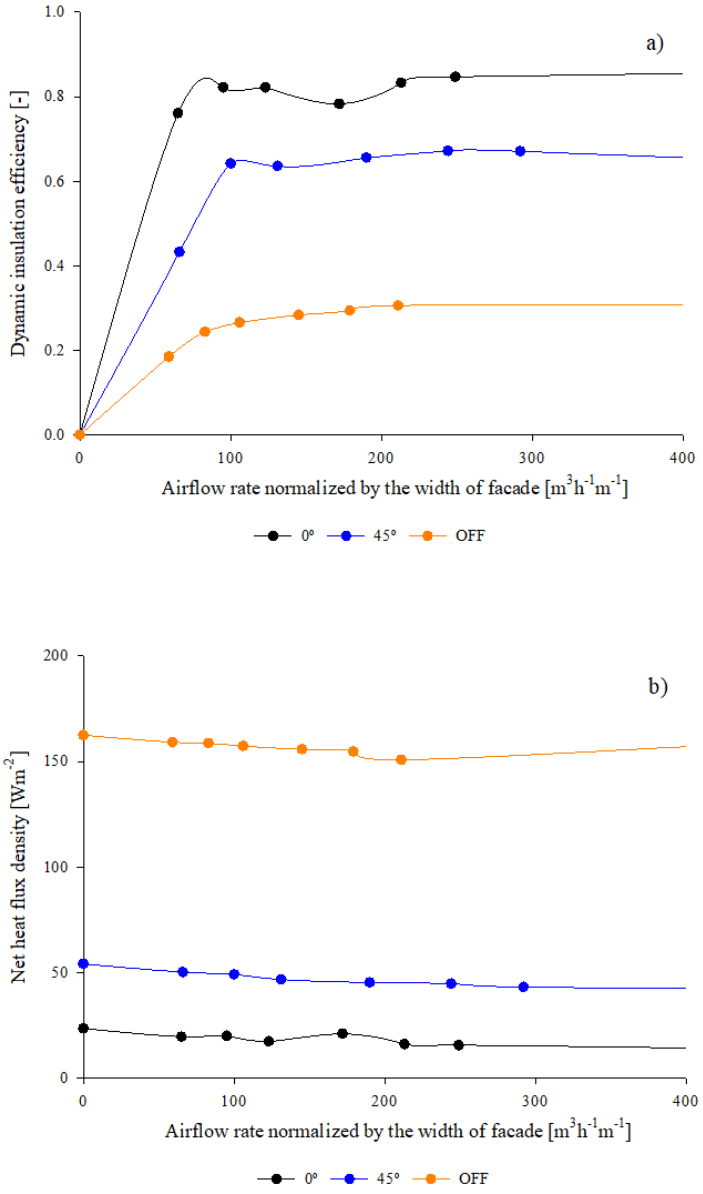

Fig. 9. - The combined effect of mechanical ventilation rate and venetian blind set up on a) the dynamic insulation efficiency and b) net heat transfer (right) in the considered summer conditions.

7.5. Discussion and conclusions

This research has shown that in the tested winter/mid-season conditions, the thermal behavior of the one-story DSF was regulated to a much greater extent by mechanical ventilation than by venetian blinds. Low ventilation rates were enough to enable positive net heat transfer, while any further rate

increase would significantly deteriorate preheating efficiency and net heat transfer. A combination of semi-opened blinds and low ventilation rates was optimal for reduced net heat transfer (energy efficiency) and fresh air delivery (indoor air quality), but also if one wants to increase the available amount of daylight, which is one of the key advantages of a highly transparent envelope. In the tested summer conditions, the thermal behavior of the DSF was almost entirely regulated by the venetian blinds, while in controlling fluid-dynamics behavior, mechanical ventilation had a primary role, but with the considerable influence of venetian blinds. The impact of forced flow on net heat transfer in the tested summer conditions was surprisingly small, indicating that the use of mechanical ventilation in the cavity did not reduce considerable heat transfer penetrating inside in steady-state conditions. However, the influence of mechanical ventilation was significant in relieving the excess heat from the cavity, which indicates that the ventilation's impact on the net heat transfer could play a (slightly) more relevant role in transient conditions when the effect of a DSF's thermal inertia is more pronounced.

Several findings arising from this research indicate that mechanical ventilation and venetian blinds can be efficiently employed to control the air preheating and the excess heat accumulated in the cavity. The DSF can be utilized as an efficient heat recuperator and a fresh air supplier with light mechanical ventilation. Furthermore, semi-opened slats led to higher preheating efficiency and the amount of heat absorbed by the airflow, most likely due to the increased turbulence and amplified heat transfer between slats and the airflow. The features of a DSF as a solar collector could be effectively controlled by mechanical ventilation. Low ventilation rates were sufficient to remove (and use if necessary) the highest amounts of accumulated heat in the cavity, increase drastically dynamic insulation efficiency and reduce the temperature in the channel. The presence of venetian blinds significantly increased the amount of heat absorbed by airflow and the dynamic insulation efficiency.

This research aimed to expand understanding of the thermophysical behavior of a one-story mechanically-ventilated DSF and to what extent controllable features of a DSF, such as shading device and fan, can be employed to utilize the collected heat in the cavity. Experimental investigations were performed using the developed experimental testbed, accompanied by certain limitations influencing the generality and applicability of obtained results. The largest was most certainly related to the inability of the climate simulator to replicate certain desired conditions, such as the offset between the projected and actual temperature in the outdoor chamber when the solar simulator is active or the inhomogeneity of solar irradiance distribution. However, we are confident that slightly different boundary conditions than those achieved in the campaign would not change the type of functional dependence of behavioral indicators. For example, a somewhat lower outdoor temperature would lift the curve describing the dynamic insulation efficiency without significant change in its

shape. Similar reasonings can be conducted to expand our results to other DSF configurations than that chosen for testing when it comes to the exact configuration of the two skins. For example, changing outer double glazing to a single, more transparent one would probably lift and stretch the curve describing preheating efficiency. Still, we believe that this would not change the nature of its functional dependence on the different variables involved in the problem. Furthermore, we trust that the inhomogeneity of solar irradiance did not significantly affect the overall behavior of the DSF due to the existence of double glazing and intensive mixing in the cavity, which most likely prevented the temperature asymmetry from being propagated further inwards. Another significant limitation was uncertainty in assessing the ventilation rate in the cavity, originating from the inadequate sealing of the ventilation system and the shortcomings of VPM related to the punctual measurements, determination of the lowest airflow rates, and their directions. That was best reflected in a mismatching in the zone where the airflows from the two techniques overlap. We sought to overcome this problem by fitting a curve with a polynomial function that smoothly connects two profiles in order to obtain a picture of the trend across the whole domain investigated. Furthermore, precision in determining high airflow velocities was not necessary since, for such ranges, the way mechanical ventilation impacts the behavior of the DSF does not change significantly.

This study deepens the understanding of the thermophysical behavior of mechanically-ventilated DSFs, especially regarding the impact of mechanical ventilation on the thermal performance of DSFs and its interaction with venetian blinds in this regard. The research showed the potential of a mechanically ventilated DSF as a dynamic envelope element to act as a solar collector or heat recoverer by manipulating the heat collected in the cavity through controllable features. One of the important findings of this paper is that high ventilation rates are not necessary to exploit accumulated heat in the DSF channel efficiently and that relatively low to medium rates can achieve this effect (up to 100 $m^3m^{-1}h$-1). The results of this study can be helpful for researchers working to optimize the size of the HVAC unit, fresh air delivery, air preheating, and utilization of heat collected in the cavity for different purposes.

The experimental data collected during the research activity presented in this paper are freely available to the scientific community for future independent studies. For instance, the interaction of mechanical ventilation and shading position with construction features that we could not manipulate in experiments (such as the optical properties of glazing or shading devices) could be further examined in numerical studies, or different boundary conditions that were not possible to recreate in a laboratory environment could be adopted to expand the performance analysis.

The Data can be found at and referenced using the following weblink: https://10.5281/zenodo.6482697/ [X] [the final link to the online repository will be updated at the level of proof-review after the paper has been potentially accepted for publication]

Acknowledgments

The activities presented in this paper were carried out within the research project "REsponsive, INtegrated, VENTilated - REINVENT – windows," supported by the Research Council of Norway through the research grant 262198, and the partners SINTEF, Hydro Extruded Solutions, Politecnico di Torino and Aalto University. The authors would like to thank M. Salman Siddiqui and Odne Oksavik for their support in developing the software for control and data acquisition. The technical partner Hydro Extruded Solutions (Hydro Building Systems) is also gratefully acknowledged for its support in developing and engineering the flexible mock-up and the in-kind contribution to its construction.

7.6. References

[1] X. Loncour, A. Deneyer, M. Blasco, G. Flamant, and P. Wouters, "Ventilated double facades. Classification & illustration of façade concepts," 2005.

[2] European Committee On Normalization, "NS-EN 12792:2003 Ventilation for buildings - Symbols, terminology and graphical symbols," 2003.

[3] D. Saelens, J. Carmeliet, and H. Hens, "Energy performance assessment of multiple-skin facades," Catholic University of Leuven, 2003. https://doi.org/10.1080/10789669.2003.10391063.

[4] X. li Xu and Z. Yang, "Natural ventilation in the double skin facade with venetian blind," Energy and Buildings, vol. 40, no. 8, pp. 1498–1504, 2008, https://doi.org/10.1016/j.enbuild.2008.02.012.

[5] A. Dama, D. Angeli, and O. K. Larsen, "Naturally ventilated double-skin façade in modeling and experiments," Energy and Buildings, vol. 144, pp. 17–29, 2017, https://doi.org/10.1016/j.enbuild.2017.03.038.

[6] H. Poirazis, Double skin façades for office buildings. Lund University, Lund Institute of Technology, 2004.

[7] D. Saelens, "Energy performance assessment of single storey multiple-skin facades," Catholic University of Leuven, 2002.

[8] S. Preet, M. K. Sharma, J. Mathur, A. Chowdhury, and S. Mathur, "Performance evaluation of photovoltaic double-skin facade with forced ventilation in the composite climate," Journal of Building Engineering, vol. 32, p. 101733, 2020, https://doi.org/https://doi.org/10.1016/j.jobe.2020.101733.

[9] H. Manz, A. Schaelin, and H. Simmler, "Airflow patterns and thermal behavior of mechanically ventilated glass double facades," Building and Environment, vol. 39, no. 9, pp. 1023–1033, 2004, https://doi.org/10.1016/j.buildenv.2004.01.003.

[10] S. P. Corgnati, M. Perino, and V. Serra, "Experimental assessment of the performance of an active transparent façade during actual operating conditions," Solar Energy, vol. 81, no. 8, pp. 993–1013, 2007, https://doi.org/https://doi.org/10.1016/j.solener.2006.12.004.

[11] A. Hazem, M. Ameghchouche, and C. Bougriou, “A numerical analysis of the air ventilation management and assessment of the behavior of double skin facades,” Energy and Buildings, vol. 102, pp. 225–236, 2015, https://doi.org/10.1016/j.enbuild.2015.05.057.
[12] J. Parra, A. Guardo, E. Egusquiza, and P. Alavedra, “Thermal performance of ventilated double skin façades with venetian blinds,” Energies, vol. 8, no. 6, pp. 4882–4898, 2015, https://doi.org/10.3390/en8064882.
[13] T. Inan, T. Basaran, and A. Erek, “Experimental and numerical investigation of forced convection in a double skin façade,” Energies, vol. 10, no. 9, 2017, https://doi.org/10.3390/en10091364.
[14] N. Safer, “Modélisation des façades de type double-peau équipées de protections solaires : Approches multi-échelles,” L’Institut National des Sciences Appliquées de Lyon, 2006.
[15] A. Guardo, M. Coussirat, E. Egusquiza, P. Alavedra, and R. Castilla, “A CFD approach to evaluate the influence of construction and operation parameters on the performance of Active Transparent Façades in Mediterranean climates,” Energy and Buildings, vol. 41, no. 5, pp. 534–542, 2009, https://doi.org/10.1016/j.enbuild.2008.11.019.
[16] N. Safer, M. Woloszyn, and J. J. Roux, “Three-dimensional simulation with a CFD tool of the airflow phenomena in single floor double-skin facade equipped with a venetian blind,” Solar Energy, vol. 79, no. 2, pp. 193–203, 2005, https://doi.org/https://doi.org/10.1016/j.solener.2004.09.016.
[17] T. E. Jiru, Y. X. Taob, and F. Haghighat, “Airflow and heat transfer in double skin facades,” Energy and Buildings, vol. 43, no. 10, pp. 2760–2766, 2011, https://doi.org/10.1016/j.enbuild.2011.06.038.
[18] R. Fuliotto, F. Cambuli, N. Mandas, N. Bacchin, G. Manara, and Q. Chen, “Experimental and numerical analysis of heat transfer and airflow on an interactive building facade,” Energy and Buildings, vol. 42, no. 1, pp. 23–28, 2010, https://doi.org/https://doi.org/10.1016/j.enbuild.2009.07.006.
[19] M. Bhamjee, A. Nurick, and D. M. Madyira, “An experimentally validated mathematical and CFD model of a supply air window: Forced and natural flow,” Energy and Buildings, vol. 57, pp. 289–301, 2013, https://doi.org/10.1016/j.enbuild.2012.10.043.
[20] J. S. Carlos, H. Corvacho, P. D. Silva, and J. P. Castro-Gomes, “Modelling and simulation of a ventilated double window,” Applied Thermal Engineering, vol. 31, no. 1, pp. 93–102, 2011, https://doi.org/https://doi.org/10.1016/j.applthermaleng.2010.08.021.
[21] I. Pérez-Grande, J. Meseguer, and G. Alonso, “Influence of glass properties on the performance of double-glazed facades,” Applied Thermal Engineering, vol. 25, no. 17–18, pp. 3163–3175, 2005, https://doi.org/10.1016/j.applthermaleng.2005.04.004.
[22] D. Faggembauu, “Heat transfer and fluid-dynamics in double and single skin facades,” Universitat Politècnica de Catalunya, 2006.
[23] A. Jankovic and F. Goia, “Impact of double skin facade constructional features on heat transfer and fluid dynamic behaviour,” Building and Environment, vol. 196, p. 107796, 2021, https://doi.org/10.1016/j.buildenv.2021.107796.
[24] A. Jankovic, M. S. Siddiqui, and F. Goia, “Laboratory testbed and methods for flexible characterization of thermal and fluid dynamic behaviour of double skin facades,” Building and Environment, vol. 210, p. 108700, 2022, https://doi.org/https://doi.org/10.1016/j.buildenv.2021.108700.
[25] A. Jankovic and F. Goia, “Characterization in a controlled environment of a naturally ventilated double-skin façade through the design of experiments (DOE) methodology,” Energy and Buildings, p. 112024, 2022, https://doi.org/https://doi.org/10.1016/j.enbuild.2022.112024.
[26] International Organization for Standardization, “ISO 9060:2018(en) Solar energy — Specification and classification of instruments for measuring hemispherical solar and direct solar radiation,” 2018.
[27] C. Popa, D. Ospir, S. Fohanno, and C. Chereches, “Numerical simulation of dynamical aspects of natural convection flow in a double-skin façade,” Energy and Buildings, vol. 50, pp. 229–233, 2012, https://doi.org/10.1016/j.enbuild.2012.03.042.
[28] A. Jankovic, G. Gennaro, G. Chaudhary, F. Goia, and F. Favoino, “Tracer gas techniques for airflow characterization in double skin facades,” Building and Environment, vol. 212, p. 108803, 2022, https://doi.org/https://doi.org/10.1016/j.buildenv.2022.108803.

[29] A. Jankovic, G. Chaudhary, and F. Goia, “Designing the design of experiments (DOE) – An investigation on the influence of different factorial designs on the characterization of complex systems,” Energy and Buildings, vol. 250, p. 111298, 2021, https://doi.org/https://doi.org/10.1016/j.enbuild.2021.111298.

[30] International Organization for Standardization, “ISO 15099: 2003 Thermal performance of windows, doors and shading devices,” 2003.

[31] M. L. Cherecheș et al., “Experimental Study on Airflow and Temperature Predicting in a Double Skin Façade in Hot and Cold Seasons in Romania,” Applied Sciences , vol. 11, no. 24. 2021. https://doi.org/10.3390/app112412139.

[32] International Organization for Standardization, “EN 16798-1:2019 Energy performance of buildings - Ventilation for buildings - Part 1: Indoor environmental input parameters for design and assessment of energy performance of buildings addressing indoor air quality, thermal environment, lighting and acous,” 2019.

[33] International Organization for Standardization, “SN-CEN/TR 16798-2:2019 Energy performance of buildings - Ventilation for buildings - Part 2: Interpretation of the requirements in EN 16798-1 - Indoor environmental input parameters for design and assessment of energy performance of buildings addressing i,” 2019.

8. Conclusions and future work

This doctoral research aims to expand the knowledge on thermal and fluid dynamics behavior of DSFs and quantify how this behavior is dictated by the construction features, operational modes, and environmental conditions. Although usually rigid, time-consuming, and expensive, an experimental approach was chosen to gain new insights into phenomena occurring in DSFs. The choice for such an approach was made since it is, in fact, the most fundamental and most reliable way in which new knowledge can be acquired. Furthermore, all findings gathered through theoretical or numerical research are worthless if observations do not validate them. The primary goal was to broaden the horizons based on experimentally collected data. However, pursuing this goal led to the development of a secondary path related to the methodological approach, i.e., how to perform the experiment and interpret the obtained data to understand DSF behavior better. Findings from both sides of the research are equally important since valid conclusions from the observation cannot be drawn without a proper experimental setup and execution. Sharing the experience from the experimental campaign and discussing the issues encountered during the course was intended to facilitate the experimental characterization of thermal and fluid-dynamics behavior of DSFs for other researchers.

8.1. Discussions

The first research activity aimed to direct the investigation and facilitate its planning through the state of the knowledge review. The review indicated that the shading device is the most influential structural element in both natural and mechanically ventilated DSFs and that venetian blinds are the most widely applied type, where the internal solar gains are effectively controlled by slat angle. Glazing, i.e., its optical characteristics, is the second most influential factor, and in mechanically ventilated facades, the forced airflow rate can be of equal importance. The ventilation mode, the aspect ratio of the cavity, and opening size may not be factors of the same significance as those listed above, but they must be well-coordinated together; otherwise, they can lead to severe underperformance in certain situations.

Furthermore, experiments in a controlled environment and CFD modeling have proven to be the only approaches capable of offering a deep insight into a delicate system of cause-and-effect relations in DSFs. The review showed that general trends and individual influence of single factors are more or less well understood. However, it identified the following research gaps manifested in the form of insufficient understanding or incomplete knowledge on

- the combined effect of several factors, e.g., the interaction between construction features;
- the overall impact of factors over a wide range of boundary conditions (not only for specified situations/boundary conditions but comprehensive depictions of thermal and fluid-dynamic behavior of DSF);
- exact balance and coexistence of buoyancy- and wind-induced flow in the cavity.

Gaps in methodology or lack of research in providing new knowledge have also been identified:

- Lack of experimental studies where multiple factors can be controlled simultaneously. That primarily relates to the experiments where in addition to thermal, radiative environment and wind conditions can be manipulated;
- Missing best practices and recommendations for developing CFD models targeting typical situations and DSF configurations;
- Lack of comprehensive sets of experimental measurements publicly available for the development and validation of numerical models;
- In CFD, the outside environment is usually not directly modeled and coupled with the model of the DSF.

Due to the volume of work, the focus was restricted to dealing with only some of the identified problems.

Unlike the individual influence of single factors, the combined effect of several factors and the overall impact of construction elements and operational features over a wide range of boundary conditions is less understood. Furthermore, only an experimental approach in a controlled environment and CFD modeling can unravel these complicated relationships and provide a comprehensive insight into the thermal and fluid-dynamics behavior of DSFs. The experimental approach, which offers strict control of boundary conditions and the possibility of systematic investigation of different DSF configurations in response to these boundary conditions, seemed like a good approach to solve the recognized problems.

Therefore, in the following research stage, a flexible experimental testbed was developed to systematically investigate thermal and fluid-dynamical DSF behavior. The testbed consisted of a flexible mock-up that could change its features: the cavity depth, the slat angle of venetian blinds, size of the opening, fan speed, and airflow path. The testbed was accompanied by a measurement system consisting of more than 70 sensors and an onboard system to monitor and control the experiment, and it was placed in a climate simulator that allowed strict control of the thermal and radiative environment. Based on the experience from the experimental campaign conducted in outdoor conditions at the Politecnico di Torino, the velocity profile method, as a more advanced

version of the velocity traverse method, was selected as an appropriate technique for airflow rate measurements in the DSF cavity.

The campaign aimed at finding the most suitable technique for airflow measurements showed that all considered techniques (constant inject, decay, and velocity traverse method) were characterized by significant limitations. However, it was concluded that some were less and others more successful in measuring airflow rate in certain conditions and airflow rate ranges. Due to the instrument's uncertainty, the velocity traverse method showed unreliability in situations where velocities in the cavity were below 0.1 ms^{-1}. Both gas tracer techniques had shown a limited capability due to the complex experimental setup and relatively high uncertainty. However, the decay method indicated the potential to be one of the few, if not the only method, that can estimate very low airflow rates. The constant injection method showed acceptable accuracy for airflow rates where velocities were over 0.1 ms^{-1}. Taught by experience in this experimental campaign, a few recommendations were shared to increase the reliability of gas tracer techniques as non-standardized and unconventional methods for measuring the airflow rate in a DSF. These tips were related to the amount of carbon dioxide dosing, the positions of the gas tracer sources and sampling points, and information on favorable or unfavorable measurement conditions.

Due to a less complex experimental setup, control and higher accuracy than the gas tracer techniques, preference was given to the velocity traverse method for future airflow measurement using the developed experimental testbed. The only difference was that the number of measuring points was increased so that the air velocity profile could be captured, and thus the airflow rate could be determined more precisely. Before conducting experiments in the climate simulator, the accuracy of the VPM was assessed through comparison with measurements of the highly precise ultrasonic flow meter. In this way, better insight into the weak points of this method was attained, such as the problem of low airflow rates, determination of airflow direction in case of minor temperature differences, and inadequacy of punctual measurements to capture complex naturally-driven flows. Finally, the experimental testbed was verified using several experimental investigation methods of different levels of complexity: standard metrics measurements, one-factor analysis, design of experiments (DOE), and dynamic profile measurements. The conclusion, and at the same time the answer to RQ2, was that for the developed flexible experimental testbed, the design of the experiments (DOE) represents the most suitable investigation method to systematically characterize the thermophysical behavior of the DSF. By applying statistical tools to the results of a predesigned series of experiments in steady-state conditions, DOE methodology quantifies relationships between factors (constructive features and boundary conditions), their interactions, and thermal and fluid-dynamics behavior of the

DSF. High material costs are required for such investigations, but based on previous experience, some practical tips on how to shorten investigation through the DOE approach were provided.

In the next step, a series of experimental runs (experimental designs/arrays) was planned, i.e., the optimal experimental design(s) were identified to characterize DSF thermophysical behavior under given conditions. Finding the optimal design was tackled through an extensive simulation study that identified features an experimental design should have to characterize the behavior of a DSF adequately and the recommended steps to be followed for the optimal design. It was concluded that the extent of nonlinearity in the process determines the resolution of the optimal design, as well as the amount of available time and material resources and the ability to perform experiments in certain conditions. Furthermore, the ability of a researcher to recognize the 'true' nature of factors and the continuous physical properties hidden behind technological implementations is also an important aspect that helps reduce the required resources for adequate characterization. For the complex behavior of dynamical envelope elements, such as a DSF, the resolution capable of assessing both the main effects and the interactions is the lowest possible resolution (resolution IV).

The extensive study provided a recommended course of action to select the optimal design that goes beyond the considered case, relating to a wide range of complex behaviors that need to be characterized by resource-limited experiments. The decision tree included several steps to be followed. The preparation of data was the first step, which included a few practical pieces of advice on selecting and classifying factors and assigning the corresponding low and high values to the levels. The subsequent step in the tree refers to decisions based on the total number of factors, where a screening procedure is recommended to narrow down important factors if there are more than five of them. Several types of experimental designs are recommended depending on the decisions made within the flow diagram. For Taguchi designs, it is recommended not to overload them with levels (a maximum of three or four levels are sufficient) to maintain a sufficiently high resolution. Furthermore, an error (unexplained part of the variance) higher than 5 % indicates possible irregularities in designing and performing the experiment and makes it challenging to establish any stronger statistical significance of the factors and interactions. If sufficient resources remain, a validation check of the obtained characterization can also be done by comparing the ANOVA results from two different designs.

Through this research activity, the answer to RQ2 is further specified by pointing out how the DOE methodology can be applied to a developed experimental testbed for future characterizations and what aspects of the thermophysical behavior should be researched. The developed approach to implement the DOE methodology was validated with physical experiments with a DSF in a climate simulator

and then employed to learn as much as possible about the thermophysical behavior of a DSF in the following research activities. Two experimental campaigns were conducted, one with a naturally- and the other with a mechanically-ventilated DSF. In the campaign with the naturally-ventilated DSF, the findings from the previous research were confirmed by comparing the ANOVA results obtained from four different designs. As an additional finding, it was concluded that designs need to evaluate a nonlinear response of the output quantity, either through the usage of quadratic models or by employing more than two points when a 2-FI model is used. Unlike the previous study, possible causes for error (the unexplained variance) arising from limitations related to physical experiments, such as uncertainty of measurement methodology and instruments, the inability of the facility to replicate desired conditions, etc., were discussed here.

Application of the DOE methodology has shown that in a naturally-ventilated DSF in a wide range of boundary conditions typical of summer, central regulators of thermophysical behavior were environmental factors. More precisely, these are temperature difference and solar irradiance, while the influence of controllable factors (venetian blind angle and opening size) was significantly limited. However, some aspects, such as the net heat transfer and the airflow rate, albeit the latter to a lesser extent, could be controlled by adjusting the angle of venetian blinds. Closure of the blinds exerted the opposite effect on these two performance indicators. The highest airflows and the amounts of heat removed by the airflow were observed for a combination of high solar irradiance and negative temperature difference (cold outside air). Furthermore, natural ventilation was quite ineffective in the removal of the heat from the cavity for the high outdoor temperature and low to moderate solar irradiance levels. ANOVA analysis further showed that the flow in the cavity was driven much more by the absorption of solar radiation than by temperature difference. By choosing a wide range of boundary conditions, a wide range of variations of behavioral indicators was obtained as well, thus including many situations in which the impact of construction elements on response quantities was not necessary. In this way, the impression was gained that the influence of controllable factors was limited, but in fact, it was overshadowed by the impact of environmental parameters.

Therefore, in the last research activity, the effect of environmental parameters was not examined, and fixed boundary conditions were chosen to gain a better insight into the influence of construction features on the thermal and fluid-dynamic behavior of the DSF. The study has shown that a DSF could be effectively used as a heat recuperator in winter/mid-season conditions by preheating air passing through the cavity from the outdoor to the indoor environment. Low ventilation rates were enough to preheat and deliver fresh air sufficiently, while the semi-opened blinds led to higher preheating efficiency than closed or no blinds. Much more than venetian blinds, mechanical ventilation regulated the net heat transfer in such an arrangement and conditions. Tests in summer

conditions demonstrated that the DSF could be efficiently employed as a solar collector. The air drawn from outside was heated by passing it through the cavity, thus removing the excess heat in significant quantities, which could be used for various purposes. Again, low ventilation rates were enough to remove the highest amounts of accumulated heat in the cavity, while the presence of venetian blinds significantly increased the dynamic insulation efficiency and the amount of heat absorbed by the airflow. The shading device almost entirely regulated the net heat transfer in such an arrangement and conditions, while the impact of mechanical ventilation was surprisingly small.

8.2. Limitations

Although the research sought to make the results as general and applicable as possible, some limitations could not be avoided. This section will list all of those that somehow impacted the interpretation of the research findings. The literature review was focused on the impact of construction features of conventional DSFs, defined as a façade element with transparent glazing on both sides and a space for ventilating in between, thicker than 20 cm, containing a traditional shading device (e.g., venetian blinds or roller screen). Due to their limited applications or still being in the testing phase, novel types of DSF (e.g., opaque DSF, green DSF, or smart DSF) and unconventional construction features (e.g., PV elements, PCM, and smart materials) were excluded from the scope of the analysis.

The developed experimental testbed offered the possibility for a thorough and systematic investigation of the thermal and fluid-dynamics behavior of double skin facades. However, it was accompanied by certain limitations originating from the used instruments, facilities, and measurement methodologies, restricting the comprehensiveness of the investigation. Limitations related to the climate simulator can be outlined through the inability to maintain the desired temperature and the existence of a vertical gradient in certain situations. The non-uniformity and fluctuating nature of emitted radiation, the inability to reproduce low radiation levels and control the direction of emitted radiation are limitations tied to the solar simulator. In the experiment with the mechanically ventilated DSF, increased infiltration was suspected in parts of the experimental testbed where the ventilation system was attached to the upper opening of the DSF, which affected the reliability of determining higher airflow rates using the ultra sonic flow meter. Finally, the climate simulator used for the investigations offered control of the thermal and radiative environment without the possibility of controlling wind conditions. Therefore, the impact of the wind as a driving factor and boundary condition could not be examined, even though it can be crucial in driving the thermal performance of DSFs.

As far as the test specimen is concerned, optical losses due to its limited dimensions were noticeable. Although it was known that some factors, such as the optical properties of glazing or shading devices, significantly influence the transport of mass and energy in a DSF, we could not examine their impact since these features could not be made alterable. The most significant limitations regarding measurement methodologies or instruments were related to the fluid-dynamic characterization, more precisely to the airflow rate measurements in the cavity. The velocity profile method was unreliable in evaluating very low airflow rates (tied to velocities below 0.1 ms^{-1}) due to the bottom threshold limit of hot wire anemometers. Furthermore, for minor temperature differences (<0.5 ^{o}C) between the fluid and the surrounding boundaries, the determination of airflow direction using this method was also problematic. The punctual measurements of the velocity profile method could not reflect the full three-dimensionality of the flow; hence, there was a possibility that sampling points were not representative of cross-sectional averages. Therefore, due to previously listed issues, the airflow rate measurement and the characterization of fluid-dynamic behavior (through the DOE methodology) were given with reduced reliability.

The research activity, which sought to develop a strategy for selecting the optimal design to characterize a complex process using a limited number of experimental runs, was supported by a series of numerical simulations of an immense number (almost half a million). Such an approach was taken since performing a large number of physical experiments would require almost unlimited time and, at the same time, material resources. However, due to the deterministic nature of simulations, experimental variation (noise, error), characterizing every physical experiment, was not present in the simulation-supported experiments. Experimental variation arises from uncontrollable factors that affect the process in a certain way, and as a result, its existence may influence the choice of the optimal design. However, the assumption was that in controlled experiments (such as those in a climate simulator), the experimental variation is minimal and does not represent a significant part of the unexplained variance.

Research showed that the DOE methodology could be successfully applied to characterize the behavior of dynamic building envelope elements (such as DSFs) through experiments in a controlled environment. However, the success of this application and the accuracy of the obtained characterization depended on many factors. If the optimal design is chosen, then the unreliability of the obtained depiction can originate from three types of sources:

- uncertainty posed by measurement methodologies;
- (in)accuracy of instruments;
- limitations of facilities intended to replicate boundary conditions.

For example, hot-wire anemometers could not register low-velocity variations (<0.1 ms^{-1}), which was reflected through blurred discernment of what factors led to the total variance of airflow rate.

8.3. Conclusive remarks and future work

The doctoral research aimed to discover to what extent and in what way the thermal and fluid-dynamics behavior of DSFs is influenced by construction elements, operational features, and boundary conditions. It was recognized that the individual influence of a single factor at a time had been more or less explained and quantified through a series of experimental and CFD studies in the past. However, there is a lack of understanding of the overall impact of factors over a wide range of boundary conditions and how the interactions between construction elements influence DSF performance. Such knowledge gaps originate from a lack of systematic research, where multiple factors are controlled simultaneously, which primarily relates to the experiments in a controlled environment. Therefore, the flexible experimental testbed was developed and paired with the DOE methodology to address the above issues and systematically investigate how structural, operational, and environmental factors influence thermophysical behavior. Furthermore, an approach was developed to optimally apply this methodology to adequately characterize the complex behavior of dynamic façade elements, such as DSFs, through resource-limited experiments.

The developed methodological approach was successfully applied to arrive at findings on the behavior of the specific façade mock-ups, which are realistically extendable to a larger range of single-story naturally- and mechanically-ventilated DSFs. It has been shown that for a wide range of boundary conditions typical of summer, environmental factors primarily regulate the thermophysical behavior of DSFs naturally ventilated in the outdoor air curtain mode. However, some aspects, such as net heat transfer and, to a lesser extent, airflow rate, can be controlled by adjusting controllable factors, i.e., venetian blind angle. It turned out that the buoyant flow in the cavity was driven far more by the solar irradiance than by the temperature difference. Therefore, the highest air flow rates and the amount of heat absorbed by it from the cavity were observed for a combination of high solar irradiance and cold outdoor air, while natural ventilation was relatively ineffective in heat removal from the channel in conditions where there was high outdoor temperature and low/moderate solar irradiance level.

However, choosing a wide range of boundary conditions in the DOE approach can make the impact of controllable factors overshadowed by driving factors, as was the case in the experimental campaign with the naturally ventilated DSF. If one wishes to know the potential of a DSF in certain situations,

where the intervention of controllable features is needed to impact the response variable, it is necessary to define a narrower range or fixed boundary conditions. Therefore, in the experimental campaign with the mechanically ventilated DSF, fixed boundary conditions were chosen for two representative cases, winter/mid-season and summer. The research showed that the DSF could be utilized as an efficient preheater and supplier of fresh air with light mechanical ventilation. The preheating efficiency can be increased even more if the slats are placed in a semi-open position, as this way, the airflow absorbs a larger amount of heat than if the slats are entirely closed or if blinds are raised. On the other hand, relatively low ventilation rates in summer conditions can efficiently control the DSF as a solar collector by removing large quantities of accumulated heat in the cavity. Dynamic insulation efficiency and the amount of heat removed by the outdoor air curtain can be increased even more with the presence of venetian blinds.

Research showed that the DOE methodology could be successfully applied to characterize the performance of dynamic building envelope elements, such as DSFs. However, the success of this application and the accuracy of the obtained characterization depends on several factors. Assuming an optimal design is chosen, the unreliability of the obtained depiction mainly originates from uncertainty posed by measurement methodologies, inaccuracy of instruments, and limitation of facilities intended to replicate boundary conditions. For example, the assessment of thermal behavior of a DSF given through DOE methodology is highly reliable, while for the fluid-dynamics behavior, the same cannot be said due to uncertainties posed by the airflow rate measurements.

Doctoral research and associated publications contributed to the scientific community through various forms of new knowledge, which can be summarized according to the following points:

- development of recommended procedures to optimally design experiments;
- providing insight into the possibilities and limitations of the DOE methodology applied for the characterization of dynamic façade elements' behavior;
- publishing the comprehensive experimental datasets freely available for further scientific investigations;
- understanding of the extent and the way certain construction and environmental factors and their interactions influence the thermophysical behavior of DSF;
- providing insight into the possibilities and challenges offered by various techniques for measuring airflow rates in DSF cavities.

A better understanding of thermal and fluid dynamics behavior is given mainly through the findings of the last two articles, the results of which can be significant to scientists and engineers working on the design and optimization of DSF. The DOE methodology is not a novel approach, but its

application in building energy or thermal performance research is quite recent and rare, especially using real 'physical' experiments. Therefore, this doctoral study opened the perspective of the possibilities and limitations of this approach to translating complex and nonlinear behaviors into understandable and practical relationships. The development of recommended procedures to optimally design the experiment can be valuable to any researcher who, through experiments, wants to efficiently characterize the behavior of complex systems, such as dynamic envelope elements, by saving resources and overall costs. All experimental campaigns in the climate simulator resulted in publicly available sets of experimental data, which is of great importance to the scientific community aiming to expand knowledge either through direct research with published data or through the development of numerical models validated with these datasets. Experiences shared from the experimental campaign could contribute to developing standardized procedures and best-practice recommendations for better and more reliable measurements of DSF performance metrics, which applies especially to airflow rate measurements and evaluation of all associated indicators.

The potential of the developed experimental testbed has not been fully realized, so further research is possible on both the processes taking place in the DSF and the methodologies by which they are investigated. For example, it would be interesting to examine the potential of DSFs when it comes to utilizing the accumulated heat in a cavity if the air is drawn from the interior. Comparing the results of such a campaign with the results of one where the air is extracted from the outdoor would be interesting. Certain activities have already been undertaken to test the reliability of the pressure difference method in determining the airflow rate in the cavity. These activities could be continued since this method showed potential primarily due to its simple experimental setup once calibration constants are determined. If this method were to be investigated in more detail, it would be possible to test the performance of several different techniques in determining airflow rates simultaneously. Comparing the methods of velocity profile, decay, constant injection, pressure difference, and measurement obtained with an ultrasonic flow meter would be interesting from the aspect of their reliability in determining airflow rates in different ranges and types of airflow (natural and mechanical). Also, impact assessment on the thermal performance of a DSF in fixed boundary conditions of all features investigable by this experimental testbed would be desirable. The influence assessment of venetian blind angle, the shading device distance to glazing, opening size, mechanical ventilation, airflow path, and cavity depth would be engaging from the aspect of comparing their extent. Activities to develop a CFD model that will be validated using measurements performed with this experimental testbed are currently underway. Such a model would be able to assess the impact of those construction features that could not be made alterable due to technical limitations, such as optical and thermal properties of glazing and shading device. Some of the aforementioned

experimental campaigns may have been conducted during the period scheduled for doctoral research. Still, it should also be recalled that for several months, due to the Covid-19 pandemic, access to the laboratory was not possible.

ISBN 978-82-326-5207-5 (printed ver.)
ISBN 978-82-326-6752-9 (electronic ver.)
ISSN 1503-8181 (printed ver.)
ISSN 2703-8084 (online ver.)

NTNU
Norwegian University of
Science and Technology